University of Glasgow

Zurita Leal, Andrea Cristina (2017) *Translesion DNA polymerases and genome maintenance in Trypanosoma brucei.* PhD thesis.

https://theses.gla.ac.uk/8897/

Translesion DNA Polymerases and genome maintenance in *Trypanosoma brucei*

Andrea Cristina Zurita Leal

BSc

Submitted in fulfilment of the requirements for the

Degree of Doctor of Philosophy

Wellcome Centre for Molecular Parasitology

Institute of Infection, Immunity and Inflammation

College of Medical Veterinary and Life Sciences

University of Glasgow

October, 2017

Abstract

Many DNA repair pathways have been documented in *Trypanosoma brucei* but less attention has been paid to damage tolerance, a reaction in which lesion bypass is needed, in particular to ensure continued genome replication. Such bypass is promoted by translesion DNA polymerases (TLS Pols). *T. brucei* has ~15 TLS polymerases candidate genes, only two of which have been functionally examined to date. Understanding the roles provided by TLS Pols could reveal new aspects of *T. brucei* biology. Here, I examine the activities of TLS Pol Nu (PolN), TbPolZ and TbPolQ (HelQ) in bloodstream cells.

RNAi against TbPolN results in slowed growth after ~24 hours, which is associated with altered DNA content, changed cell morphology and sensitivity to DNA damage. Surprisingly, growth and morphology defects are reduced after ~48 hours, without apparent RNAi reversion. In addition, depletion of the protein seems to lead to an aberrant distribution of the chromosomes, as visualised by telomere fluorescent in situ hybridization. TbPolN epitope tagging demonstrates a discrete localisation of the protein at the periphery of the nucleus in the absence of damage, with a more widespread, but non-uniform localisation after damage. EdU labelling and γH2A analysis after TbPolN knockdown reveal a decrease in proliferating cells, which accumulate nuclear DNA damage. Finally, we show that TbPolN interacts with a nuclear putative non-canonical PolyA polymerase. Taken together, these data suggest TbPolN may be involved in *T. brucei* nuclear DNA maintenance.

RNAi of TbPolZ (zeta) did not impair growth but resulted in increased sensitivity to methyl methanesulphonate (MMS) damage and UV radiation, suggesting a possible role in the response against both genotoxic agents. Generation of TbPolZ null mutants confirmed that the protein is non-essential and plays a role in genotoxic damage repair. Surprisingly, TbPolZ epitope tagging not only showed a nuclear signal, but a mitochondrial signal was also detected. These data were supported by immunoprecipitation, where mitochondrial proteins were obtained as potential interaction partners. These data suggest a contribution of TbPolZ to both nuclear and kinetoplast genome maintenance.

Targeted RNAi of the third putative TLS-related factor, TbHelQ, was unsuccessful. Despite this, sequence analysis of the protein indicates that its current annotation as a PolQ homologue is inaccurate, since the predicted protein is not a joint polymerase-helicase like in other eukaryotes, but only a putative helicase. Hence, it is suggested it should be renamed TbHelQ. Immunoprecipitation and colocalisation analyses indicate a possible role of TbHelQ in homologous recombination, given the potential interaction of the factor with BRCA2 and other factors involved in this repair process. Notably, the predicted interactome of TbHelQ differs from that of TbPolN, suggesting discrete functions in *T. brucei*.

Taken together, these data reveal widespread and variant functions of three putative TLS DNA polymerases in the parasite genome biology, suggesting a possible role in the maintenance of genome integrity in *T. brucei*.

Table of contents

List of Tables

List of Figures

Acknowledgements

First of all, I would like to thank my supervisor Richard McCulloch for his constant guidance and encouragement over these four years. It was really a pleasure to work with him. I would also like to thank my assessors, Elmarie Myburgh and Markus Meissner for their helpful suggestions, Leandro for his help with the microscopy images, and SENESCYT, Ecuador, for funding my Ph.D.

To all the amazing people that I have met over these four years (Sammy, Mari, Amy, Becky, Fernando, Jeziel, Cat, Jenny, Sam, Emma, Dan, Chris, Jim, Elaine, etc), you guys made Glasgow feel like home to me.

To past and present members of the McCulloch lab, thanks! Craig for his constant support. Cat, Becky and Jenny for teaching me everything when I first arrived. Dan, for being a great friend and making TC days more fun. Sam, for her friendship and for trying to solve all my computational problems (I still do not know how I manage to break my computer so often). I really want to thank Emma for being such an amazing friend. Thanks for all those evening chats, of course with tea and cake, and for always being there for me.

My wonderful friends Vivi, Carmen and Nati and for all those adventures together; things would not have been the same without these girls. Helena and Mario, for all your advice and chats, you are great guys.

To Fer, my soul sister, I really do not know how to thank you for all you have done for me. Thanks for all those laughs, advice, encouraging words and for all the gourmet food that you have cooked for me (especially the tuna bread, hahaha).

I especially want to thank my family. My mom for being my role model, with her love and support she taught me to pursue my dreams. My dad, although he is not with us anymore, he always inspires me to be a better person. My sister, for always being by my side. I love you all so much!

Author's Declaration

I, the author, hereby declare that this thesis and the results presented within are the result of my own work unless otherwise stated. None of the results presented here have been previously used to obtain a degree at any university.

Andrea Cristina Zurita Leal

List of Abbreviations and definitions

AP/C	Anaphase promoting complex or Cyclosome
ATM	Ataxia-telangiectasia mutated
ATP	Adenosine triphosphate
ATR	Rad3-related protein
AUK	Aurora B kinase
BER	Base excision repair
BES	Blood stream form expression site
BLAST	Basic Local Alignment Search Tool
BLASTp	BLAST(protein)
bp	Base pairs
BRCA	Breast cancer associated
BSA	Bovine serum albumin
BSD	Blasticidin
BSF	Blood stream form
CAK	CDK-activating kinase
cDNA	Complementary DNA
CDK	Cycline-dependent kinase
CDS	Coding sequence
CIF1	Cytokinesis Initiation Factor1
CL	Cross-link
coIP	Co-immunoprecipitation
C-terminal	Carboxyl terminal
CTCF	Corrected total cell fluorescence
CYC	Cyclin
DAPI	4',6-diamidino-2-phenylindole
ddH$_2$O	Double distilled water
DIC	Differential interference contrast
D-Loop	Displacement loop
DNA	Deoxyribonucleic acid
dNTP	Deoxynucleotide triphosphate
DSB	Double strand break
dsDNA	Double stranded DNA
EDTA	Ethylenediaminetetraacetic acid
EdU	5-Ethynyl-2'-deoxyuridine
EF1α	Elongation factor 1-alpha
EGTA	Egtazic acid
EM	Electron microscoy
ES	Expression site
ESAG	Expression site associated genes
ESB	Expression site body
FA	Fanconi Anemia
FACS	Fluorescence activated cell sorting
FAZ	Flagellar attachment zone
FITC	Fluorescein isothiocyanate
FP	Flagellar pocket
G1	Gap 1
G2	Gap 2
gDNA	Genomic DNA
GFP	Green fluorescent protein

HAT	Human African trypanosomiasis
HelQ	Helicase theta
HMI	Hirumi's modified Isocove's medium
HR	Homologous recombination
Hrs	Hours
HSP	Heat shock protein
HYG	Hygromycin
ICL	Interstrand cross-link
IFA	Immunofluorescence assay
Ig	Immunoglobulin
IP	Immunoprecipitation
IMDM	Isocove's modified Dulbecco's medium
K	Kinetoplast
kbp	Kilobase pairs
kDa	Kilo-dalton
kDNA	Kinetoplast DNA
Mb	Megabase
MBC	Megabase Chromosome
MMEJ	Microhomology-mediated end joining
MMR	Mismatch repair
MMS	Methyl methanesulfonate
MOPS	3-(N-morpholino) propanesulfonic acid
MRN	Mre11-Rad50-Nbs1
mRNA	Messenger RNA
MUB	Mono-ubiquitination
N	Nucleus
nDNA	Nuclear DNA
NEO	Neomycin
NER	Nucleotide excision repair
NHEJ	Non-homologous end joining
Nr	Non-redundant
N-terminal	Amino terminal
ORC	Origin recognition complex
ORF	Open reading frame
PAGE	Polyacrylamide gel electrophoresis
PBS	Phosphate buffered saline
PBST	PBS-tween
PCNA	Proliferating cell nuclear antigen
PCR	Polymerase chain reaction
PFA	Paraformaldehyde
PLK	Polo-like kinase
Pol	Polymerase
PolI	Polymerase I
Polα	Polymerase alfa
Polδ	Poymerase delta
Polε	Poymerase epsilon`
Polη	Polymerase eta
Polι	Poymerase iota
Polκ	Polymerase kappa
Polλ	Polymerase lambda
Polμ	Polymerase mu
PolN	Polymerase Nu

Polσ	Polymerase sigma
PolQ	Polymerase theta
PolZ	Polymerase zeta
PUR	Puromycin
Rev3	Poymerase zeta catalytic subunit
RNA	Ribonucleic acid
RNA pol I	RNA polymerase I
RNAi	RNA interference
ROS	Reactive oxygen species
RPA	Replication protein A
RT	Reverse transcriptase
qPCR	Quantitative polymerase chain reaction
S	Synthesis
Scc1	α-kleisin protein
SEM	Scanning electron microscopy
SDS	Sodium dodecyl sulphate
SMC	Structural maintenance of chromosome
SOC	Super optimal broth supplemented with glucose
ssDNA	Single stranded DNA
TAE	Tris acetit acid EDTA buffer
Tb	*Trypanosoma brucei*
TC	Telomere conversion
TEM	Transmission electron microscopy
Tet	Tetracycline
Tet-	Without tetracycline
Tet+	With tetracycline
TLS	Translesion synthesis
TLS	Translesion synthesis polymerases
TOEFAZ1	Tip Of The Extending FAZ 1
UTR	Untranslated region
UV	Ultraviolet
VSG	Variant surface glycoprotein
WT	Wild type

1 Introduction

1.1 Kinetoplastids

Kinetoplastids (class Kinetoplastae) are flagellated protozoans, which belong to the phylum Euglenozoa (Moreira, López-García and Vickerman, 2004). The members of this group are characterised by the presence of a unique organelle known as kinetoplast, which is the single copy mitochondrion and contains a genome composed of a concatenated network of two classes of circular DNA (Moreira *et al.* 2004). This is not the only biological peculiarity that differentiates these organisms from other eukaryotes. The ability to edit their mitochondria RNA, their organisation of nearly all genes as multigene transcription units, near universal trans-splicing to generate mature mRNA, and the compartmentation of glycolysis are a few of the characteristics that make kinetoplastids unusual among the eukaryote domain (Simpson, Stevens and Lukeš, 2006).

The class Kinetoplastae is divided into two subclasses known as the Prokinetoplastina and Metakinetoplastina, the latter of which is subdivided in four clades: the Parabodonida, Eubodonida, Neobodonida and Trypanosomatida (Lukeš *et al.*, 2014). The Trypanosomatida clade consists of uniflagellar obligate parasites, which are associated with pathogenic infections in humans and animals. This grouping includes *Trypanosoma brucei, T. cruzi* and *Leishmania* spp (Simpson, Stevens and Lukeš, 2006; Kaufer *et al.*, 2017). *T. brucei* is the etiological agent of African trypanosomiasis, which is a parasitic disease of humans (sleeping sickness) and cattle (Nagana disease). *T. cruzi* infection provokes American trypanosomiasis, which is known as Chagas disease and is found mainly in south and central America (Simpson, Stevens and Lukeš, 2006; Kaufer *et al.*, 2017). On the other hand, *Leishmania* spp. are responsible for a range of pathologies collectively referred to as the disease leishmaniasis, which is divided into cutaneous, mucocutaneous and visceral leishmaniasis (Murray *et al.*, 2005). Leishmaniasis is endemic to the tropics, subtropics and Mediterranean basin (Simpson, Stevens and Lukeš, 2006; Oryan and Akbari, 2016).

1.2 Human African Trypanosomiasis

African trypanosomiasis affects humans and animals in sub-Saharan Africa (Franco *et al.*, 2014) (Figure 1-1). In humans, Human African trypanosomiasis

(HAT), or sleeping sickness, is frequently fatal if untreated. Furthermore, the disease also has a wider impact on the economy, since sleeping sickness contributes to the reduction of labour resources (Simarro, Jannin and Cattand, 2008). Meanwhile, animal infection, or Nagana, greatly impacts food sources (Simarro, Jannin and Cattand, 2008) since it affects cattle, which are normally used for farming activities (Steverding, 2008). The infected animals develop a range of symptoms like fever, discharge from the eye, anaemia and paralysis, subsequently generating weakness in the animal rendering it unable to work (Steverding, 2008). Due to these effects, African trypanosomiasis is a public health problem which affects not only the economy but the cultural development of rural communities (Steverding, 2008).
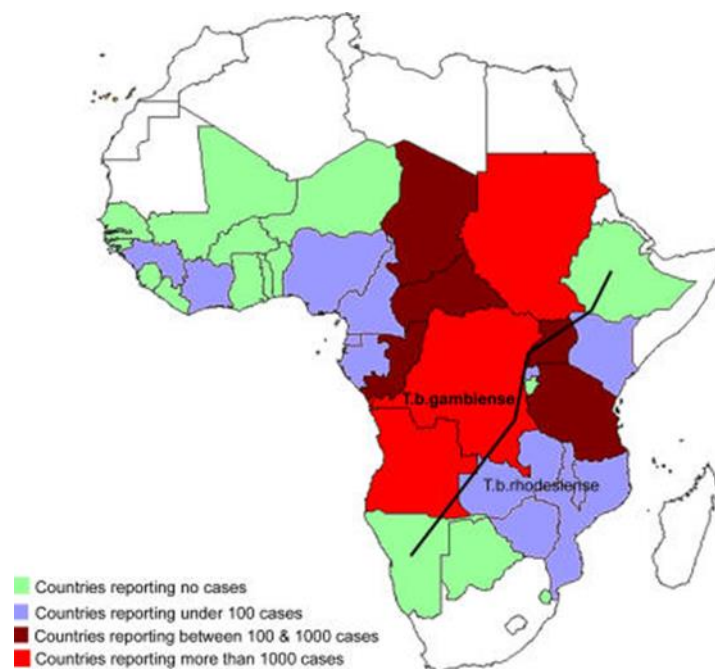
Figure 1-1. Map showing the distribution of sleeping sickness across the African continent. Adapted from (Simarro *et al.*, 2010).

The causative agent of trypanosomiasis, in humans, is the flagellate parasite *Trypanosoma brucei*, of the class Kinetoplastida, order Trypanosomatidae (Rotureau and Van Den Abbeele, 2013). The parasite is transmitted by the bite of the flies from the genus *Glossina* (*Diptera*; *Glossinidae*) (Rotureau and Van Den Abbeele, 2013; Franco *et al.*, 2014). This parasite is divided in three subspecies, *Trypanosoma brucei brucei*, *T.b. gambiense*, and *T.b. rhodesiense*. *T.b. gambiense* and *T.b. rhodesiense* are

human infective and responsible for HAT (Rotureau and Van Den Abbeele, 2013; Franco *et al.*, 2014). *T.b. brucei* is not human infective but instead is responsible for causing Nagana disease, though two further species, *T. vivax* and *T. congolense*, are a much greater source of the animal disease (Steverding, 2008).

HAT has two stages. The first stage is called the haemolymphatic stage, where parasites are found in the lymph and the blood system. During this stage the symptoms that manifest include fever, headache, pruritus lymphadenopathy, weakness, asthenia, anaemia and hepato-splenomegaly (Franco *et al.*, 2014). However, considering that these symptoms are usually not severe, patients do not typically seek medical care (WHO, 2013). In the second, or meningoencephalitic stage, the parasites cross the blood brain barrier and invade the central nervous system, producing neurological disorders (Franco *et al.*, 2014). The common symptoms in this stage include confusion, tremors, fasciculation, motor weakness, akinesia or dyskinesia, sensory disturbances, abnormal movements and speech disorders (Malvy and Chappuis, 2011; Franco *et al.*, 2014). Early sleeping sickness symptoms are general and variable, making it possible to confuse this disease with others such as malaria, enteric fever, tubercular meningitis and HIV (Wastling and Welburn, 2011). Depending on the parasite subspecies, the progression of the disease can vary. *T.b. gambiense* (responsible of 90% of HAT cases) results in a chronic infection, in which the patients may be infected for months, even years, without presenting any neurological symptoms (Simarro, Jannin and Cattand, 2008). By the time infected individuals display specific HAT symptoms (headaches, fever, sleep disturbances, alteration of mental state and other neurological disorders), the disease is already in the meningoencephalitic stage (Simarro, Jannin and Cattand, 2008; Franco *et al.*, 2014). In contrast, *T.b. rhodesiense* causes an acute infection where neurological symptoms can manifest a few weeks or months after the infection and subsequently progress rapidly to the meningoencephalitic stage (Simarro, Jannin and Cattand, 2008; Franco *et al.*, 2014).

Recent studies have shown that *T. brucei* parasites are found outside the vasculature in the adipose tissue, suggesting this location may provide a

significant reservoir for *T. brucei*, where the parasites use fatty acids as a carbon source. Parasite localisation in this tissue could be beneficial for parasite survival, hindering the action of the immune system (Trindade *et al.*, 2016). Though it is still uncertain if *T. brucei* has the capability to undergo VSG switching in the adipose tissue, if this is the case it would be an advantage during blood repopulation (Trindade *et al.*, 2016). However, further studies are needed in order to determine if the insect vector, the tsetse fly, is able to ingest parasites from the subcutaneous fats in order to continue the infection cycle (Trindade *et al.*, 2016). In further work, the skin has also been recently identified as a similar extravascular reservoir for *T. brucei*. In the same way as adipose tissue, parasites localised in the skin may play an important role during blood repopulation and transmission (Capewell *et al.*, 2016).

1.2.1 **Treatment**

The treatment for HAT involves highly toxic drugs, whose administration depends upon the phase of the disease. In the case of infections with *T.b. gambiense,* early stage disease is treated with pentamidine, while a combination of eflornithine and nifurtimox is used for the late stage (Kennedy, 2013). In the case of infections with *T.b. rhodesiense* the early stage of the disease is treated with suramin, and the late stage disease with melarsoprol (Kennedy, 2013). The problem with these drugs is the severe side-effects for the patient and difficulties during administration of the drug, since nifurtimox is the only drug administered by the oral route (Kennedy, 2013).

1.3 Life Cycle

The life cycle of *T. brucei* involves two hosts, an insect (tsetse fly) and a mammal (Figure 1-2). The cycle begins when an infected fly feeds on a mammal and inoculates metacyclic trypomastigotes, which invade the bloodstream from the bite site via the lymphatic system. In the bloodstream the metacyclic form cells differentiate into long slender bloodstream form trypomastigotes, and start to replicate by binary fission (Rotureau and Van Den Abbeele, 2013). This form of the parasite can also differentiate into short stumpy trypomastigote forms, which are non-dividing and are pre-adapted for inhabiting the vector, where

replicative bloodstream form cells do not survive. When a fly feeds on an infected mammal, short stumpy form parasites are able to differentiate into procyclic form cells in the midgut of the fly (Rotureau and Van Den Abbeele, 2013). Short stumpy form cells therefore have a crucial role in perpetuating the trypanosome life cycle. These forms are also associated with infection chronicity since they contribute, along with antigenic variation (see below), to the regulation of parasitemia (Matthews and Gull, 1994; Rico *et al.*, 2013).

Procyclic form cells establish an infection in the midgut by resuming cell replication and undergoing a major change in the proteins displayed on the cell surface of the parasite. The Variant Surface Glycoprotein (VSG) 'coat' expressed on the plasma membrane of bloodstream form and metacyclic form cells is replaced by expression of procyclin. Each coat is required for survival in the different host environments (Rotureau *et al.*, 2012). In bloodstream forms, the VSG coat has an important function evading the mammalian host immune system (Sheader *et al.*, 2005; Taylor and Rudenko, 2006). The role of the procyclin coat is still uncertain, but it is believed to have a similar role to the VSG coat in bloodstream forms (Ruepp *et al.*, 1997; Acosta-Serrano *et al.*, 2001). It has been proposed that the coat in procyclic form cells is essential for the establishment of infection in the fly, probably by contributing to the evasion of the fly immune system and protecting the cells from lysis in the midgut environment (Ruepp *et al.*, 1997; Acosta-Serrano *et al.*, 2001; Sheader *et al.*, 2005). The next stage in the life cycle begins when procyclic form cells differentiate into mesocyclic forms, which migrate from the midgut and then differentiate into epimastigotes. In the salivary glands, epimastigote cells multiply and differentiate into metacyclic trypomastigotes and, in this way, the cycle starts all over again (Rotureau & Van Den Abbeele, 2013)

Previous studies have analysed mRNA expression levels of pleomorphic slender forms, *in vivo* generated stumpy forms and cells undergoing synchronous differentiation (from stumpy to procyclic forms); in order to compare gene expression in different life cycle stages (Jensen *et al.*, 2009; Kabani *et al.*, 2009; Nilsson *et al.*, 2010). Despite the different techniques used for the analysis, microarrays (Jensen *et al.*, 2009; Kabani *et al.*, 2009) and splice leader trapping (Nilsson *et al.*, 2010), the results were comparable. Expression of

distinct genes was seen depending on the life cycle stage, at least some of which might be related with the requirement for diverse proteins for the adaptation to a new environment, or growth and survival within that environment (Jensen *et al.*, 2009; Kabani *et al.*, 2009; Nilsson *et al.*, 2010; Rico *et al.*, 2013).Significant changes in transcripts levels involved in metabolism, cell division, protein transport, cell structure, proteolysis and translation, were detected in slender and stumpy forms. For example, in the slender forms an up-regulation of expression site-associated genes (ESAG), histones, DNA replication/repair and translation transcripts was detected (Jensen *et al.*, 2009; Kabani *et al.*, 2009). On the other hand, in the stumpy form, there was an up-regulation of procyclins and proteins associated with differentiation (PAD) (Jensen *et al.*, 2009; Kabani *et al.*, 2009). In the case of the procyclic forms, there was a down-regulation of ESAG transcripts and an up-regulation of procyclin transcripts (Jensen *et al.*, 2009; Kabani *et al.*, 2009; Nilsson *et al.*, 2010).
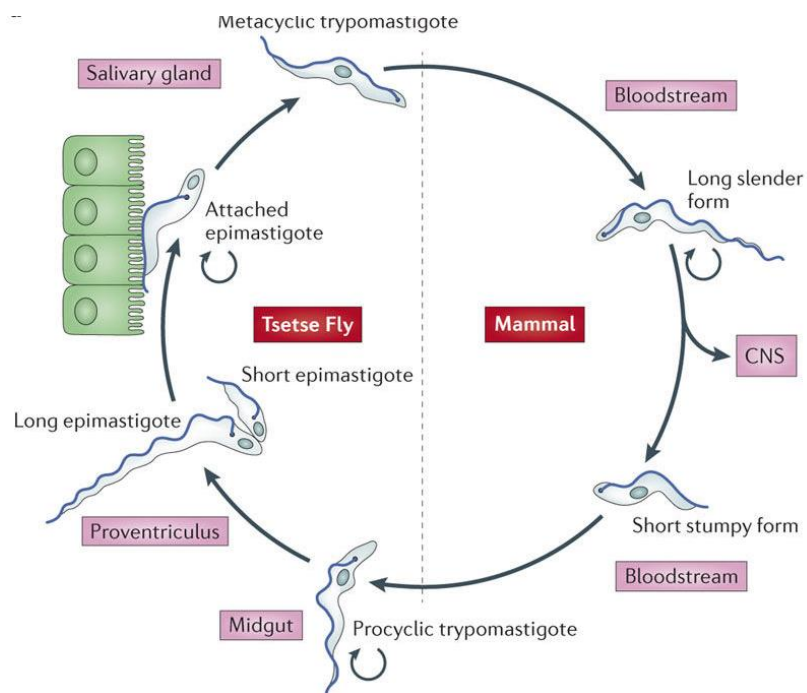
Figure 1-2. Life cycle of *T. brucei*. Simplified diagram of the life cycle of the parasite inside the fly and mammal host. Adapted from (Langousis and Hill, 2014).

1.4 *Trypanosoma brucei* architecture

T. brucei is an elongated unicellular organism with a single flagellum. The parasite contains a network of sub-pellicular microtubules that gives shape and

polarity to the cell (Matthews, 2005). The flagellum is essential for parasite survival as it facilitates motility and attachment to the salivary glands in the insect vector (Matthews, 2005; Ooi and Bastin, 2013). This structure is attached laterally along the cytoskeleton of the cell by the flagellar attachment zone (FAZ) (Ooi and Bastin, 2013). The flagellum is organised as two main structures: the axoneme and paraflagellar rod, which arise from the flagellar pocket that is linked to the basal body. The flagellar pocket is the only region in the parasite where endo- and exocytosis occurs (Matthews, 2005). The basal body consists of a 9+0 microtubule configuration (Ooi and Bastin, 2013), which is connected to the kinetoplast by the tripartite attachment complex (Matthews, 2005; Field and Carrington, 2009). The *T. brucei* cell contains a number of single copy organelles, including a nucleus, mitochondrion and Golgi apparatus, all being localised towards the posterior end of the cell (Matthews, 2005; Hammarton, 2007) (Figure 1-3). However, the parasite cell presents morphological differences depending on the life cycle. The reorganization of the kinetoplast and the basal body with respect to the nucleus is one of the main alterations that the cell undergoes during their transition from epimastigotes to trypomastigotes (Matthews, 2005). In the case of the epimastigotes, the kinetoplast and the basal body lie anterior to the nucleus. In the case of the trypomastigotes, the kinetoplast and the basal body are positioned posterior to the nucleus (Matthews, 2005; Ooi and Bastin, 2013).

1.	Nucleus	7.	Lysosome
2.	Kinetoplast	8.	Endosomes
3.	Flagellar pocket	9.	Mitochondrion
4.	Basal body and probasal body	10.	Microtubule cytoskeleton
5.	Axoneme and paraflagellar rod	11.	Glycosomes
6.	Golgi		
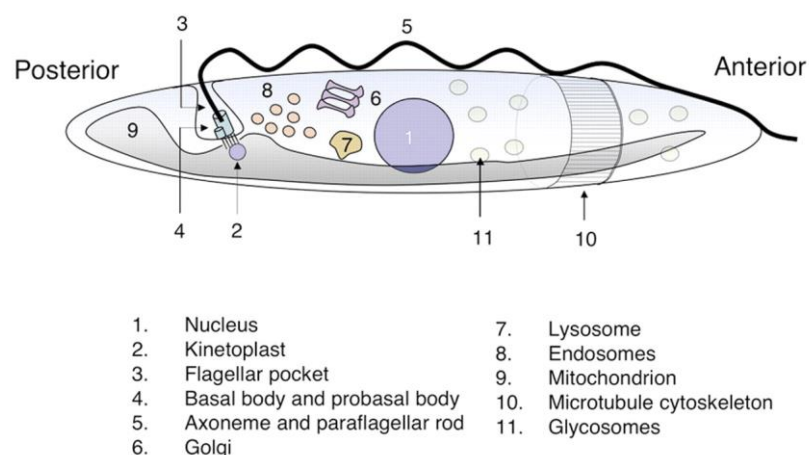
Figure 1-3. Cell architecture. Internal structure of *T. brucei*; for details refer to the legend. Adapted from (Matthews, 2005).

1.5 Cell Cycle

1.5.1 Cell cycle in eukaryotes

The cell cycle of eukaryotes consists of four stages, separated by checkpoints, which ensure the integrity of the cell (see below). The diverse checkpoints are essential for the regulation of different mechanisms such as cell growth, replication and chromosome segregation during mitosis (Barnum and O'Connell, 2014). Cyclin-dependent kinases (CDKs), which are serine/threonine protein kinases, play an important role during cell cycle progression. These protein kinases are not only involved in cell cycle regulation, but also have a critical role during transcription, autophagy and differentiation (Hisanaga and Endo, 2010; Yang *et al.*, 2010; Malumbres, 2014).

Like all kinases, CDKs structure consists of two lobes: a C-terminal lobe containing α- helix, and an N-terminal lobe containing ß-sheets. Between these structures the active site is localised (Malumbres, 2014). CDK activation is regulated by two events, the binding of a cyclin subunit and the phosphorylation by CDK-activating kinase (CAK) (Malumbres, 2014). The cyclin subunit binds to the C-terminal lobe. In the absence of the subunit, the active site is blocked by a flexible loop, also known as T-loop, impeding the binding of ATP (Malumbres, 2014). The binding of the cyclin reorders the α-helix, facilitating the phosphorylation of Thr161, localised in the active site, by CAK (Malumbres, 2014). Once the cyclin-CDK complex is activated, it has the capacity to phosphorylate several substrates, including substrates which promote new DNA synthesis and mitotic progression (Harashima, Dissmeyer and Schnittger, 2013; Barnum and O'Connell, 2014).

The activated form of CDK is regulated during the cell cycle by the interaction with cyclin-dependent kinase inhibitor proteins (Wee1 or Myt1). These proteins phosphorylate the Thr14 and Tyr15 residues in the N-terminal lobe, reducing the affinity of the cyclin-CDK complex for its substrate (Malumbres, 2014). Cdc25 phosphatase is able to reverse the inactive state by cleaving the phosphate group of the Thr14 and Tyr15 residues (Malumbres, 2014).

Cell cycle progression is regulated by the action of various cyclin-CDK complexes. In each step of the cell cycle, a different cyclin is required, leading to a continuous process of synthesis and degradation of the proteins. On the other hand, CDK synthesis remains constant during the cycle (Harashima, Dissmeyer and Schnittger, 2013). In mammalian cells there are four CDKs that are involved in cell cycle progression. The first stage of the cell cycle is gap1 (G1), in which the cell increases its size preparing for replication, ensuring the accessibility of nutrients and cell integrity (Harashima, Dissmeyer and Schnittger, 2013; Barnum and O'Connell, 2014). Once the cell is ready for replication, CDK4 or CDK6 binds with cyclin D; followed by phosphorylation by CAK. This will result in the progression to S phase (Malumbres, 2014). The retinoblastoma protein (Rb) is inactivated during this process, as a consequence of phosphorylation by CDK4 or CDK6 activated kinase. Rb is associated with the repression of genes that encode for proteins involved in DNA synthesis (Malumbres, 2014). In S phase, cyclin E binds to CDK2; the activation of this complex promotes replication during S-phase. During this process there is the presence of two checkpoints, which are activated in the case of DNA damage. The checkpoints are regulated by the Chk1 (G1/S) and Chk2 (G2/M) kinases, and by ATM and ATR (serine/threonine kinases) (Harashima, Dissmeyer and Schnittger, 2013; Barnum and O'Connell, 2014). ATM and ATR are activated by DNA damage, phosphorylating ChK1 and Chk2, which subsequently phosphorylate Cdc25, impeding the activation of the cyclin-CDK complex (Harashima, Dissmeyer and Schnittger, 2013; Barnum and O'Connell, 2014).

The transition to mitosis is regulated by the binding of cyclin A and B to CDK1. The cyclin-CDK complex is essential during this stage, promoting mitotic entry, chromosome condensation and spindle maturation and migration (Malumbres, 2014). The transition from metaphase to anaphase is regulated by the Anaphase promoting complex or Cyclosome (AP/C) (Manchado, Eguren and Malumbres, 2010; Barnum and O'Connell, 2014), which is an E3 ligase that consists of approximately 12 subunits and is regulated by the cofactors Cdc20 (cell division cycle 20) and Cdh1. When sister chromatids and kinetochores are properly attached to the poles of the mitotic spindle, the cyclin A- or B-CDK1 complex phosphorylates AP/C, promoting the binding with Cdc20 (Manchado, Eguren and Malumbres, 2010; Barnum and O'Connell, 2014). AP/C[Cdc20] degrades

securin and cyclin A and B, promoting the release of separase (cysteine protease), whose role is to cleave the kleisin protein of the cohesin complex (Figure 1-4)(Manchado, Eguren and Malumbres, 2010). The cohesin complex is a multiple subunit complex, composed of proteins that are members of the Structural Maintenance of Chromosomes (SMC) family (SMC1, SMC3), a α-kleisin protein (Scc1), and Scc3 (Peters, Tedeschi and Schmitz, 2008). Scc1's N-terminal domain binds to SMC3 and the C-terminus binds with SMC1, forming a ring structure, which is followed by the binding of Scc3 with Scc1 (Figure 1-4)(Peters, Tedeschi and Schmitz, 2008). In the case of unattached kinetochores, the mitotic checkpoint proteins, known as Bub1R (serine/threonine kinase) in mammals and Bub1 in yeast, inhibit the action of Cdc20, impeding the activation of the AP/C complex (Barnum and O'Connell, 2014). Cdh1 is also involved in the regulation of AP/C complex activity. The association of AP/C^{Cdh1} promotes mitotic exit by degrading cyclins A and B and other molecules, such as Aurora kinase and Plk1, which are involved in the removal of bulky cohesin during prophase (Peters, Tedeschi and Schmitz, 2008; Barnum and O'Connell, 2014).
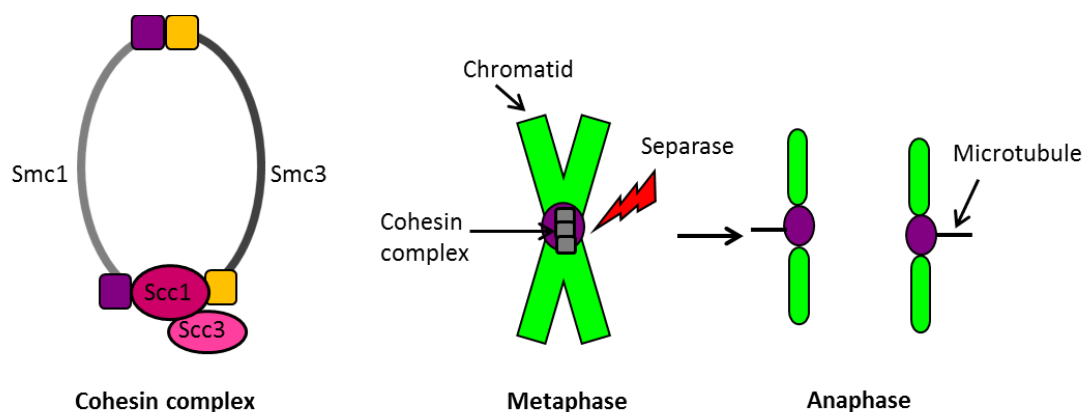
Figure 1-4. Diagram representing the cohesin complex and metaphase-anaphase transition. Cohesin subunit Smc1 is in light grey and purple, Smc3 in dark grey and yellow, Scc1 and Scc3 in pink. Representation of the cleavage of the cohesion complex, inducing the transition from metaphase to anaphase.

1.5.1.1 Mitosis

Mitosis is an important process during cell division, permitting equal distribution of genomic material into two daughter cells. In eukaryotes there two types of mitosis: 'open' and 'closed'. The first is characterised by the

breakdown of the nuclear membrane before chromosome segregation, and in the latter the nuclear envelope remains intact during chromosome distribution (Boettcher and Barral, 2012). Plants and animals are known to have an 'open' mitosis, while the members of the Excavata subgroup, which includes trypanosomes, are characterised by having a 'closed' mitosis. Interestingly, organisms such as fungi and amoeboid protists may go through 'closed' to 'semi-open' and 'open' mitosis (Boettcher and Barral, 2012).

Mitosis is subdivided into four stages: prophase, metaphase, anaphase and telophase (Figure 1-5). During each stage, the cell undergoes diverse changes. In a typical prophase, chromatin condensation occurs by formation of distinct visible chromosomes. This event is driven by the condensin complex, which consist of two SMC proteins and three non-SMC proteins. This complex forms a ring, encircling two strands of DNA (Mitchison and Salmon, 2001; Antonin and Neumann, 2016). The sister chromatids are joined by the centromere, the microtubule spindle is connected to the centromere via the kinetochore, and with the poles of the cell by the centrosome structure (Mitchison and Salmon, 2001). Another main change during prophase is the disappearance of the nuclear membrane (Mitchison and Salmon, 2001), though, as mentioned above, not all eukaryotes undergo this event (Boettcher and Barral, 2012). In the case of 'closed' mitosis, the chromosomes tend to localise close to the nuclear membrane (Ebrahimi and Cooper, 2012).

In metaphase, the chromosomes line up along the centre of the nucleus, which is a consequence of the opposing forces generated by the microtubules (Mitchison and Salmon, 2001). On the other hand, during anaphase there is the separation of the sister chromatids, which start to migrate to the poles of the cell (Barnum and O'Connell, 2014). The transition between metaphase-anaphase is regulated by the AP/C complex, as described above.

During the final stage of the cell cycle, termed telophase, the spindles disappear, there is a redistribution of the chromosomes and the formation of a new nuclear membrane (Salic and Mitchison, 2008). Mitosis is then followed by cytokinesis, which completes cell division by cytoplasm separation, normally

resulting in two identical daughter cells (Harashima, Dissmeyer and Schnittger, 2013).
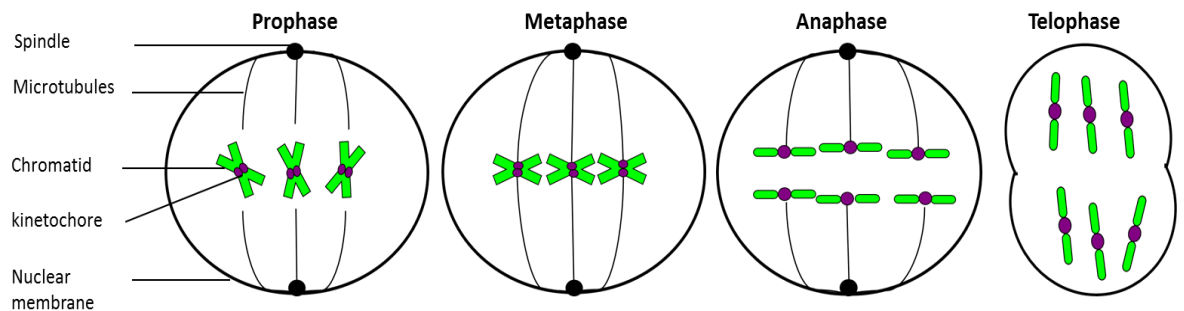
Figure 1-5. Stages of mitosis. Diagram describing the different stages of mitosis. Prophase shows the condensation of the chromatin by the formation of distinct visible chromosomes. In metaphase the chromosomes align to the centre of the nucleus, while in anaphase the sister chromatids are separated and start migration to opposite poles. The last stage is telophase in which there is a reorganisation of the chromosomes.

1.5.2 Cell cycle in *Trypanosoma brucei*

The parasite *T. brucei* follows the typical route of the eukaryotic cell cycle, but with certain peculiarities. A prominent variation relative to a canonical eukaryote is the lack of chromatin condensation or dissolution of the nuclear membrane during mitosis, though these are also observed in other eukaryotes. As it was previously mentioned the organisms belonging to the Excavata subgroup are characterised by having a 'closed' mitosis, maintaining the nucleus envelope (Boettcher and Barral, 2012). On the other hand, the lack of chromatin condensation is not unique for *T. brucei* (Belli, 2000; Hammarton, 2007), with the absence of chromatin compaction also detected in *T. cruzi* and *Leishmania* (Belli, 2000).

The cell cycle progression in *T. brucei,* as in other eukaryotes, is regulated by cyclin-kinase complexes. In the parasite, 11 cyclin related kinases (CRK1-4, CRK6-12) and ten cyclins (CYC2-11) have been identified. Of these the roles of just two kinases and two cyclins have been elucidated (Monnerat *et al.*, 2013). Depletion of CRK1 and CRK3 by RNAi has shown these proteins to have an important role during G1/S and G2/M progression (Tu and Wang, 2004). On the

other hand, depletion of cyclin CYC2 by RNAi results in the accumulation of cells in G1/S phase in procyclic forms (Li and Wang, 2003; Hammarton, Engstler and Mottram, 2004), and the depletion of CYC6 blocks mitosis in procyclic and in bloodstream forms (Hammarton *et al.*, 2003). *In vivo* analysis have confirmed the interaction of CRK3 with CYC2 and CYC6 in *T. brucei* and their role in the regulation of G1/S and G2/M transition (Van Hellemond *et al.*, 2000; Hammarton *et al.*, 2003; Monnerat *et al.*, 2013), though it is still uncertain with which cyclins CRK1 is interacting in the parasite. It is known that in yeast CRK1 interacts with cyclins CYC2, CYC4 and CYC5, but whether this is conserved in *T. brucei* remains to be tested (Monnerat *et al.*, 2013). A role for the CYC9-CRK12 complex has also been demonstrated in bloodstream cell proliferation, though in procyclic forms the depletion of the cyclin-kinase complex does not affect the cell cycle (Monnerat *et al.*, 2013).

As mentioned above (section 1.4), the parasite has single copy organelles and structures, which must be correctly replicated. Such replication includes the unusual genome composition of both the nucleus (which has many more chromosomes than most eukaryotes) and the mitochondrion (the unusual kinetoplast network)(Hammarton, 2007). For this reason, replication and segregation of the organelles maintain a specific order during the different phases of the cycle, assuring a viable progeny (Hammarton, 2007).

During the G1 phase, duplication of the basal body and elongation of the new flagellum can be observed (Hammarton, 2007). It has been shown that polo-like kinase (PLK) plays an important role during basal body duplication (Hammarton, 2007). PLK is a serine-threonine kinase that has been shown to have an important role in the context of cell progression in all eukaryotes (Harashima, Dissmeyer and Schnittger, 2013; Barnum and O'Connell, 2014). The depletion of PLK in procyclic *T. brucei* cells by RNAi results in cells with two nuclei but one kinetoplast, one basal body and one flagellum (reviewed by Hammarton 2007). The elongation of the new flagellum is followed by duplication of the Golgi apparatus, but the signals that initiate duplication are still uncertain (Hammarton, 2007). The Golgi apparatus is positioned alongside the basal body and kinetoplast, and Vps34 kinase is involved during this process (Hall *et al.*, 2006; Hammarton, 2007).

The replication of the kinetoplast and nuclear DNA occurs during S phase, though completion of kinetoplast replication and division occurs prior to completion of nuclear DNA replication (Hammarton, 2007; Li, 2012). It has been shown that the nucleus and the kinetoplast possess their own, distinct replication machinery (Hammarton, 2007). In the case of the nucleus, replication initiation is regulated by a divergent origin recognition complex (ORC), containing at least two proteins related to other eukaryotic ORC subunits, TbORC1/CDC6 and TbORC4, as well as further more diverged factors (De Melo Godoy *et al.*, 2009; Tiengwe *et al.*, 2012; Marques *et al.*, 2016). How ORC activity is regulated is unclear, since no protein kinases that act on TbORC have been described. Indeed, the recruitment of one ORC-like protein, TbORC1B, to the nucleus only occurs during S phase, which may suggest very unusual regulation, since conventionally ORC is thought to be loaded to replication initiation sites during G1 phase (Dang and Li, 2011; Marques *et al.*, 2016). It was suggested that kDNA replication is regulated by the abundance of TbPIF2, though the detailed regulation processes in this organelle are still uncertain (Li, 2012), at least in part because the kinetoplast recruits many novel replication or repair factors, including DNA polymerases, DNA ligases and further DNA helicases that appear either to have no counterparts in the nucleus or are exclusively found in the kinetoplast (Engel and Ray, 1999; Grams *et al.*, 2002; Downey *et al.*, 2005; Onn *et al.*, 2006; David F Bruhn, Sammartino and Klingbeil, 2011).

During the G2 phase, another checkpoint is present to ensure the integrity of the cell prior to mitosis. The transition from G2 to mitosis is regulated by the kinase CRK3 and the cyclin CYC6 (Hammarton *et al.*, 2003). Mitosis in *T. brucei* is a complex process due to the number of chromosomes (~200) that are redistributed within the nucleus (Hammarton, 2007). Minichromosome and megabase chromosome segregation occur by different mechanisms: the 11 diploid megabase chromosomes are segregated by a kinetochore-centromere dependent mechanism (Gull, Alsford and Ersfeld, 1998; Akiyoshi and Gull, 2014; D'Archivio and Wickstead, 2017), whereas the ~100 minichromosomes are segregated before the megabase chromosomes along pole-to-pole microtubules (Gull, Alsford and Ersfeld, 1998; Echeverry *et al.*, 2012; Li, 2012). As shown in other eukaryotes, the transition from metaphase to anaphase is regulated by the APC/C complex. Tandem affinity purification and mass spectrometry analysis

was used to identify 10 subunits of *T. brucei* APC/C complex, including APC1, APC2, APC10/DOC1, APC11, CDC16, CDC23, CDC27, AP2, AP3 and APC4 (Kumar and Wang, 2005; Bessat *et al.*, 2013). Although the general structure of AP/C is closely related to that observed in the rest of eukaryotes, it was possible to detect certain peculiarities, such as the absence of a securin homologue in the parasite, the lack of interaction between CDC20 and APC/C, as well as the lack of association of APC/C with mitotic checkpoint proteins (Bessat *et al.*, 2013). Taken together, these data may suggest that *T. brucei* APC/C regulation differs from the rest of the eukaryotes (Bessat *et al.*, 2013). The depletion of the subunits APC1, APC2 and CDC27 in procyclic cells results in an arrest in metaphase, suggesting that, despite the differences, *T. brucei* APC/C complex is involved in metaphase-anaphase transition (Kumar and Wang, 2005; Li, 2012; Bessat *et al.*, 2013)

The culmination of mitosis gives rise to cytokinesis, which occurs along the longitudinal axis of the cell (Zhou *et al.*, 2016). A furrow forms initially in the anterior end of the new flagellum, and ingression of the furrow divides the cellular organelles and structures equally between progeny, resulting in two viable cells (Hammarton, 2007; Zhou *et al.*, 2016). Cytokinesis in *T. brucei* is regulated by three proteins, CIF1 (Cytokinesis Initiation Factor1), which is also called TOEFAZ1 (Tip Of The Extending FAZ 1), Aurora B kinase (TbAuK) and Polo-like kinase (TbPLK). CIF1 works like a substrate for both kinases (Zhou *et al.*, 2016). Although TbAuK and TbPLK have an important role during this process, these two proteins never interact during the cell cycle (Zhou *et al.*, 2016). In S phase, TbPLK phosphorylates and recruits CIF1 to the tip of the new FAZ. TbAUK concentrates to the kinetochore and central spindle during G2 and early anaphase, while TbPLK and CIF1 remain in the FAZ tip. During late anaphase, CIF1 recruits TbAUK to the new FAZ tip, while TbPLK diffuses into the cytoplasm (Li *et al.*, 2010; Zhou *et al.*, 2016). The recruitment of TbAUK initiates a cascade of signals that result in the formation of the initial cleavage furrow (actomyosin contractile ring) (Minoshima *et al.*, 2003; Li, Umeyama and Wang, 2009). Interestingly, depletion of CIF1 results in a 'back-up' cytokinesis, where the furrow ingression is originated in the posterior region (Sinclair-Davis, 2013; Zhou and Li, 2016).

1.6 Variant Surface Glycoprotein Coat and Immune evasion

Certain microorganisms, including species of viruses, bacteria, fungi and protozoa, have evolved a strategy to avoid the host immune system by changing their surface molecules; this strategy is collectively known as antigenic variation (Deitsch, Lukehart and Stringer, 2009; Duraisingh and Horn, 2016; Palmer, Bankhead and Seifert, 2016). During the infection process, the host generates idiotypic antibodies to eliminate the pathogen and the pathogen changes the surface coat to temporarily avoid being recognized. Therefore, there is a constant coevolution between the host and infectious organism in which the most competent will survive (Barry, Hall and Plenderleith, 2012; Sironi *et al.*, 2015). Though the strategy of antigenic variation is a common route for surviving the host immune attack, the underlying molecular mechanisms and machinery in the different organisms are highly variable, suggesting independent evolutionary events. African trypanosomes are remarkable in that they utilise two commonly observed mechanisms for antigenic variation (transcription-based and recombination-based antigen switching), whereas most other organisms employ a single strategy (McCulloch, 2004; Horn, 2014; Duraisingh and Horn, 2016).

In the mammalian bloodstream, each *T. brucei* cell is covered with approximately five million dimers of one type of variant surface glycoprotein (VSG), which is thought to form a protective coat that shields invariant surface antigens from immune recognition (Pays, Vanhamme and Pérez-Morga, 2004; Smith *et al.*, 2009; Stijlemans *et al.*, 2016; Bartossek *et al.*, 2017), though this view has been challenged due to the discovery of an invariant surface glycoprotein that may project beyond the VSG coat (Overath *et al.*, 1994; Schwede and Carrington, 2010). A VSG monomer is composed of a C-terminal domain and an N-terminal domain, with the C-terminus arranged towards the cell surface, where it is anchored by GPI, and the N-terminal domain predominantly exposed to the host immune system (Hall, Wang and Barry, 2013). During an infection, the parasites have the capacity to express different VSG coats; as the host immune system recognizes the currently expressed surface VSG and eliminates the infecting parasites, a population of cells that have switched to express a new VSG variant coat allow part of the infectious

population to survive, proliferate and continue the infection (Jackson *et al.,* 2012). The success of this strategy appears to rely on a number of features, in common with antigenic variation in all organisms that use this strategy. First, trypanosomes have an 'archive' of new surface antigen genes, ready to be expressed (Jackson *et al.,* 2012). Second, trypanosomes ensure that only a single VSG coat is expressed in a single cell at one time, a control termed monoallelic expression. Third, trypanosomes have mechanisms to execute a switch in the expressed VSG (Hovel-Miner *et al.,* 2015).

1.6.1 Organization of VSG genes

T. brucei has >1000 silent VSG genes, which are distributed among the chromosome subtelomeres of all types of chromosome in the genome (Berriman *et al.,* 2005), including the 11 large, diploid megabase chromosome (MBC) and specialised, aneuploid intermediate and minichromosomes, which seem to have evolved to provide a reservoir of new VSGs (Barry *et al.,* 2003; Morrison, Marcello and McCulloch, 2009). The vast majority of the VSG archive is found in silent, subtelomeric arrays in the megabase chromosomes (Marcello and Barry, 2007), and variations in these parts of the chromosome appear to underlie the observed flexibility in the chromosome (and perhaps genome) size amongst strains of *T. brucei* (Callejas *et al.,* 2006). However, most of the silent VSG archive is not composed of intact VSGs, with ~85% found to be either pseudogenes or gene fragments (Berriman *et al.,* 2005). The requirement that only a single VSG gene is expressed in one cell at any given time is achieved by VSG expression in the mammal being limited to specialised bloodstream form expression sites (BES) that are located in the telomeres of the MBCs and some intermediate chromosomes. BES consist of a defined structural organisation (Figure 1-6) (Vanhamme *et al.,* 2001). During transcription, the active VSG-ES promoter recruits RNA Polymerase I within a putative subnuclear structure known as the expression-site body (ESB) (López-Farfán *et al.,* 2014; Glover *et al.,* 2016). In this site, a single VSG gene, in combination with expression site associated genes (ESAGs), is transcribed (Günzl *et al.,* 2015). This contrasts with metacyclic forms, where one VSG gene is transcribed in a metacyclic expression site that does not encode ESAGs (Ginger *et al.,* 2002).
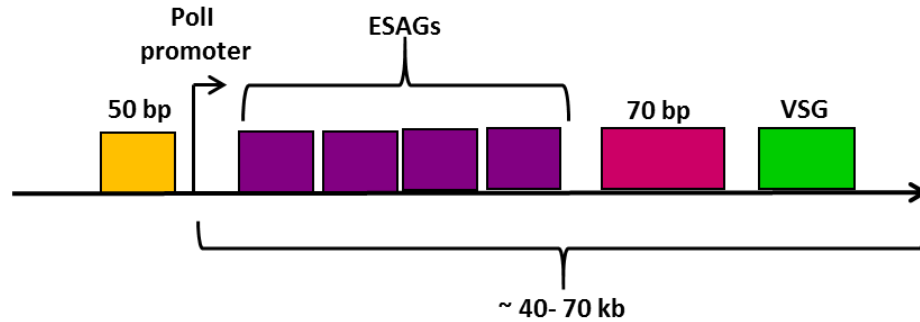
Figure 1-6. Schematic representation of BES architecture. 50 bp repeats (yellow), whose function is unknown, is localised upstream of the promoter (black arrow). Downstream of the promotor are localised multiple ESAG genes (purple), the 70 bp repeat sequence (pink) and the VSG (green), which is located proximal to the telomere. Not to scale.

1.6.2 Monoallelic expression

Surprisingly, approximately 20-40 ES have been estimated in the *T. brucei* genome, and 15 have been documented and sequenced in the strain Lister 427 (Chapter5, Figure 5-17) (Borst and Ulbert, 2001; Hertz-Fowler *et al.*, 2008; Landeira *et al.*, 2009). However, only one BES is active at a time, ensuring singular VSG expression, though the details of how such 'monoallelic expression' is achieved are still being determined (Nguyen *et al.*, 2014). Chromatin structure is an important factor in the regulation of monoallelic expression. Studies have demonstrated that the active BES contains a reduced number of nucleosomes relative to the silent BES, suggesting that this event may be regulating Pol I transcription and monoallelic expression (Figueiredo and Cross, 2010; Hovel-Miner *et al.*, 2015). Moreover, histone deposition proteins are also associated with BES promoter silencing. Depletion of these proteins (FACT, NLP, Asf1A or Caf-19), results in an increase in transcription of silenced BES (Narayanan *et al.*, 2011; Alsford and Horn, 2012). Another factor involved is the histone modifier DOT1B, depletion of this factor delays the active to silent transition, resulting in parasites expressing two VSGs for a prolonged time period (Figueiredo, Janzen and Cross, 2008). Recent studies have shown a novel factor, VEX1, as a positive and negative regulator of BES that appears to co-localise with the ESB (Glover *et al.*, 2016). The origin recognition complex, or at least ORC1/CDC6, has also been associated with the maintenance of monoallelic expression (Benmerzouga *et al.*, 2013).

1.6.3 VSG switching

T. brucei has two switching strategies: transcriptional switching, and recombination. In the first strategy, often called in situ switching, an activated BES is silenced and a silent BES is activated. This mechanism may predominantly occur during the early infection stage, since only the VSG genes that are already located in the BES can participate in this switching process (Figure 1-7 A) (McCulloch and Barry, 1999; Vanhamme *et al.*, 2001; Taylor and Rudenko, 2006). Recombination is the more common switching mechanism, allowing the parasite to move a silent VSG into a BES and thereby become expressed. A number of mechanisms have been described that account for VSG recombination switching. The most common is a gene conversion mechanism, sometimes called duplicative transposition (Figure 1-7 B), where the VSG gene that is located in the active BES is deleted and replaced by a copy of a silent gene. Gene conversion can use functionally intact silent VSGs, which are able to be translated and form a VSG coat(Horn, 2014). Alternatively, the VSG pseudogenes and fragments can be recombined by segmental gene conversion reactions, using multiple silent genes to form novel VSG 'mosaics'(Figure 1-7 C)(Marcello and Barry, 2007; Hall, Wang and Barry, 2013). A final form of recombination is termed reciprocal recombination (Figure 1-7 D), where there is a telomere exchange, moving a silent gene into the active BES and the transcribed VSG gene to the silent telomere (Horn, 2014). It is suggested that recombination-based VSG switching takes advantage of the parasite's homologous recombination (HR) pathway, which is a general strategy for repair of genome damage or replication stalling (McCulloch and Barry, 1999; Vanhamme *et al.*, 2001). Whether or not parasite-specific factors or processes direct such recombination events during VSG switching, and whether mosaic VSG formation also uses HR, is largely unclear. For instance, it has been suggested that DNA breaks within the BES initiate recombination, but how these form and whether they are sequence-specific remains undetermined (Boothroyd *et al.*, 2009; Glover *et al.*, 2013). Recent studies have alternatively suggested that replicative lesions may trigger VSG switching in the parasite (Devlin *et al.*, 2016). VSG switching is essential for the survival of the parasite, allowing it to change its coat and avoid the host immune system, and indeed some further work suggests that expression of the VSG itself is essential, since RNAi ablation of VSG is lethal *in vitro* (Sheader *et al.*, 2005).

The switching rate of laboratory-adapted lines is 10^{-6} cells per generation, but it can occur at much higher rates (10^{-2}-10^{-5}) if the cells have been recently recovered from field isolates (Vanhamme *et al.*, 2001). Switching is not induced by antibodies, and is largely stochastic, though some order of VSG expression is seen during infections (Morrison *et al.*, 2005), and it may have an important functional relationship with long slender to short-stumpy form differentiation (Batram *et al.*, 2014).
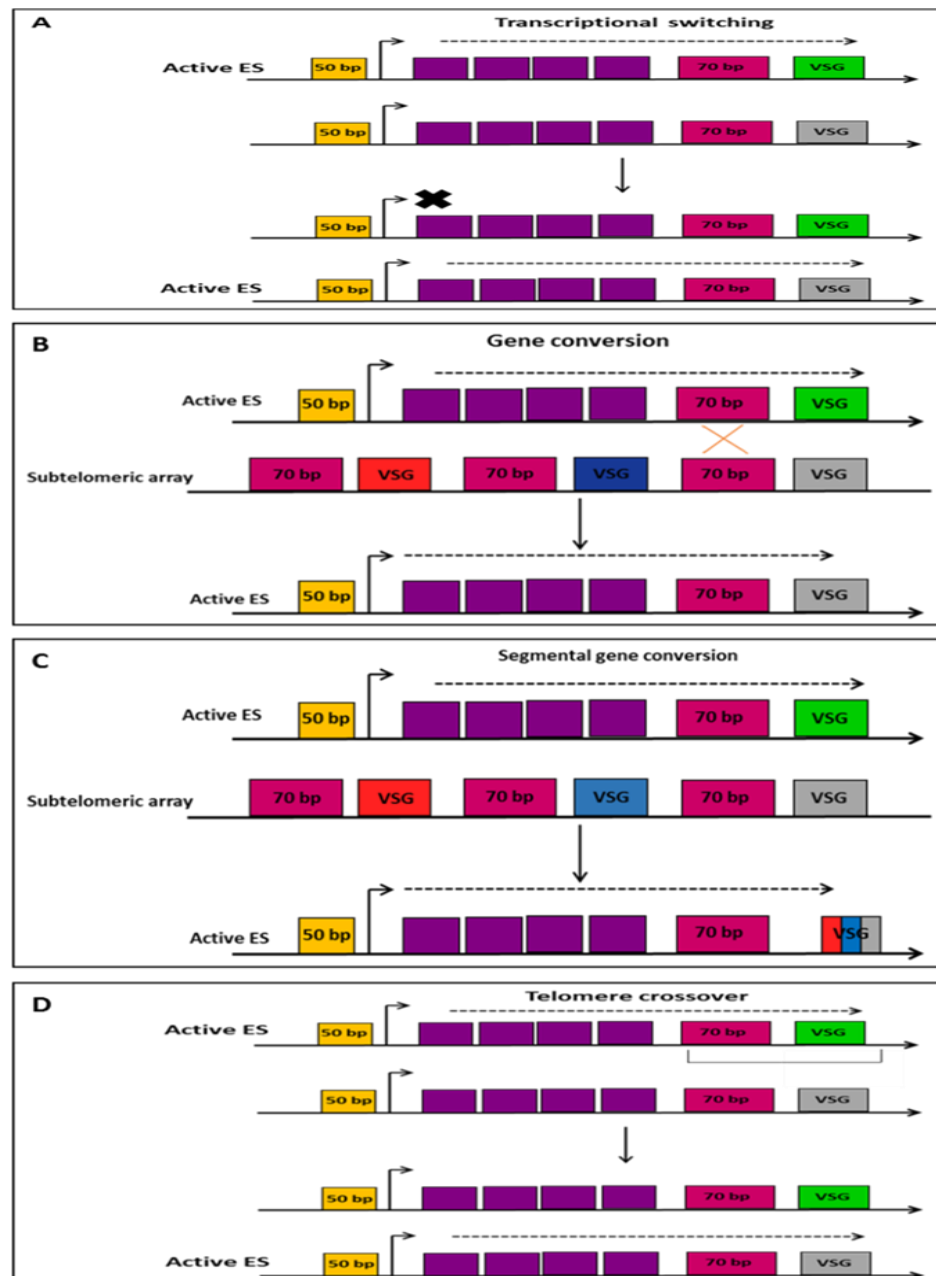
Figure 1-7. VSG switching strategies. A. In the transcriptional switching, the telomere of the 'active' BES (green) is exchanged for a 'silent' VSG (grey). **B.** A silent VSG is duplicated to the active 'BES' replacing the active VSG. **C.** A new VSG is generated by segments of other VSG genes, resulting from a segmental

gene conversion. **D.** Telomere exchange, result in the replacement of the active VSG by another telomeric VSG.

1.7 DNA Polymerases

DNA Polymerases (Pols) play important roles in all organisms, both during genome replication and repair. These enzymes are divided into four families based on sequence homology: A, B, X and Y (Table 1-1). Despite the differences between members of these diverse families, the catalytic reaction is conserved, with few exceptions. DNA Pols have the capacity to add nucleotides in order to synthesise a DNA strand. For DNA synthesis, the polymerases normally require a single-stranded DNA template and a primer (a short DNA or RNA molecule), which anneals to the template and provides a 3'-OH group that is the starting point for new synthesis (Cotterill & Kearsey, 2002; Rothwell & Waksman, 2005). Apart from these elements, the Pols require four deoxyribonucleotide triphosphates (dATP, dTTP, dGTP and dCTP) that are incorporated into the new strand, following Watson and Crick pairing rules (A•T and G•C), in a 5'-3'direction (Cotterill & Kearsey, 2002). Mg^{2+} ions have an important function in this process, facilitating the bond between the 3'-OH group of the primer and the α-phosphate of the dNTP (Cotterill and Kearsey, 2002). In the case of repair DNA Pols, they have the capacity to extend the sequence using mismatched primers, and new synthesis does not necessarily follow the Watson and Crick pairing rules (Cotterill and Kearsey, 2002).

Family	Polymerase	Proposed role
A	γ (gamma)	Base excision repair, Non-homologous end joining, mitochondrial replication
A	θ (theta)	Homologous recombination, translesion synthesis
A	ν (nu)	Homologous recombination, translesion synthesis
B	α (alpha)	Primase
B	ε (epsilon)	Replication
B	δ (delta)	Replication, repair of double strand breaks
B	ζ (zeta)	Translesion synthesis
X	Β (beta)	Base excision repair
X	λ (lambda)	Non-homologous end joining, Base excision repair
X	μ (mu)	Non-homologous end joining
X	σ (sigma)	Sister chromatin cohesion
Y	ι (iota)	Translesion synthesis
Y	Κ (kappa)	Translesion synthesis
Y	η (eta)	Translesion synthesis
Y	REV1	Translesion synthesis

Table 1-1.Eukaryotic DNA polymerases. Members of the A, B, X and Y family of polymerases and their proposed role in the cell. Table based on (Cotterill and Kearsey, 2002).

1.7.1 Polymerase families

1.7.1.1 A family

A family of DNA Polymerases (Pols) are involved in replication and repair processes and are known for their high fidelity due to their 3'-5' exonuclease activity, which allows the excision of incorrectly inserted nucleotides. In bacteria, polymerase I (Pol I) is a member of the A family and was the first DNA Pol ever described (Bebenek and Kunkel, 2004; Johansson and Dixon, 2013), with a total of five bacterial DNA Pols subsequently described (I, II, III, IV and V) (Bebenek and Kunkel, 2004). Bacterial DNA PolI is involved in repair and the maturation of Okazaki fragments during DNA replication (Rothwell and Waksman, 2005; Garcia-Diaz and Bebenek, 2007). In eukaryotes, the A family is composed of DNA polymerases gamma (Pol ɣ), theta (Pol θ) and nu (Pol N), with Pol ɣ being associated with mitochondrial replication, base excision repair (BER) and non-homologous end joining (NHEJ) (Bebenek and Kunkel, 2004; Garcia-Diaz and Bebenek, 2007). On the other hand, Pol θ and Pol N are characterised by the absence of the 3'-5' proofreading activity, suggesting roles in translesion DNA synthesis (TLS) (Garcia-Diaz and Bebenek, 2007)(discussed below).

1.7.1.2 B family

In eukaryotes, the B family is formed by polymerase alpha (Pol α), polymerase delta (Pol δ), polymerase epsilon (Pol ε) and polymerase zeta (PolZ). Pol δ and Pol ε are high fidelity polymerases with the ability to excise incorrectly inserted nucleotides due to their 3'-5' proofreading activity (Rothwell and Waksman, 2005). Polδ and Polε are directly involved in the synthesis of the leading and lagging strands during DNA replication (Shcherbakova, Bebenek and Kunkel, 2003; Bebenek and Kunkel, 2004). Polymerase α and polymerase zeta (PolZ) lack proofreading activity. The former is involved in the initiation of DNA synthesis due to its ability to elongate RNA primers at replication origins and in the lagging DNA strand (Bebenek and Kunkel, 2004; Garcia-Diaz and Bebenek, 2007). The latter is suggested to be involved in translesion synthesis (Goodman, 2002; Garcia-Diaz and Bebenek, 2007). *E*. coli Pol II is also a member of the B family of polymerases, harbouring a 3'-5' proofreading activity, associated with replication restart and TLS (Bebenek and Kunkel, 2004).

1.7.1.3 X family

The members of the X family, which includes polymerase beta (Pol ß), polymerase sigma (Pol σ), polymerase mu (Pol μ) and polymerase lambda (Pol λ), operate in the context of DNA repair (Rothwell and Waksman, 2005; Garcia-Diaz and Bebenek, 2007). Pol ß is known to participate in the nuclear base excision repair pathway (Garcia-Diaz and Bebenek, 2007)(see below). In *T. brucei,* Polß and Polß-PAK are localised to the mitochondrion, showing nonredundant roles. Polß has an active role during the maturation of the Okazaki fragments and Polß-PAK is associated with gap filling during the final stage of minicircle replication (Saxowsky *et al.*, 2003; David F Bruhn, Sammartino and Klingbeil, 2011). Studies in *T. cruzi* have demonstrated a potential role of Polß in BER of oxidative damage, since the overexpression of Tc Polß increased the survival rate of epimastigotes in the presence of H_2O_2 (Schamber-Reis *et al.*, 2012). This contrasts with *L. infantum,* where Pol ß has a nuclear localisation, like higher eukaryotes, thus suggesting an important role for Pol ß in nuclear BER (Alonso *et al.*, 2006). Pol μ and Pol λ participate in non-homologous end-joining, and Pol λ has also been implicated in BER (Bebenek and Kunkel, 2004; Garcia-Diaz and Bebenek, 2007). Finally, studies in *S. cerevisiae* indicate Pol σ has a role in sister chromatid cohesion, assuring equal chromosomal segregation (Edwards *et al.*, 2003a).

1.7.1.4 Y family

All members of the Y family are known as translesion polymerases (TLS pol), though the same activity is found in a few members of the A (Polv, Polθ) and B (PolZ) families (Garcia-Diaz and Bebenek, 2007). These polymerases have an important role in the survival of the cell, permitting the cell to tolerate damage during replication. Even though the replicative machinery is known to be highly efficient, this process can be interrupted by unresolved lesions, resulting in replication fork stalling (Sale, Lehmann and Woodgate, 2012). TLS Pols are involved in the bypass of unrepaired lesions by replacing the replicative polymerases and extending through the damage (Garcia-Diaz and Bebenek, 2007; Sale, Lehmann and Woodgate, 2012; Vaisman and Woodgate, 2017). During this process, they are prone to insert mutations due to their lack of 3'-5' proofreading activity (Garcia-Diaz & Bebenek, 2007; Sale et al., 2012; Vaisman &

Woodgate, 2017). The average rate of mutation is between 10^{-2}-10^{-4} errors per base replicated (Rothwell and Waksman, 2005), of which some mutations will be lethal for the cell (Sale, Lehmann and Woodgate, 2012). In humans, seven polymerases are suggested to have TLS activity: PolZ, Polν, Polθ, Polι, Polη, PolΚ and Rev1 . On the other hand, *S. cerevisiae* only harbour three TLS Pols, PolZ, Polη and Rev1. These polymerases are not restricted to eukaryotes (Bebenek and Kunkel, 2004). *E. coli* contains three TLS pols: two Y family members (Pol IV (DinB) and Pol V (UmuD$_2$C)), and one B family member (Pol II), which are known to be involved in the SOS repair pathway (Goodman, 2002; Bebenek and Kunkel, 2004).

1.7.2 Polymerase Structure

The general structure of DNA polymerases is highly conserved among the different families, though with certain variations. The overall structure resembles a right hand, containing palm, finger and thumb subdomains (Figure 1-8). The palm domain harbours the catalytic carboxylate-metal ion complex, whereas the finger and the thumb grasp the template and the primer, creating an active site (Rothwell and Waksman, 2005). In the case of the Y family DNA pols, the finger and thumb are smaller, thus facilitating the binding of DNA lesions (Chun and Jin, 2010). In addition, Y family DNA pols have an extra structure called the little finger, wrist or polymerase-associated domain (Figure 1-8); this domain may be involved in the substrate specificity of these Pols (Garcia-Diaz and Bebenek, 2007; Sale, Lehmann and Woodgate, 2012).
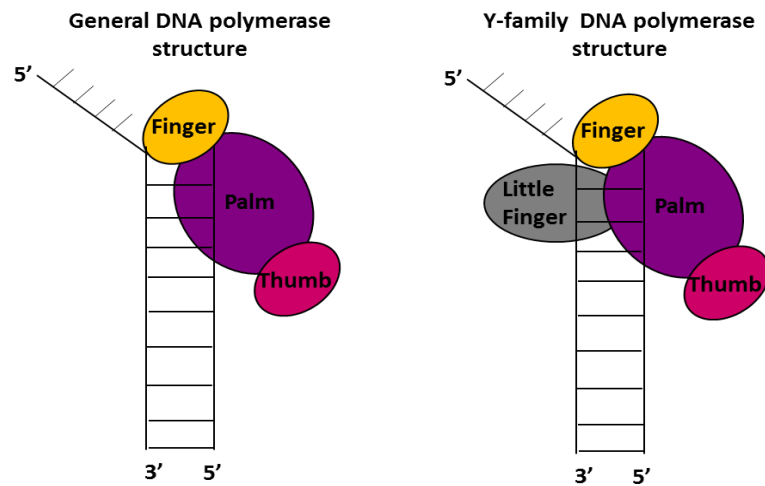
Figure 1-8. Structural similarities of DNA polymerases. Comparison between the general DNA polymerase structure and the structure of Y- family polymerases. Diagram showing the different subdomains: palm (purple), thumb (pink), finger (yellow) and little finger (grey), in the particular case of the Y-family polymerases.

1.8 Damage repair pathways

DNA damage originates from many sources such as UV or gamma radiation, chemical agents and reactive oxygen species, some generated within the cell (Waters *et al*. 2009). Several mechanisms to repair these lesions have been described and are conserved across all domains of cellular life: nucleotide excision repair, base excision repair, mismatch repair, homologous recombination, non-homologous end joining and microhomology-mediated end joining (Figure 1-9)(García-Díaz and Bebenek, 2007; Waters *et al*. 2009). Despite the abundance and diversity of these repair mechanisms, a tolerance pathway is also needed under circumstances where the lesion cannot be eliminated, thereby preventing the collapse of cell integrity and function (L S Waters *et al*., 2009).
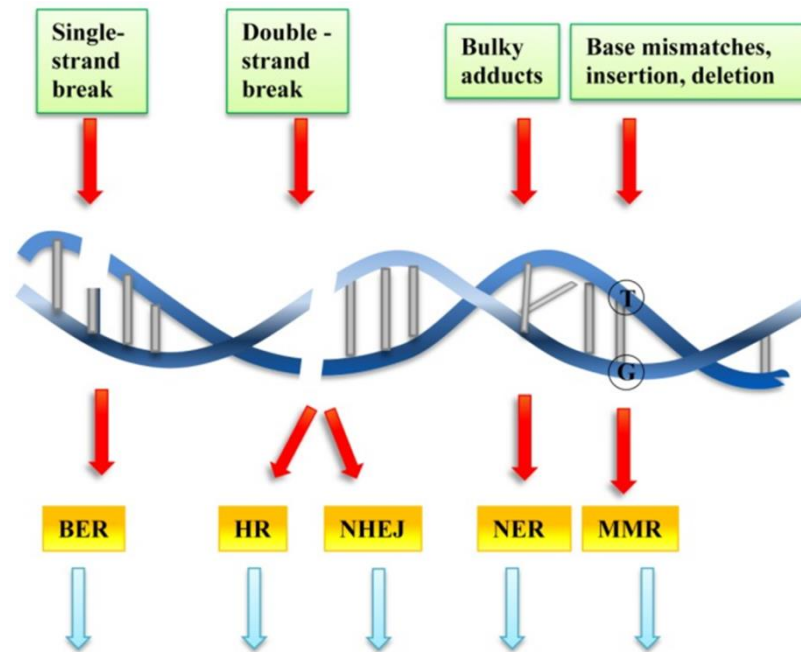
Figure 1-9. DNA damage and possible DNA repair pathways. Figure shows mechanisms of DNA repair such as base excision repair (BER), homologous recombination (HR), non-homologous end joining (NHEJ), nucleotide excision repair (NER) and mismatch repair (MMR). Figure adapted from (Cervelli et al. 2012).

1.8.1 Base excision repair (BER)

The BER pathway commonly repairs lesions generated by oxidation, alkylation and deamination of bases (Krokan and Bjørås, 2013) by removing the damaged base(s), and thus preventing the insertion of mutations or possible breaks during DNA replication (Krokan and Bjørås, 2013). DNA glycosylases are critical for recognizing and removing the incorrect base, thus leaving an apurinic/apyrimidinic site(AP) site. AP endonucleases then cleave the AP site, generating a 3'hydroxyl end and a 5' deoxyribosephosphate, which will facilitate new DNA synthesis, most commonly catalysed by Pol ß (Krokan and Bjørås, 2013). In *Leishmania* spp (Passos-Silva *et al.*, 2010; Genois *et al.*, 2014) Polß is localised in the nucleus and a BER activity has been demonstrated. It has been proposed that Polß BER activity is critical especially during the amastigote stage, where the parasite has to survive the hostile environment of the macrophages (Taladriz *et al.*, 2001). In the case of *T. cruzi* and *T. brucei,* Polß and Pol ß-PAK have a mitochondrial localisation, suggesting a role during the maintenance of the kinetoplast (Saxowsky *et al.*, 2003; Lopes *et al.*, 2008; Genois *et al.*, 2014).

Why there is such a putative BER functional dichotomy within the kinetoplastids has not been explored.

1.8.2 **Nucleotide excision repair (NER)**

The NER mechanism is divided in two pathways, global genome NER (GG-NER) and the transcription coupled NER (TC-NER). GG-NER is associated with repair throughout the genome, and TC-NER is associated with repair of lesions that block transcription (Compe and Egly, 2012). NER is involved in the repair of helix distorting lesions, including those caused by UV radiation, which results in DNA adducts including thymidine dimers and 6,4 photoproducts (Schärer, 2013). This repair pathway acts by removing short oligonucleotides containing the lesion, leaving a 3' hydroxyl end and 5' deoxyribosephosphate. Gap synthesis is catalysed by Pol δ, Pol ε or Polκ, and DNA is rejoined by DNA ligase III (Schärer, 2013). *T. brucei, T. cruzi* and *Leishmania* lack ligase III, suggesting that this enzyme is replaced by the activity of DNA ligase I (Passos-Silva *et al.*, 2010). It is known that the general transcription factor TFIIH, together with XPG, is necessary for the cleavage of the 3' site, and XPF is involved in the cleavage of the 5' site. XPD and XPB, which are part of TFIIH, unwind the DNA strands (Compe and Egly, 2012).

The transcription factor complex, TFIIH, has a critical role during NER. This complex consists of two subcomplexes, the first formed by two helicases (XPB and XPD) and five associated proteins (p62, p52, p44, p34 and p8/TTD-A), and the second by the kinase activating complex, CAK. Helicases XPA, XPC, XPE, XPF and XPG also participate in the NER pathway (Compe and Egly, 2012). In *T. brucei,* two genes have been identified that encode for two XPB proteins, one of 105 kDa (XPB) and a second one of 89 kDa (XPBz) (Badjatia *et al.*, 2013). Deletion of *T. brucei* XPBz has demonstrated that the protein is non-essential and that its loss increases the sensitivity of the cells to UV radiation and cisplatin (Badjatia *et al.*, 2013). Therefore TbXPBz has been associated with the TC-NER pathway (Machado *et al.*, 2014). RNAi studies targeting XPG, XPD and XPB have also been performed, suggesting that NER activity is uniquely associated with XPG, which shows a similar effect to RNAi against CSB, which initiates TC-NER. Thus, only CSB, XPBz and XPG appear to act in NER, suggesting

that the TC-NER mechanism seems to predominate in the parasite (Machado *et al.*, 2014).

1.8.3 **Mismatch repair (MMR)**

The MMR pathway is highly conserved in all kingdoms and is required during the repair of erroneous base insertions produced by DNA synthesis or homologous recombination (HR) (Marinus, 2012). *T. brucei* and *T. cruzi* express many proteins involved in this process, including MSH2 and MLH1, suggesting that these organisms are fully capable of repairing lesions requiring the MMR pathway (Augusto-Pinto and Bartholomeu, 2001; Bell *et al.*, 2004; Passos-Silva *et al.*, 2010).

1.8.4 **Non-homologous end joining (NHEJ)**

The NHEJ pathway is involved in the repair of DNA double-strand breaks (DSBs) by promoting the re-ligation of the lesion, without relying on a template (Schärer, 2013). *T. brucei*, *T.cruzi* and *L. major* harbour several proteins known to be involved in this pathway, such as Mre11, Rad50, KU70 and KU80. In spite of the presence of the proteins, studies suggest that each of the parasites lacked NHEJ activity and, instead an alternative repair pathway, termed microhomology-mediated joining (MMEJ) predominates (Burton *et al.*, 2007; Glover, Jun and Horn, 2011; Genois *et al.*, 2014). MMEJ is another repair pathway that is considered a non-homologous mechanism, though in this case it requires between 5-25 bases of imperfect homology in order to promote re-ligation of a DSB (Truong *et al.*, 2013). This mechanism is associated with chromosome aberrations such as translocation, deletion and inversions (Truong *et al.*, 2013) and is readily detected in kinetoplastids, perhaps due to the lack of NHEJ (Burton *et al.*, 2007; Peng *et al.*, 2015).

1.8.5 **Homologous recombination (HR)**

The HR repair pathway is involved in the repair of DSBs and the restart of stalled replication forks (Costes and Lambert, 2013). The repair of DSB lesions involves the activity of a group of proteins which lead the recombination steps (Figure 1-10). The first step is the recognition of the DSB by the MRN complex

(Mre11-Rad50-NBS1) in humans, or the MRX (Mre11-Rad50-Xrs2) complex in *S. cerevisiae*. This is followed by the binding of replication protein A (RPA; SSB in bacteria) and recombination mediators such as RAD52 and RAD54 to the ssDNA, stimulating RAD51 (Renkawitz, Lademann and Jentsch, 2014). The loading of Rad51 to ssDNA depends of BRCA2 and Rad51 paralogs (RAD51B, RAD51C, RAD51D, XRCC2 and XRCC3) (Sung and Klein, 2006; Suwaki, Klare and Tarsounas, 2011; Costes and Lambert, 2013). It is known that Rad51 interacts with BRCA2 via BRC repeat motifs present in the latter protein (Lord and Ashworth, 2007). The precise role of Rad51 paralogs during this process is still uncertain, but it has been demonstrated that in the absence of these proteins there is an inefficient HR process (Suwaki, Klare and Tarsounas, 2011). It has also been proposed that Rad51C and XRCC3 play a role during branch migration (Badie *et al.*, 2009; Suwaki, Klare and Tarsounas, 2011). Moreover, it has been suggested that Rad51C, XRCC2 and XRCC3 are involved in chromosome segregation and centrosome integrity (Griffin *et al.*, 2000; Renglin Lindh *et al.*, 2007).

Once Rad51 binds onto ssDNA, it forms a helical protein filament known as presynaptic filament (Sung and Klein, 2006; Costes and Lambert, 2013). Rad51 is universally conserved, with close homologues in bacteria and archaea called RecA and RadA, respectively. The presynaptic filament next binds to the DNA duplex (synaptic complex), initiating the search for homology along the duplex (Sung and Klein, 2006). The strand invasion is promoted by the action of accessory factors (including Rad54, Rad54B), forming a DNA joint known as a displacement (D)-loop (Sung and Klein, 2006; Costes and Lambert, 2013). DNA synthesis starts from the 3' broken end, using the homologous sequence as a template and the invaded ssDNA as a primer. This process commonly results in the formation of a recombination intermediate known as the Holliday junction (HJ). The dissolution of the HJ is performed by branch migration (Renkawitz, Lademann and Jentsch, 2014). There is an alternative pathway known as synthesis-dependent strand annealing (SDSA), where the HJ is not formed due to the migration of the DNA strand after DNA synthesis (Renkawitz, Lademann and Jentsch, 2014).

In kinetoplastids, HR is the main mechanism involved in the repair of DSBs. *T. brucei, T. cruzi* and *L. major* encode for the main HR proteins, BRCA2

and Rad51 (Passos-Silva *et al.*, 2010). Rad51 has been characterised amongst the three species, demonstrating a role during this repair mechanism (Passos-Silva *et al.*, 2010). As in other eukaryotes, Rad51 interacts with the BRC repeat motifs of BRCA2. Interestingly the parasite has evolved an expansion of BRC repeats, with 15 predicted BRC repeats (Hartley and McCulloch, 2008), which contrasts with mammals that have eight BRC repeats, and *T. cruzi* and *L. major,* where BRCA2 harbours two BRC repeats (Hartley and McCulloch, 2008; Carreira and Kowalczykowski, 2011; Genois *et al.*, 2012). Unlike other organisms, such as *Leishmania* and mammals, it is proposed that BRCA2 in *T. brucei* is not solely involved in the recruitment of Rad51. Instead, it is suggested that is associated with the subnuclear redistribution of Rad51 (Genois *et al.*, 2012; Trenaman *et al.*, 2013; Lord and Ashworth, 2016). BRCA2 also contributes to VSG switching, since its loss impedes the reaction (Hartley and McCulloch, 2008).

Rad51 paralogues also play an important role in *T.brucei* HR. Six Rad51-like proteins were identified in the parasite. Mutants have been made in all the proteins, demonstrating they all act in repair, presumably through HR (Proudfoot and McCulloch, 2005; Dobson *et al.*, 2011). Interestingly, the disruption of Rad51-3 also results in a decrease of VSG switching rate (Proudfoot and McCulloch, 2005), like RAD51, reaffirming an association of HR and VSG switching in the parasite (McCulloch and Barry, 1999; Proudfoot and McCulloch, 2005).
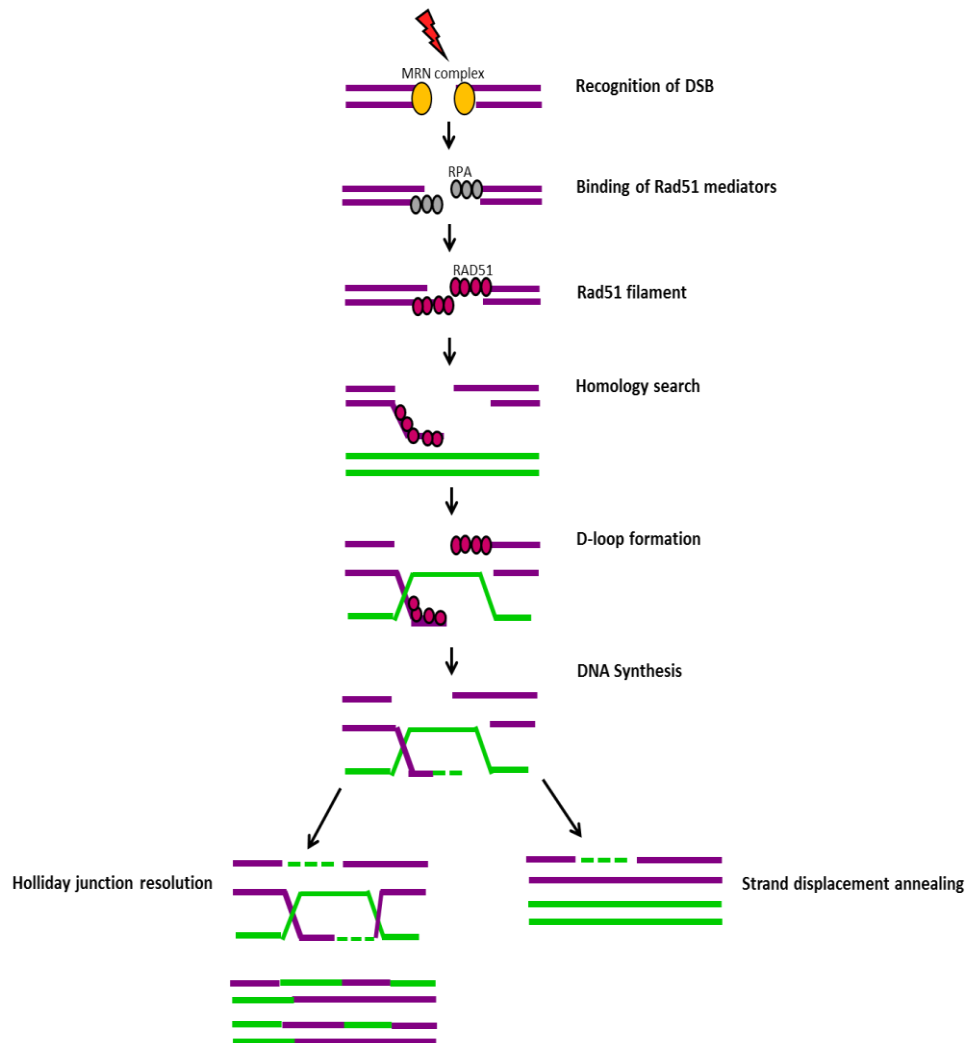
Figure 1-10. Activity of Rad51 during homologous recombination. Diagram detailing the homologous recombination pathway. In yellow is represented the MRN complex, in grey replication protein A (RPA) and in pink Rad51.

1.8.6 Translesion synthesis (TLS)

It is thought that when the replicative DNA pols α, ε and δ, encounter replication fork-blocking lesions, all or some of the replicative DNA pols are replaced by a TLS polymerase (Garcia-Diaz and Bebenek, 2007). TLS pols have the ability to insert nucleotides opposite to damage and, in this way, permit the replication process to continue. Depending on the lesion, TLS synthesis can be performed by one TLS pol or by the collaboration of two TLS pols (Bebenek and Kunkel, 2004) (Figure 1-11). This process is known as a tolerance mechanism, since the damage may not be corrected (L S Waters *et al.*, 2009). When TLS pols synthesize DNA on a damaged template, the error rate can be as high as 1 incorrect nucleotide for every 10 bases replicated (L S Waters *et al.*, 2009).

Recent studies have demonstrated that TLS pols can replace each other since, when a specific TLS Pol is not present, other Pols can be recruited and synthesise on the template. This may result in an increased probability of generating mutations (Friedberg, Lehmann and Fuchs, 2005). An example includes Xeroderma pigmentosum (XPV) syndrome, which is a type of skin cancer caused by the incapacity of the cells to repair UV lesions (Kannouche and Stary, 2003). XPV can be the result of a mutation in the XPV gene, impeding the activation of Polη, interrupting the repair of UV lesions. It has been proposed that in the absence of Polη, an alternative TLS pol acts to bypass the damage, increasing the mutation probability and leading to the development of the disorder (Kannouche and Stary, 2003; Jansen *et al.*, 2014). Studies suggest that Polι may be one of the Pols able to compensate for the absence of Polη (Jansen *et al.*, 2014).
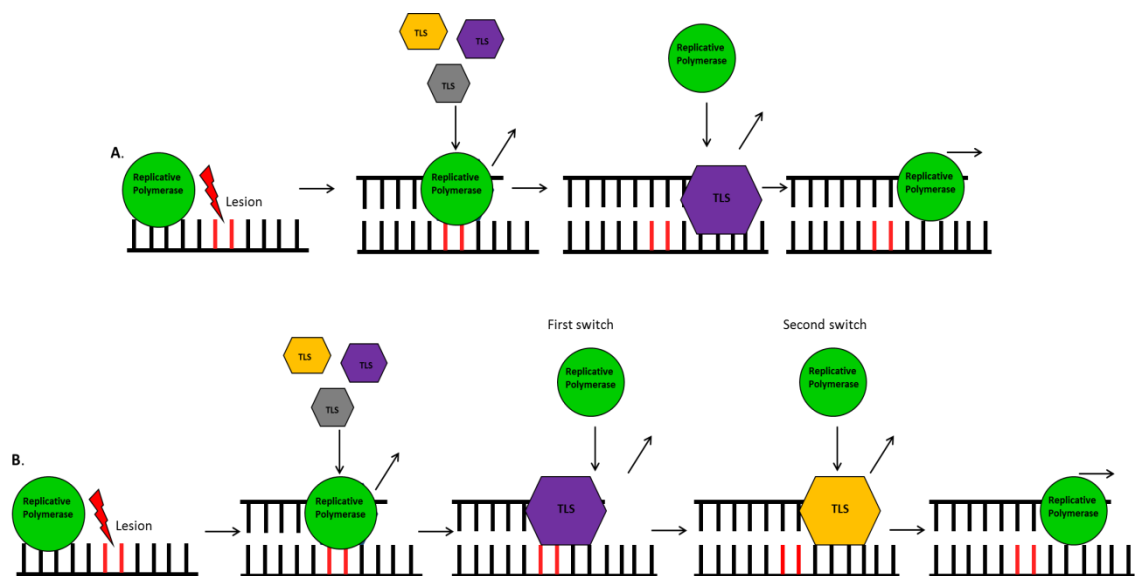
Figure 1-11. Schematic representation of DNA damage repair by translesion synthesis. A. Translesion synthesis by a single TLS pol, showing the replacement of the replication polymerase (green) by the translesion polymerase (purple), the one that is subsequently replaced by the replicative polymerase **B.** Translesion synthesis by two TLS pols. Showing two subsequent switches between two different TLS pols, the first inserts the nucleotide and the latter extends the strand. As in the first mechanism the TLS pol is replaced by the replicative polymerase.

But TLS pols may have multiple functions. In *S. cerevisiae* Pol Z is able to synthesise through UV damage-associated lesions, such as TT dimers (an activity also seen in PolH) and is also capable of elongating mismatched primers (Rattray and Strathern, 2003; L S Waters *et al.*, 2009), thereby increasing its capacity to retain mutations in the genome. In yeast, Pol Z is the cause of 50-70% of spontaneous mutations (Goodman, 2002). While in mammals this enzyme has an essential role during embryogenesis; experiments performed in mice show that a knockout of PolZ causes death during embryonic development (Esposito *et al.*, 2000; Gómez-Llorente *et al.*, 2013), suggesting the Pol Z might have an important role during cell division (Esposito *et al.*, 2000). In mammals, PolQ (Polθ) has a helicase domain and a polymerase domain (Li, Gao and Wang, 2011). This polymerase has been associated with several repair pathways apart from TLS, including MMEJ, BER and HR (Beagan *et al.*, 2017). Studies performed on PolN in humans, suggest that this polymerase is involved in cross-link repair and HR (Moldovan *et al.*, 2010) . A notable feature of these two enzymes is that the polymerase domain of mammalian PolN is similar to the polymerase domain of mammalian PolQ (Marini *et al.*, 2003). Studies in the fly, *Drosophila melanogaster,* show a close relation between HEL308 (ortholog of human PolQ) and PolN due to an ancient gene duplication event; it was also shown that expression of both genes overlaps, which suggests that these two polymerases might function together in the cell (Marini *et al.*, 2003).

1.8.6.1 Recruitment of translesion polymerases

The proliferating cell nuclear antigen (PCNA) is a homotrimeric protein whose role is to encircle the DNA and orchestrate the recruitment of proteins involved in DNA damage repair, DNA replication and chromatin structure maintenance (Andersen, Xu and Xiao, 2008). It has been demonstrated that TLS Pols are able to interact with PCNA through a motif known as the PIP box (Boehm, Spies and Washington, 2016). The interaction between the polymerase and the PCNA clamp increases the processivity of the polymerase, which can be described as the number of nucleotides that are incorporated by the polymerase in a single association (Zhuang and Ai, 2010). Furthermore, mono-ubiquitination (MUB) of PCNA promotes the switch between the replicative polymerase and the translesion polymerase, while polyubiquitination (POLYUB) is linked with an

error-free repair pathway (Lehmann *et al.*, 2007; Boehm, Spies and Washington, 2016).

Blockage of the replication fork leads to a prolonged single-stranded DNA (ssDNA), followed by the association of the RPA with the ssDNA. This event triggers MONOUB of the PCNA by the RAD18-RAD6 complex (Mailand, Gibbs-Seymour and Bekker-Jensen, 2013; Boehm, Spies and Washington, 2016). This then leads the switch of the replicative polymerase with the TLS pol, facilitating the bypass of the lesion. MUB of the PCNA can be reversed by the deubiquitylating enzyme known as ubiquitin-specific processing protease 1 (USP1) (Mailand, Gibbs-Seymour and Bekker-Jensen, 2013). The PCNA can also undergo POLYUB, and this event is driven by the E3 ligase Rad5 in association with the MMS2-UBC13E2 ubiquitin-conjugating enzyme complex (Mailand, Gibbs-Seymour and Bekker-Jensen, 2013; Boehm, Spies and Washington, 2016). POLYUB in higher eukaryotes leads to the recruitment of the helicase-nuclease ZRANBR3, suggesting that this molecule facilitates the binding of the PCNA to the stalled replication fork (Mailand, Gibbs-Seymour and Bekker-Jensen, 2013). Studies have shown that certain genotoxic agents, such as UV irradiation, methyl methanesulfonate, cisplatin and benzo[α]-diolepoxide are more prone to cause MONOUB of PCNA (Stelter and Ulrich, 2003; Solomon, Cardoso and Knudsen, 2004; Lehmann *et al.*, 2007). In mammalian cells, UV irradiation mainly causes mono-ubiquitination (Stelter and Ulrich, 2003; Kannouche, Wing and Lehmann, 2004; Lehmann *et al.*, 2007).

1.8.7 Translesion Polymerases in kinetoplastids

Studies to date on TLS Pols in kinetoplastids are relatively limited. Recent work in *L. infantum* demonstrated TLS activity of LiPolθ, which is capable of bypassing oxidative damage (Fernández-Orgiler *et al.*, 2016). Moreover, *T. cruzi* Polη is linked with the bypass of oxidative and UV damage. In addition, this polymerase has been shown to have an active role during HR (De Moura *et al.*, 2009). TcPolκ has also been shown to possess TLS activity, with the capability to bypass 8-oxoG, a lesion commonly generated by oxidative agents (Rajão *et al.*, 2009). Studies performed in *T. brucei* have demonstrated the presence of two primase-polymerase-like proteins (PPL), TbPPL1 and TbPPl2 (of which the second

protein has been shown to be essential for cell survival). TbPPl2 was shown to have translesion synthesis activity, and depletion of the protein leads to a G2 arrest, perhaps because of unrepaired DNA gaps (Rudd et al. 2013). Although these findings have given us a better understanding of the TLS pathway in kinetoplastids, essentially nothing is known about the functions of the ~14 conventional TLS gene candidates of *T. brucei* (Table 1-2). In this context, whether or not these orthologs are involved in the TLS synthesis, in repair pathways, or in parasite-specific reactions is unknown.

Polymerase	Family	Chromosome localisation in *T. brucei*	Number of copies
PolK (kappa)	Y	11	10
PolH (eta)	Y	10	1
PolZ (zeta)	B	8	1
PolN (nu)	A	11	1
PolQ-Helicase domain (theta)	A	8	1

Table 1-2. Predicted translesion DNA polymerases in *T. brucei*.

1.9 Project objectives

To date, most of our understanding of TLS Pols is based on studies in bacteria, mammals and model eukaryotes. Therefore investigating the roles of these polymerases in *T. brucei* will address questions as to whether they conform to these predictions, or if they harbour *T. brucei* specific functions. Given the large number of translesion polymerases present in the parasite, three candidates, which belong to the A and B family of polymerases, were selected for further studies.

The main aim of this research was to understand the functions of polymerase nu (TbPolN), polymerase theta helicase domain (TbPolQ) and polymerase zeta (TbPolZ) during genome maintenance in the bloodstream form of *T. brucei*. The study tried to address the importance of the three TLS pols in the parasite survival, analysing a potential contribution in DNA damage repair.

2 Material and Methods

2.1 General Bioinformatics

2.1.1 Sequence retrieval and analysis

T. brucei gene and protein sequences were retrieved from TriTrypDB version 33 (http://tritrypdb.org/tritrypdb/) (Aslett *et al.*, 2009). Sequences from other organisms were retrieved from NCBI database (http://www.ncbi.nlm.nih.gov/). CLC genomic Workbench, version 7.5.1 (Qiagen) was used for sequence alignments, plasmid map construction and primer design.

2.2 Protein homology search and domain prediction

The protein homology searches were performed using the NCBI database Basic Local Alignment Tool (BLASTp) (https://blast.ncbi.nlm.nih.gov/Blast.cgi) (Altschul *et al.*, 1990). Smart BLAST (http://blast.ncbi.nlm.nih.gov/smartblast/smartBlast.cgi?CMD=Web&PAGE_TYPE=BlastDocs) was used for further analysis of the sequences. For protein domain analysis two web-based programs were used: InterPro 64.0 (https://www.ebi.ac.uk/interpro/) and Pfam 31.0 (http://pfam.xfam.org/).

2.3 General Molecular Techniques

2.3.1 Genomic DNA extraction

Genomic DNA was extracted by harvesting $2x10^6$ cells and processed through the Qiagen Blood and Tissue kit (Qiagen), according to the manufacturer's instructions. Genomic DNA was eluted in 50 µl of Buffer AE and stored at 4°C.

2.3.2 Primer design

Primers were designed based on *T. brucei* reference strain TREU927, using the CLC genomic Workbench 7.0 and synthesised by Eurofins Genomics (http://www.eurofins.com/). The lyophilised DNA was reconstituted in ddH$_2$O to give a final concentration of 100 pmol/µl. The primer working concentration was of 10 pm/µl.

2.3.3 **Polymerase Chain Reaction (PCR)**

For general fragment amplification NEB Taq DNA polymerase was used, in the case of cloning fragment amplification Phusion® high fidelity polymerase (NEB) was used.

For the amplification of the different DNA fragments, specific primers were used (**Error! Reference source not found.**). The amplification reaction was performed in a final volume of 50 µl containing: 1x Phusion Buffer (NEB) or 10 x ThermoPol® Buffer (NEB; Taq), 0.2 mM dNTPs mix, 10 ng of genomic DNA from Lister 427 *T. brucei*, 2 µl of each primer (10 pmol/µl stock) and 20 U/ml of Phusion® (NEB) or Taq DNA polymerase (NEB) and ddH$_2$O to obtain a final volume of 50 µl. The amplification was carried out as follows: initial denaturation step of 5 min at 98°C, 30 cycles of 30 s-1 min at 98°C, the annealing temperature varied depending of the pair of primers but in general was 30s between 52°C-60°C and an extension of 30 s-1min at 72°C (Phusion®) or 68°C (Taq) ; with a final extension step of 10 min at 72°C. The resulting products were analysed in agarose gel electrophoresis (Section 2.3.5).

Gene ID	Gene	Sense	Sequence	Restriction site	Annealing Tº	Purpose	Plasmid backbone	Linearisation enzyme
Tb927.8.3290	TbRev3	Fw	ggggacaagtttgtacaaaaaagcaggctacctgtcttggttctgtggg	attB sites	52 ºC	Gateway cloning	pGl2084	AscI
		Rv	ggggaccactttgtacaagaaagctgggtcgcagcttcctttactggac	attB sites				
		Fw	gcatacgcgtgcggccgcttggaaactcggctattgga/ gcatggatccgcggccgcttggaaactcggctattgga	MluI/BamHI, NotI	60 ºC	KO (5'UTR)	pmtl23	NotI
		Rv	gcattctagattcccttcagtggttgtgta	XbaI				
		Fw	gcatgagctctttctatccagtcggaaga	SacI	60 ºC	KO (3'UTR)		
		Rv	gcatatcgatgcggccgctcacgtttgccttgagacac	ClaI,NotI				
		Fw	tacttgtgtcgatgcatgcg	N/A	60 ºC	Integration verification KO	N/A	N/A
		Rv_ NEO	gcgtgcaatccatcttgttc	N/A				
		Rv_ BSD	gggtggattcttcttgagac	N/A				
		Fw	aaagagttacgttccgcgtg	N/A	60 ºC	ORF verification KO	N/A	N/A
		Rv	acttgttgtgtcctgagctc	N/A				
		Fw	gcattctagagcgagtcgttacgtagtctt	SacI	52 ºC	C-terminal myc tag	pNAT	HpaI
		Rv	gcatgagctccagatggctattaaaatgct	XbaI				
Tb927.11.5550	TbPolN	Fw	ggggacaagtttgtacaaaaaagcaggcttcagcacactcagttccgtc	attB sites	52 ºC	Gateway cloning	pGl2084	AscI
		Rv	ggggaccactttgtacaagaaagctgggtacccgcaacgaaaatacttg	attB sites				
		Fw	gcataagcttgcggccgcaaacatgcttatgtttttgt	HindIII, NotI	60 ºC	KO (5'UTR)	pmtl23	NotI
		Rv	gcattctagattcccttcagtggttgtgta	XbaI				
		Fw	gcatgagctcttcacgaaaggcgtcacgac	SacI	60 ºC	KO (3'UTR)		
		Rv	gcatatcgatgcggccgcccccacaacaataacaacaa	ClaI,NotI				
		Fw	tggacgaagctgttgccttg	N/A	60 ºC	Integration verification KO	N/A	N/A
		Rv_ NEO	gcgtgcaatccatcttgttc	N/A				
		Rv_ BSD	gggtggattcttcttgagac	N/A				
		Fw	aacactgttcttacgccctc	N/A	60 ºC	ORF verification KO	N/A	N/A
		Rv	aacgccgacgcatcattcat	N/A				
		Fw	gcatgagctcacgagttgctcattaagcac	SacI	60 ºC	C-terminal myc tag	pNAT	PstI
		Rv	gcattctagaaggaacatcaagtttctcga	XbaI				
Tb927.8.1090	Putative Polσ	Fw	gcatgagctcagatgctttaaacgtacgga	SacI	60 ºC	C-terminal HA tag	pNAT	HpaI
		Rv	gcattctagaacgtcgggtcaatgaccga	XbaI				
Tb927.8.3350	TbHelQ	Fw	gcatgagctcctggagtttgtcgcgattgg	SacI	60 ºC	C-terminal HA tag	pNAT	XhoI
		Rv	gcattctagagtaggttgaagattggaggg	XbaI				

Table 2-1. Primer sequences. List of primer sequences used for gene deletion (KO), endogenous tagging and Gateway cloning.

2.3.4 **RT-qPCR**

Gene knockdown was tested by quantitative reverse transcriptase polymerase chain reaction (RT-qPCR). For this, 4×10^6 cells were harvested by centrifugation (405 g for 10 minutes). RNA was isolated by using the Qiagen RNeasy kit, following the manufacturer's protocol entitled "Purification of Total RNA from Animal Cells using Spin Technology".

For the RT-qPCR primers were designed by using the software 'Primers Express 3.0' (Table 2-2). For the amplification, the One Step SYBR® Prime Script™ RT PCR kit (TAKARA) was used. The amplification reaction was performed in a final volume of 20 μl containing: 10 μl of Buffer4, 0.8 μl of each primer (10 μM), 0.4 μl OF Reoxdyell, 5.2 μl of H_2O and 2 μl of RNA. Actin primers were used as the endogenous control (Table 2-2) and ddH_2O as a negative control. Each sample set was performed as a technical triplicate.

For testing the RNA levels of silent VSGs, first the RNA of each sample was converted to complementary DNA. 1 μg of total RNA from each sample was converted into complementary DNA. For this process the SuperScript™ III Reverse Transcript Kit (Invitrogen™, Life Technologies) was used, following the manufacturer's protocol entitled 'First Strand cDNA Synthesis'. Random primers were used. The cDNA was stored at -20 °C until analysis. For the RT-qPCR, specific primers were used (Table 2-2). Prior to the RT-qPCR, cDNA was extracted. The master mix was prepared at 4°C (but not in direct contact with ice) as follows: 12.5 μl SYBR® Green PCR Master Mix (Applied Biosystems), 5 μl RNase free ddH_2O (Qiagen), 2.5 μl of each primer (300 nM stock) and 2.5 μl of the appropriate cDNA. The master mix was pipetted into a MicroAmp® Optical 96-well reaction plate (Thermo Fisher). As mentioned above, actin was used as endogenous control and ddH_2O as negative control.

The AB 7500 RT PCR system thermocycler conditions for all reactions were 50 °C for 2 min (x 1), 95 °C for 10 min (x 1), 95 °C for 15 sec followed by 60 °C for 1 min (x 40) then a dissociation step was added as follows, 95 °C for 15 secs, 60 °C for 1 min, 95 °C for 15 secs and finally 60 °C for 15 secs (x 1). Analysis of

the amplification and dissociation curves was performed as described in the Applied Biosystems® manual. The fluorescence intensity was quantified by calculated by using the $\Delta\Delta C_t$ method (Livak and Schmittgen, 2001).

Number	Name	Sense	Sequence	Use
*	PolZ_b	Fw	cgcaacgttcggcagta	TbPolZ RT-PCR
*	PolZ_b	Rv	ggtgcacccccgtaaca	
CT_OL29	Actin	Fw	cggacgaggaacaaactgc	RT-PCR endogenous control
CT_OL30	Actin	Rv	tttccatgtcatcccaattgg	
CT_OL33	VSG221	Fw	agcagccaagaggtaacagc	VSG221 RT-qPCR
CT_OL34	VSG221	Rv	caactgcagcttgcaaggaa	
CT_OL35	VSG13	Fw	ataacgcatggccatcttgac	VSG13 RT-qPCR
CT_OL36	VSG13	Rv	cagcgcaagtacaggacg	
CT_OL37	VSGV02	Fw	cagccaagtacaggacg	VSGV02 RT-qPCR
CT_OL38	VSGV02	Rv	tgcttcgtcgtcgcttac	
CT_OL39	VSG224	Fw	gacgcagcagaatcaacac	VSG224 RT-qPCR
CT_OL40	VSG224	Rv	gcttattttgtgtctgtcgc	
CT_OL41	VSG800	Fw	acagaccgccgacagtatc	VSG800 RT-qPCR
CT_OL42	VSG800	Rv	gtatctttgtaggccgctgc	

Table 2-2. Primers used for RT-qPCR.

2.3.5 Agarose Gel

1% agarose gels were performed by melting UltraPureTM Agarose (Invitrogen) in 1x TAE (40 mM Tris Base, 19 mM acetic acid, 1 mM EDTA). SYBR® Safe DNA Stain (Life technologies) was added in a proportion of 1:20,000 for DNA visualization under ultraviolet light. The PCR product, which was pre-mixed with 4x NuPAGE® LDS Sample Buffer in a final concentration of 1x, was loaded onto the gel along with the 1 Kb Plus ladder (Invitrogen™, Life Technologies). The gel was left running at 100 V for 50 minutes on a Mini-Sub® Cell GT Cell tank (Bio Rad). DNA was visualized by using a GelDocTM XR+ system (BioRad).

2.3.6 DNA fragment purification

For the DNA purification, the gels were visualised under a Dark Reader blue Transilluminator (Clare Chemical Research) and the fragment of interest was excised from the agarose gel using a sterile scalpel blade. The QIAquick Gel purification kit (Qiagen) was used for the DNA purification following the manufacturer's instructions.

2.3.7 Restriction Enzyme digestion

The purified PCR fragment and vector backbone used for cloning (excluding Gateway Cloning) were digested with the appropriate restriction enzymes. The reaction was performed as follows: 5 µl of 10x buffer, 20 units of the restriction enzyme, 20 µl of the PCR product or 10 µl of the vector (~5 µg) and made up to a final volume of 50 µl with ultra-pure water. In the case of a double digestion, it was determined the best buffer for the optimal function of both enzymes. The reaction was incubated for 2 h at the temperature recommended by the manufacturer (NEB). Once the incubation period concluded, the product was separated in a 1% agarose gel (Section 2.3.4) and purified with the QIAquick Gel purification kit (Section 2.3.6).

2.3.8 Fragment ligation

The fragment was ligated into the appropriate vector using 1 µl (400 units) of T4 ligase (NEB), 1 µl of 10x buffer, 2 µl of digested vector and 6 µl of the digested product (1:3 ratio; vector: PCR product). Reactions were left overnight at room temperature. In the case of the KO plasmids, the ligation of the inserts was performed in two ligation steps: in the first step, one of the inserts was ligated to the vector and, after confirmation, the next insert was ligated to the same vector.

2.3.9 Transformation of competent cells

Chemically competent DH5α *E. coli* (in house) bacteria were thawed on ice for 5 minutes. Next, 50 µl of bacteria were added to 10 µl of ligation product and incubated on ice for 30 minutes. The cells were 'heat shocked' at 42 °C for

45 seconds and immediately placed on ice for 5 minutes. Next, 250 µl of SOC media (5 g yeast extract, 20 g tryptone, 0.5 g NaCl, 10 ml 1M $MgCl_2$, 10 ml 2M glucose, 10 ml 1M MgS04 /L) was added and left for shaking at 37 °C for 1 h. The cells were pelleted at 7000x g for 1 minute and re-suspended in ~50 µl of the remaining supernatant. The cells were plated onto LB broth (5 g yeast extract, 10 g tryptone, 10 g NaCl /1L ddH20; pH 7.0 and 20 g agar) agar plates supplemented with 100 µg/ml ampicillin and incubated overnight at 37 °C.

2.3.10   **Plasmid extraction**

A colony containing the required plasmid was inoculated into 5 ml of liquid LB supplemented with 100 µg.ml^{-1} of Ampicillin and incubated overnight at 37 °C, with agitation. 800 µl of the culture was stored in 50:50 'peptone-glycerol' mix for long term storage at -80 °C. The rest of the liquid culture was centrifuged for 10 minutes at 2000x g and the pellet was used for plasmid purification.

In order to purify the plasmid from the pellet of the transformed *E. coli* DH5α bacteria, the QIAprep Spin Miniprep Kit (Qiagen) was used according to the manufacturer's instructions. The plasmid concentration was measured by using the NanoDrop 1000™ Spectrophotometer (Thermo Scientific). To test if the plasmid has successfully recombined, 5 µg of the plasmid was digested with the appropriate restriction enzymes. The product was loaded o n a 1% agarose gel to visualize the digestion pattern. Once the correct digestion pattern was achieved, the plasmid was sent for sequencing (Eurofins Genomics, Germany) to confirm that the product was free of mutations. Primers used for the sequencing are in Table 2-3. The resulting chromatogram files were analysed using CLC Workbench, version 7 (QIAGEN), by assembling the sequence peaks to the reference file.

Primer Number	Name	Sense	Sequence	Purpose
MP 15	HA/myc	Fw	cgttggccgattcattaatgc	C-terminal myc tag sequence
MP 16	HA/myc	Rv	taatgacgaacgggaaatgc	C-terminal myc tag sequence
M13 (-43)	M13 (-43)	Fw	agggttttcccagtcacgacgtt	KO plasmid sequence
M13 (-49)	M13 (-49)	Rv	gagcggataacaatttcacacagg	KO plasmid sequence

Table 2-3. Primers used for the confirmation of insert integration.

2.3.11 Plasmid preparation prior to transfection

10 µg of plasmid was linearised with appropriate restriction enzyme (Table 2-1) for 4 hours. The digested product was purified using the DNA Clean and Concentrator™ -25 kit (ZYMO). 1 µl of the purified product was loaded onto a 1% agarose gel, alongside the undigested plasmid for confirmation. If correct, 10 µg of the product was used for transfection (Section 2.6.4).

2.4 Gateway Cloning

The RNAi constructs for bloodstream form cells (BSF) were generated as described in (Jones *et al.*, 2014). The primers were designed to include the site-specific attachement sites (attB) (ggggacaatttgtacaaaaaagcaggct/ggggaccactt tgtacaagaaagctgggt) The primer sequence was identified using TrypanoFAN RNAit software (http://trypanofan.bioc.cam.ac.uk/software/RNAit.html).The PCR amplification was performed using Phusion® High fidelity DNA polymerase, as described in section 2.3.3. The PCR product was tested on a 1% agarose gel (Section 2.3.5); the expected band was extracted and purified as described in section 2.3.6.

The insert was cloned into the plasmid by using the Gateway Cloning Technology. Which consist of a BP reaction, catalysed by the bacteriophage λ integrase and *E. coli* integration host factor proteins, which promote the recombination between the attB sites of the PCR product and the attP sites of the pGL2084 vector (Katzen, 2007). The pGL2084 vector consist of two sets of attP sites, which flank a counter selectable marker (*ccdB*), and are separated by a 150 bp stuffer (Figure 3-6). Resulting in the insertion of the gene-specific

fragment in a 'tail to tail' orientation, separated by the 'stuffer'. Allowing the expression of a dsRNA hairpin loop, which is under the control of the PRNA promoter, regulated by a tetracycline operator (Jones *et al.*, 2014)

The BP reaction (section 3.3) was performed by using the Gateway® BP Clonase® II Enzyme mix by adding 5 µl attB-PCR product, 1 µl pGL2084, 3.75 µl TE buffer and 0.25 µl of the BP enzyme. The reaction was incubated for 1 h at room temperature; after the incubation 1 µl of proteinase K (2 µg/µl) was added. The 10 µl BP reaction was added to 50 µl of *E. coli* MAX Efficiency® DH5α™ competent cells (Life Technologies), which were transformed as described in section 2.3.9. The plasmid was purified as described in section 2.3.10. The verification of the plasmid was performed by enzymatic digestion using the following enzymes: BamHI/XbaI (excise both inserts), StuI (sense insert), ClaI (anti-sense insert) and AscI (linearisation site). The enzymatic reaction was prepared as follow: 2 µl of Buffer 4 with BSA or CutSmart™ buffer (NEB), 0.25 µl of restriction enzyme (NEB), 3 µl of plasmid and 14.75 µl of ddH$_2$O (final volume 20 µl); and incubated for 1 h at 37 ˚C. The digestion product was separated on a 1% agarose gel for plasmid confirmation.

2.5 Construct design

2.5.1 C-terminal endogenous tagging

The pNAT12myc or pNAT6HA vector (Alsford and Horn, 2008) was used. The construct integrates into the gene of interest through single-crossover recombination, guided by the 3' ORF region present in the vector. Resulting in the incorporation of the tag (Myc or HA) into the 3' end of the gene's ORF, together with the *T. brucei* βα tubulin, the drug resistance marker gene and the *T.brucei* actin. Tubulin and actin are necessary for the expression of the drug resistance gene by regulating trans-splicing. There is also a duplication of the target sequence downstream of the tagged locus. The duplicated sequence lacks the start codon, suggesting an inactive ORF, not compromising the gene (McCulloch *et al.*, 2004) (Figure 2-1).

The primers used in this assay, amplify a 3' region of the ORF excluding the stop codon (Table 2-1). The cloning was performed as described above (Section 2.3.7 - 2.3.10.)
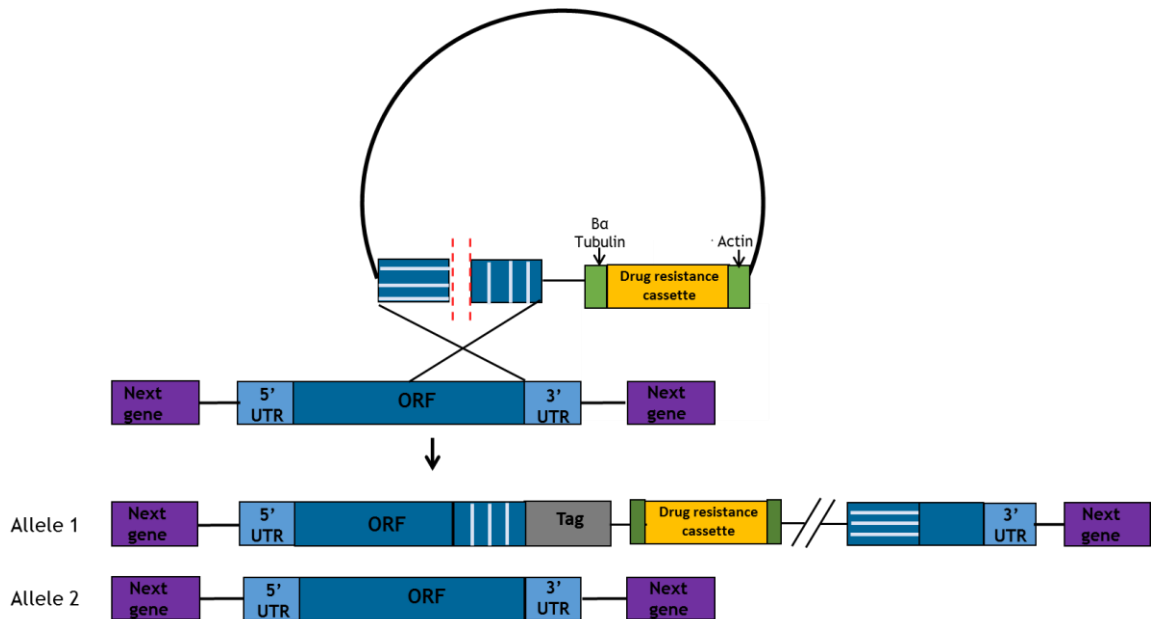
Figure 2-1. C-terminal endogenous tagging strategy. Integration of the linearised construct via a single recombination (black cross) using the homologous regions (white lines), within the 3' region of the endogenous locus. Not to scale.

2.5.2 Knockout construct

The knockout mutant cell lines were generated by the replacement of the endogenous locus with an antibiotic selection marker (blasticidin or neomycin) by homologous recombination (HR) (section 4.3). For this approach the pmtl23 vector was used (Devlin *et al.*, 2016). There are two modified versions, containing either the blasticidin (ΔORF::BSD) or the neomycin (ΔORF::NEO) antibiotic cassette. The *NEO* and *BSD* vectors contain *T. brucei* Actin and *T. brucei* β/αTubulin, which facilitate the trans-splicing and polyadenylation required for mRNA processing. Primers were designed to amplify the 3' region of the 5' UTR upstream, and the 5' region of the 3' UTR downstream. The amplification of the fragments was performed as described in section 2.3.3. The cloning strategy is described in sections 2.3.7-2.3.10. 10 µg of the plasmid (ΔORF::BSD or ΔORF::NEO) was linearised and concentrated as described in section 2.3.11.

2.6 *In* vitro cultivation of bloodstream forms of *Trypanosoma brucei*

2.6.1 Strains

The monomorphic bloodstream strain, Lister 427, was used for gene deletion and protein tagging assays. Lister 427 is a laboratory adapted strain, frequently used for genetic manipulation (McCulloch *et al.*, 2004).

For the RNAi interference assays the genetically modified Lister 427 cell line (2T1) was used. The 2T1 cell line contains a modification in chromosome 2a. For the construction of the RNA interference (RNAi) cell lines, an RNAi cassette integrates in the ribosomal locus of chromosome 2a in the 2T1 parental cell line. Permitting the expression of a RNA stem loop, which is under the control of the RNA polymerase I promoter, regulated by a tetracycline operator (Alsford and Horn, 2008). Facilitating the knockdown of the gene of interest by RNAi. The procedure is explained in detail in section 3.3.

2.6.2 Maintenance of cultures

Lister 427 (WT) cells were grown in HMI-9 (Gibco®) (Hirumi and Hirumi, 1989), supplemented with 20% (v/v) heat inactivated fetal bovine serum (FBS; Sigma Aldrich) and 1% penicillin-streptomycin solution (stock at 10,000 U/ml) (Gibco®). In the case of the 2T1 cell line, the cells were grown in HMI-11 thymidine-free media, consisting of Iscove's Modified Dulbecco's Medium (IMDM) (Gibco®), 10% (v/v) of FBS (Gibco®,tetracycline free), 1% of penicillin-streptomycin solution (10.000 U.ml^{-1})(Gibco®).

For the RNAi cell lines used for the replication assays with EdU (Section 2.8), the cells were grown in HMI-11 thymidine free media, consisting of Iscove's Modified Dulbecco's Medium (IMDM) (Gibco®), 10% (v/v) of FBS (Gibco®, tetracycline free), 1% of penicillin-streptomycin solution (10,000 U.ml^{-1}; Gibco®),4% (v/v) of HMI-9 mix (0.05 mM of bathocuproine disulphonic acid, 1 mM of sodium pyruvate, and 1.5 mM of L-cysteine (Sigma Aldrich), 1 mM of hypoxanthine (Sigma Aldrich) and 0.0014% of 2-mercaptoethanol (Sigma Aldrich).

For Lister 427 (WT) no drugs were added to the media. The selective drugs used for 2T1 cells were puromycin and phleomycin and for RNAi cell lines phleomycin and hygromycin. For the tagged lines the drug depends on the plasmid (blasticidin or phleomycin) and for the knockout cell lines blasticidin and neomycin (G418). The concentrations are detailed in Table 2-4. For culture maintenance the cells were seeded at ~$1x10^4$ and were cultured up to a maximum of $2x10^6$ cells.ml^{-1}. The cells were grown in vented flasks at 37°C in a 5% CO_2 humidified incubator.

Manufacturer	Drug	Concentration
InvivoGen	Hygromycin	5 μg/ml
InvivoGen	Neomycin (G418)	2.5μg/ml
InvivoGen	Blasticidin	10μ/gml
InvivoGen	Phleomycin	2.5μg/ml
Calbiochem	Puromycin	0.2μg/ml

Table 2-4. Antibiotic concentration used for cell maintenance and transfection in bloodstream forms.

2.6.3 Cryopreservation of bloodstream forms

For cryopreservation of the cells, 800 μl of a mid-log phase culture was added to 200 μl of 50:50 solution of glycerol and HMI-9 media. The samples were wrapped in cotton wool and stored at -80 °C for 24 hours. Subsequently, the cells were transferred to liquid nitrogen tanks. The respective information of each stabilate was submitted to the Wellcome Trust Centre for Molecular Parasitology (WTCMP) Freeze works samples management database (http://www.freezerworks.com/).

For the revival of the cells, the cells were thawed at room temperature and added to 9 ml of HMI-9 (lacking drugs). If required, selective drugs were added 24 hours later. The cells were maintained as described in section 2.6.2

2.6.4 Transfection

$3x10^7$ cells were harvested by centrifugation at 405x g for 10 minutes. The pellet was re-suspended in remaining media and transferred to a 1.5 ml tube.

The cells werere centrifuged at 665x g for 2 minutes. The pellet was re-suspended in 100 µl of Amaxa Human T Cell Nucelofactor kit solution (Lonza) and transferred to an electroporation cuvette (Lonza), containing 10 µg of linearised plasmid (Section 2.3.11). The cells were electroporated using the programme X-100, pre-programmed into the Amaxa Nucleofector II machine (Lonza). The cells were transferred into a conical tube containing 27 ml of HMI-9 medium in the absence of selective drugs. Two further serial dilutions were performed, adding 3 ml of the cells to a new conical tube containing 27 ml, resulting in three tubes with the following concentrations: $1x10^6$ cells.ml^{-1}, $1x10^5$ cells.ml^{-1} and $1x10^4$ cells.ml^{-1}. One ml of the cell suspension was plated into 24 well plates and incubated overnight at 37 °C with 5% CO_2. The following day, 1 ml of medium containing double the required concentration of drugs was added to each well (Table 2-4). The plates were incubated with 5% CO_2 for 5 to 7 days. The surviving clones were confirmed by PCR (Section 2.3.3) or Western blot analysis (Section 2.12.1).

2.7 Cell growth assays

2.7.1 Growth analysis after RNA interferance induction

The cell lines with inducible RNAi were used to test the gene essentiality in *T. brucei* survival. In order to test the importance of the different genes in the parasite growth, on the day before of the experiment, the parental cell line 2T1 (untransformed cell line) and the RNAi cell lines (transformed cell lines) were set up at a concentration of $1x10^5$ cells.ml^{-1} in 10ml of HMI-11 thymidine-free medium (Section 2.6.2). Containing puromycin and phleomycin for the 2T1 (untransformed) and phleomycin and hygromycin for the RNAi cell lines (Table 2-4). The following day, the culture (2T1and RNAi cell lines) was diluted to $5x10^4$ cells.ml^{-1} in HMI-11 medium with the selective drugs and devided into two flasks. Resulting in two flasks containing 2T1 cells (used as a control cell line) and two flasks containing the RNAi inducible cell line. Tetracycline (1µg/ml) was added to one flask (Tet+) containing 2T1 cells and to one flask containing the RNAi inducible cell line. In the case of the RNAi inducible cell line, the tetracycline controls the expression of the dsRNA hairpin loop, permitting the knockdown of the gene. After the addition of the tetracycline 1 ml of each of the four flasks was pipetted into 24 well plates. The cells were left to grow at 37 °C for 48-72

hr. Growth was monitored every 24 hours: 10 μl of each culture was loaded onto the Neubauer improved hemocytometer for parasite counting. The concentration was plotted using Prism 6 (GraphPad software Inc.), where the y-axis represents the number of parasites in a Log10 scale and the x-axis the days post induction.

The growth of the cells was also assessed after genotoxic stress, using methyl methanesulfonate (MMS) (0%, 0.001%, 0.0002%, 0.0003%) and UV radiation (0 J/m^2, 500 J/m^2, 750 J/m^2, 1000 J/m^2 and 1500 J/m^2). The experiment was set up as described above. The appropriate concentration of MMS was added to each well of Tet- and Tet+ cells. In the case of UV exposure, Tet- and Tet+ cells were UV irradiated 24 hour post induction using a Stratagene Stratalinker UV Crosslinker 2400 and left to grow for 72 h.

2.7.2 Growth analysis of knockout cells

The day before the experiment, cells were set up at a concentration of $1x10^5$ cells.ml^{-1} in 10 of HMI-9 medium (Section 2.6.2), containing blasticidin for the heterozygous and null mutants. G418 was slowing the growth of the cells, and so it was not added to the medium containing null mutants. In the case of the WT (Lister 427), no drugs were added to the medium. The following day, the culture was diluted to $5x10^4$ cells.ml^{-1} in HMI-9 medium with the respective drugs and 1 ml of each flask (WT and KO cells) was pipetted to 24 wells plate. Different concentrations of MMS (0%, 0.0001%, 0.0002% and 0.0003%) was added to each well. As no induction was required, cells were exposed to UV (0 J/m^2, 500 J/m^2, 750 J/m^2, 1000 J/m^2 and 1500 J/m^2) immediately.

The cells were left to grow at 37 °C for 48-72 hr. Growth was monitored every 24 h hours post treatment. 10 μl of each culture was loaded onto the Neubauer improved hemocytometer for parasite counting. The concentration was plotted using Prism 6 (GraphPad software Inc.), in where the y-axis represents the number of parasites in a Log10 scale and the x-axis the days post induction. As described the growth was monitored every 24 hours.

2.7.3 Cell Cycle analysis

The day before the experiment, RNAi cell lines and 2T1 cells were set up at a concentration of $1x10^5$ cells.ml^{-1} in 10 ml of HMI-11 thymidine-free media (2.6.2), containing the selective drugs. The following day, the culture (2T1 and RNAi cells) was diluted to $5x10^4$ cells.ml^{-1} in HMI-11 media with the selective drugs and divided into two flasks. Tetracycline (1µg/ml) was added to one flask (Tet+). Every 24 hours the cells were counted and harvested by centrifugation (405xg for 10 minutes at room temperature). Cells were stained with DAPI as described in section 2.10.1.

2.7.4 Flow cytometry

For the assay, $5x10^6$ cells were harvested by centrifugation (405xg for 10 minutes) and washed once with 1x PBS. Cells were re-suspended in the residual supernatant before adding 200 µl of 1% paraformaldehyde (PFA; diluted in 1xPBS) for 10 minutes at room temperature. Fixed cells can be stored at 4 °C before harvesting. Next, the cells were centrifuged at 1620x g for 10 minutes and washed once in 1x PBS. The cells were then re-suspended in 1ml 1x PBS containing 10 µg/ml of propidium iodide (PI; Sigma Aldrich) and 10 µg/ml of RNAse A (Sigma Aldrich), and incubated at 37 °C for 45 minutes in the dark. Samples were filtered through a fine mesh gauze prior analysis using a FACS Calibur (BD Biosciences). Data was acquired from the FL2-A channel and analysed using Flow Jo software (TreeStar).

2.8 Replication assay

Cells were grown in thymidine free media for 24 h. The following day, 4 ml with $1x10^5$ cells were transferred to a vented flask, one with tetracycline and other without tetracycline. After 20 hours, 32 hours and 44 hours the cells were incubated with EdU (Click-iT® EdU Alexa Fluor® 555 Imaging Kit – Life Technologies) for 4 hours at 37 °C with 5% CO_2. Next, the cells were centrifuged at 1000x g for 5 minutes and washed with 1x PBS. The pellet was re-suspended in 20 µl of 1x PBS and the cell suspension was pipetted onto a 12 well slide, pre-treated with poly-L-lysine, and left to settle for 5 minutes. The supernatant was removed and 25 µl of 3.7% paraformaldehyde was added and left for 4 minutes,

followed by a wash with 3% BSA in 1x PBS. The cells were permeabilised by adding 20 µl of 0.2% Triton X-100 (Promega) in 1x PBS for 10 minutes at room temperature. The wells were washed twice with 3% BSA in 1x PBS. The supernatant was removed and 25 µl of the Click-iT reaction was added (Life Technologies) (21.25 µl of 1x Reaction Buffer, 1 µl of $CuSO_4$, 0.25 µl Alexa Fluor 555 Azide and 2.5 µl of 1x Reaction Buffer) for 1 hour at room temperature. The solution was removed and the cells were washed six times with 3% BSA in 1x PBS. The cells were stained with DAPI as described in section 2.10.1.

2.9 Telo FISH analysis

For the Telo-FISH analysis, $5x10^6$ cells were harvested (405x g for 10 minutes) and washed in 1x PBS at 660x g for 3 minutes. The supernatant was removed and the pellet re-suspended in 4% FA in 1x PBS for 20 minutes at room temperature. The cells were washed and re-suspended in 65 µl of 1xPBS and spread onto a pre-treated poly-L-lysine (Sigma Aldrich) slide (left to settle for 20 minutes). The supernatant was removed and the cells permeabilised with 0.1 % TritonX-100 in 1x PBS for 3 minutes. The cells were washed and dehydrated with pre-chilled ethanol in ascending concentration (70-90-100%) for 5 minutes each concentration. The slide was left to dry.

In the meantime, the probe (10 µl) in the hybridization solution (60 µl) (50 % Formamide, 10% Dextran, 2x SSPE buffer [1x SSPE: 0.18 M NaCl, 10 mM NaH_2PO_4, 1 mM EDTA, pH 7.7: use buffer at pH 7.9]) was heated at 85 °C in a water bath for 7 minutes and added to the slide. The slide was sealed and incubated at 95 °C for 5 minutes (water bath), followed by a 16 hours incubation at 37 °C. The telomeric probe recognizes the TTAGGG repeats. Then, the slide was washed for 30 minutes with 2x SSC (Thermo Fisher)/50% Formamide solution at 37 °C (incubator), 60 minutes with 0.2x SCC at 50 °C and a final wash with 4x SSC at room temperature for 10 minutes. Cells were stained for DAPI as described in section 2.10.1.

2.10 Microscopy protocols

2.10.1 DAPI staining

For DAPI staining, $2x10^6$ cells were harvested by centrifugation at 405x g for 10 minutes. The pellet was washed in 1x PBS at 405x g for 3 minutes and the supernatant was removed, leaving ~25 µl in which the cells were re-suspended. The cell suspension was settled on a pre-treated poly-l-lysine (Sigma Aldrich) slide (Menzel-Gläser) for 5 minutes at room temperature. A hydrophobic circle was drawn on the slide by using a PAP pen (Life Technologies). The supernatant was removed and 25 µl of 4% PFA was added for 4 minutes. The PFA was removed and the cells were washed three times in 50 µl of 1xPBS for 5 minutes. 5 µl of DAPI (SouthernBiotech) was added to each well and left at room temperature for 5 minutes. The slide was covered with a coverslip and sealed with nail varnish. Slides were stored at 4 °C.

2.10.2 Immunofluorescence analysis

The cells were prepared as described above (Section 2.10.1). After the fixation step, the cells were permeabilised with 25 µl 1x PBS/Triton X-100 (Thermo Scientific) for 10 minutes. Free-aldehyde groups were neutralised by the addition of 100 mM glycine for 20 minutes. The glycine binds the free aldehyde groups, impeding its binding with the primary and secondary antibody, minimizing the background in the immunofluorescence.   The wells were washed three times with 1x PBS for 5 minutes. To each well, 25 µl of blocking solution (1 % BSA [Sigma], 0.2 % Tween-20 in 1 x PBS) was added for 1 hour (wet chamber). The blocking solution was removed and 25 µl of the primary antibody diluted in blocking solution was added and incubated for 1 hour in a wet chamber (antibody concentration Table 2-5). The wells were washed two times and the secondary antibody was added and incubated for one hour. The cells were washed and DAPI stained as described in section 2.10.1. In the case of the fluorophore-conjugated antibody, the incubation with the secondary antibody was not necessary. The rest of the protocol was followed as described above.

Double immunofluorescence using primary antibodies from the same host specie was performed. For this assay, the samples were incubated with the first

primary and secondary antibody, following the protocol described above with the exception of the DAPI staining. Sequentially the cells were incubated with the blocking solution for a second occasion, followed by the incubation with the fluorophore-conjugated antibody and DAPI staining.

Antibody	Serotype	Target	Clone	Concentration	Manufacturer
α-myc Alexa Fluor 488 conjugated	Mouse (IgG)	Myc	4A6	1:500	Millipore
α-HA	Mouse (IgG)	HA	HA-7	1:1000	Sigma Aldrich
α-myc	Rabbit (IgG)	Myc	4A6	1:100	Millipore
α-γH2A	Mouse (IgG)	Phosphorylated H2A	N/A	1:1000	T. Donatelli Serafim
Alexa Fluor® 488 α- mouse	Goat (for IgG H+L)	Mouse	N/A	1:1000	ThermoFisherScientific
Alexa Fluor® 594 α- mouse	Goat (for IgG H+L)	Mouse	N/A	1:1000	ThermoFisherScientific
Alexa Fluor® 488 α- rabbit	Goat (for IgG H+L)	Rabbit	N/A	1:1000	ThermoFisherScientific
Alexa Fluor® 594 α- rabbit	Goat (for IgG H+L)	Rabbit	N/A	1:1000	ThermoFisherScientific

Table 2-5. Antibody concentration used for immunofluorescence assay.

2.10.3 Measurement of fluorescence intensity

The software Fiji (ImageJ) was used for the measurement of the fluorescence intensity. For the fluorescence analysis, the image has to be in grayscale and the background must be subtracted. The cell of interest was selected by using the drawing/selection tool (circle). A circle of 2.1 x 2.1 pixel region of interest (ROI) was drawn around the cell. The option 'measure' was selected from the 'analyse' menu. This provides, for the area, integrated density (area and the mean gray value) and mean fluorescence value of each cell. For each image a region that has no fluorescence was selected, which corresponds to the background control. The fluorescence was obtained by calculating the corrected total cell fluorescence (CTCF) using the following formula:

$$CTCF = Integrated\ density - (Area\ of\ selected\ cell \times mean\ fluorescence\ of\ background\ readings)$$

The fluorescence was plotted onto a vertical scatter plot using Prism 6 (GraphPad software Inc.).

2.11 Electron microscopy protocols (EM)

Fixation and imaging of the cells was performed by L.Lemgruber-Soares.

2.11.1   Scanning Electron Microscopy (SEM)

Cells ($5x10^6$) were fixed in a solution containing 2.5% glutaraldehyde and 4% PFA in 0.1 M phosphate buffer. Samples were stored at 4 °C until used. The cells were settled on a pre-treated poly-L-lysine cover slip and washed with 0.1 M phosphate buffer. The cells were dehydrated with ethanol in ascending concentration (from 30% to 100%). The cover slip was left to dry and metal coated (gold/palladium). The samples were visualized on a Jeol 6400 scanning electron microscope (Jeol, Japan).

2.11.2   Transmission Electron Microscopy (TEM)

For the TEM $5x10^6$ cells were fixed in a solution containing 2.5% glutaraldehyde and 4% PFA in 0.1 M cacodylate buffer (pH 7.2). The post-fixation was performed for 45 minutes by adding 1 % osmium tetroxide and 2.5 % potassium ferrocyanide (pH7.3) in 0.1 M sodium cacodylate buffer (in the dark). The cells were washed several times with 0.1 M cacodilate buffer. Next, they were stained with 2 % aqueous uranyl acetate and dehydrated in acetone solutions (30, 50, 70, 90 and 100 %). The samples were embedded in Epon resin and sectioned. The visualisation of the sample was performed on a Tecnai T20 transmission electron microscope (FEI, Netherlands).

2.11.3   Image analysis

For images captured on the Axiscope 2 (Zeiss) fluorescence microscope, the 63 x DC magnification lens was used. The images were acquired using the ZEN software package (Zeiss; http://www.zeiss.com/corporate/en_de/home.html). For images captured in the Deltavision RT deconvolution fluorescence microscope, the 1.4/63 x lens was used. Z-stacks were acquired and images de-convolved using SoftWoRx suite 2.0 (Applied Precision, GE). High resolution images were captured on an Elyra PS.1 super resolution microscope (Zeiss) using the 1.4/63 x lens. The images were acquired using the ZEN software.

2.12 Protein analysis

2.12.1   Western blot

$2.5x10^6$ cells were harvested by centrifugation at 1620x g for 10 minutes and washed with 1x PBS by centrifugation (405x g). The pellet was re-suspended in 10 µl of 2x NuPAGE® LDS sample buffer (Invitrogen) and denatured at 100 °C for 10 minutes. Samples were loaded in a NuPAGE 10% Bis-tris protein gel 1.0mm (Life Technology), along with a NovexSharp prestained Standard (Life Technology) that was used as a protein size marker, and 5% NuPAGE MOPS SDS Run buffer (Life Technology). The gel was left to run for 50 minutes at 200 V in a XCell SureLock™ Mini-Cell Electrophoresis System (Life Technologies).

For the protein transfer a PVDF (Amersham Bio) membrane, activated with methanol (GE Healthcare Life Science) was used. The transfer was performed by electrophoresis at 100 V for 1 hour, in a Mini Trans-Blot Electrophoretic Transfer Cell tank (Bio Rad) containing 1x transfer buffer (25 mM Tris pH 8.3, 192 mM Glycine, and 20% (v/v) methanol). After the transfer the membrane was incubated in Ponceau-S solution (Sigma) for one minute, in order to confirm a successful transfer of proteins.

The membrane was washed in 1xPBS-Tween for 5 minutes and incubated in blocking solution (1x PBS, 0.01% Tween and 5% milk) for 1 hour, preventing nonspecific antibody binding. The membrane was incubated with agitation with the primary antibody (Table 2-6), diluted in blocking solution for 1 hour. The membrane was washed twice with agitation for 10 minutes with 1x PBS with 0.001% Tween. After the washes, the membrane was incubated for 1 hour with the blocking solution containing the secondary antibody (Table 2-6). Next, the membrane was washed three times in 1x PBS with 0.001% Tween, in order to reduce the background. For the developing, the membrane was incubated for 1 minute with SuperSignal WestPico Chemi-luminescent Substrate (Thermo Scientific) and exposed onto X-rayfilm (Kodak). In the cases that protein detection failed, the membrane was incubated in ECL Prime western blotting Development Reagents (GE Healthcare Life Sciences) and exposed onto the Hyperfilm ECL film (GE Healthcare Life Sciences).

Antibody	Serotype	Target	Clone	Concentration	Manufacturer
α-HA	Mouse (IgG)	HA	HA-7	1:10000	Sigma Aldrich
α-myc	Mouse (IgG)	Myc	4A6	1:7000	Millipore
α-γH2A	Rabbit (IgG)	Phosphorylated H2A	N/A	1:10000	T. Donatelli Serafim
Ef1α	Mouse (IgG)	Ef1α	CBP-KK1	1:25000	Millipore
α-mouse HRP conjugate	Goat (gor IgG H+L)	Mouse	N/A	1:3000	ThermoFisher Scientific
α-rabbit HRP conjugate	Goat (gor IgG H+L)	rabbit	N/A	1:3000	ThermoFisher Scientific

Table 2-6. Antibody concentrations used for Western Blot.

2.12.2 Immunoprecipitation

2.12.2.1 Preparation of magnetic beads

Approximately 50 μl of Dynabeads® M-28 Sheep α-mouse IgG (Novex®, Life Technologires) magnetic beads were washed twice in cold blocking solution (0.5% BSA in 1x PBS, pH 7.2) for 1 minute, vortexed gently and placed on a DynaMag™-2 magnet (Life Technologies). The supernatant was discarded and the beads were re-suspended in 125 μl of blocking solution containing 5 μg of mouse α-Myc clone 4A6 antiserum (Milipore) or α-HA antiserum (Sigma Aldrich). Due to the lack of polymerase specific antibodies, it was necessary to tag the proteins rather with Myc tag or HA tag, in order to perform the immunoprecipitation. The beads were left overnight on mixing rotor at 4°C.

2.12.2.2 Cell lysis

A total of 5×10^8 cells were harvested by centrifugation at 1620x g for 10 minutes (two flasks were set up for each cell line). The cells were washed once in 1x PBS by centrifugation. Approximately 2.5×10^6 cells were re-suspended in 4x NuPAGE® LDS Sample Buffer (pre-lysis sample). The rest of the sample was re-suspended in 1 ml of whole extract buffer (WCE; 50 mM of HEPES pH 7.55,100 mM NaCl, 1 mM EDTA pH 8, 1 mM EGTA pH 8, 10% Glycerol, 1%Triton X-100, 1 mM DTT, and 2x complete protease inhibitor cocktail - Roche) and lysed at 4°C for 30 minutes. Next, the sample was centrifuged at 15000x g for 30 minutes at

4°C. From the supernatant 30 μl was re-suspended in 4x NuPAGE® LDS Sample Buffer (Input sample) and the remaining 900 μl were saved for the immunoprecipitation.

2.12.2.3   Immunoprecipitation and Elution

The remaining 900 μl was added to the 50 μl of magnetic beads, which were pre-washed three times in blocking solution, and left at 4 °C for 2 hours. The sample was placed on the magnet and 30 μl of supernatant was re-suspended in sample buffer (Flowthrough sample). The remaining supernatant was discarded and the beads were washed five times with washing buffer (50 mM Hepes pH 7.55, 100 mM NaCl, 1 mM EDTA pH 8.0, 1 mM EGTA pH 8.0, 10 % glycerol, 0.1 % Triton X-100, and 2x complete protease and phosphatase inhibitor cocktail; Roche). For this step the washing buffer was added to the beads, the beads were gently shaken and placed on the mixing rotor for 5 minutes. After the last wash, the supernatant was discarded and the beads were centrifuged at 1000x g for 3 minutes. The beads were placed on the magnet, in order to discard the supernatant, and the beads were re-suspended in 15 μl of 1x NuPAGE® LDS Sample Buffer (gently vortexed). The beads were incubated at 70 °C for 10 minutes, then the beads were placed on the magnet and the supernatant collected (Eluate sample). 1 μl of the eluate sample was added to 1 μl of 1x NuPAGE® LDS Sample Buffer for Western blot analysis (Section 2.12.1)The remaining 14 μl were saved for SYPRO® Ruby staining and for mass spectrometry analysis (Glasgow Polyomics). For this reason two samples were set up for each cell line.

2.13 SYPRO® Ruby staining

After electrophoresis, the gel was placed in a clean polypropylene container with fixation solution (100 ml 7 % (v/v) acetic acid and 50 % (v/v) methanol diluted in MilliQ water) and left to agitate for 30 minutes. The fixation solution was discarded and 60 ml SYPRO® Ruby gel stain (Molecular ProbesTM, Life Technologies) was added and left agitating overnight. Next, the gel was transferred to a clean container with wash solution (7 % (v/v) acetic acid and 10% (v/v) methanol diluted in MilliQ water) and left to agitate for 30 minutes. The wash solution was discarded and the gel washed twice with MilliQ water for

5 minutes on agitation. The gel was imaged using a Typhoon 8600 Variable Mode Imager (Amersham Biosciences) using the 457 mm Blue I and Blue II emission filters.

3 The importance of Translesion DNA Polymerases in *Trypanosoma brucei*

3.1 Introduction

3.1.1 Translesion DNA synthesis pathway in Eukaryotes

DNA replication is a high fidelity mechanism, with an error incidence of 10^{-7} to 10^{-8} in *Escherichia coli* (Kunkel, 2004). It is suggested that, in eukaryotes, A and B family DNA polymerases (Pols) have an error incidence of 10^{-7} to 10^{-8} during DNA synthesis (Kunkel, 2004). This pathway is extremely efficient in part because of the capacity of the replicative DNA Pols to recruit the correct nucleotide, allied to the proofreading activity of the DNA Pols permitting the excision of incorrectly inserted nucleotides. In addition, the overall error rate of replication is reduced further by post-replicative repair strategies to remove mispaired bases (Sale, 2013). Even though these characteristics are required for efficient replication, the replication machinery can be unstable in the presence of damage, provoking a stall of the replication fork (Sale 2013). For this reason, the cells have evolved diverse repair mechanisms to maintain the integrity of the genome (Iyama and Wilson, 2013; Gao *et al.*, 2017)

Several DNA repair pathways can be found in eukaryotes, including base excision repair (BER), mismatch repair (MMR), nucleotide excision repair (NER), homologous recombination (HR) and non-homologous end joining (NHEJ). In addition, there is a damage tolerance pathway, termed translesion synthesis (TLS) (Iyama and Wilson, 2013; Gao *et al.*, 2017). The first three repair mechanisms directly remove lesions from the DNA template before the replication fork encounters them, ensuring synthesis on a damage free template. Unfortunately, these repair mechanisms can fail, risking the integrity of the cell (Iyama and Wilson, 2013; Gao *et al.*, 2017).

When replicative DNA Pols encounter an unrepaired lesion, this can result in the replication fork stalling and the subsequent death of the cell if the blockade is not tackled (Sale, 2013). Therefore, the presence of HR, NHEJ and and TLS are necessary to ensure cell survival (Iyama and Wilson, 2013; Sale, 2013).The difference between the three mechanisms is the ability to tackle the lesions in 'error free' or 'error prone' manners (Gao *et al.*, 2017). HR is generally considered error-free, since it relies on copying sequence from an intact template. NHEJ is frequently error-prone, since DNA breaks are processed

to allow rejoining. However, NHEJ normally occurs during G0/G1, meaning lesions in S-phase are normally tackled by HR (Karanam *et al.*, 2012; Iyama and Wilson, 2013).

The TLS pathway has the ability to insert nucleotides opposite DNA lesions, meaning the lesion is not immediately repaired. In addition, this pathway is notable for its low fidelity, due to the lack of proofreading activity in most of the translesion DNA pols (TLS pols) involved in this process (Li, Gao and Wang, 2011; Sale, 2013). Such lack of proofreading activity may increase the probability of spontaneous mutations but, despite this, TLS has been conserved throughout evolution, revealing its importance for cell viability (Friedberg, Wagner and Radman, 2002; Sale, 2013). In fact, mutations generated during TLS can have a role in evolution or adaptation, an effect that has been demonstrated in bacteria, showing that genome sequence changes generated by the TLS pathway can have important functions during population diversification, which is a decisive event during adaptive evolution (Taddei *et al.*, 1997; Rosenberg, 2001; Friedberg, Wagner and Radman, 2002). Moreover, TLS pols in human cells are involved in somatic hypermutation, increasing the diversification of immunoglobulin genes by the insertion of mutations within the variable region (Friedberg, Wagner and Radman, 2002; Saribasak *et al.*, 2012). An example of this positive function was confirmed in experiments showing that inhibition of DNA PolZ provokes a decrease in somatic hypermutation (Friedberg, Wagner and Radman, 2002; Saribasak *et al.*, 2012). Although the activity of the TLS pathway can be beneficial, it can also represent a risk for the cells (Friedberg, Wagner and Radman, 2002). For instance, in organisms such as humans, these mutations increase the probability of cancer (Friedberg, Wagner and Radman, 2002). For this reason, cells have efficient mechanisms to regulate the intervention of TLS pols during replication (Friedberg, Wagner and Radman, 2002).

3.1.2 Translesion DNA synthesis pathway in trypanosomes

In trypanosomes, many DNA repair pathways have been documented, but less attention has been paid to the TLS pathway (Passos-Silva *et al.*, 2010; Genois *et al.*, 2014). In *T. brucei, T. cruzi* and *L. major,* several TLS pols have been reported to be present in the parasites including Polymerase kappa (Pol κ),

Polymerase eta (Polη), Polymerase zeta (PolZ), Rev1 and two PrimPol-like proteins (PPL1 and PPL2) (Passos-Silva *et al.*, 2010; Rudd *et al.*, 2013) .

The overexpression of Polκ and Polη in *T. cruzi* results in an increase in tolerance to H_2O_2, suggesting that these enzymes are capable of inserting nucleotides opposite oxidative lesions (Rajão *et al.*, 2009; Passos-Silva *et al.*, 2010). The ability of the cells to tolerate oxidative stress is of high importance, given that *T. cruzi* parasite cells, especially amastigotes, have to deal with reactive oxygen species (ROS) inside the host cell (Passos-Silva *et al.*, 2010) .

It has been hypothesized that the TLS pathway in *T. cruzi, T. brucei and Leishmania*, may have an important role during genetic diversification of surface protein genes (Passos-Silva *et al.*, 2010), due to its capacity to insert mutations during lesion bypass (Passos-Silva *et al.*, 2010). If correct, this might increase the efficiency of the evasion mechanism of the parasite when confronted by the immune system of the host (Passos-Silva *et al.*, 2010). However, to date concrete evidence of a role of any TLS pol, or the wider pathway, in immune tolerance is lacking. Indeed, experimental evaluation of the importance of the range of TLS Pols in parasite biology, and their modes of action, is notably absent.

Little research has been conducted to investigate the tolerance repair pathway in *T. brucei*, beyond two Primase-Polymerase (Prim Pol) putative proteins, PPL1 and PPL2 (Rudd *et al.*, 2013). Prim Pol proteins belong to the archaeo-eukaryotic primase (AEP) superfamily. In archaea and prokaryotes, AEP proteins are known to have a nucleotidyltransferase activity (Iyer *et al.*, 2005). In certain bacteria, such as *Mycobacterium tuberculosis*, is known to be involved in DNA repair (Della *et al.*, 2004). In *T. brucei,* TLS activity of PPL1 and PPL2 have been confirmed; revealing their capacity to insert nucleotides opposite T-T 6-4 photoproducts (Rudd *et al.*, 2013). As such, there is a lack of information about the range of function of TLS pols in the parasite. Three TLS pols were chosen for this study: Polymerase Zeta catalytic subunit (TbRev3), Polymerase Nu (also known as Polymerase Theta polymerase domain; TbPolN) and Polymerase Theta helicase domain (TbHelQ). TbPolZ was obtained as a hit in an RNAi screen which demonstrated that depletion of the protein generates an

increase in cell sensitivity towards the alkylating agent Methyl methanesulfonate (MMS) (Stortz *et al.*, 2017). The same study suggested a similar effect following loss of Pol κ, but as this is encoded from a multicopy gene family (Berriman *et al.*, 2005; Passos-Silva *et al.*, 2010), it was more problematic to evaluate. Unpublished studies conducted in procyclic *T. brucei* cells demonstrated the possible interaction of TbHelQ with proteins involved in HR (Marko Prorocic, unpublished). TbPolN was chosen due to its potential interaction with TbHelQ, as has been proposed in other organisms (Marini *et al.*, 2003).

The aim of this chapter was to study the effect of depletion by RNAi of three putative TLS pols, TbPolN, TbHelQ and TbPolZ (Rev3), on BSF parasite growth *in vitro*. These data will contribute to understanding if these proteins are involved in the survival of the cells.

3.2 Bioinformatics Analysis

3.2.1 Blast Analysis

Due to the lack of information about TLS pols in *T. brucei*, it was important to search for homologues in other species, with the aim of elucidating if the function of these proteins resemble the functions described in other organisms. Available information for the three TLS pols of interest is shown in Table 3-1, which summarises the product annotation of each gene in tritrypDB, plus chromosome and predicted protein size. To evaluate if the annotations are accurate, the predicted polypeptides were used firstly in standard protein-protein Basic Local Search Tool (Blastp) searches (https://blast.ncbi.nlm.nih.gov/Blast.cgi).

Name	Gene ID	Chromosome localization	Protein Size
Polymerase Nu or Polymerase Theta DNA polymerase domain **(TbPolN)**	Tb927.11.5550	Chromosome 11	98.829 kDa
Polymerase Theta helicase domain **(TbPolQ (HelQ))**	Tb927.8.3350	Chromosome 8	115.095 kDa
Polymerase Zeta catalytic subunit **(TbRev3)**	Tb927.8.3290	Chromosome 8	216.883 kDa

Table 3-1-General information of TbPolN, TbHelQ and TbRev3. Gene ID of the specific gene that encodes for each particular protein, the chromosome localization and the expected protein size (data obtained from TriTrypdb.org; correct as of June 2017).

The protein sequences of TbPolN, TbHelQ and TbRev3 were each used as query sequences against the protein non-redundant (nr) database (Li *et al.*, 2013), in an effort to identify homologous proteins. A second analysis of the protein sequences was then conducted by using the SmartBLAST (http://blast.ncbi.nlm.nih.gov/smartblast/) tool, whose aim is to identify potential matches from distantly related organisms compared to that of the input sequence. The top five 'hits' identified by Blastp and SmartBLAST are summarized in Table 3-2 and Table 3-3, respectively.

Description	Query cover	E value	Ident	Accession	Protein Query
DNA polymerase theta [*Trypanosoma brucei brucei* TREU927]	100%	0.0	100%	XP_828630.1	TbPolN
DNA polymerase theta, putative [*Trypanosoma brucei gambiense* DAL972]	100%	0.0	99%	XP_011779772.1	TbPolN
putative DNA polymerase theta [*Trypanosoma congolense* IL3000]	99%	0.0	41%	CCC95167.1	TbPolN
DNA polymerase theta (polymerase domain only) [*Trypanosoma grayi*]	88%	0.0	41%	XP_009311251.1	TbPolN
DNA polymerase theta (polymerase domain only) [*Trypanosoma cruzi* strain CL Brener]	95%	1e-179	39%	XP_818250.1	TbPolN
DNA polymerase theta (helicase domain only) [*Trypanosoma brucei brucei* TREU927]	100%	0.0	100%	XP_847166.1	TbHelQ
DNA polymerase theta (helicase domain only), putative [*Trypanosoma equiperdum*]	100%	0.0	99%	SCU66137.1	TbHelQ
DNA polymerase theta (helicase domain only),putative [*Trypanosoma brucei gambiense* DAL972]	100%	0.0	99%	XP_011775640.1	TbHelQ
putative DNA polymerase theta (helicase domain only) [*Trypanosoma congolense* IL3000]	99%	0.0	59%	CCC92122.1	TbHelQ
ATP-dependent RNA helicase, putative [*Trypanosoma cruzi*]	88%	0.0	60%	EKG08646.1	TbHelQ
DNA polymerase zeta catalytic subunit [*Trypanosoma brucei brucei* TREU927]	100%	0.0	100%	XP_847160.1	TbRev3
DNA polymerase zeta catalytic subunit, putative [*Trypanosoma equiperdum*]	100%	0.0	99%	SCU66131.1	TbRev3
DNA polymerase zeta catalytic subunit, putative [*Trypanosoma brucei gambiense* DAL972]	100%	0.0	99%	XP_011775634.1	TbRev3
putative DNA polymerase zeta catalytic subunit, fragment [*Trypanosoma vivax* Y486]	99%	0.0	46%	CCC49665.1	TbRev3
DNA polymerase delta catalytic subunit, putative [*Trypanosoma cruzi*]	91%	0.0	52%	CCC49665.1	TbRev3

Table 3-2. Top Five Blastp 'hits' for TbPolN, TbHelQ and TbRev3, obtained from the NCBI database. Comparing the query sequence with closely related *Trypanosome* species. Blastp hits, showing the E value and the percentage of identity for each hit (Data recovered June, 2017).

Description	Query cover	E value	Ident	Accession	Protein Query
DNA polymerase theta (polymerase domain only), putative (*Leishmania donovani*)	57%	9e-84	33%	XP_003861182.1	TbPolN
DNA polymerase theta [*Danio rerio*]	36%	8e-27	28%	XP_009293682.1	TbPolN
MUS308 and mammalian DNA polymerase-like protein [*Arabidopsis thaliana*]	36%	1e-25	28%	NP_001078482.1	TbPolN
DNA polymerase theta isoform X4 [*Mus musculus*]	35%	5e-24	28%	XP_006522799.2	TbPolN
DNA polymerase theta isoform X6 [*Homo sapiens*]	35%	8e-24	27%	XP_011510656.1	TbPolN
Hypothetical protein DDB_G0279107 [*Dictyostelium discoideum* AX4]	76%	7e-143	34%	XP_641869.1	TbHelQ
Helicase POLQ-like isoform X3 [*Homo sapiens*]	75%	2e-142	35%	XP_005262770.1	TbHelQ
Helicase POLQ-like [*Mus musculus*]	76%	3e-141	35%	NP_001074576.1	TbHelQ
Helicase and polymerase-containing protein TEBICHI isoform X2 [*Glycine max*]	72%	1e-130	34%	XP_014622422.1	TbHelQ
MUS308 and mammalian DNA polymerase-like protein [*Arabidopsis thaliana*]	71%	1e-123	34%	NP_001078482.1	TbHelQ
DNA polymerase zeta catalytic subunit, putative [*Leishmania donovani*]	50%	0.0	55%	XP_003861052.1	TbRev3
Recovery protein 3 [*Arabidopsis thaliana*]	50%	4e-132	36%	NP_176917.2	TbRev3
DNA polymerase zeta catalytic subunit isoform X2 [*Glycine max*]	37%	1e-130	36%	XP_006577240.1	TbRev3
Rev3p [*Saccharomyces cerevisiae* S288c]	37%	4e-121	39%	NP_594068.1	TbRev3
DNA polymerase zeta catalytic subunit Rev3 (predicted) [*Schizosaccharomyces pombe* 972h-]	30%	7e-119	38%	NP_594068.1	TbRev3

Table 3-3. Top five SmartBlast 'hits' for TbPolN, TbHelQ and TbPolZ (Rev3), obtained from the NCBI database. Comparing the query sequence with distantly related organisms. SmartBlast five top 'hits', showing the E value and percentage of identity for each hit. Data recovered June, 2017.

The 'hits' obtained with standard Blastp indicate that TbPolN, TbHelQ and TbRev3 are conserved amongst the class kinetoplastida, with syntenically conserved genes identified in different *Trypanosoma* species. For *T. brucei brucei, T. brucei gambiense* and *T. congolense,* PolN gene is localised in chromosome 11. Unlike the other species, in *T. cruzi* PolN is found in chromosome 26. In the case of *T. grayi,* the localisation of the gene has not been assigned. On the other hand, HelQ gene is localised in chromosome 8 with exception of *T. cruzi,* which is found in chromosome 32. PolZ gene is found in chromosome 8 on *T. brucei brucei, T. brucei gambiense* and *T. congolense*. The localisation of PolZ gene in *T. equiperdum* and *T. cruzi* genome still unknown. The level of sequence homology followed predictions of phylogenetic distances between species, with *T. cruzi* always the most distantly related to the *T. brucei* subspecies. The Smart Blast analysis revealed *Leishmania* homologues for TbPolN and TbRev3 (Table 3-3).

Notably, in all cases DNA PolN and PolQ were encoded from separate genes, suggesting that none of the kinetoplastids encode a single protein with both polymerase and helicase domains. PolQ with dual domain (polymerase and helicase domain), has so far has only been described in metazoan organisms, including humans, *D. melanogaster* and *C. elegans* (Wood and Doublié, 2016; Wyatt *et al.*, 2016).

From the SmartBLAST analyses, homologues in organisms aside from the kinetoplastid group were identified. One species appeared as a common 'hit' in the analysis of the three proteins; *Arabidopsis thaliana*, with an E value of 1e-25, 1e-123 and 4e-132 for TbPolN, TbHelQ and TbRev3, respectively. *Homo sapiens* was one of the top 'hits' for TbPolN (8e-24; XP_011510656.1) and for TbHelQ (2e-142; XP_005262770.1). For TbPolN it was notable that the genes identified did not encode proteins with only a polymerase domain, but instead DNA Pol theta was recovered, which encodes both a helicase-like domain and a polymerase-like domain (Yousefzadeh and Wood, 2013). Thus, this reinforces the close evolutionary relationship between the dual-domain and single-domain proteins. Nonetheless *H. sapiens* helicase PolQ-like (2e-142; XP_005262770.1), which is just a predicted helicase, was a top 'hit' for TbHelQ, suggesting this protein may be more homologous to the parasite helicase.

3.2.2 Protein domain predictions

The study of protein structure is of high relevance, permitting a better prediction of the functions played in the organism (Karplus and Kuriyan, 2005). Due to this the domain organization of TbPolN, TbHelQ and TbRev3 was analysed, in the attempt to comprehend their roles in the parasite.

To identify potential protein domains, analysis using two software packages, Pfam (http://pfam.xfam.org/) and InterPro (https://www.ebi.ac.uk/interpro/), was performed. These software are databases of known protein families, which includes their domains and functional sites (Sonnhammer *et al.*, 1998; Finn *et al.*, 2017). Pfam and Interpro align the unknown proteins to the database, finding the conserved domains present in the protein of interest(Sonnhammer *et al.*, 1998; Finn *et al.*, 2017).

The protein structures were subsequently compared to their respective human homologues. The structure of TbPolN and TbHelQ resemble the domain organization of *H. sapiens* PolN and HelQ, respectively. In the case of TbPolN (Figure 3-1 A-D), the presence of a polymerase palm domain, which is characteristic of A family polymerases, was seen. On the other hand, TbHelQ is composed of a helicase domain and a DEAD/DEAH box domain, both domains of which are characteristic of SF2 family helicases (Fairman-Williams, Guenther and Jankowsky, 2010). Thus, TbHelQ resembles the domain organization of the human HelQ (Figure 3-1C-D). These data confirm that neither TbPolN nor TbHelQ harbour both domains, as can be found in *A. thaliana* and *H. sapiens* PolQ (Figure 3-1 E-F).

In the case of TbRev3, a polymerase domain, a multifunctional domain (characteristic of B family DNA polys) and an N- terminal exonuclease domain are conserved between *T. brucei. H. sapiens* and *A. thaliana* (Figure 3-2). The human PolZ catalytic Rev3 subunit has the presence of an N-terminal domain, with unknown function, that is absent in the other two species. There is also the presence of an extra C-terminal exonuclease domain and a C-terminal zinc finger domain in the human and the plant proteins that is not present in the *T. brucei* polymerase subunit (Figure 3-2 B-C).
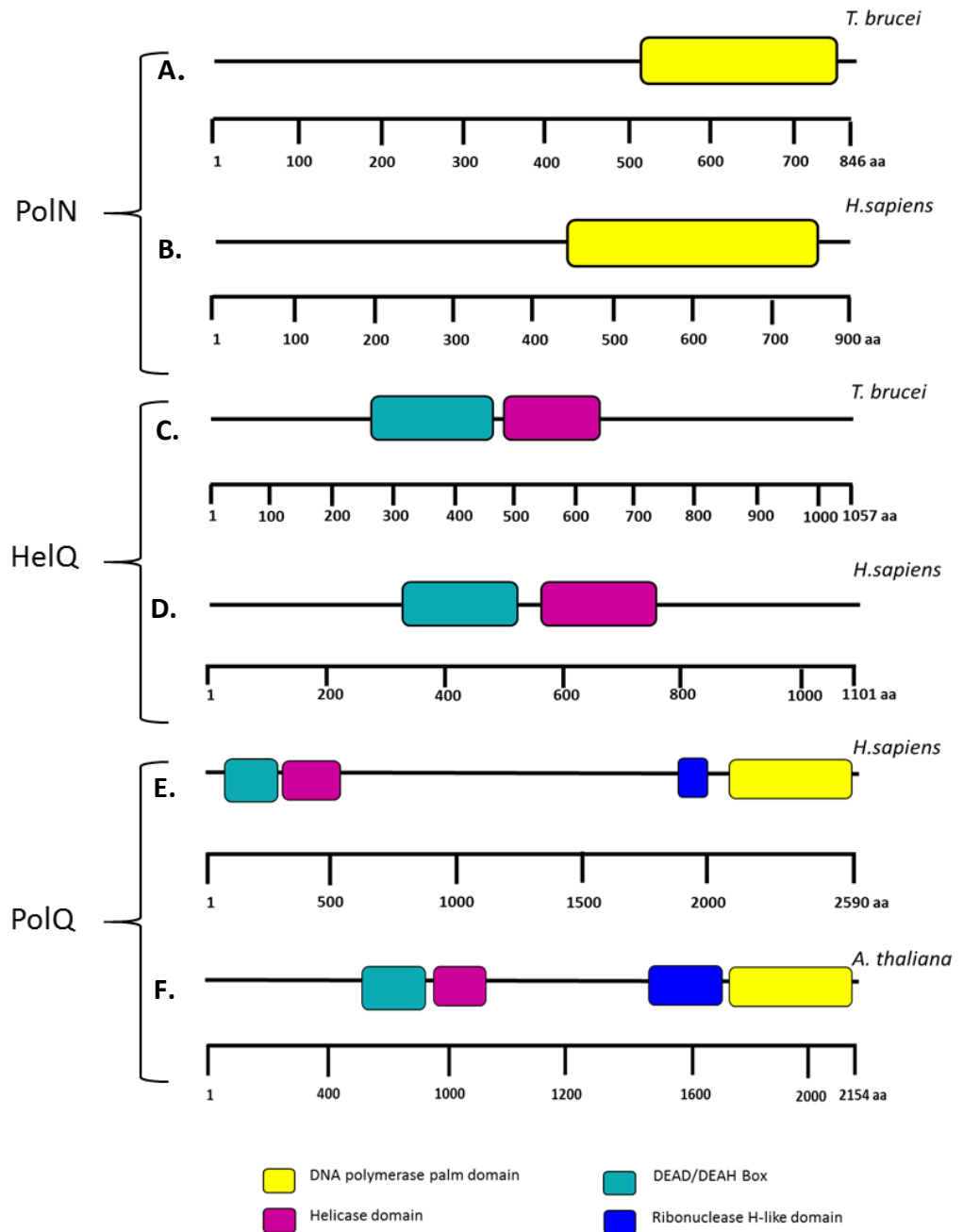
Figure 3-1. Schematic representation of conserved domains of TbPolN and TbHelQ compared against human and plant homologues. A-B. Domain organization of TbPolN and *H. sapiens* PolN. **C-D.**Domain organization of Tb HelQ and *H. sapiens* HelQ. **E-F.** Domain organization of *H. sapiens* and *A. thaliana* PolQ. See legend for domain colour coding.
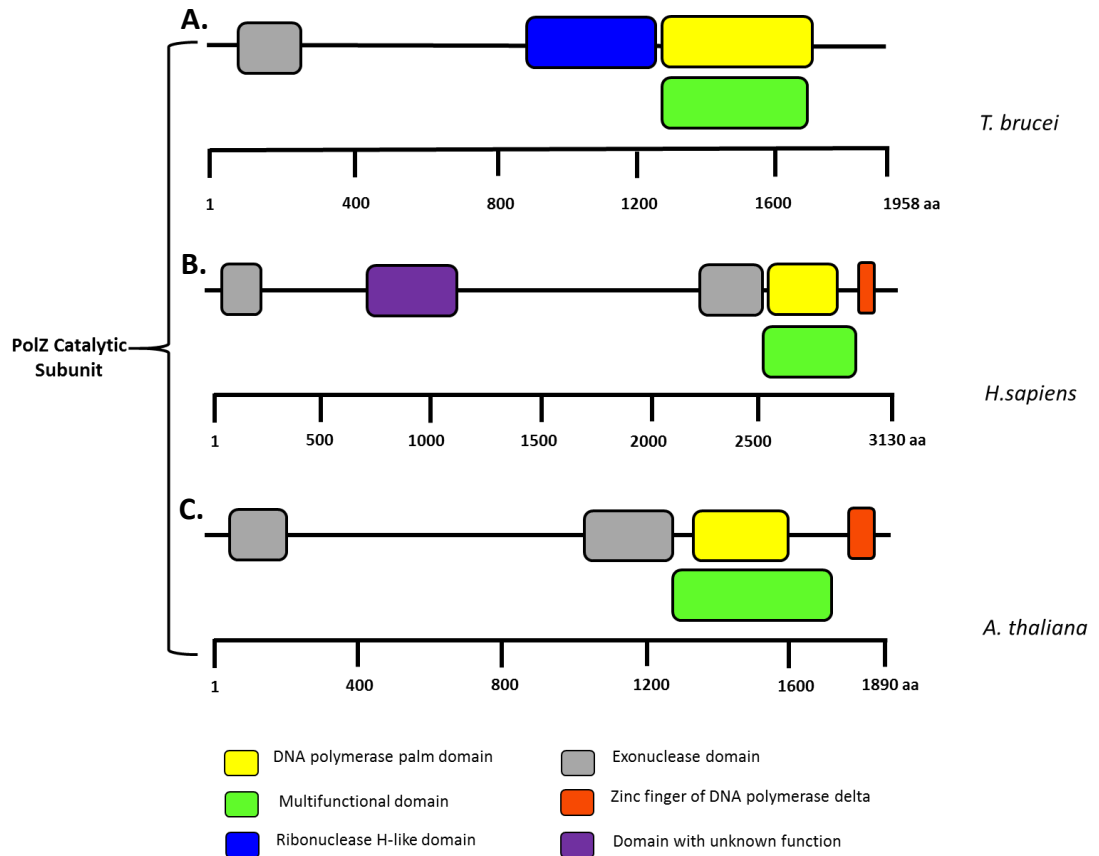
Figure 3-2. Schematic representation of conserved domains of PolZ catalytic subunit Rev3. Conserved domains of TbRev3, compared against *H. sapiens* and *A. thaliana* homologous proteins. The color-coded legend identifies the distinct domains constituting each protein.

3.2.3 Conserved Motifs

To identify conserved motifs in the putative *T. brucei* TLS pols, the protein sequences of TbPolN (Tb927.11.5550) and TbHelQ (Tb927.8.3350) were obtained from TriTrypDB v. 33 and compared against the human protein sequences of PolQ (XP_011510656.1), PolN (Gene ID: 353497) and HelQ (XP_005262770.1), for which the protein sequences were obtained from the NCBI database. The alignment was carried out using the multiple sequence alignment software ClustalW2. In the case of the polymerase domain, it was possible to observe the presence of six conserved motifs (Figure 3-3) characteristic of A family polymerases (Delarue *et al.*, 1990; Yousefzadeh and Wood, 2013). On the other hand, TbHelQ displayed conservation within the helicase domain across 7 conserved motifs characteristic of the SF2 helicase family (Figure 3-4) (Hall and Matson, 1999; Fairman-Williams, Guenther and

Jankowsky, 2010). The presence of sequence inserts in the polymerase domain of *Drosophila melanogaster* (Mus308) and the human dual helicase-polymerase, PolQ, which are absent in TbPolN, suggest the parasite protein is closer in function to the stand alone human polymerase, *H. sapiens* PolN.

The same analysis was conducted for TbPolZ catalytic subunit Rev3 (Tb927.8.3290) and compared against *H. sapiens* (Gene ID: 5980) and *A. thaliana* Rev3 (NP_176917.2) (Figure 3-5). In this alignment, it was possible to identify six conserved motifs that characterize members of the B family polymerases (Lin, Wu and Wang, 1999).

A.

Motif	Sequence
1	(F)N••(S)••QL•••(L)
2	(T)(G)(R)
3	(D)•(S) ••(E)
4	(K)•••(Y)(G)
5	V(H)(D)(E)
6	(Q)(G)(S)

B.

```
                                  1
T. brucei_PolN      SKYSGGC FSVRE--ATAEVM VDCLRDTYGYNLSVNGSFDKQLQKLYRGAGKGNESGRKLA
H. sapiens_PolN     HFVAGER FLITSNNQLREIL FGKLKLHLLSQRN------------------S---LPRTG
H. sapiens_PolQ     YQLAGHS FSFTSSDDIAEVL FLELKLPPNRB MKNQGS-KKTLGS----TRRGIDNGRKLR   Insert 1
D.melanogaster_Mu308 YEQHGSR TNLGSSQAVAKVL GLHRKAK-------------------------
                         *   * . .      ::: :          :

T. brucei_PolN      HVWLAIRERTDFMRTLRSNVENMNM---LDRIVDVATQVASNEEDEGANDCSGSGGSSVG
H. sapiens_PolN     LQK-YPSTSEAVLNALRDLHPLPKIILEYRQVHKIKSTF-----VDGLLACMKKG-----
H. sapiens_PolQ     LGR-QFSTSKDVLNKLKALHPLPGLILEWRRITNAITKV-----VFPLQREKCLN-----
D.melanogaster_Mu308 --G-RVTTSRQVLEKL--NSPISHLILGYRKLSGLLAKS-----IQPLMECC--------
                         .:. *             :      ::     :
                                         2
T. brucei_PolN      STKKAVCYSVHPHWAV HHTSTGRLYCSRPNLQT VPKTAQKCTY--VS--PL---------
H. sapiens_PolN     ---SI-----SSTWNQ TGTVTGRLSAKHPNIQG ISKHP-IQITT------PKNFK-----
H. sapiens_PolQ     ---PFLGMERIYPVSQ SHTATGRITFTEPNIQN VPRDFEIKMPT LVGESPPSQAVGKGLL   Insert 2
D.melanogaster_Mu308 ------QADRIHGQSI TYTATGRISMTEPNLQN VAKEFSIQVGSDVV------------
                                 * ***:  ..**:* : :
                                                                3
T. brucei_PolN      ----------------------TSDYGLLFTNPEWTMRHLYGPAP- GCVLLSFDFNQM
H. sapiens_PolN     ----------G-----------KEDKIL---TISPRAMFVS-SK GHTFLAADFSQI
H. sapiens_PolQ     PMGRGKYKKGFSVNPRCQAQMEERAADRGMPF---SISMF HAFVPFP- GGSILAADYSQL
D.melanogaster_Mu308 ----------------------HISCRSPFMPTDE SRCLLSADFCQL
                                         : *   :     .  :*: *: *:
         3                                                        4
T. brucei_PolN      ELRVL AHLSGDELLIKHLSS--EYDVLSAMTRHITGLSDDEQVPPHLF ETVKVVVYGLFY
H. sapiens_PolN     ELRIL THLSGDPELLKLFQESERDDVFSTLTSQWKDV-PVEQVTHADF EQTKKVVYAVVY
H. sapiens_PolQ     ELRIL AHLSHDRRLIQVLNT--GADVFRSIAAEWKMI-EPESVGDDLF QQAKQICYGIIY
D.melanogaster_Mu308 EMRIL AHMSQDKALLEVMKS--SQDLFIAIAAHWNKI-EESEVTQDLF NSTKQVCYGIVY
                     *:*:*:*:* *  *::  :.  :     *:: ::: ..:  ..* *:.* : .:..*

T. brucei_PolN      GMGLATMKERVKILMDSAHSVPSSQRKFTADTLLRAFHQRYPAAGKFLTRARIRAFHEAR
H. sapiens_PolN     GAGKERLAACLGVPIQE-----------AAQFLESFLQKYKKIKDFARAAIAQCHQTGC
H. sapiens_PolQ     GMGAKSLGEQMGIKEND-----------AACYIDSFKSRYTGINQFMTETVKNCKRDGF
D.melanogaster_Mu308 GMGMRSLAESLNCSEQE-----------ARMISDQFHQAYKGIRDYTTRVVNFARSKGF
                     * *    :   :   :.           *      *  . *   .:   .   . .
                                             6
T. brucei_PolN      CVTLT-------GINDLSSEKDGNF RRQHSIARILQGSSSTLFQS AMVKVHERRHDIVPN
H. sapiens_PolN     VVSIMGRRRPLPRIHAHDQQLR-AQ AERQAVNFVVQGSAADLCKL AMIHVFTAVAASH--
H. sapiens_PolQ     VQTILGRRRYLPGIKDNNPYRK-AH AERQAINTIVQGSAADIVKI ATVNIQKQLET FHST   Insert 3
D.melanogaster_Mu308 VETITGRRRYLENINSDVEHLK-NQ AERQAVNSTIQGSAADIAKN AILKMEKNIERYREK
                     ::         *:           :.:::  :***: : : * :::
                                                       5
T. brucei_PolN      -------------------------LPA APFALVLCIHDELIYSVV EGYVDVVARKI
H. sapiens_PolN     ----T-------------------- LTARLVAQIHDELLFEVE DPQIPECAALV
H. sapiens_PolQ     FKSHGHREGMLQSDQTGLSRKRKLQGMFCPIR GGFFILQLHDELLYEVA EEDVVQVAQIV
D.melanogaster_Mu308 LALGD-------------------- NSVDLVMHLHDELIFEVP GKAKKIAKVL
                                             ::  :****::.*         *  :
```

Figure 3-3.Diagram illustrating the characteristic motifs within members of A family polymerases. A. Conserved sequence motifs within A family polymerases. "()" represents an amino acid (aa) residue known to be located in a specific position and that is conserved in almost all four sequences; "aa" represents an aa known to occupy a specific position but that can be replaced by another aa; "•" denotes any aa can occupy that position. A family of polymerase conserved sequences obtained from (Delarue *et al.*, 1990; Yousefzadeh and Wood, 2013) **B.** Characteristic motifs of the A family polymerases are labeled in yellow and, in purple, polymerase domain inserts in *H. sapiens* PolQ are labelled.

A.

Motif	Conserved Sequence
Q	(L)••••(Q)
I	++•••∘G•(G)(K)(T)
Ia	(P)••••L(A)
II	(V)(D)(E)•(H)
III	+•+(S)(A)(T)•••
IV	++(F)••∘•∘
IVa	CH(G)••••••(R)••••••(F)
V	+•(T)•••••(G)+∘+•
VI	(Q)••(G)(R)••(R)

B.

```
                                              Q                        I
H. sapiens_PolQ      --LLLANWGLPKAVLEKYHS-FGVKH MFEWQAE CLLLGQVLEGKNI VYSAPTSAGKT VA
T. brucei_PolQ(HelQ) VDDPDFFYDLPVSVKDFYATRRGIKH LYNWQHE VLMRDDIRAGGSI VYSLPTSGGKT VA
H. sapiens_HelQ      SNDLGPFYSLPSKVRDLYAQFKGIEH LYEWQHT CLTLNSVQERKNL IYSLPTSGGKT VA
                       :.**  *  :  *    *::.:::**    *  ..:   :.** ***.******

                                     Ia
H. sapiens_PolQ      ELLILKRVLEMRKKALFIL PFVSVAH EKKYYLQSLFQEVGIKVDGYMGSTS---PSRHFS
T. brucei_PolQ(HelQ) EISLLRCLINRGQSCLFVL PFVSLAE EKTDAMIPLGDVLGFTVDGHYSTRGRFPLPV---
H. sapiens_HelQ      EILMLQELLCCRKDVLMIL PYVAIVQ EKISGLSSFGIELGFFVEEYAGSKGRFPPTKRRE
                     *: :*: ::   :. *::**:*::..:**   :  :    :*: *:  :

                                           II
H. sapiens_PolQ      SLDIAVCTIERANGLINRLIEENKMDLLGM VVVDELHM LGDSHRGYLLELLLTKICYITR
T. brucei_PolQ(HelQ) SKAVFVCTIEKANSLVNHMLEENTIGRIGT IVVDELHM LGETSRGATLELLLTKLLCLR-
H. sapiens_HelQ      KKSLYIATIEKGHSLVNSLIETGRIDSLGL VVVDELHM IGEGSRGATLEMTLAKILYTS-
                     .  : :.***:.:.*:* ::*  .:* .:**:*******:*:  **  **: *:*:

                                   III
H. sapiens_PolQ      KSASCQADLASSLSNAVQI VGMSATLPN LELVASWLNAELYHTDFRPVPLLESVKVGNSI
T. brucei_PolQ(HelQ) --------------HKVQI IGMSATIPN LPDIARWLRASCYIGNYRPVPLRQYAVVGGEV
H. sapiens_HelQ      --------------KTTQI IGMSATLNN VEDLQKFLQAEYYTSQFRPVELKEYLKINDTI
                           :  .**:*****: *:  :  :*.*. *   ::*** *:   :... :

                                                          IV
H. sapiens_PolQ      YDSSMKLVREFEPM--L-------QVKGDEDHVVSLCYETICDNHS VLLFCPSKKI CEKL
T. brucei_PolQ(HelQ) LEDGREVCRSLVAA----------GHTSESSQ-LVF-LTTEVKGAS VLVFCASRQQ TVST
H. sapiens_HelQ      YEVDSKAENGMTFSRLLNYKYSDTLKKMDPDHLVAL-VTEVIPNYS CLVFCPSKKI CENV
                       : .  .:        .  :  .:  : :       . * *:** *::    .

H. sapiens_PolQ      ADIIAREFYNLHHQAEGLVKPSECPPVILEQKELLEVMDQLRRL-PSGLDSVLQKTVPWG
T. brucei_PolQ(HelQ) ARLIARSRKEEVDKEGGVR---------YNASSLALVADLRAL-DSEESSLLSQLVPYG
H. sapiens_HelQ      AEMICKFLSKEYLKHKE-----------KEKCEVIKNLKNIGNGNLCPVLKRTIPFG
                     * :*.:  :   :  :       .  ::  :*:  :   :*.:  :*:*

                       IVa                    V
H. sapiens_PolQ      VAF HHAGLTFEERDIIEGAF RQGLIRVL AATSTLSSGVNLPAR RVIIRTPIFGGRPLDIL
T. brucei_PolQ(HelQ) VAF HHGGLVAEERTLIETAF RRRSIGVL CCTSTLAAGVNLPAR RVIFKTPFVAVDFLTKS
H. sapiens_HelQ      VAY HHSGLTSDERKLLEEAY STGVLCLF TCTSTLAAGVNLPAR RVILRAPYVAKEFLKRN
                     **:**.**. :** ::* *:     :  : .****::**********:::*  ..   *

                       VI
H. sapiens_PolQ      TYK QMVGRAGR KGVDTVGESILICKNSEKSKGIALLQGSLKPVRSCLQRREGEEVTGSMI
T. brucei_PolQ(HelQ) RYL QMCGRAGR AGLDEFGESFLFLSRKDRNRGCELMQQEVE---ACVSQLLEE-KSTVE-
H. sapiens_HelQ      QYK QMIGRAGR AGIDTIGESILILQEKDKQQVLELITKPLE---NCYSHLVQE-FTKGIQ
                     * ** ***** *:* ,***:*: ...::.:  *:   ::    * .:   * :
```

Figure 3-4. Diagram illustrating the characteristic motifs within members of SF2 Helicase family. A. Conserved sequences within SF2 helicase family characteristic motifs. "()" represents an amino acid residue (aa) known to be localized in a specific position and that is conserved in almost all three sequences. The "aa" represents an aa that is known to occupy a specific position but that can be replaced by another one; "•" denotes any aa can occupy that position. "+" Represents hydrophobic aa occupying a specific position and "∘"represents hydrophilic aa. SF2 family conserved sequences obtained from (Hall and Matson, 1999; Fairman-Williams, Guenther and Jankowsky, 2010) **B.** Characteristic motifs of the SF2 helicase family are labelled in pink.

Figure 3-5. Diagram illustrating the characteristic motifs within the catalytic subunit of PolZ, Rev3. Yellow boxes showing the conserved sequences within PolZ catalytic subunit Rev3 in three different species, *T. brucei. A. thaliana* and *H. sapiens*. B family of polymerases conserved sequences obtained from (Lin, Wu and Wang, 1999).

3.3 Construction of TbPolN, TbHelQ and TbRev3 RNAi cell lines

In order to generate the RNAi cell lines against TbPolN, TbHelQ and TbRev3, the Gateway® technology was used for the construction of the stem loop plasmids. The TbHelQ RNAi cell line was kindly provided by M. Prorocic.

The plasmid pGl2084 (constructed as described in (Jones *et al.*, 2014)), originally modified from the pRPAiSL construct (Alsford & Horn 2008), was used for this assay. The RNAi target sequences were amplified using appropriate

primers, incorporating attachment sites (attB) which facilitates the integration of the fragment into the vector (Jones *et al.*, 2014).

The pGl2084 plasmid is composed of two sets of attachement sites (attP), which flank a counter selectable marker (ccdB), and are separated by a 150 bp stuffer (Figure 3 6). The attP sites are compatible with attB sites of any fragment of interest. The compatibility between the attP (vector) and the attB (fragment) sites facilitates the integration of the fragment into two specific regions of the vector in a single cloning step, replacing the ccdB gene (Hartley *et al.* 2000; Katzen 2007). This approach results in a final vector with the gene-specific fragment inserted in a 'tail to tail' orientation separated by the 'stuffer' (Figure 3-7), which permits the expression of a dsRNA hairpin loop, which is under the control of the ribosomal RNA promoter (P$_{RRNA}$), regulated by a tetracycline operator (Jones *et al.*, 2014). Resulting in a tetracycline inducible RNAi plasmid, thus facilitating knockdown of a gene of interest by RNAi (Jones et al., 2014). The plasmid also contains HindIII, XbaI, BamHI, ClaI and StuI restriction sites, which allow the verification of the correct integration of the fragment into the plasmid (described in N. Jones PhD thesis, 2014). On the other hand, an AscI restriction site allows the linearisation of the plasmid prior to transfection (Jones *et al.*, 2014). Additionally, the plasmid harbours the remaining sequence of the HYG ORF.

The pGl2084 plasmid leads the integration of a gene-specific RNAi cassette into the ribosomal locus of chromosome 2a in the 2T1 parental strain (Jones *et al.*, 2014). 2T1 is a genetically adapted strain of *T. brucei*, in which the ribosomal spacer of chromosome 2a is modified to contain inserts consisting of a 3' Hygromycin (HYG) fragment (see below) and a puromycin (PUR) selectable marker (Alsford & Horn 2008). A detailed description of the construction of the cell line is found in (Alsford & Horn 2008). After transfection into 2T1 cells, the plasmid integrates into the ribosomal locus replacing the PUR marker and reconstructing the HYG ORF (Figure 3-8). The correct integration of the plasmid will result in cells resistant to hygromycin and sensitive to puromycin (Jones *et al.*, 2014). The successful cloning will result in tetracycline-inducible RNAi gene knockdown cell lines.
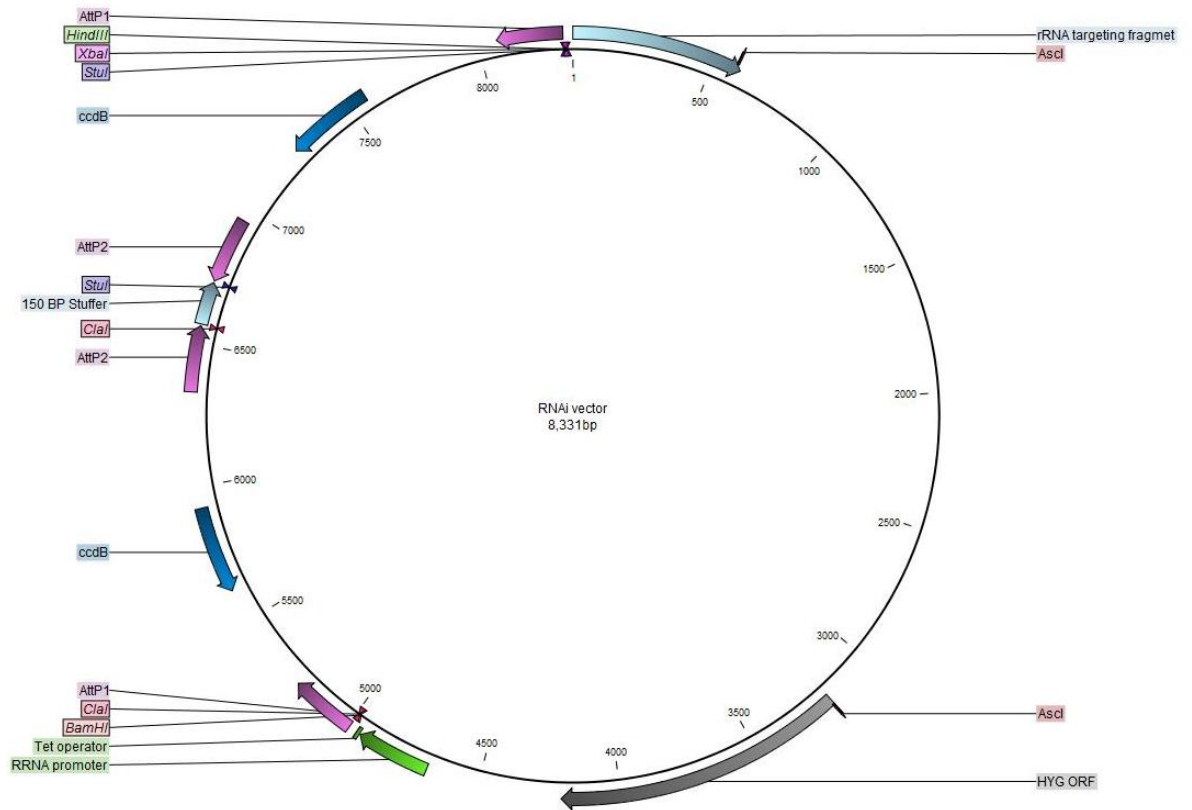
Figure 3-6. RNAi plasmid pGL2084 Map. The purple arrows represent the Attp1 and Attp2 sites; the Attp sites are separated by a 150 bp stuffer (light blue arrow). The RRNA promoter and the tetracycline operator, which regulates the activation of the expression of an RNAi insert, are represented in green. The dark blue arrows represent the selectable marker (*ccdB*). The gray arrows show the incomplete *HYG* resistance gene. The linearization sites (AscI) are localized next to the *HYG* sequence and the rRNA targeting fragment (blue arrow). The restriction enzyme sites used for validation (BamHI, ClaI, HindIII, StuI and XbaI) are shown in pink.
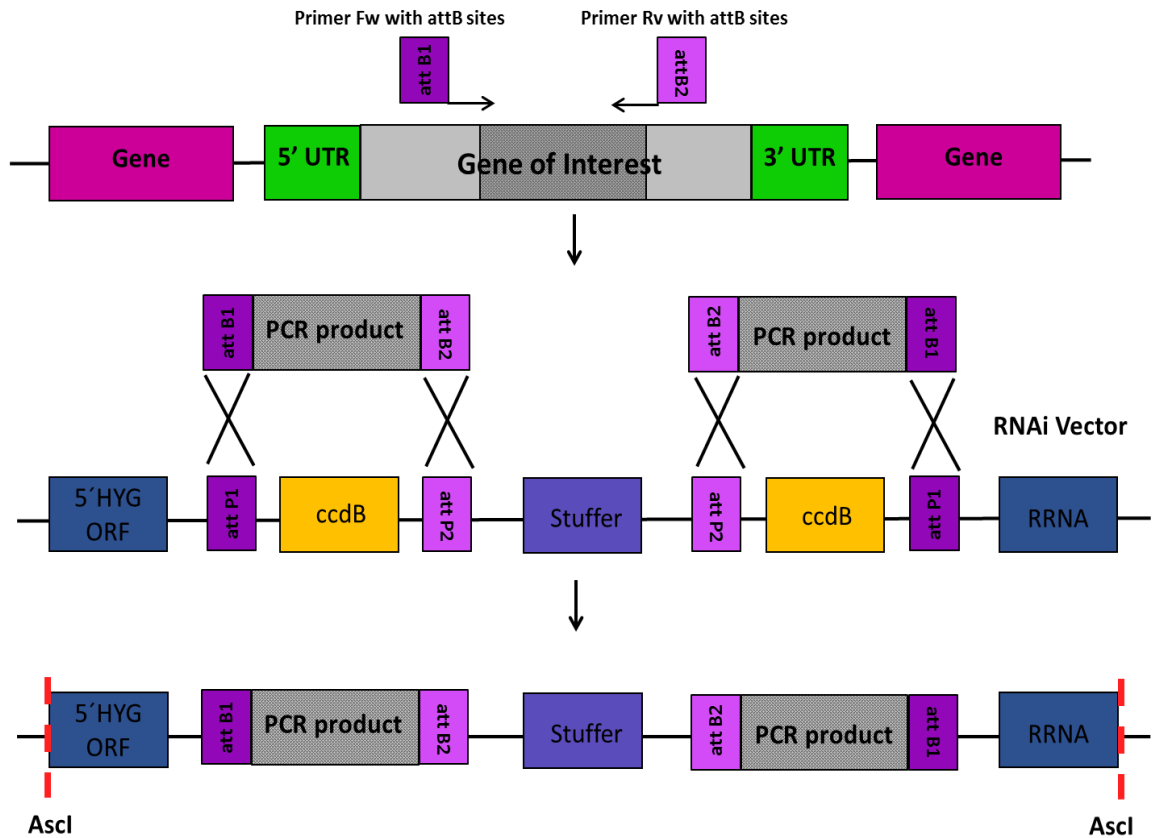
Figure 3-7. Schematic representation of the integration of PCR products into the RNAi vector. Graphic showing the integration of an att B flanked PCR product into the vector in a single cloning step, replacing the *ccdB* gene (selection marker) by recombination of the attP sites.
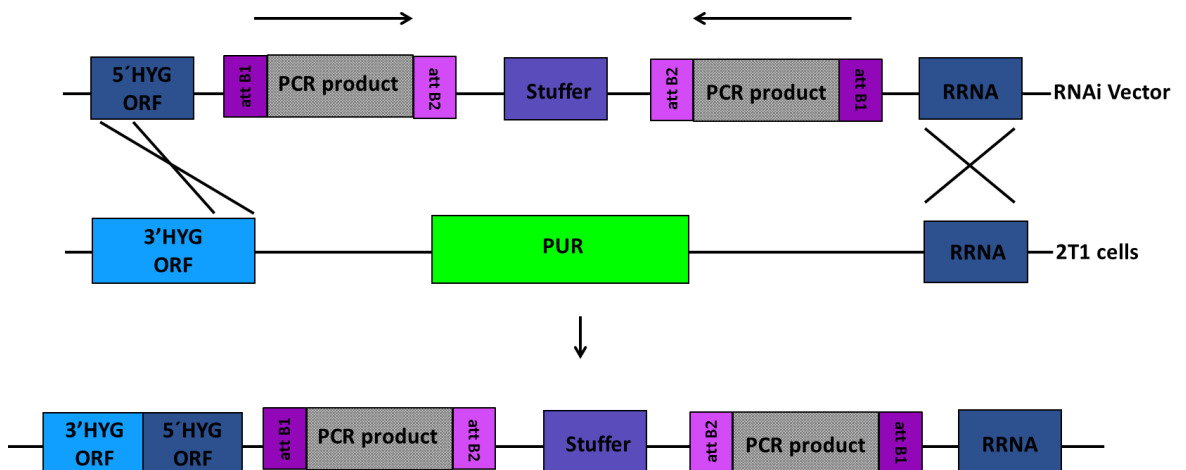
Figure 3-8. Schematic representation showing the integration of linearized RNAi vector into the ribosomal spacer of the 2T1 cell line. Integration of the RNAi vector into the genome of 2T1, replacing the *PUR* cassette and reconstructing the *HYG* ORF.

3.3.1 Growth analysis after the depletion of Polymerase Nu, Polymerase Theta and Polymerase Zeta catalytic subunit Rev3 in *T. brucei*

To determine the effect of TbPolN, TbHelQ and TbRev3 depletion in BSF *T. brucei* parasites, RNAi mediated tetracycline inducible knockdown of the three genes were performed. This will provide a better understanding of the essentiality of TbPolN, TbHelQ and TbPolZ in the survival of the parasite.

The RNAi cell lines used for this analysis were generated as described in the section above (Section 3.3). To confirm the correct integration of the RNAi target fragment into the vector prior to transfection, a diagnostic restriction digest was performed using the following combination of enzymes: BamHI+XbaI, ClaI, StuI and AscI alone (Figure 3-9). The double digestion with BamHI and XbaI result in the excision of the opposite fragments and the attL sites (comprised of sequences from the attB and attP sites). ClaI digestion results in the excision of one of the PCR fragments and the attL sites. Equally to StuI digestion, which excises the other PCR fragment including the attL sites. AscI digestion excises the entire fragment including the two PCR fragments and the HYG ORF. This was performed for both the TbPolN and TbRev3 plasmids. This restriction digest analysis was not performed on the TbHelQ RNAi plasmid, as the cell line was kindly provided by M. Prorocic.

A.

B.

C.

	1	2	3	4
	BamHI+XbaI	ClaI	StuI	AscI
	1.3-1.6Kb+5013bp	~600bp+5790	~600bp+5788bp	2610+~3797
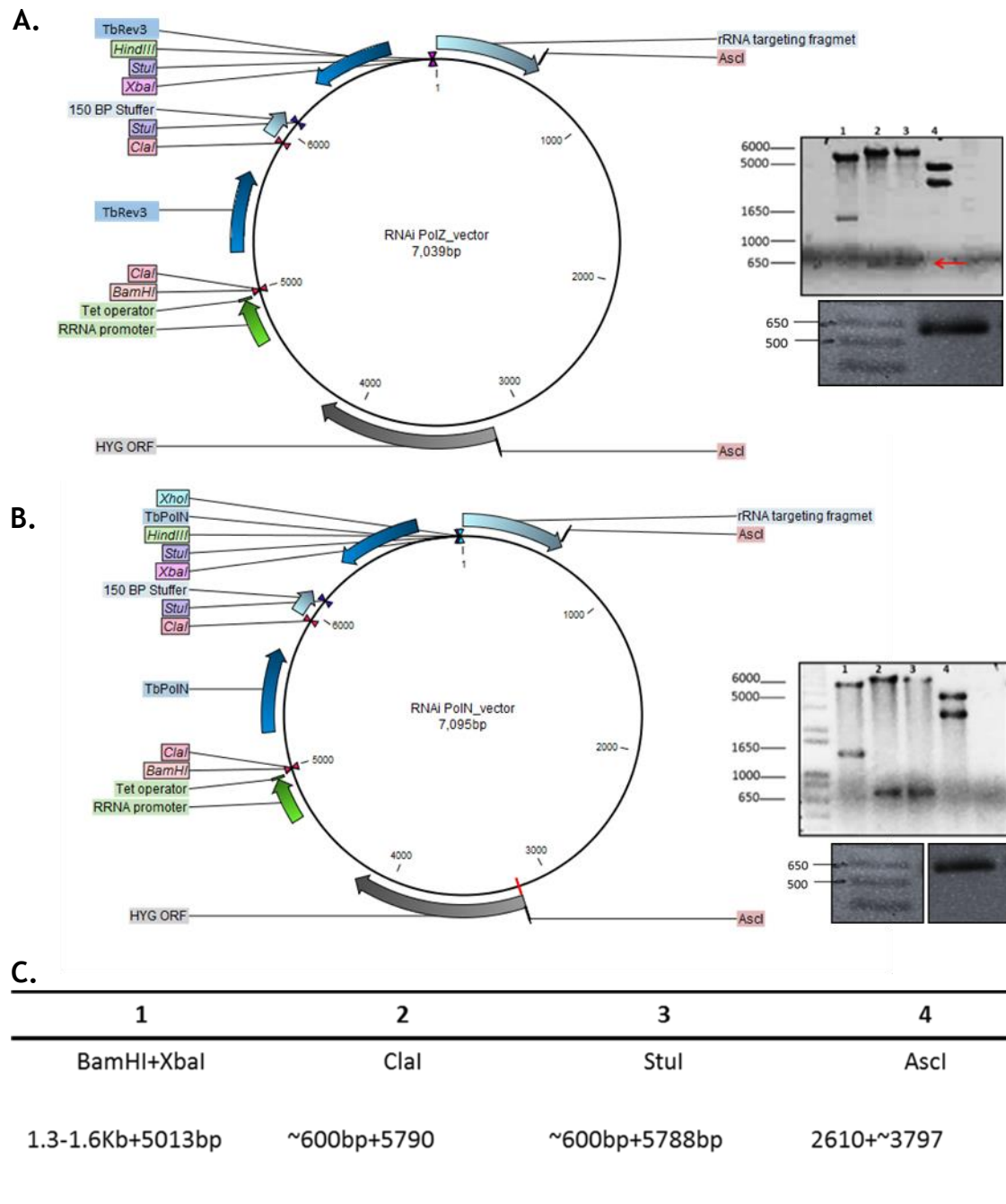
Figure 3-9. Validation of RNAi vectors and transformants for TbPolN and TbRev3. Enzymatic digestion confirming the insertion of the PCR fragment into the RNAi vector and PCR on 2T1 cells transformed with above RNAi vector confirming the insertion of the cassette into the genome of 2T1. **A.** RNAi vector map for TbPolZ and confirmatory enzymatic digestion. Red arrow shows the band corresponding to the TbRev3 insert. Smaller gel shows PCR on 2T1 cells transformed with RNAi TbPolZ (Rev3) vector confirming the insertion of the cassette, represented by the ~600 bp band. **B.** RNAi vector map for TbPolN and confirmatory enzymatic digestion. Second gel showing a band of ~600bp confirming integration of TbPolN RNAi vector into the genome of 2T1. Image has been cropped to show the corresponding band next to the DNA molecular weight marker. **C.** Expected band size in bp after the digestion with the different enzyme combination is shown.

Following the diagnostic digestion, the vectors were linearised with AscI and transformed into the 2T1 cell line and hygromycin resistant clones were selected. To confirm the integration of the cassette, the transformants were tested for puromycin sensitivity (0.2 µg/ml). As it was mentioned above, the integration of the cassette replaces the *PUR* marker and reconstructs the *HYG* ORF. The puromycin resistant cells were discarded and the rest of transformants were further tested for hygromycin (5µg/ml) resistance. The integration of the cassette was further analysed by PCR using the primers OL4161-taatgccaactttgtacaaa and OL4212-taatgccaactttgtacaag, expecting a band of approximately 600 bp, which correspond to the insert and the attB sites (Figure 3-9). To understand the effect of RNAi against each gene, cultures were diluted to 5×10^4 cells.ml^{-1} and grown with or without the addition of tetracycline at 1 µg/ml. Cell proliferation for each cell line was monitored over 72 hours, with the growth analyses repeated three times.

Following the putative RNAi depletion of TbRev3 and TbHelQ, no clear proliferative defects could be observed when compared to the uninduced controls (Figure 3-10 A-B). In contrast, 24 hours after the putative depletion of TbPolN, cell proliferation was reduced. However, growth did not cease, but instead was slowed from 24 hours onwards. The phenotype was confirmed by testing two independent clones; a similar reduction in growth was observed following putative TbPolN depletion in both clones (Figure 3-10 C-D). Since the two different clones displayed the same behavior, clone B was chosen for further analysis.

To test for loss of TbPolN and TbHelQ after RNAi, the cell lines were transformed with constructs that result in the expression of each protein, from its own locus, as a variant fused to 12 copies of the myc tag. This manipulation was achieved using the 12Myc pNAT BSD vector (Alsford and Horn, 2008). The procedure is described in detail in Chapter 5 (section TbPolN 5.3.1; section 5.7.4 TbHelQ), the only difference being the parental cell line used for the transformation. For this specific case the RNAi cell lines against TbPolN and TbHelQ were used instead of WT Lister427 cells. Apart from this difference, the same primers and procedure were performed in both assays.

Anti-myc antiserum was then used to test for loss of the myc-tagged proteins after RNAi by Western blot analysis (Figure 3-10 B,D). For TbRev3, RT-qPCR was performed to test for loss of transcript (Figure 3-10 A) (procedure described in section 2.3.4), as myc-tagged clones could not be generated in the RNAi cells. The reasons behind this are unclear, as TbRev3 was successfully myc-tagged in non-RNAi BSF *T. brucei* cells (section 4.2).

RT-qPCR of TbRev3 demonstrated a 50% reduction of the RNA transcript relative to uninduced cells at 24 hours post RNAi induction (Figure 3-10 A), suggesting the RNAi was successful. western blotting of whole cells extracts to detect TbPolN-myc revealed the depletion of the protein from 24 hours and throughout the 72 hours growth post induction (Figure 3-10 D). However, In the case of TbHelQ, the Western blot revealed no evidence for loss of TbHelQ-myc (Figure 3-10 B), suggesting an inefficient RNAi cell line following tetracycline addition, or an unusually stable protein. No attempt was made to evaluate growth and protein levels over a more prolonged period of TbHelQ RNAi induction. Irrespective of the explanation, the lack of growth alteration after RNAi cannot be said to be because loss of the protein does not affect BSF *T. brucei* viability. An attempt to generate a new TbHelQ RNAi cell line was conducted, in case the available cell line was defective. In order to do this, a vector containing different TbHelQ ORF fragments was used. As it was mentioned above, the correct integration of the fragments into the vector was tested by enzymatic digestion (Figure 3-11). The plasmid was used to transform competent *E. coli* cells (DH5 α). Unfortunately, it was not possible to recover transformants.
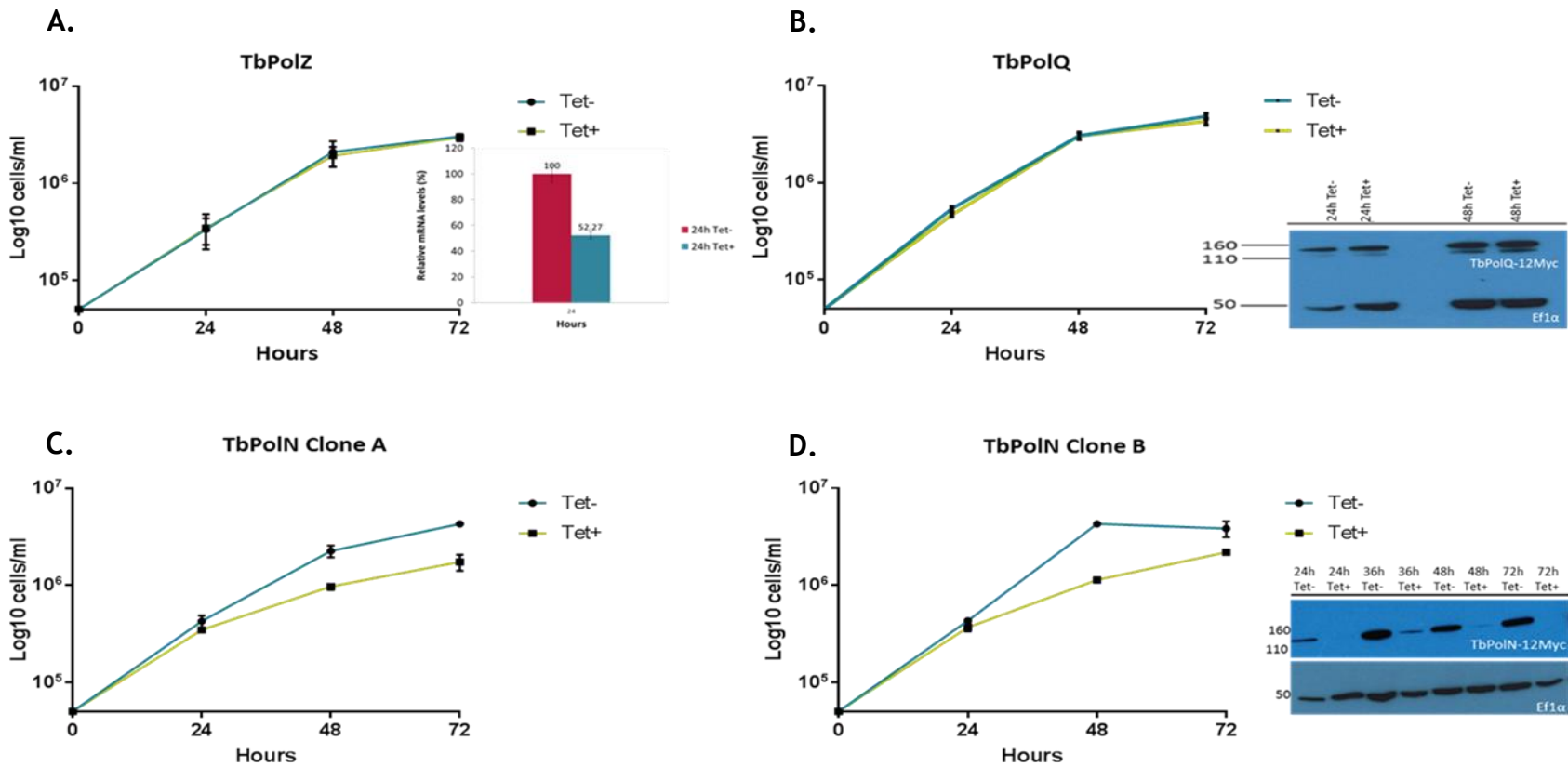
Figure 3-10 Effect of RNAi against the three T. brucei putative TLS Pols. Growth curves are shown of T. brucei bloodstream form cells over 72 hrs in the absence (Tet-) or presence (Tet+) of tetracycline induction of RNAi against TbRev3 (**A**), TbHelQ (**B**) and TbPolN (**C-D**). Error bars represent the standard deviation of the mean of three experimental repetitions. Inserts in B and D show Western blot analysis using anti-myc antiserum. Ef1α was used as a loading control. Insert (**A**) show RT-qPCR comparing the relative amounts of TbRev3 RNA after 24 hours with or without addition of Tet.
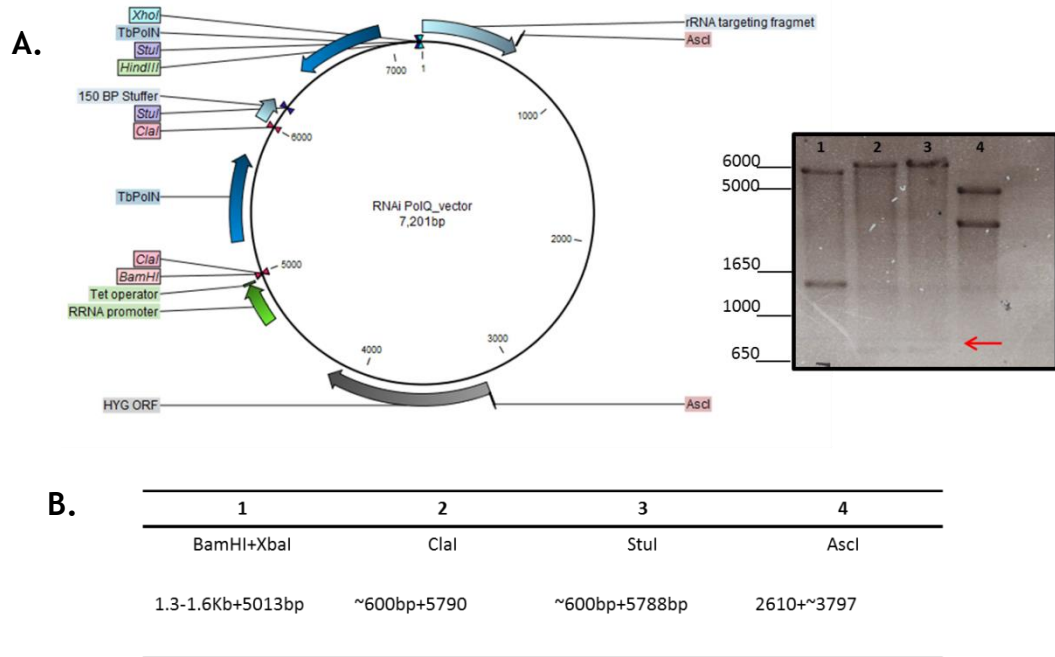
Figure 3-11. Verification of TbHelQ RNAi vector. **A**. RNAi vector map for TbHelQ and confirmatory enzymatic digestion. **B.** Expected band size in bp after the digestion with the different enzymes combination is shown, and size markers of the digest gels are shown.

3.3.2 Cell cycle analysis following depletion of Polymerase Nu and Polymerase Zeta catalytic subunit Rev3

As it was demonstrated in section 3.3.1 the proliferation of *T. brucei* cells was affected by the depletion of TbPolN, the cell cycle was analysed in order to ask if the loss altered progression. Even though the cells did not show an obvious phenotype after the knockdown of TbPolZ, it was important to test if the lack of a growth defect masked cell cycle defects.

The cell cycle was analysed using the RNAi cell line against TbPolN and TbRev3, in the absence and presence of tetracycline induction at 24 hours, 48 hours and 72 hours. The cells were stained with 4 ',6-diamidino-2-phenylindole (DAPI), allowing the visualization of the nucleus and the kinetoplast, before and after the depletion of the protein, allowing the characterization of the cell cycle. Depending on the stage of the cell cycle the DNA content will vary, because replication and segregation of the nucleus and kinetoplast differ in their timing (Siegel, Hekstra and Cross, 2008). Cells containing 1 nucleus and 1 kinetoplast (1N1K) are predominantly in G1, though some may have entered

nuclear S (which can be seen by an elongated K configuration and perhaps increased N). Cells with 1 nucleus and 2 kinetoplasts (1N2K) are predominantly in G2/M; and cells that have completed mitosis and are undergoing cytokinesis have 2 nuclei and 2 kinetoplasts (2N2K). Changes in the distribution of these configurations in mutants or after RNAi indicate altered cell cycle dynamics, and it is frequently observed that non-standard configurations arise after mutation or depletion ofspecific genes (Hammarton, 2007; Monnerat *et al.*, 2009). The morphology of the parasites was also observed by differential interference contrast (DIC) microscopy, asking if cells with an aberrant body shape arose.

Following depletion of TbPolN, the DNA content distribution of the population and body shape at 24 hours post RNAi induction did not seem to be strongly affected (Figure 3-12 A). However, a minor increase in the number of 1N2K cells could be observed, as well as a small decrease in 2N2K cells and a small increase in non-standard configurations ('other') (Figure 3-12 B). Flow cytometry of propidium iodide stained cells appeared to confirm this, as slightly decreased numbers of cells with 2N content were detected after RNAi relative to the control, as well as slightly increased numbers of cells with 4N content (Figure 3-12 C). At 48 hours post RNAi induction there was a significant decrease of 1N1K cells and a further loss of 2N2K cells; the numbers of 1N2K cells did not appear to increase relative to 24 hours, but instead there was a very significant accumulation of cells with aberrant DNA content (Figure 3-12 A-B). At the same time, the cells had lost their typical trypomastigote shape and were highly abnormal (Figure 3-12 A). The abnormal DNA content was hard to classify, but most cells had multiple kinetoplasts and abnormal, enlarged nuclei (Figure 3-12 A-Figure 3-13). The phenotype observed after DNA characterization was confirmed by flow cytometry, showing a very pronounced decrease in 2N cells and an accumulation of >4N cells (Figure 3-12 C).

The cell cycle data suggest an initial, partial arrest in G2/M, which explains the increase in 1N2K cells. However, it appears this stall is overridden and the cells progress to mitosis but cannot complete it, preventing the correct division of the cell and explaining the reduction of 2N2K cells, the accumulation of abnormal cells with increased nuclear DAPI signal, and the strong decrease of 1N1K (G1) cells (Figure 3-12 B).

Remarkably, the time course revealed that the cell cycle perturbations following depletion of TbPolN are transient phenotypes, since at 72 hours the cells started to recover: in the IFA images it was possible to observe more cells with normal DNA content and regular body shape than at 48 hours (Figure 3-13) and the DNA characterisation demonstrated an increase of 1N1K cells and a decrease of aberrant cells relative to 48 hours. The basis for this change is unclear, since Western blot analysis indicated that TbPolN-myc was still absent at 72 hours, suggesting the RNAi depletion was still present (Figure 3-10 D). In addition, the cell cycle changes were not associated with increased growth, as the RNAi cells were still growing more slowly (Figure 3-10 C-D) than the controls.

In the case of TbRev3, no differences between the control cells and the RNAi induced cells at 24 hours and 48 hours growth could be observed (Figure 3-14). The DNA content and the body shape of the parasite was not affected following depletion of the protein (Figure 3-14 A), suggesting that TbPolZ is unlikely to have an essential role in bloodstream form *T. brucei*.
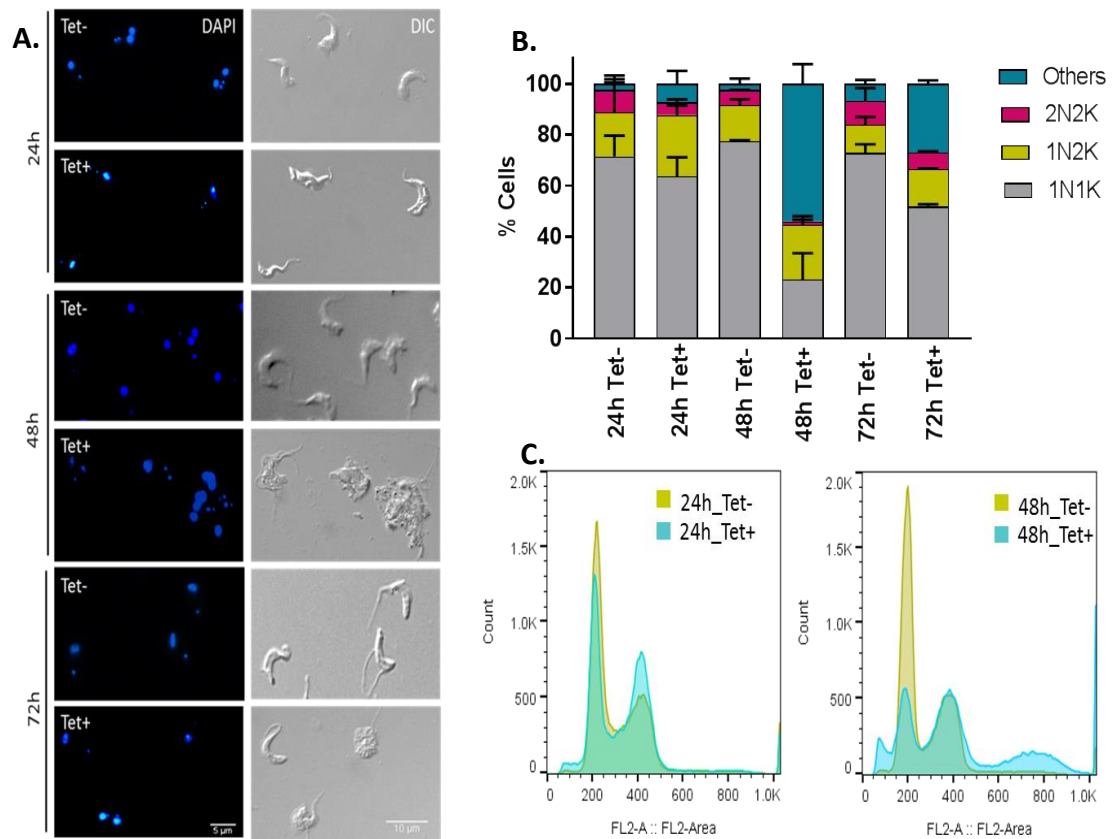
Figure 3-12. Analysis of the cell cycle after RNAi depletion of TbPolN. A. Cell cycle analysis by DAPI staining at 24 h, 48 h and 72 h in the absence (T-) and presence (T+) of tetracycline induction. Immunofluorescence analysis allowing the visualization of the DNA content. Visualization of the cell body was performed by differential interference contrast microscopy (DIC). **B.** Characterisation of DNA content by DAPI counting, allowing the classification into 1N1K (G1/S), 1N2K (G2/M) and 2N2K (mitosis) cells; other denotes cells that deviate from these classifications. Values depict the mean of each classification in the total population, and error bars represent the standard deviation of the mean of two biological repetitions. >200 cells were counted at each time point and in each experiment. **C.** FACS analysis: histogram profiles of cells labelled with propidium iodide, at 24 h and 48 h post-induction (Tet+, blue) or in uninduced cells (Tet-, yellow).
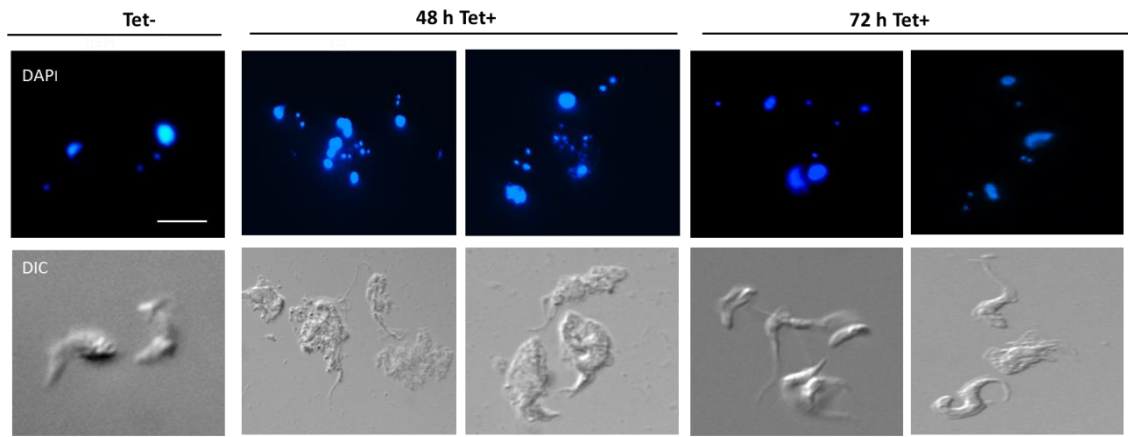
Figure 3-13. Cell phenotype after the depletion of TbPolN in bloodstream forms. Immunofluorescence analysis at 24 h and 48 h in the absence (Tet-) and presence (Tet+) of tetracycline. First panel show DAPI staining of the nucleus and kinetoplast and second panel visualization of the cell body by differential interference contrast microscopy (DIC). Scale bar: 5 µm
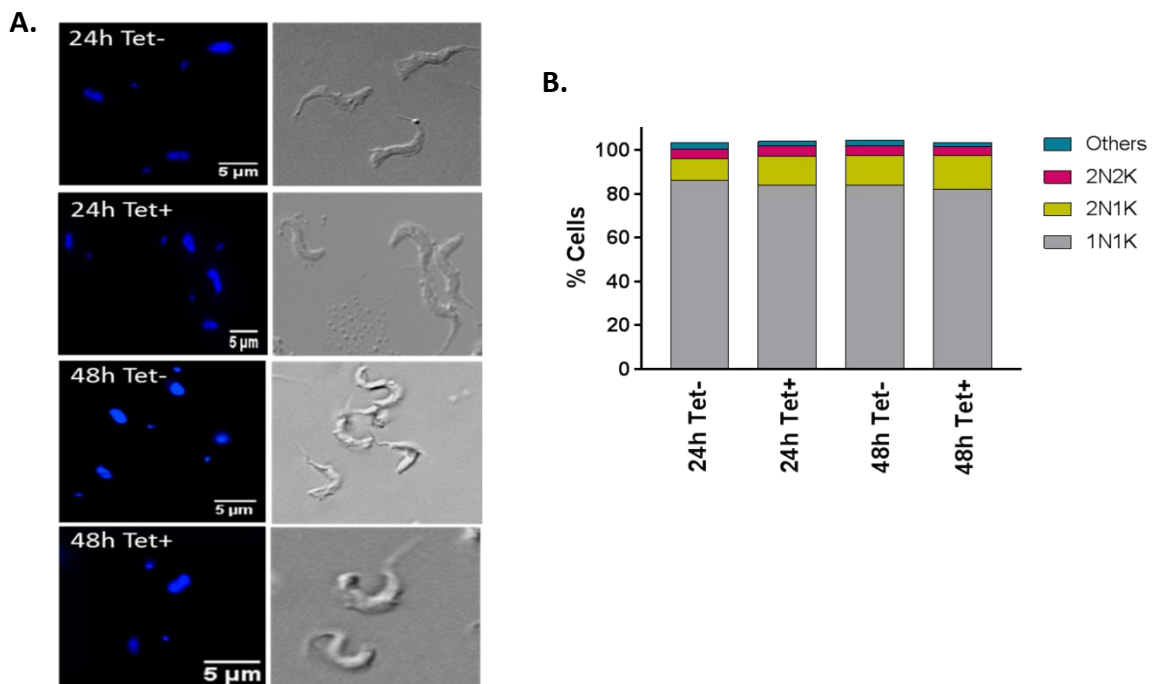
Figure 3-14. Analysis of the cell cycle after RNAi of TbRev3. A. Cell cycle analysis by DAPI staining at 24 h and 48 h in the absence (T-) and presence (T+) of tetracycline induction. Immunofluorescence analysis allowing the visualization of the DNA content. Visualization of the cell body was performed by differential interference contrast microscopy (DIC). **B.** Characterisation of DNA content by DAPI counting, allowing the classification into 1N1K (G1/S), 1N2K (G2/M) and 2N2K (mitosis) cells; other denotes cells that deviate from these classifications. Values depict the mean of each classification in the total population of two biological repetitions. >200 cells were counted at each time point and in each experiment.

3.3.3 Analysis of cell sensitivity to genotoxic agents after TLS RNAi

The deletion of PolN and PolZ have been linked with an increase of sensitivity to genotoxic agents (UV, MMS, cisplatin, etc), responsible for DNA cross-links and breaks, including DSBs (Ho and Schärer, 2010; Sharma, Helchowski and Canman, 2013a). The depletion of human PolN increases the sensitivity against cisplatin and mitomycin C, suggesting a role in interstrand cross-link repair (ICL) (Ho and Schärer, 2010). On the other hand, the depletion of PolZ in chicken and mammalian cells lead to an increase in the sensitivity to UV radiation, MMS and other cross-linkinkig agents (Sale, 2013; Sharma, Helchowski and Canman, 2013b). These observations indicate that these proteins have a role in the maintenance of genome integrity following damage (Ho and Schärer, 2010; Sharma, Helchowski and Canman, 2013a). For this reason, we next tested if the depletion of TbPolN and TbRev3 increased the sensitivity of *T. brucei* cells to exposure by the genotoxic agents UV radiation and MMS.

3.3.3.1 Sensitivity of BSF cells to MMS damage after depletion of TbPolN and TbRev3

Sensitivity of *T. brucei* BSF cells to the alkylating agent MMS was tested by evaluating growth of RNAi cell lines targeting TbPolN and TbRev3, in the absence (Tet-) and presence (Tet+) of tetracycline, over 72 hours. Growth was compared at three different concentrations of MMS (Figure 3-15). Depletion of either TbPolN or TbRev3 resulted in reduced growth in comparison to the uninduced cells exposed to MMS, particularly at the highest concentration (0.0003%).

Depletion of TbRev3 may have had a more severe effect than depletion of TbPolN, since the former cells began to loose proliferation after the 24 hours post-induction at 0.0003% MMS and were unable to recover at 72 hours (Figure Figure 3-15 C-D), unlike the latter. However, this is hard to evaluate, since the extent of growth impairment of the TbRev3 uninduced cells was more severe than the uninduced TbPolN cells, perhaps due to MMS dilution variation. Nonetheless, these data suggest that both TLS Pols contribute to cell viability following exposure to MMS stress.
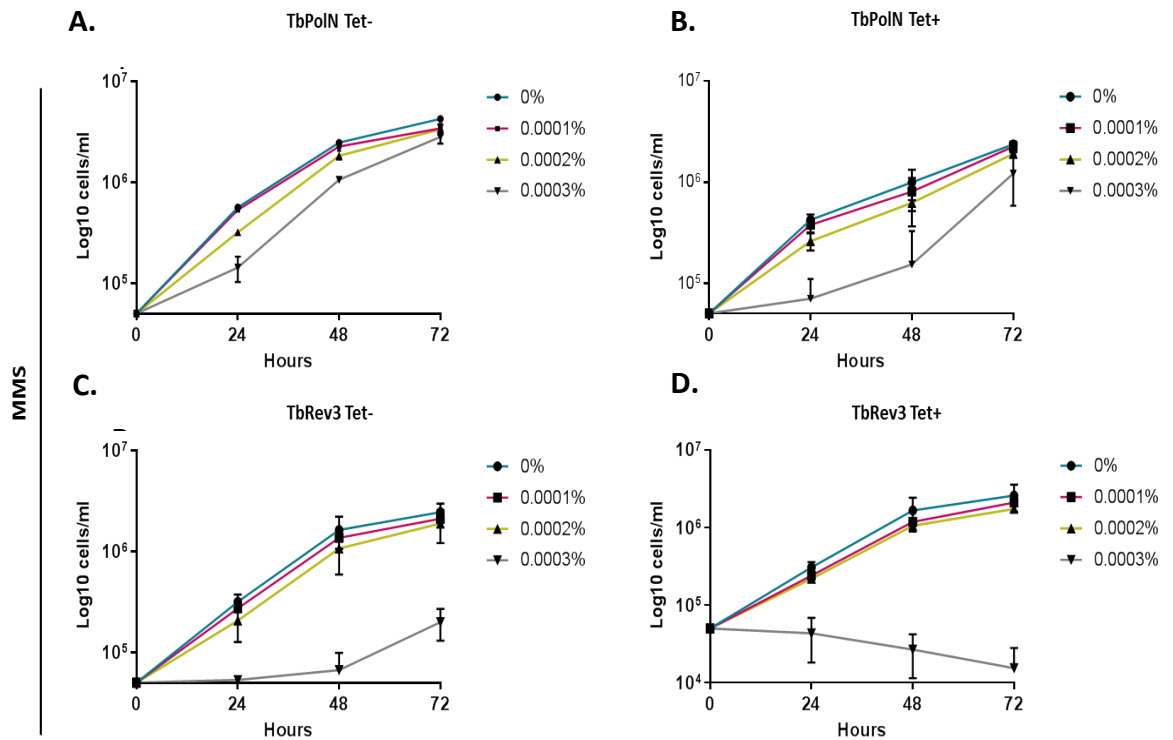
Figure 3-15. Growth of *T. brucei* cells in the presence of MMS and after RNAi depletion of TbPolN or TbRev3. Growth curves of *T. brucei* bloodstream form RNAi cell in the absence (Tet-) or presence (Tet+) of tetracycline induction, with or with various concentrations of MMS (0%, 0.0001%, 0.0002%, 0.0003%). **A-B.** Growth curve in the absence and presence of tetracycline RNAi induction against TbPolN. **C-D.** Growth curve in the absence and presence of tetracycline induction against TbRev3. Error bars represent the standard deviation of the mean of three biological repetitions.

3.3.3.2 Sensitivity of BSF cells to UV radiation damage after depletion of TbPolN and TbRev3

The sensitivity of TbPolN and TbRev3 RNAi cell lines to UV radiation was tested by examining cell proliferation, following TbPolN or TbREv3 RNAi depletion, after exposure to five different UV intensities (0 J/m^2, 500 J/m^2, 750 J/m^2, 1000 J/m^2 and 1500 J/m^2).

As seen during MMS exposure, depletion of either protein increased the sensitivity of the cells to UV exposure; cell proliferation in the induced cells (Tet+) was reduced when compared to the control, uninduced cells (Tet-) at the equivalent UV dose. However, the growth impediment in the presence of UV was more pronounced after depletion of TbPolN (Figure 3-16 A-B), with TbRev3 depletion having only a minor effect (Figure 3-16 C-D). Due to the active role of

PolZ in UV lesion repair described in other organisms (Sharma, Helchowski and Canman, 2013a), this was unexpected.
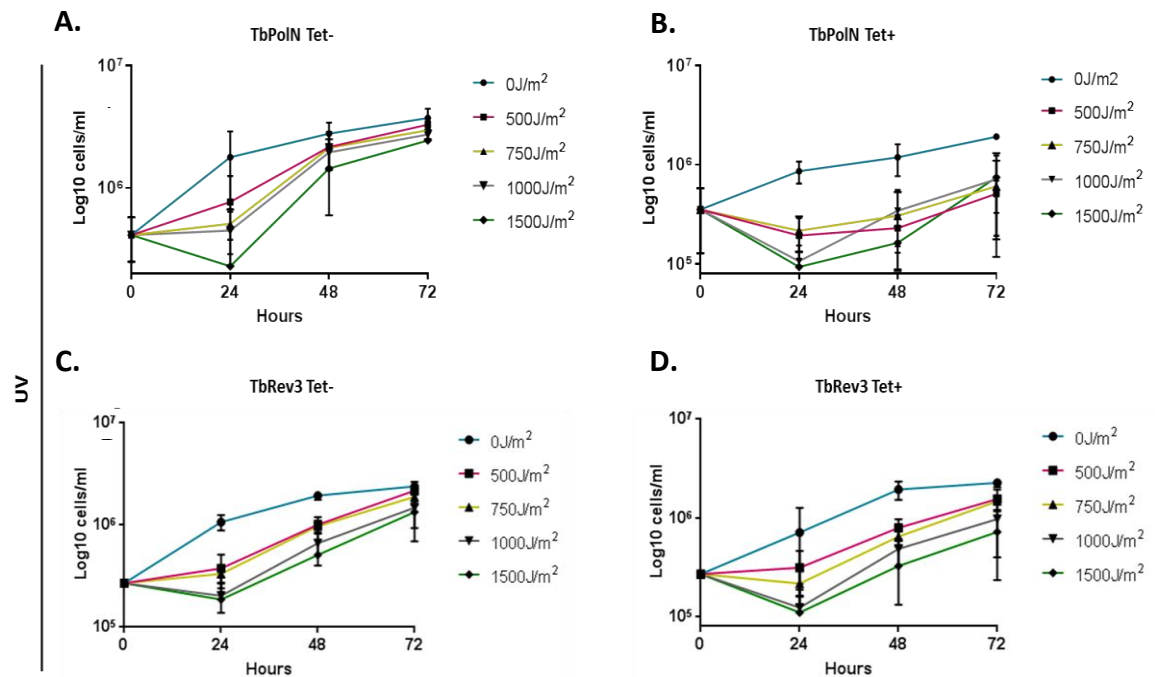
Figure 3-16.Growth curve of *T*. *brucei* bloodstream RNAi cell lines against TbPolN and TbPolZ in the absence (Tet-) and presence (Tet+) of tetracycline induction, after the exposure to different intensities of UV (0 J/m^2, 500 J/m^2, 750 J/m^2, 1000 J/m^2, 1500 J/m^2). A-B. Growth curve in the absence and presence of tetracycline induction against TbPolN, after the exposure to different UV intensities. **C-D.** Growth curve in the absence and presence of tetracycline induction against TbRev3, after the exposure to different UV intensities. Error bars represent the standard deviation of the mean of three biological repetitions.

3.4 Discussion

This chapter provides a first analysis of the importance of three putative TLS DNA Pols in *T. brucei* BSF cells. Loss of TbPolN was shown to be severely detrimental to growth over 48 hours (approximately 8 generations), with an accumulation of cells showing aberrant nuclei, suggesting a critical role in nuclear genome maintenance. RNAi of TbPolZ, or at least the TbRev3 polymerase catalytic subunit, did not impair growth, but resulted in increased sensitivity to methyl methanesulphonate (MMS) and, to a greater extent, UV radiation damage, phenotypes which were also observed after the depletion of TbPolN. Thus, both TLS pols provide a role in the response to alkylation and UV radiation effects. Unfortunately, targeted RNAi of a third factor, TbHelQ, was

unsuccessful. Taken together, these data reveal variant functions for two TLS DNA polymerases in *T. brucei* genome biology.

3.4.1 Bioinformatics and protein domain prediction

TbPolN, TbHelQ and TbRev3 were analysed using the SmartBlast software, with the aim of identifying related sequences in other organisms. The three proteins all recognized putative homologues in a common eukaryote, *A. thaliana* (Table 3-3); this plant is known to encode for orthologues of most proteins involved in genome maintenance in eukaryotes (Hays, 2002). *A. thaliana* encodes for four TLS pols, Polη, PolZ, Polκ and Rev1, polymerases that are also known to be present in *T. brucei* (Hays, 2002; Passos-Silva *et al.*, 2010).

The single *A. thaliana* PolQ-like protein was a common match for TbPolN and TbHelQ. The plant protein is composed of a C-terminal polymerase-like domain and an N-terminal helicase-like domain (Yousefzadeh and Wood, 2013), explaining its homology with TbPolN, which harbours a C-terminal A-family polymerase domain (Figure 3-1 A), and TbHelQ, which consist of a N-terminal helicase domain (Figure 3-1 C) (Delarue *et al.*, 1990; Hall and Matson, 1999; Yousefzadeh and Wood, 2013). Additionally, the absence of an exonuclease domain in TbPolN suggests a possible role in the TLS pathway. The exonuclease domain is associated with the capacity of DNA polymerases for editing wrong nucleotides, an activity that is commonly found in replicative polymerases (Johansson and Dixon, 2013). The absence or alteration of this domain increases the possibility of spontaneous mutations, which was confirmed by alterations in the *S. cerevisiae* Polδ and Polε exonuclease domain resulting in frameshift and base substitution during synthesis (Tran, Gordenin and Resnick, 1999). It is known that polymerases involved in the TLS pathway are characterised by lacking 3'-5' proofreading activity, impeding the excision of wrong nucleotides. Although this mechanism increases the probability of mutations, it is still essential for the survival of the cell (Goodman and Woodgate, 2013).

SmartBlast analysis of TbPolN also identified the *H. sapiens* PolQ as a 'hit', and, similar to *A. thaliana*, the human PolQ has a C-terminal A- family polymerase domain and an N-terminal SF2-helicase domain (Figure 3-1 E)

(Takata *et al.*, 2010; Yousefzadeh and Wood, 2013). Surprisingly, *H. sapiens* PolN, the human protein that consists only of a C-terminal polymerase domain (Figure 3-1B), did not score as highly in searches with TbPolN. The polymerase domains of human PolQ and PolN are closely related (Yousefzadeh and Wood, 2013), and previous studies suggest that PolN and PolQ diverged from one another before the origin of the vertebrate lineage (Yousefzadeh and Wood, 2013). Whether *T. brucei* had a PolQ dual domain protein that was discarded, leaving TbPolN and TbHelQ (below), or whether the two proteins were generated by separation of an ancestral PolQ is unknown. However, a true dual-domain PolQ was not observed in any of the kinetoplastids examined, and detailed investigation of functional motifs suggests divergence between TbPolN and *H. sapiens* PolQ.

When the protein sequences of TbPolN and TbHelQ were compared to the corresponding putative human homologues, the presence of several characteristic motifs in the polymerase and helicase domains could be identified. In the case of the polymerase domain, the aa sequence shown in Figure 3-3 was highly conserved across the functional motifs of the A family polymerase members, suggesting TbPolN is likely to be an active polymerase, though this remains to be tested. Studies performed in vertebrate and invertebrate PolQs indicate that these motifs are separated by three important inserts, all of which are characteristic of the PolQ polymerase domain (Hogg *et al.*, 2011; Yousefzadeh and Wood, 2013). The first insert is located in the thumb domain, between the first and second motifs. The second insert resides in the palm domain between the second and third motifs, and the third insert is located in the palm domain, between the fifth and sixth motifs (Figure 3-3). Deletion of insert 1 affects the enzyme's processivity. On the other hand, the deletion of inserts 2 and 3 affects the enzyme's activity and its ability to bypass abasic sites (Hogg *et al.*, 2011; Yousefzadeh and Wood, 2013; Wood and Doublié, 2016). TbPolN lacks two of the three inserts that are characteristic of PolQ, whereas human PolN lacks all the inserts (Figure 3-3). This may suggest closer homology between TbPolN and vertebrate PolN homologues, but is not definitive. Indeed, it is unclear how any PolN activity is altered by the loss of these inserts, though activity of this TLS pol may be mediated by interaction with another protein. Further work will be needed to evaluate activity.

In contrast to TbPolN, TbHelQ appears to be more homologous in sequence to the human helicase HelQ than PolQ. HelQ shows clear sequence homology to the PolQ SF2-helicase domain (Takata *et al.*, 2010; Yousefzadeh and Wood, 2013). From the alignment of the proteins (performed in section 3.2.3), TbHelQ also belongs to the SF2-family. Indeed, detailed analysis shows TbHelQ harbours specific motifs characteristic of this group of helicases (Figure 3-4)(Hall and Matson, 1999; Tanner and Linder, 2001; Fairman-Williams, Guenther and Jankowsky, 2010). The Q motif within this domain has been suggested to be involved in the DNA binding (Ding *et al.*, 2015). Moreover, the motifs I, II and VI have been shown to be responsible for the binding and hydrolysis of nucleotide triphosphate (Fairman-Williams, Guenther and Jankowsky, 2010). Motifs Ia and IV are also involved in substrate binding (Tanner and Linder, 2001), while motifs III and V are involved in communication between the nucleoside triphosphate and the nucleic acid binding site (Tanner and Linder, 2001; Fairman-Williams, Guenther and Jankowsky, 2010). It seems, likely, therefore that the protein has helicase activity, given its homology with human HelQ. HelQ homologues are also found in archaea, where they are termed Hel308 (Northall *et al.*, 2017).

To date, the activity of the helicase domain of PolQ remains uncertain, considering the polymerase domain confers the functions of this protein (Yousefzadeh and Wood, 2013). Several roles for PolQ have been reported across a diverse range of eukaryotes. For instance, the enzyme has been shown to be involved in somatic hypermutation in chicken cells, since the absence of PolQ provokes a decrease in the immunoglobulin gene diversity in this organism (Yousefzadeh and Wood, 2013). Additionally, studies have shown that PolQ in eukaryotes is required during several repair pathways, such as microhomology mediated end joining (MMEJ), non-homologous end joining (NHEJ), homologous recombination (HR), base excision repair (BER) and translesion DNA synthesis (TLS) (Yousefzadeh and Wood, 2013; Wood and Doublié, 2016). To date, the PolQ related proteins, PolN and HelQ, have been shown to act during HR and crosslink repair, where they interact with proteins that are directly involved in this pathway. Immunoprecipitation analysis suggests a possible interaction between human PolN, Rad51 and FANCD2 (Moldovan *et al.*, 2010). On the other hand, there is evidence of a possible interaction of mice HelQ and Rad51 paralogues

(Adelman *et al.*, 2013). In the case of HelQ, it is suggested that the deficiency of this protein in mammalian cells affects the recruitment of RAD51 to the damage replication fork (Adelman *et al.*, 2013; Takata *et al.*, 2013). On the other hand it has been proposed that RAD51 stimulates the recruitment of PolN for the synthesis of the invaded strand (Moldovan *et al.*, 2010). More recent data has suggested that human PolN may have a more restricted role in meiotic recombination (Takata *et al.*, 2017), though this is incompatible with the pronounced phenotypes seen after PolN loss in *T. brucei*. Whether this is because TbPolN has assumed some of the functions of PolQ from other eukaryotes is unknown.

One problem in assessing this is the fact that RNAi against TbHelQ did not work, and we cannot evaluate if the effects of its loss compare with or differ from TbPolN (discussed further below). For instance, it is unclear why the parasites encode two separate proteins instead of one protein with both activities. It is unknown if the separate expression of the proteins provides an advantage to the parasite, perhaps allowing the two separate proteins to work independently in diverse pathways. Moreover, the question still remains as to whether the two proteins interact with each other in order to compensate for the lack of a protein with both domains, or do TbPolN and TbHelQ provide completely different roles in the parasite?

As described in section 3.2.2, the putative Rev3 component of TbPolZ was compared with the PolZ catalytic subunit of *A. thaliana* and *H. sapiens*. From this analysis, we could identify the presence of six conserved motifs characteristic of the B family of polymerases (Lin, Wu and Wang, 1999; Gan *et al.*, 2008). The alignment of the sequences shows high homology across the motifs, suggesting that the Rev3 catalytic subunit is conserved between the three members of the B family of polymerases and that the *T. brucei* protein is likely active (see below). What is not known, however, is whether TbRev3 forms part of a conventional multisubunit PolZ, as interacting subunits have not been described.

Domain predictions using Pfam and InterPro software (Section 3.2.2) show a similarity between the domain organization of *T. brucei, H. sapiens* and *A.*

thaliana Rev3, with each constituted by a C-terminal polymerase domain, a C-terminal multifunctional domain and an N-terminal exonuclease domain. In spite of the presence of the exonuclease domain in the three species, it has not been demonstrated that this domain provides a nuclease function (Vaisman and Woodgate, 2017). The presence of a conserved, dormant exonuclease domain suggests TbPolZ, through TbRev3, plays a role in a TLS pathway, though activity assays are necessary to test this prediction. The only difference between Rev3 in *T. brucei* and the other two species is the lack of the C-terminal zinc finger domain in the parasite catalytic subunit. The zinc finger domain has been associated with an interaction between PolZ and PCNA, regulating the binding of the polymerase to the DNA template (Vaisman and Woodgate, 2017). However, previous experiments performed in *S. cerevisiae* demonstrate that the absence of PCNA does not affect the recruitment of the protein to the DNA template (McVey et al., 2016; Waters et al., 2009). There is the possibility that in the parasite, as well as in *S. cerevisiae*, the recruitment of TbPolZ is regulated by another mechanism. The zinc finger domain has also been associated with the possible interaction of the PolZ catalytic subunit and Pol δ accessory subunits. A Fe-S cluster that localizes next to the zinc finger is known to coordinate the interaction between the two proteins (Baranovskiy *et al.*, 2012). In humans it has been suggested that Polδ is able to regulate the TLS pathway by the recruitment of TLS polymerases that bind to the C-terminal domain (Tian *et al.*, 2016). Whether the lack of the zinc finger domain in the parasite protein interrupts the interaction between both proteins is unknown.

3.4.2 Cell cycle analysis after the depletion of TbPolN and TbRev3

DNA replication is characterized by its efficiency and high fidelity, ensuring the viability of cells (Sale, 2013). Under optimal conditions, most lesions are repaired during the G1 phase of the cell cycle, thus assuring replication can proceed in the presence of a damage free DNA template (Ziv *et al.*, 2014). However, if DNA damage can escape the DNA repair machinery during G1 phase, or new lesions are formed during replication, the presence of a tolerance repair pathway to avoid the collapse of the cell is required (Ziv *et al.*, 2014). TLS pols play active roles during this process; these polymerases primarily function during S and early G2 phases of the cell cycle, thus ensuring the

culmination of replication (Ziv *et al.*, 2014). Previous studies have shown that members of the Y family of polymerases are involved in the TLS pathway; other proteins, such as PolN, PolQ and PolZ, though they do not belong to the Y family of polymerases, play active roles during this tolerance process and in other repair mechanisms (Garcia-Diaz and Bebenek, 2007).

TbPolN and TbRev3 were successfully depleted by RNAi with the aim of better understanding their role(s) in bloodstream from *T. brucei* cells. Foremost, the depletion of TbPolN resulted in a notable decrease in cell proliferation (Figure 3-10) and a rise in the number of aberrant cells in the population (Figure 3-12). The aberrant cells contained multiple kinetoplasts and abnormal nuclear content, with this phenotype most pronounced at 48 hours, at which time ~60% of the cell population was comprised of aberrant cells. Furthermore, a significant decrease (~50%) of 1N1K cells occurred, thus suggesting an impairment of mitosis that may prevent cytokinesis.

It was suggested that the replication of the kinetoplast is coordinated distinctly, and perhaps independently, from nuclear replication (Hammarton *et al.*, 2003), where kinetoplast S phase starts before nuclear S phase, and kinetoplast segregation occurs in early G2 phase (Hammarton *et al.*, 2003). Independent control of the two replication processes would explain the accumulation of cells with multiple kinetoplasts and abnormal nuclei, in that even in the absence of effective nuclear replication and division, TbPolN RNAi cells successfully complete the kinetoplast replication and segregation, and perhaps continue to replicate again. These data link TbPolN with nuclear functions.

In *S. cerevisiae* it has been suggested that HR is essential for a successful cell division, since unrepaired DSBs affect chromosome segregation, impeding a proper division of the cell (Guirouilh-Barbat *et al.*, 2014). As mentioned previously, it has been proposed that PolN has a role during HR (Moldovan *et al.*, 2010). Taken together, these data may suggest that TbPolN has a role during this repair process. However, what aspect of repair provided by TbPolN is so central to nuclear replication and division is unclear. Nonetheless, depletion of TbPolN leads to a transient and not terminal phenotype, since cells continued to

proliferate after 48 hours of RNAi, and the cell cycle impediments were reduced. One potential explanation is redundancy between TLS pols; in the absence of one polymerase, others may have the ability to take over the function of the absent enzyme (Friedberg, Wagner and Radman, 2002). Numerous studies in other organisms have indicated the activity of other TLS pols during this process; for example, in the case of multicellular eukaryotes, PolQ plays an important role in HR (Wood and Doublié, 2016). As previously mentioned, *T. brucei* lacks PolQ, but in other organisms, PolZ has an active role during HR (Sharma, Helchowski and Canman, 2013a); perhaps this is the reason why the phenotype of the cells begins to reverse after the depletion of TbPolN. One other TLS Pol that may contribute to such redundancy is PrimPol2, another nuclear factor (Rudd *et al.*, 2013). RNAi against PrimPol2 also affects the cell cycle after G2 phase, but here the effect is lethal, unlike TbPolN. In addition, localisation of PrimPol2 is modulated by MMS treatment, perhaps indicating a role in repair (Rudd *et al.*, 2013).

The catalytic subunit of PolZ has been linked to other processes; in mice, the depletion of this protein leads to embryonic lethality, suggesting an important role during cell development and embryogenesis (Vaisman & Woodgate, 2017). Due to this, we hypothesized depletion of TbPolZ might also affect *T. brucei* proliferation. However, in contrast to TbPolN, cell growth was not affected by RNAi of TbRev3, suggesting this protein does not have an essential role in this stage of the parasite's life cycle. Generation of a TbRev3 null mutant would confirm the non-essential nature of this enzyme for the *in vitro* survival of *T. brucei*, and this is explored in Chapter 4.

3.4.3 Cell Sensitivity against genotoxic stress

DNA damage sensitivity after RNAi was tested by the exposure of *T. brucei* cells to two damaging agents, UV radiation and MMS, with the aim to elucidate a possible role in the repair of cross-link and DSB lesions. The exposure to UV radiation results in the formation of cyclobutane pyrimidine dimers and pyrimidine (6-4) pyrimidine photoproducts. The main repair pathway for tackling these lesions is the NER pathway (Genois *et al.*, 2014; Shah and He, 2015). Studies made in *T. brucei* have demonstrated the presence of this repair

machinery in the parasite, including its role in the removal of UV lesions (Machado *et al.*, 2014).The helicase XPB-R has an important role during this process. The knockout of this gene results in an increase in the sensitivity of cells against UV radiation and cisplatin (Badjatia *et al.*, 2013). It is proposed that XPB-R may have an important role in unwinding the site of damage, permitting the repair of the lesion (Badjatia *et al.*, 2013). In contrast, MMS, an alkylating agent, has the capacity to generate DNA breaks, including both single and DSBs (Wyatt and Pittman, 2006); this type of lesion is commonly tackled by HR (Lundin *et al.*, 2005). In *S. cerevisiae*, it has been demonstrated that alteration of the HR pathway results in increased sensitivity of cells to alkylating agents (Lundin *et al.*, 2005). Similar results have been observed in *T. brucei* in the absence of RAD51, RAD51 paralogues and BRCA2. An increase in the sensitivity to the alkylating agent MMS was observed in the absences of the Rad51 paralogues, RAD51-4 and RAD51-6 (Dobson *et al.*, 2011). The same effect was detected in BRCA2 mutants and Rad51 mutants, associating this protein with the repair of DSB (McCulloch and Barry, 1999; Hartley and McCulloch, 2008).

RNAi against TbPolN and TbRev3 showed sensitivity to both damaging agents. We hypothesized that we would observe a strong growth effect following depletion of TbRev3 after exposure to UV radiation, due to the active role that PolZ has in the repair of lesions caused by photoproducts, in collaboration with Polκ and ι, in other organisms (Zhu and Zhang, 2003; Shah and He, 2015). However, the *T. brucei* cells presented only a mild sensitivity, which suggests other TLS pols are more involved during the repair of UV induced lesions. An important TLS pol that plays a crucial role in this process in other organisms is Polη (Shah and He, 2015). This enzyme is able to repair UV lesions in an error-free manner, being capable of both base insertion and template extension without requiring another polymerase (Shah and He, 2015). Due to the polymerase's ability to complete synthesis without the help of other proteins, there is the potential that *T. brucei* Polη provides the predominant activity during the repair of UV lesions, with TbPolZ playing a lesser role. Polη has not been examined here, or by others, in *T. brucei*, so further experiments would be needed to test this prediction. It was, however, observed that TbPolN depleted cells show increased sensitivity to UV radiation compared toTbRev3 depleted cells (Section 3.3.3.2), suggesting PolN plays a pronounced role. Previous studies

have shown the activity of PolN during cross-link repair in avian cells (Moldovan *et al.*, 2010). It has been proposed that the repair of DNA cross-links involves the action of three DNA repair pathways: NER, TLS and HR. Since NER mutants in *T. brucei* are also sensitive to UV, it is possible that NER is in charge of generating the incision at the lesion, and TLS bypass of the lesion, or HR, is in charge of later repair. As PolN functions within these pathways, its depletion may explain the increase in sensitivity to cross-link and DSB agents after its depletion in *T. brucei*, as in avian cells (Moldovan *et al.*, 2010). Further support for this suggestion is that RNAi depletion of PolN also sensitises the cells to MMS, whose is known to generate DSBs, which are commonly repaired by HR (Lundin *et al.*, 2005; Wyatt and Pittman, 2006).

Perhaps surprisingly, TbRev3 depleted cells showed greater sensitivity to MMS than TbPolN depleted cells, a result consistent with the readout of whole genome RITseq of putative MMS repair factors (Stortz *et al.*, 2017). PolZ has been shown to function in the context of HR repair in other organisms (Sharma, Helchowski and Canman, 2013a): its deletion sensitises avian and mammalian cells to MMS and UV (Van Sloun *et al.*, 2002; Okada *et al.*, 2005; Sharma, Helchowski and Canman, 2013a). In *S. cerevisiae,* an active role for PolZ during HR repair has been determined (Sharma *et al.*, 2012). These studies propose that the ability of this TLS pol to extend mismatched primers plays an important role during the early stages of HR; here the polymerase has the capacity to extend mismatch primers in the 3' invading strand, thereby facilitating the initiation of this pathway (Sharma *et al.*, 2012). Whether such activities are shared by TbPolZ is currently unknown.

4 Understanding the function of DNA Polymerase Zeta in *T. brucei*

4.1 Introduction

4.1.1 DNA Polymerase Zeta in Eukaryotes

4.1.1.1 Structure and possible interactions

DNA Polymerase Zeta (PolZ) is a member of the B family of DNA Pols. Yet unlike other members of this family, PolZ is characterized by its low fidelity due to the lack of 3'- 5' proofreading activity (Sharma, Helchowski and Canman, 2013a). It is suggested that PolZ consists of a core, which contains the catalytic subunit Rev3 and the structural subunit Rev7 (Gan *et al.*, 2008). There is also the presence of two accessory subunits that are known as Pol31/Pol32 in *S. cerevisiae* and P50/P66 in humans (Lee, Gregory and Yang, 2014).

Interestingly, in *S. cerevisiae* it has been demonstrated that the accessory subunits, Pol31/Pol32, are shared with Pol δ (Baranovskiy *et al.*, 2012; Lee, Gregory and Yang, 2014). Polymerase δ is a member of the B family polymerases, which are characterized by their high fidelity (Baranovskiy *et al.*, 2012) and have an important role in replication of both the leading and lagging DNA strands (Johansson, Majka and Burgers, 2001). In yeast this polymerase is composed of three subunits, Pol3 (catalytic subunit), Pol31 and Pol32 (Johansson, Majka and Burgers, 2001), the latter two of which are shared with PolZ (Makarova and Burgers, 2015).

 It was suggested that when Polδ encounters a lesion within the DNA template, the replication fork stalls, activating an unknown signal that in turn provokes the dissociation of Pol3 from Pol31 and Pol32 (Baranovskiy *et al.*, 2012). The last two subunits remain associated with the site of damage, forming a complex with Rev3 and Rev7 (Baranovskiy *et al.,* 2012; Makarova and Burgers, 2015). The Polδ catalytic subunit replaces Rev3 and Rev7 after PolZ bypasses the DNA lesion, allowing the culmination of the replication process (Baranovskiy *et al.*, 2012). This interaction suggests a possible role of Polδ in the regulation of the TLS pathway (Baranovskiy *et al.*, 2012).

It has also been demonstrated that Rev3 and Rev7 interact with Rev1, another TLS pol member of the Y family of DNA pols. Together they are able to

extend through mismatched primers and DNA secondary structures (McVey *et al.*, 2016). It is believed that Rev1, similar to Polδ, is involved in the regulation of the TLS pathway, working as a platform protein recruiting TLS pols by interactions with its C-terminal domain (McVey *et al.*, 2016). The TLS pols that are known to interact with Rev1, apart from PolZ (Rev3 and Rev7), are Polη, Polι and Polκ (McVey *et al.*, 2016). Previous studies have suggested the interaction of PolZ with Polη, Polι and Polκ occurs during the error tolerance repair pathway. During this process PolZ works like an extender and the other three TLS pols are in charge of the nucleotide insertion (Zhao & Washington 2017a).

4.1.1.2 The role of DNA Polymerase Zeta

PolZ is characterised by its ability to bypass through cyclobutane pyrimidine dimers (CPD), produced by UV irradiation, with a high probability of inserting mutations during the process (Zhao & Washington 2017a). This capacity has been demonstrated by the overexpression of Rev3, provoking an increase in spontaneous mutations (Singh *et al.*, 2015). The repair of UV lesions is not the only role of PolZ, however. Deletion of the PolZ catalytic sub-unit (Rev3) results in embryonic lethality in mice (Sharma, Helchowski and Canman, 2013a; Makarova and Burgers, 2015; Singh *et al.*, 2015), revealing that PolZ has an essential role during the early stage of mammalian embryonic development, which cannot be replaced by any other Pols (Sharma, Helchowski and Canman, 2013a).

There are also studies suggesting a role of PolZ during HR. Experiments performed in human and chicken cells, showed that the deletion of Rev1, Rev3 or Rev7 provokes an increase in sensitivity to DNA cross-link and DNA DSBs (Sharma, Helchowski and Canman, 2013a). A decrease in HR by 50% was observed in mammals and *Drosophila melanogaster* in the absence of the PolZ catalytic subunit (Sharma *et al.*, 2012; Sharma, Helchowski and Canman, 2013a). The depletion in mammalian cells of Rev1, Rev3 and Rev7 by siRNA, generates the accumulation of foci of Rad51, an essential protein involved in HR (Sharma *et al.*, 2012). This suggests a relevant role of the three proteins during this repair pathway (Sharma *et al.*, 2012).

It was proposed that PolZ (Rev3 and Rev7) works in association with Rev1 during the initial step of the HR pathway (Sharma *et al.*, 2012). Due to PolZ's ability to extend mismatched primers, the complex Rev1/PolZ (Rev3 and Rev7) is able to proceed with the extension step in the presence of a 3'mismatch in the invading DNA strand (Sharma *et al.*, 2012).

Even though TLS Pols are known to be preferentially expressed in the nucleus, the presence of some of these proteins has also been documented in the mitochondria. Previous studies have shown the presence of Rev1, Rev3 and Rev7 in yeast mitochondria (Zhang, Chatterjee and Singh, 2006). Experiments performed in *S. cerevisiae* using single mutants of mtRev1, mtRev3 and mtRev7 show a decrease of spontaneous mutations, proposing a role for these proteins in mitochondrial genome mutagenesis (Zhang, Chatterjee and Singh, 2006). On the other hand, in humans uniquely the catalytic subunit has been localized in the organelle (Singh *et al.*, 2015). Here, the deletion of Rev3 is linked with the alteration of the oxidative phosphorylation system, suggesting a role in the regulation of the mitochondrial metabolic pathway (Singh *et al.*, 2015). Interestingly, this is not the only possible role of mtRev3 in humans; chromatin immunoprecipitation analysis has shown a high affinity of PolZ catalytic subunit towards D-loop regions (Singh *et al.*, 2015). These regions are known to be highly sensitive to UV radiation, proposing a role for PolZ in the maintenance of mitochondrial integrity (Singh *et al.*, 2015).

In *T. brucei* the presence of PolZ subunits in the mitochondria has not been reported. In the parasite, there are five polymerases that are involved in the maintenance of the organelle's genome integrity: Polß, Polß PAK, PolIB, PolIC and PolID (Klingbeil, Motyka and Englund, 2002; David F Bruhn, Sammartino and Klingbeil, 2011). The first two polymerases are members of the X family of polymerases and are known to be involved in a late stage of the minicircle replication, during which they collaborate in the processing and gap filling of the Okazaki fragments (Saxowsky *et al.*, 2003; David F. Bruhn, Sammartino and Klingbeil, 2011). The last three polymerases are members of the A family of polymerases and are known to be involved in kinetoplast replication (Klingbeil, Motyka and Englund, 2002; Chandler *et al.*, 2008; Bruhn *et al.*, 2010).

The aim of this chapter was to perform a more in-depth characterisation of TbPolZ, analyzing its subcellular localization, the effects seen after the loss of the protein and its link with damage repair, in order to have a better understanding of its function in the parasite.

4.2 Intracellular localization of the catalytic subunit of Polymerase Zeta (TbRev3)

4.2.1 Verification of TbRev3 endogenous epitope tagging via Western blot analysis

As it was mentioned above, although PolZ predominantly is localised in the nucleus it has also been detected in the mitochondria of *S. cerevisiae* and humans, suggesting a role in the maintenance of both organelles (Zhang, Chatterjee and Singh, 2006; Singh *et al.*, 2015). Evaluation of the intracellular localisation of TbRev3 is of high importance, as this information will help the elucidation of a role for this protein in the parasite. For instance, does it play a role in the nucleus or kinetoplast, and does it display discrete or generalised localisation within an organelle?

For this, the Rev3 component of TbPolZ was endogenously tagged, meaning that the Rev3 gene was modified *in situ* to express TbREV3 as a C-terminal fusion with 12 copies of the myc epitope. This manipulation was achieved using the 12Myc pNAT BSD vector (Alsford and Horn, 2008), inserting 1592 bp of the C-terminal end of Tb*Rev3* after PCR-amplification with the primers Fw-gcatgagctccagatggctattaaaatgct (SacI site) and Rv-gcattctagagcgagtcgttacgtagtctt (XbaI site) (Figure 4-1 A). Plasmid and PCR fragment were digested with SacI and XbaI, followed by ligation. The resulting plasmid was sequenced to verify correct construction and then digested by HpaI and transformed into Lister 427 BSF *T. brucei*, allowing integration by 'single crossover' homologous recombination (2.5.1). To check if the TbRev3 variant was expressed as a fusion with the 12 myc tag, a Western blot was performed using an anti-myc antibody. A band of approximately ~231 kDa (216.8kDa for Rev3, 14.4 kDa for 12myc), was seen in cell extracts of two blasticidin resistant transformants (Figure 4-1 B).

A.

B.
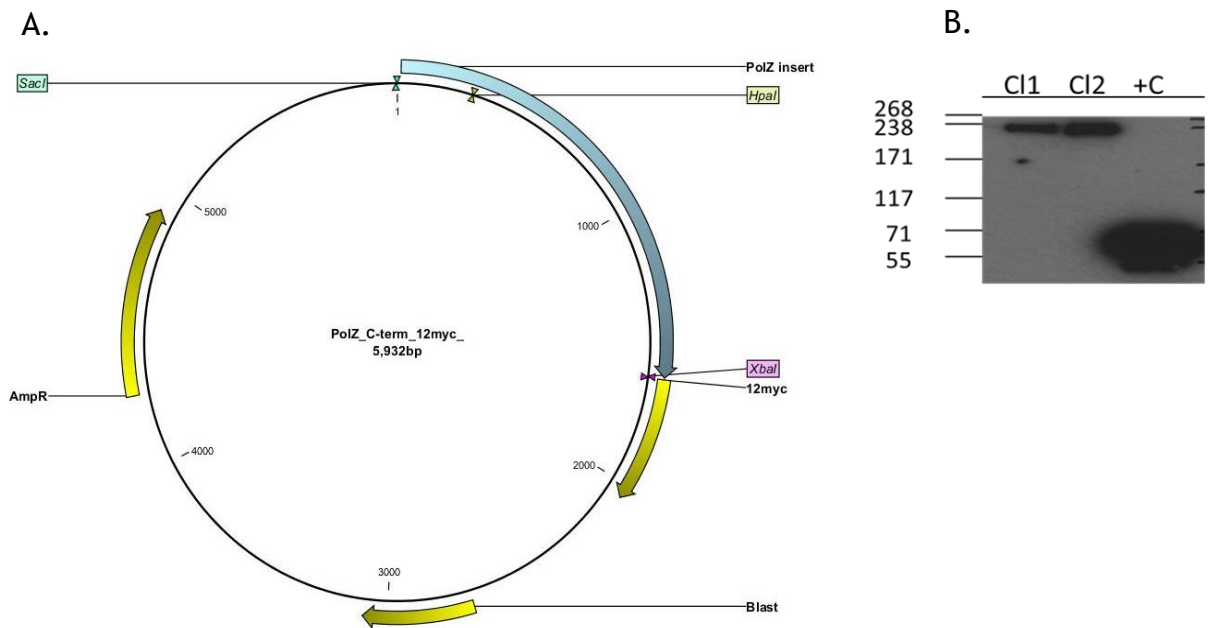
Figure 4-1. C- terminal plasmid map and and confirmatory Western blot showing the correct fusion of the myc tag. A. Map of the C-terminal tagging vector containing a 12 Myc tag sequence (represented in yellow) and (in blue) the TbRev3 insert, derived from the C-terminus of the complete ORF. Cloning restriction sites are labelled in green and pink (SacI and XbaI) **B.**Western blot of whole cell extracts from two blasticidin resistant transformants and from a cell line expressing the protein kinase TbAUK2-12myc as a control (+C), detected using anti-myc antibody. The Wt untagged cell line is not shown in the Western blot.

4.2.2 TbREV3 localization in the absence and presence of DNA damage

Localisation of TbRev3-12myc was assessed by immunofluorescence of permeabilised cells, using an anti-myc antibody. The intracellular localisation of the protein was tested before and after exposure of the cells to the alkylating agent MMS (0.0003%) for 18 h. In both conditions, the predominant signal was present in the nucleus, though some extra-nuclear staining was also apparent (Figure 4-2). The extra-nuclear signal was considered as background staining, due to the fact that signal was also detected in WT (untagged) cells (Figure 4-3 A). Surprisingly, a signal was also observed in the kinetoplast (Figure 4-2). The nuclear signal appeared to be present throughout the organelle and did not notably change when analysed inthe different cell cycle stages (Figure 4-3 B). In contrast, the kinetoplast staining was more pronounced after exposure to MMS (Figure 4-2), though it was still not seen in every cell, in common with the

nuclear signal. The kinetoplast signal seems to predominate in the 1N1K cells, although it was also possible to detect a weak signal in other cell cycle stages (Figure 4-4). From a total of 50 cells, it was possible to detect the myc signal in the kinetoplast of 6% of undamaged cells and in 21% of damaged cells. These data may suggest that at least the TbRev3 component of TbPolZ may act in the kinetoplast.
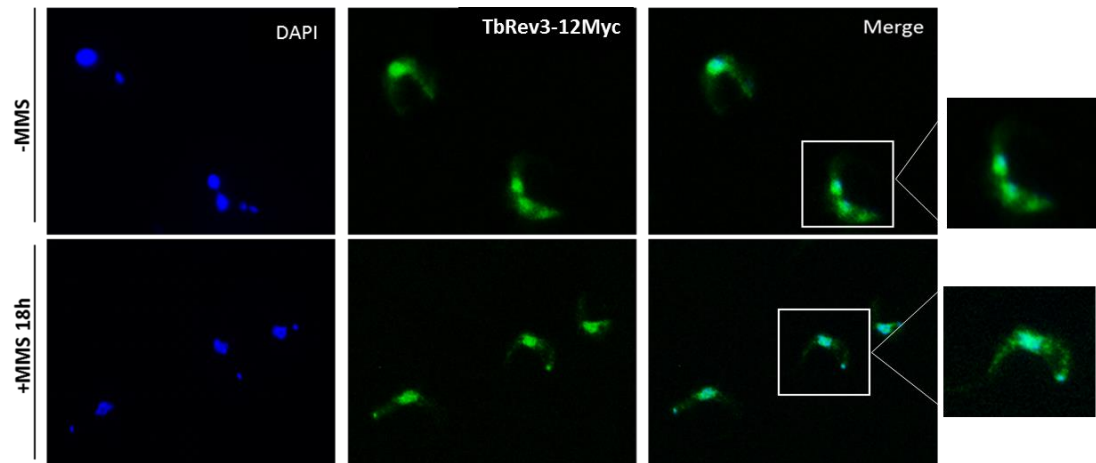
Figure 4-2. Immunolocalisation of C-terminally 12myc-tagged TbRev3 in the absence and presence of MMS damage. Immunolocalization of REV3-12myc in *T. brucei* BSF cells: first panel showing DAPI staining of the nucleus and kinetoplast, the second panel shows localization of Rev3-12myc using a conjugated Alexa Fluor® 488 anti-myc antibody, and the third panel is merged images of both signals. Cells are shown after culture without damage (-MMS) or after growth for 18 hrs in the presence of 0.0003% methyl methanosulphonate (+MMS 18 h). Larger images of boxes show the nuclear and kinetoplastid signals.
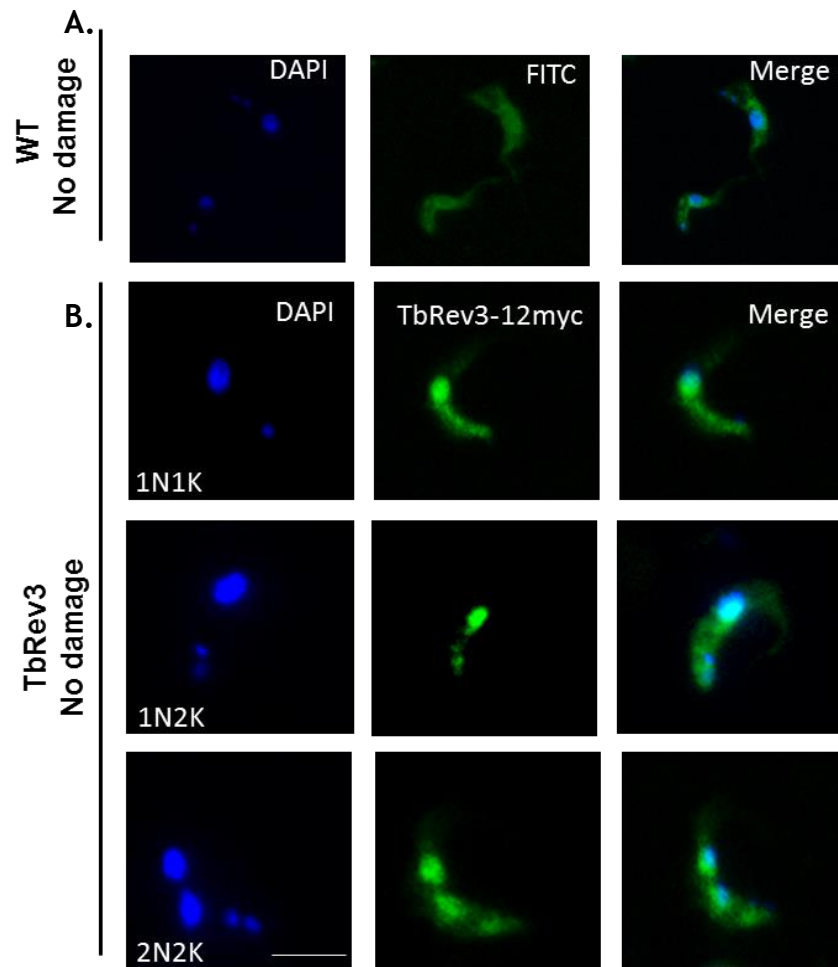
Figure 4-3. Nuclear immunolocalisation of TbRev3-12myc throughout the different cell cycle stages. A. The top panels show representative field of view images from WT cells (Lister 427) stained with DAPI (to visualise the nDNA and kDNA) and conjugated Alexa Fluor® 488 anti-myc antibody. **B.** The lower panels show the detection of anti-myc signal throughout the three stages of the cell cycle in TbRev3-12myc expressing cells. The left panel shows DAPI staining of the nucleus and kinetoplast, the middle panel shows localisation of TbRev3-12myc using a conjugated Alexa Fluor® 488 anti-myc antibody, and the right panel is merged images of both signals. Scale bar 5 μm.
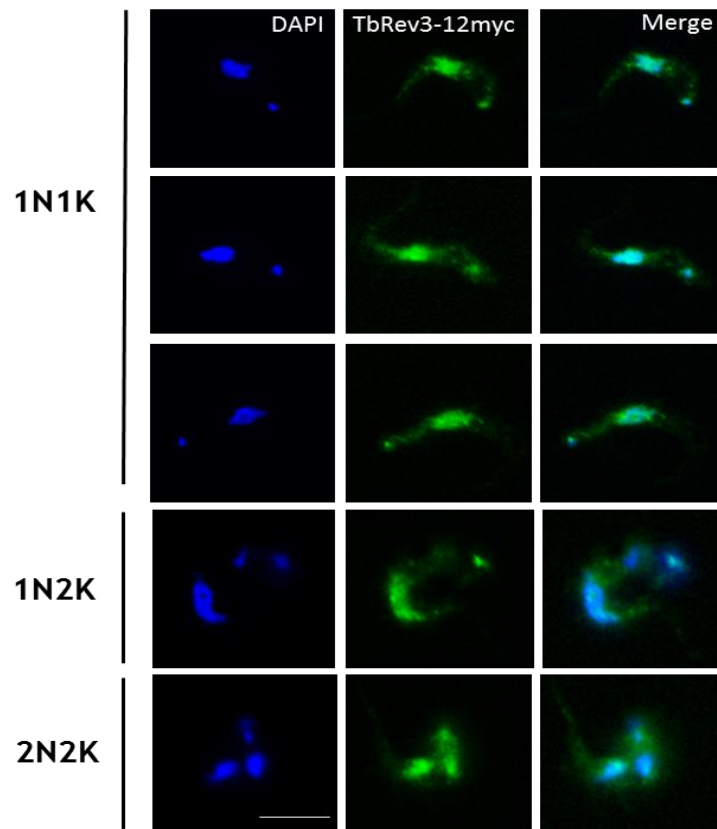
Figure 4-4. Mitochondrial immunolocalisation of TbRev3-12myc throughout the different cell cycle stages after growth for 18 hrs in the presence of 0.0003% methyl methanosulphonate. Detection of anti-myc signal throughout the three stages of the cell cycle in TbRev3-12myc expressing cells. The left panel shows DAPI staining of the nucleus and kinetoplast, the middle panel shows localisation of TbRev3-12myc using a conjugated Alexa Fluor® 488 anti-myc antibody, and the right panel is merged images of both signals. Scale bar, 5 µm.

4.3 Generation of TbRev3 knockout cell lines

As discussed previously (section 3.3.1), depletion of TbPolZ by TbRev3 RNAi did not suggest an essential role in BSF cells. However, these data do not mean that TbPolZ does not have an important role in the parasite, or indeed are definitive. High stability of the protein could confound the effectiveness of RNAi knockdown, or the cellular function may require only a low concentration of the enzyme. For these reasons, a full knockout of Tb*Rev3* was attempted to more rigorously test the prediction that TbRev3 is non-essential and ask if the complete absence of the gene affects the growth of the cells. Disruption of the *TbRev3* gene was performed by two sequential rounds of transformation into wild type (WT) BSF cells (*T. brucei* Lister 427) using two constructs: one containing a BSD cassette (ΔPolZ:: BSD) (Figure 4-5 A) and the other a NEO cassette (ΔPolZ:: NEO) (Figure 4-5 B).

A region of approximately 500 bp was PCR-amplified, which includes a part of the UTR and ORF of the gene of interest, from both the 5'and 3' regions. The forward and reverse primers used for the amplification were designed to include a specific restriction site, important for the cloning step. In this specific case, two variations of the 5' region forward primer were designed, one containing MluI and NotI restriction sites (gcatacgcgtgcggccgcttggaaactcggctattgga) and the other BamHI and NotI sites (gcatggatccgcggccgcttggaaactcggctattgga). The first primer was used for the amplification of the product that was ligated into the NEO vector and the second was used for the amplification of the insert cloned into the BSD vector. In the case of the 5' reverse primer the XbaI restriction site was included (gcattctagattcccttcagtggttgtgta). The 3' region forward primer contains SacI restriction site (gcatgagctcttttctatccagtcggaaga) and ClaI and NotI for the 3' reverse primer (gcatatcgatgcggccgctcacgtttgccttgagacac).

The PCR products and vectors were digested with MluI/BamHI+XbaI and SacI+ClaI allowing the correct ligation of the inserts into the BSD and NEO vector (Figure 4-6). The resulting plasmid constructs were checked by sequencing and linearised with NotI. The 5´and 3´UTRs in the constructs, flanking the drug resistance cassettes, allowed HR, replacing the ORF of the gene with the antibiotic resistance cassette (Figure 4-7).
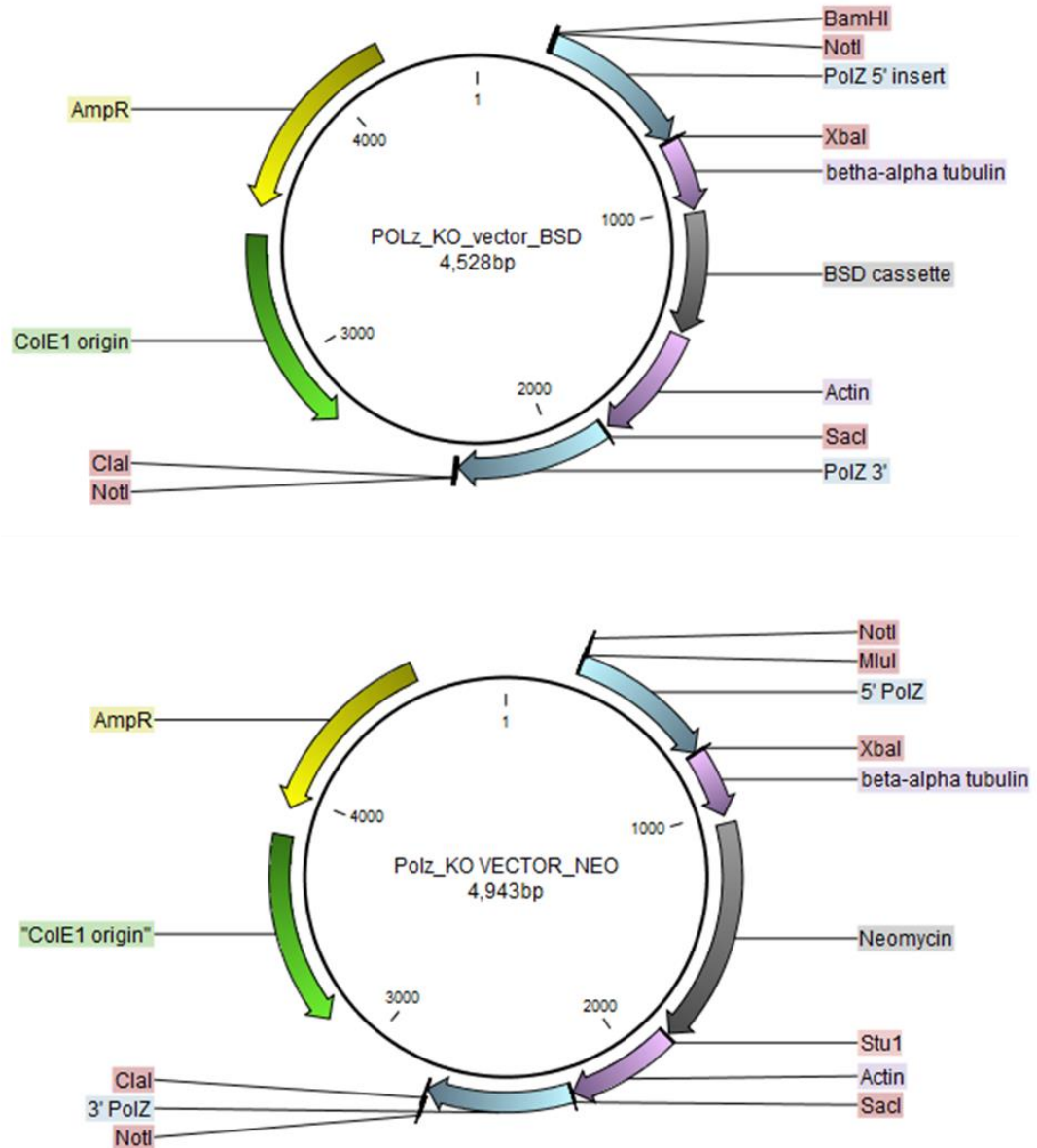
Figure 4-5. Plasmid maps of the constructs used for the deletion of TbREV3. In grey are represented the *BSD* and *NEO* cassettes, encoding the drug resistance markers used for the selection of clones. Flanked by ß-α tubulin and actin, represented in purple. In blue are represented sequences of approximately 200 bp that have homology with the 5'and 3' regions surrounding the *REV3* ORF, respectively, which provide homology for recombination and integration of the cassettes after transfection.
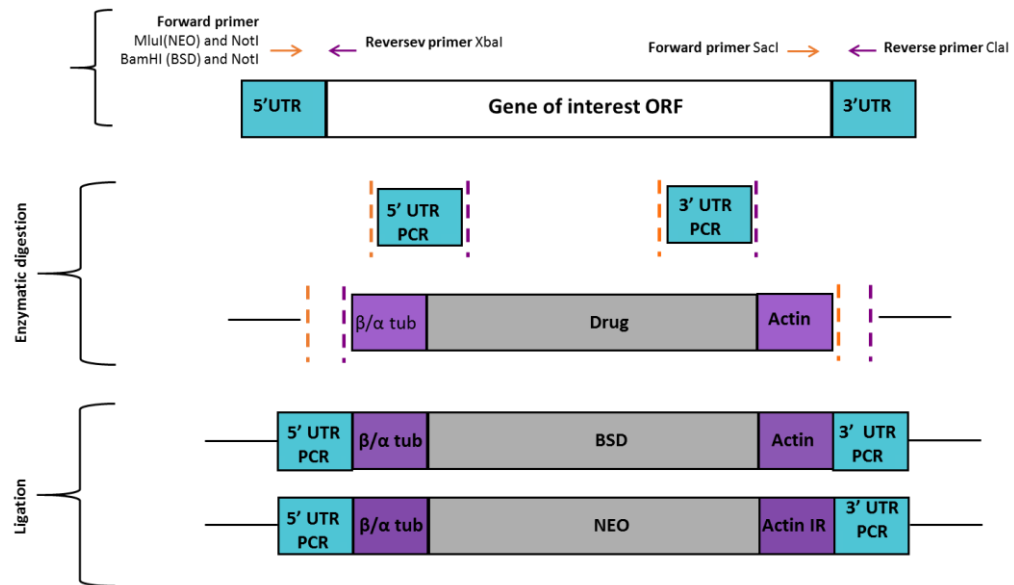
Figure 4-6. Schematic representation of the ligation of the 5'and 3'UTR PCR product into the BSD and NEO vector. The 5'and 3' intergenic regions of the gene (UTR) are represented in blue, the ORF of the gene in white and the arrows show the amplification region. The drug resistance cassettes are represented in grey; the intergenic regions are represented in purple. The diagram shows the cloning of the targeting regions (PCR product) into the vectors.
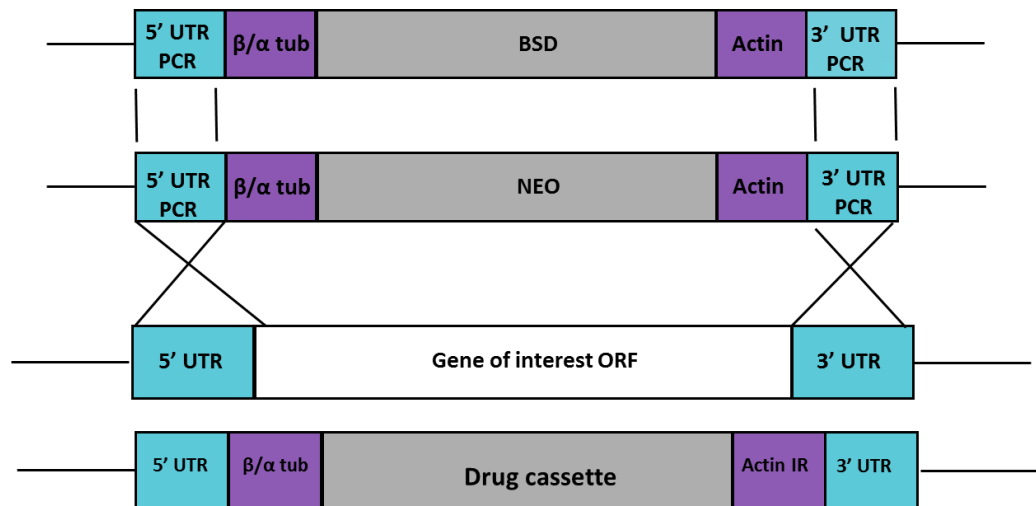
Figure 4-7.Schematic representation of the replacement of the ORF of a gene of interest with the drug resistance cassette, mediated by homologous recombination. The targeting regions in the vector and the homology sequence in the gene are represented in blue. The mediated HR is represented by the crosses, showing the replacement of the ORF (white) with the drug cassette (grey).

The ΔPolZ:: NEO construct was first transformed into WT cells, generating putative heterozygous mutants (*TbRev3-/+*). Though G418 (NEO)-resistant cells were recovered, it was noticed that the addition of the antibiotic provoked a slowed growth of the transformant cells relative to wild type (data not shown). The drug was therefore removed during growth and transformation of the putative Tb*Rev3-/+* cells with the ΔRev3:: BSD construct. To test for the successful generation of the heterozygous and knockout cell lines, genomic DNA was extracted from putative *TbRev3-/+* and *TbRev3 -/-* null mutants for use as a template in PCR analysis. For the PCR, specific primers were used targeting the drug resistance cassettes and a region of the TbRev3 ORF (Table 2-1), testing for the presence of these genes (Figure 4-8 A). The clones were analysed by PCR, demonstrating the integration of the antibiotic resistance cassettes and the deletion of the ORF in the case of the null mutants to suggest the absence of TbRev3 and the successful generation of KO cell lines. Figure 4-8 B shows a comparison of the PCR products generated using WT, *TbRev3-/+* and two *TbRev3-/-* clones, demonstrating the presence of the expected cassettes and the presence or absence of the TbRev3 ORF.
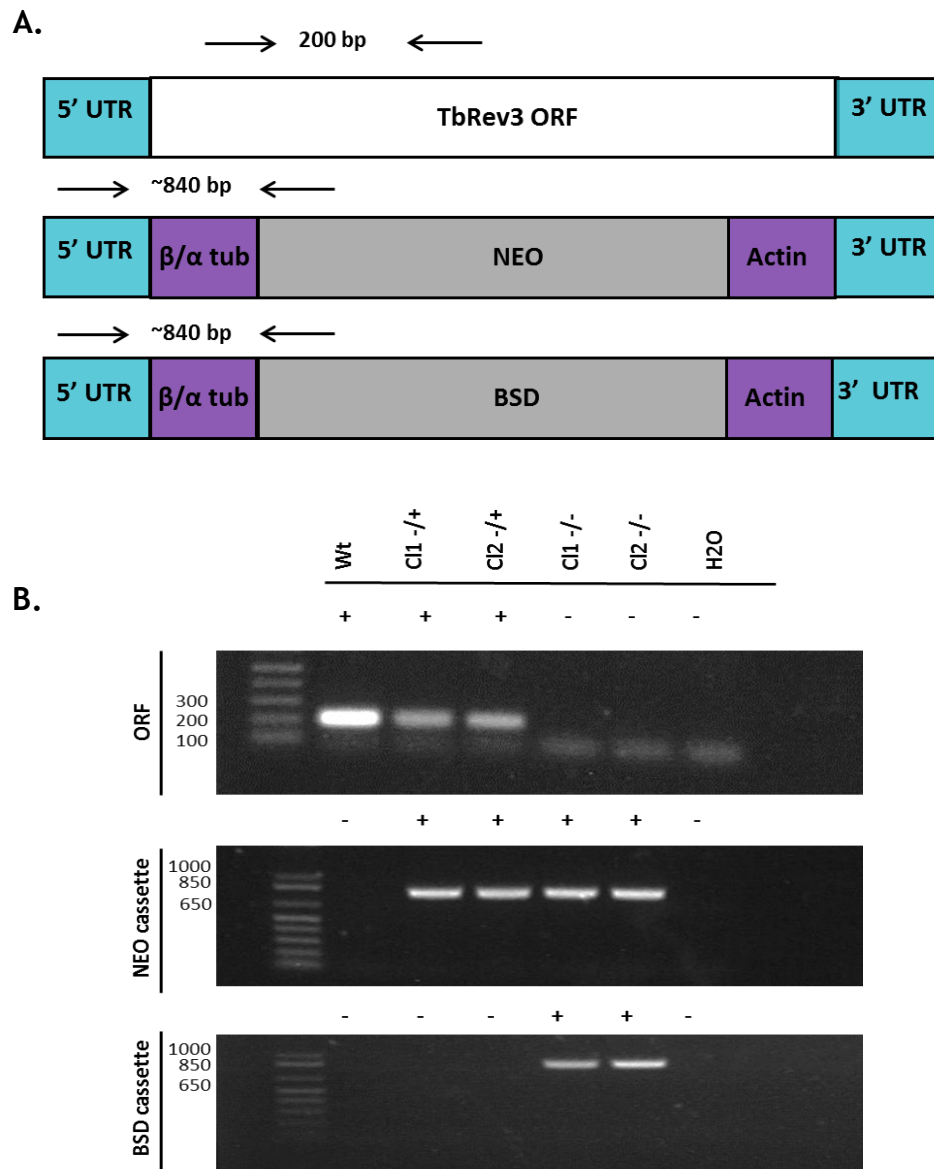
Figure 4-8. Confirmatory PCR of TbRev3 heterozygotes and null mutants. A. Schematic representation of expected fragment sizes amplified by PCR (bp), diagnostic primers used (black arrows) and their position in the genome. Primer sequences are available in Table 2-1. Not to scale. **B.** Agarose gels of diagnostic integration PCRs, testing the presence of TbRev3 ORF and integration of NEO or BSD cassette in wild type (Wt) cells, heterozygote +/- cells and null mutants -/-; ddH2O was used as a negative control. All PCRs were performed on the same gDNA samples.

4.3.1 Loss of TbRev3 is associated with increased sensitivity of BSF cells to DNA damage

To ask if the loss of TbRev3 had any stronger effect than RNAi, the growth of the two *TbRev3-/-* clones was compared with WT (Figure 4-9A). No difference in population doubling time was apparent, suggesting that loss of TbRev3 had no

effect on the cells survival in culture. The growth of the *TbRev3-/-* mutants was compared with WT cells in the presence of three concentrations of MMS, asking if loss of TLS pol increases sensitivity of the cells to damage. Though the effect was not very pronounced, growth of the *TbRev3-/-* cells was notably slower than WT at the highest concentration of MMS (0.0003%) and perhaps slightly reduced at 0.0002% MMS (Figure 4-9 B), suggesting that TbPolZ is involved in the repair of MMS induced damage. To ask if this effect is only seen in the null mutants, growth of the *TbRev3-/+* cell line was also compared with WT, though in a separate experiment. In this experiment greater slowing of WT growth was seen, perhaps due to pipetting differences during drug dilution, but it appeared that it was possible to observe a slightly increased growth reduction of the heterozygous mutants relative to WT at 0.0003% MMS (Figure 4-9 C). The results obtained, with TbRev3-/+ and TbRev3-/-, resemble the growth effect observed in the RNAi cell line against TbRev3 after MMS damage (section 3.3.3). Showing a growth effect after the exposure with the highest concentration of MMS. This appears to confirm a role for TbPolZ in MMS repair.
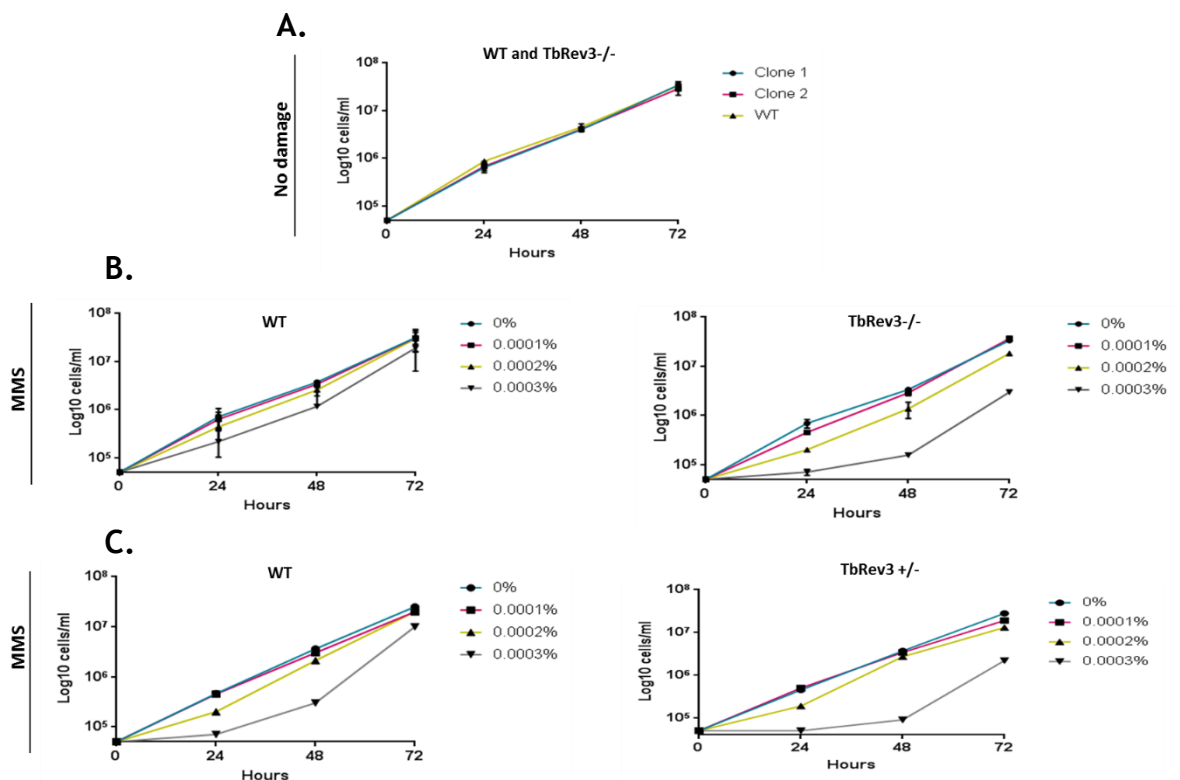
Figure 4-9. Proliferation of *TbRev3 +/-* and *TbRev3 -/-* cell lines under different concentrations of MMS. A. Growth curve of Wt427 and TbRev3 -/- full knockout in the absence of damage, showing no effect on the growth of the cells after the deletion of both alleles. B. Growth curve of Wt427 and null mutant

TbRev3 -/- cell line under different concentrations of MMS; showing an increase of sensitivity, at the highest concentration of MMS after the loss of one allele. C.Growth curve of Wt427 and heterozygote *TbRev3* +/- cell line under different concentrations of MMS; showing an increase of sensitivity, at the highest concentration of MMS after the loss of one allele.

4.4 Identifying potential TbRev3 interaction partners

4.4.1 Immunoprecipitation and mass spectrometry using TbRev3-12myc

PolZ in other eukaryotes is known to cooperate with diverse proteins facilitating the bypass of DNA lesions. An example is the interaction of *S. cerevisiae* and human Rev3 with the TLS pol Rev1 (Sharma *et al.*, 2012). In *S. cerevisiae*, it has been demonstrated that Polδ shares accessory subunits with PolZ (Pol31/32), resulting in PolZ forming a four subunit complex (Makarova and Burgers, 2015).

In order to try and examine TbPolZ function further, we next sought to ask what factors TbRev3 might interact with. For instance, if TbPolZ is conserved as a four subunit complex in *T. brucei*, it might be predicted that TbRev3 interacts with proteins related to the three other factors, including some overlap with DNA Pol δ.

To perform this analysis, extracts from WT cells and the cells expressing TbRev3-12myc were incubated with Dynabeads® (Invitrogen), magnetic beads coated with anti-myc antibody. After five washes with washing buffer (50 mM Hepes pH 7.55, 100 mM NaCl, 1 mM EDTA pH 8.0, 1 mM EGTA pH 8.0, 10 % glycerol, 0.1 % Triton X-100, and 2x complete protease and phosphatase inhibitor cocktail; Roche) the eluate was collected and re-suspended in 15 µl of 1x protein loading buffer (duplicates for each sample were performed). One of the eluates from each WT and TbRev3-12myc, was separated on 10% Bis-Tris gel by SDS-PAGE and stained with SYPRO®Ruby, revealing several bands that were only present in the tagged sample (Figure 4-10 A). With the second eluate, the specificity of the antibody of the two immunoprecipitations (IP) was confirmed by Western blot, detecting the presence of TbRev3-12myc exclusively in TbRev3-

12myc IP (Figure 4-10 B). After assessing the proper performance of the IPs, the remaining eluates of the WT IP and TbRev3-12myc IP were analysed by mass spectrometry (Glasgow Polyomics Facility).
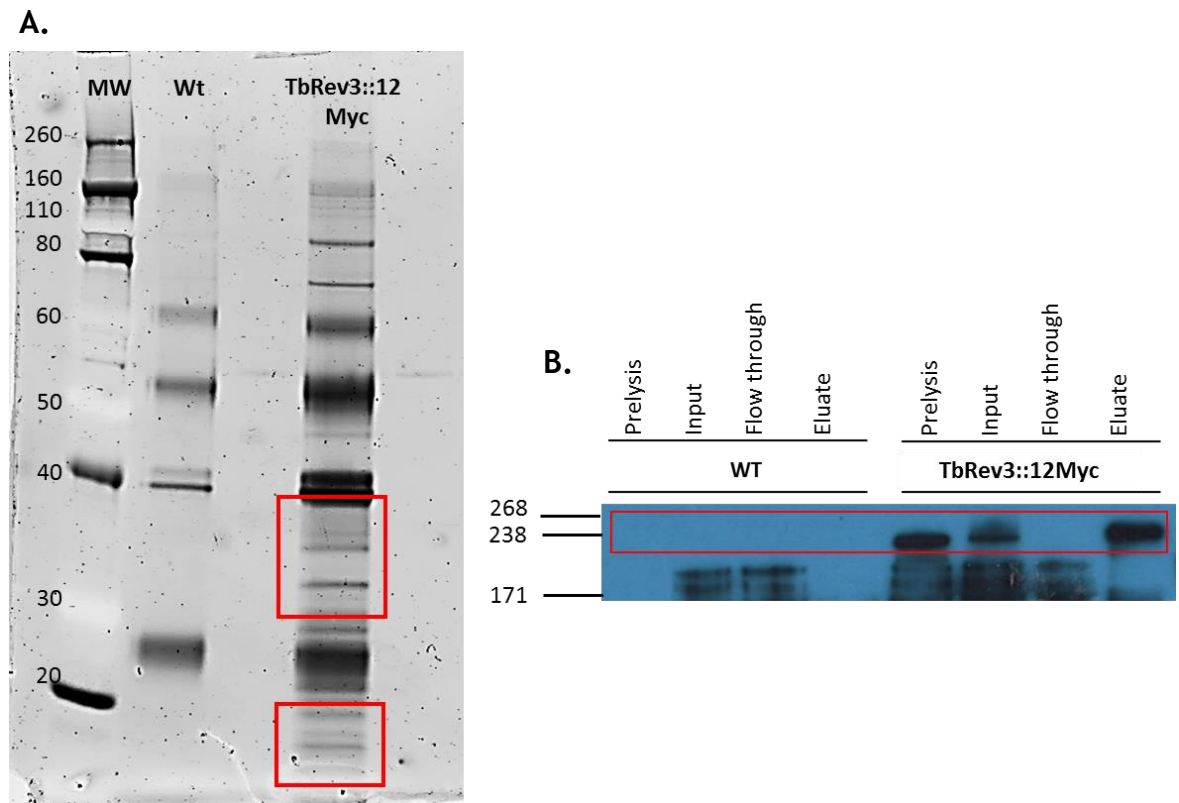
Figure 4-10. Validation of TbrEV3-12Myc immunoprecipitation. **A.** Syrpo ruby stained gel of anti-myc immunoprecipitated proteins from WT427 (un-tagged cell line) and TbRev3-12myc lysates. Some specific bands in the TbRev3-myc are enclosed in the red box. **B.** Western blot on all fractions of the IP from WT and TbRev3-12myc cells. Fractions from left to right: prelysis, input, flow-through and eluate from TbRev3-12myc and WT, showing the absence of bands in the untagged cell line. Red box show bands corresponding to TbRev3-12myc.

The mass spectrometry results show the immunoprecipitation of several possible interacting partners. Proteins were compared between the hits obtained with the WT cell line and the tagged cell line, in order to select only the proteins that were uniquely immunoprecipitated with the tagged cell line, ignoring those pulled down in both. In the WT immunoprecipitation, peptide hits were recovered for 87 proteins. Any proteins recovered in both samples were excluded, which amounted to removing 45 proteins from the TbRev3-12myc IP and left a total of 49 hits for the tagged cell line (Table 4-1). Next, the available

genome annotations of the remaining 49 proteins were examined for the exclusion of possible contaminants such as VSG and ribosomal proteins. The rest of the hits were analysed by BLASTp and those with insufficient information were also excluded, leaving eight potential TbRev3 interaction partners (Table 4-2).

Gene ID	Annotation	Score
Tb927.1.3180	40S ribosomal protein S11, putative	256
Tb10.389.0910	60S ribosomal protein L34, putative	183
Tb10.70.2170	ribosomal protein S27a, putative	156
Tb10.70.5650	TEF1 elongation factor 1-alpha	138
Tb927.2.450	retrotransposon hot spot (RHS) protein, putative	135
Tb10.70.1380	40S ribosomal protein S9, putative	126
Tb09.211.0540	FBPase fructose-1,6-bisphosphate, cytosolic	120
Tb11.01.6640	hypothetical protein, conserved	113
Tb09.244.2730	60S ribosomal protein L5	108
Tb927.7.7030	hypothetical protein, conserved	106
Tb10.61.1810	mitochondrial carrier protein, putative	104
Tb09.160.2490	1L12.125 ribosomal protein S7, putative	93
Tb10.70.1670	40S ribosomal protein S10, putative	93
Tb09.211.4850	60S ribosomal protein L26, putative	92
Tb927.1.710	PGKB phosphoglycerate kinase	89
Tb11.01.1790	60S ribosomal protein L29, putative	89
Tb09.211.4511	kinetoplastid membrane protein	85
Tb927.7.180	hypothetical protein	76
Tb927.5.2080	inosine-5'-monophosphate dehydrogenase, putative	75
Tb09.211.2650	60S ribosomal protein	69
Tb10.61.1390	40S ribosomal protein S13	62
Tb10.70.7020	RPS23 40S ribosomal protein S23, putative	62
Tb09.211.3680	HSP40 heat shock protein	60
Tb09.211.3830	Tb09.211.3830 hypothetical protein, conserved	60
Tb10.05.0060	hypothetical protein, conserved	54
Tb10.100.0080	40S ribosomal protein S6	53
Tb927.2.480	retrotransposon hot spot protein	50
Tb927.7.7460	hypothetical protein, conserved	48
Tb927.1.2430	histone H3, putative	43
Tb09.211.1150	hypothetical protein, conserved	41
Tb11.02.0740	60S ribosomal protein	40
Tb927.4.2070	antigenic protein	40
Tb927.4.1860	ribosomal protein S19	36
Tb927.4.3890	ATP-dependent RNA helicase, putative	35
Tb09.244.2720	ribosomal protein L15	35
Tb11.55.0013	cysteine desulfurase, putative	33
Tb927.6.2090	hypothetical protein, conserved	33
Tb09.160.4250	TRYP1 tryparedoxin peroxidase	28
Tb10.70.2465	nucleolar RNA-binding protein, putative	26
Tb09.v4.0057	variant surface glycoprotein (VSG, pseudogene)	25
Tb927.6.2210	hypothetical protein, conserved	23
Tb927.4.1390	hypothetical protein, conserved	23
Tb927.8.7260	kinetoplast-associated protein	23
Tb11.02.1566	variant surface glycoprotein (VSG)-related, putative	23
Tb927.3.1130	DNA polymerase delta subunit 2	22
Tb10.70.3290	DHH1 ATP-dependent DEAD-box RNA helicase	22
Tb09.160.5580	60S ribosomal protein L11	22
Tb11.02.5450	glucose-regulated protein 78, putative/Hsp70	19
Tb09.211.1750	mitochondrial carrier protein, putative	14

Table 4-1. Recovered proteins from TbRev3-12myc IP after Mass Spectrometry analysis. Proteins shown were only present in TbRev3 anti-myc IP; hits also identified in IP from WT cells were excluded. Interesting 'hits' are labelled in red. Samples were analysed using MASCOT software.

Gene ID	Annotation	Predicted domains	Score
Tb10.61.1810	mitochondrial carrier protein, putative	ADP/ATP transporter on adenylate translocase	104
Tb09.211.3680	HSP40 heat shock protein	DnaJ-class molecular chaperone with C-terminal Zn finger domain	60
Tb11.55.0013	cysteine desulfurase, putative	Aminotransferase class-V	33
Tb09.160.4250	TRYP1 tryparedoxin peroxidase	Peroxiredoxin (PRX) family,	28
Tb927.8.7260	kinetoplast-associated protein	No putative conserved domains	23
Tb927.3.1130	DNA polymerase delta subunit 2	PolD2 (DNA polymerase delta, subunit 2), C-terminal domain	22
Tb11.02.5450	glucose-regulated protein 78, putative/Hsp	Heat shock protein 70kD (HSP70), peptide-binding domain	19
Tb09.211.1750	mitochondrial carrier protein, putative	Mitochondrial carrier protein	14

Table 4-2. Potential TbRev3 interaction partners identified by Mass Spectrometry analysis. Proteins shown were only present in IP from TbRev3-12myc. Proteins were analysed using MASCOT. Protein sequence for each 'hit' was examined by BLASTp.

After excluding the possible contaminants, heat shock proteins, mitochondrial proteins and DNA polymerase δ subunit 2 were classified as potential interaction partners. The obtained hits have not been verified by further analysis and so must be considered as preliminary data.

Blastp analysis of DNA polymerase delta subunit 2 (Tb927.3.1130) demonstrated homology (E- value of 2e-40 and 25% identity) with the *S. cerevisiae* Polδ subunit, Pol31 (Gene ID EEU05433.1). In *S. cerevisiae*, the interaction between the accessory subunits of Polδ and the catalytic subunit of PolZ have been confirmed, showing an important role in the regulation of the TLS pathway (McVey *et al.*, 2016). Homologues of neither Pol32 nor Rev7, the other two subunits of *S. cerevisiae* PolZ, were found in the eluate of TbRev3-12myc. Blastp analysis of the yeast PolZ subunits Pol32 (NP_012577.1) and Rev7 (Gene ID NP_012127.1) was performed revealing, interestingly, no homologues were found in *T. brucei*. These findings may suggest that TbPolZ is not a four unit complex and TbPolδ lacks one of the accessory subunits, differing from the yeast proteins where PolZ consists of four subunits and Polδ is organized in three subunits (Figure 4-11). It will be important to elucidate if the possible absence of the accessory subunits (Rev7 and Pol32) affects the functions of TbPolZ and TbPolδ. It should be noted that these are speculations and further analysis need to be performed to confirm the absence of Pol32 and Rev7 homologues in *T. brucei*.

On the other hand, the recovery of the heat shock proteins, HSP40 (Tb09.211.3680) and HSP70 (Tb11.02.5450), is potentially interesting, as these have been suggested to be involved in the maintenance and replication of the mitochondrial DNA in *T. brucei* (Týč, Klingbeil and Lukeš, 2015). The interaction of TbPolZ with HSP40 and HSP70 is still uncertain, but if this interaction is proven, it will confirm a role of TbPolZ in the maintenance of the *T. brucei* mitochondria. Furthermore, the mitochondrial carriers (Tb10.61.1810, Tb09.211.1750, Tb11.55.0013) are of high relevance in *T. brucei*; previous studies have demonstrated that carriers allow the exchange of metabolites across the mitochondrial membrane for the proper function of different metabolic pathways (Colasante *et al.*, 2009). The key question would be whether or not the parasite is using these carriers to enter to the mitochondria. TRYP1 is another potential interactor and is involved in the detoxification of peroxide, although its localisation in the mitochondria is still uncertain (Tetaud *et al.*, 2001).
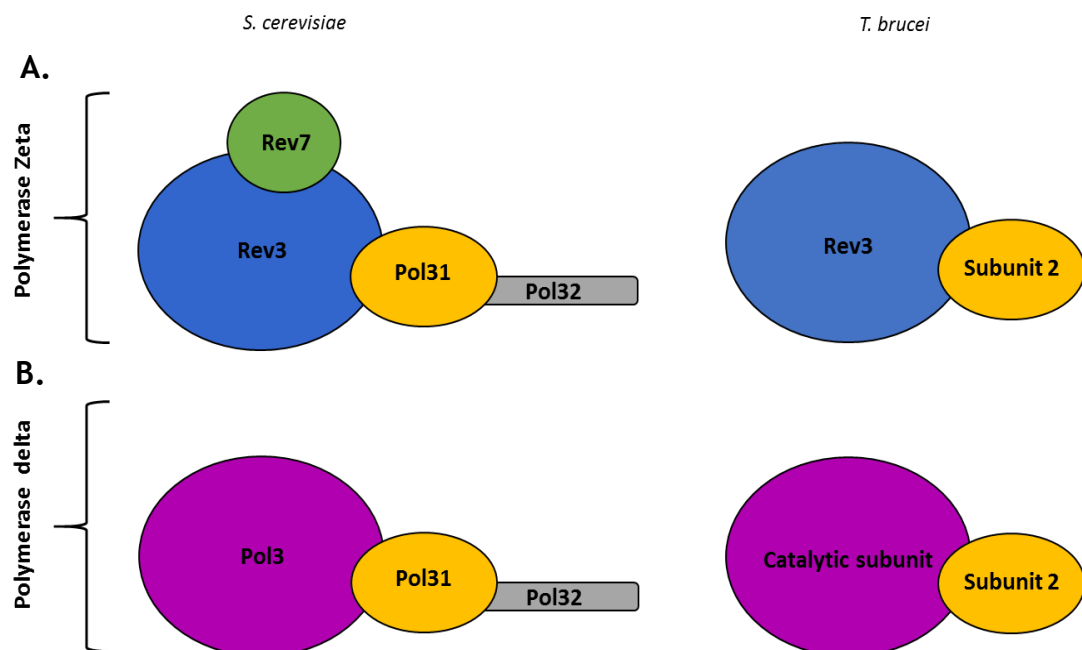
Figure 4-11. Schematic representation of Polδ and PolZ in *S. cerevisiae* and *T. brucei*. A. Schematic representation *S. cerevisiae* and *T. brucei* PolZ. In blue is represented the catalytic subunit; in yellow, green and grey are represented the accessory subunits. **B.** Diagram of *S. cerevisiae* and *T. brucei* Delta. In purple is represented the catalytic subunit and in yellow and grey the accessory subunit. *S. cerevisiae* polymerase delta structure was based on (Makarova and Burgers, 2015).

4.5 Discussion

Several interesting outcomes resulted from the analysis of the catalytic subunit of TbPolZ (TbRev3). First, TbRev3 is localized preferentially in the nucleus, but presents a mitochondrial signal in some cells, a localisation that is more evident after the generation of damage with MMS. TbRev3 double knockout cells show no growth effect, but there was an increase in sensitivity to MMS and UV damage, suggesting that this enzyme contributes to the repair of this type of DNA damage. Lastly, potential interaction partners were identified, suggesting that TbPolZ may have a role in mitochondrial maintenance.

4.5.1 TbRev3 displays both nuclear and mitochondrial localization

The mitochondrion is an important organelle in eukaryotes, having an essential role in the production of ATP by oxidative phosphorylation (Kaniak-Golik and Skoneczna, 2015). Trypanosome mitochondria are uncommon as they are only found in a single copy in each parasite cell and are characterized by the presence of a uniquely unusual genome, which is composed of an interlinked lattice of few dozens of maxicircles and ~1000 minicircles, forming a specialized structure known as the kinetoplast (Lukes *et al.*, 2002). Interestingly, in *T. brucei* the mitochondrion in the bloodstream stages is reduced in function and structural complexity, since glycolysis provides the main source of the generation of ATP (Fenn and Matthews, 2007; Cristodero, Seebeck and Schneider, 2010). On the other hand, during the insect stages, this organelle has an active role in the production of ATP (Cristodero, Seebeck and Schneider, 2010).

Studies have shown that in mammalian cells chemicals such as platinum-based chemotherapy agents, cigarette components, the fungal toxin aflatoxin B1, and UV light result in mitochondrial DNA damage. Indeed, in the case of endogenous factors, it is well known that reactive oxygen species (ROS), which are generated during the synthesis of ATP, are the main source of mitochondrial DNA damage (Akhmedov & Marín-García, 2015; Cline, 2012). ROS are not the only endogenous factors that generate mitochondrial DNA damage, however, as spontaneous errors of the replication machinery can provoke point mutations and deletions (Akhmedov & Marín-García, 2015). Given all the above

considerations, it seems likely that active repair mechanisms must be present to protect the unusual genome of the single copy trypanosome mitochondrion.

In *T. brucei* the presence of several mechanisms to protect the nucleus have been described (Passos-Silva *et al.*, 2010), including base excision repair (BER), mismatch repair (MMR), nucleotide excision repair (NER), homologous recombination (HR) and microhomology-mediated end-joining. If trypanosomes follow the profile of other eukaryotes, the mitochondrion may have more restricted options for DNA repair (Cline, 2012). In mammalian cells, BER appears to be the main mechanism involved in DNA repair in the mitochondria. In this pathway, DNA Pol ß acts to fill short gaps in the DNA template (Lopes *et al.*, 2008; Sykora *et al.*, 2017). *T. cruzi* and *T. brucei* have revealed two DNA Pol ß variants, Polß and Pol ß-PAK, that are associated with mitochondrial DNA maintenance (Lopes *et al.*, 2008), either acting in replication or repair (Saxowsky *et al.*, 2003). Studies of *Leishmania infantum* have shown a nuclear localization for Polß (Mejia *et al.*, 2014). Interestingly, neither *T. cruzi* nor *T. brucei* shows the presence of this polymerase in the nucleus (Saxowsky *et al.*, 2003; Schamber-Reis *et al.*, 2012). Like Polß, *T. brucei* POLIB, POLIC and POLID, are targeted to the kinetoplast (Bruhn et al. 2011).

Interestingly the immunofluorescence assay performed with the TbPolZ catalytic subunit demonstrates nuclear and mitochondrial localization of this protein, which suggests that TbRev3 is the first polymerase in *T. brucei* to be localized in both organelles. In *T. cruzi* Pol κ, a TLS pol, has been examined and its main roles appear to be in the kinetoplast. *In vitro* overexpression of Polκ, showed an increase in the cells resistance to hydrogen peroxide and gamma radiation (Rajão *et al.*, 2009), revealing the ability of Polκ in bypassing 8-oxoguanine lesions (lesion caused by oxidative agents) and in the repair of DSBs, indicating a possible function in HR (Rajão *et al.*, 2009). If and how these activities are used in *T. brucei* are unknown.

Previous studies have demonstrated a mitochondrial localization of PolZ in *S. cerevisiae* and mammals. The specific role of the TLS polymerase in both organisms is still unclear, but it has been suggested that it may be involved in mitochondrial maintenance (Kaniak-Golik and Skoneczna, 2015; Singh *et al.*,

2015). Recent studies in yeast have reported the interaction of yeast PolZ with Polη, another translesion polymerase, preventing the accumulation of mutations caused by UV-radiation (Kaniak-Golik and Skoneczna, 2015).

In the case of mammalian cells, it has been possible to identify two isoforms of Rev3, the catalytic subunit of PolZ (Singh *et al.*, 2015). In the nucleus, it is feasible to detect both isoforms, while one is specifically seen in the mitochondria (Singh *et al.*, 2015). It has been proposed that an interaction between Rev3 and Polγ in the mitochondria takes place, in order to maintain the integrity of the organelle (Singh *et al.*, 2015).

The data in this chapter provide indications that TbPolZ might also act in the nucleus and in the mitochondrion of *T. brucei*, since TbRev3-12myc showed a clear and robust nuclear signal as well as evidence for kinetoplast expression, especially after MMS treatment. It is uncertain if these data reflect dynamic relocalisation of a single isoform of TbRev3, or if the signals might be due to expression of more than one isoform, perhaps due to alternative start codon usage. In mammals Rev3 gene has two alternative translation sites (AUG). If translation initiates from the first start codon the result is a long isoform, and if it starts from the second AUG, a smaller isoform is generated (Singh *et al.*, 2015). There is evidence that shows that *T. brucei* also has differential splicing: the genes that encode for tRNA synthetases have two translational start codons, allowing the generation of a short and a long isoforms (Rettig *et al.*, 2012).

The basis for the observed stronger mitochondrial signal after the generation of damage with MMS is unclear, but could be explained by increased expression of a mitochondrial-targeted TbRev3 in the presence of damage or the migration of some of the nuclear TbRev3 to the kinetoplast. In the IFA performed with TbRev3-12 myc, the mitochondrial signal was present in some, but not all cells, regardless of the cell cycle phase. The lack of signal in some cases may simply be explained by low expression levels of the protein, making visualization of the signal in all the cells difficult. However, it is also conceivable that kinetoplast localisation only occurs in the cells in the population that reach a critical level of organellar genome damage or functional impairment.

Previous studies have suggested that PolZ in other eukaryotes is mainly involved in the repair of lesions provoked by UV (Zhao & Washington 2017b). It is unlikely that *T. brucei* is exposed to UV in natural conditions, but UV treatment in culture has been shown to cause both nuclear and kinetoplast damage (J.P da Rocha, personal communication). In the nucleus, UV damage is tackled by NER (Machado *et al.*, 2014), but what route is used for kinetoplast repair is unknown. Recent studies in mammalian cells suggest the presence of BER, MMR and HR in the mitochondrion (Akhmedov and Marin-Garcia, 2015), but not the NER pathway, which is commonly in charge to repair UV induced lesions (Akhmedov and Marin-Garcia, 2015).

PolZ's role in HR has been demonstrated in humans and yeast, where it is seen as a key factor in the repair of DSBs (McVey *et al.*, 2016). Though these studies considered the function of nuclear PolZ, there is a possibility that the polymerase plays a similar role in both the mitochondrion and nucleus. If so, the role of TbRev3, and perhaps TbPolZ, in providing HR activity in the kinetoplast is a feasible hypothesis, both for repair and perhaps during the recombination process the minicircles must undergo as part of the replication of the kinetoplast network (Rajão *et al.*, 2009). This hypothesis needs further analysis, however, including tests to show that loss of TbRev3 leads to impaired integrity of the nuclear and mitochondrial genomes of *T. brucei*.

4.5.2 Increase in the cells sensitivity after partial and total deletion of TbRev3

As it was mentioned above, PolZ has been linked with several repair pathways such as cross-link repair and HR (Gan *et al.*, 2008; Makarova and Burgers, 2015). In mammalian cells this protein seems to have a critical role during cell development, since the deletion of the gene leads embryonic lethality in mice (Esposito *et al.*, 2000). It was suggested that this protein is essential during the early stages of cell development, by avoiding the stalling of the replication fork (Esposito *et al.*, 2000; Makarova and Burgers, 2015). Studies in *S. cerevisiae* and *D. melanogaster* have demonstrated that mutations in the PolZ catalytic subunit result in an increase in sensitivity to UV radiation and alkylating agents (Eeken *et al.*, 2001; Lawrence, 2002; Gan *et al.*, 2008). In *A. thaliana,* mutations in a Rev3 homologues resulted in an increase in sensitivity to

UV radiation. However, AtRev3 mutants did not present sensitivity toward MMS damage (Takahashi *et al.*, 2005).

At the moment the role of this DNA polymerase in *T. brucei* remains uncertain, but based on the DNA damage sensitivity experiments performed after the depletion of the protein using RNAi, it is possible that the protein is involved in the repair of DNA lesions. In this chapter a Tb*rev3-/-* null mutant was generated, demonstrating that the protein, and probably TbPolZ, is not essential for BSF cell survival, at least in culture. Given a predicted function in repair, it may have been expected that the null mutants would display a stronger sensitivity to MMS in comparison to RNAi depletion and heterozygote deletion cell lines. Surprisingly, though there was some evidence for the strongest MMS sensitivity phenotype in the *Tbrev3-/-* mutants, this was rather mild. MMS damage sensitivity might be expected, as it is known this alkylating agent has the ability to generate base mispairing, replication blocks and DNA double strand breaks, most of which PolZ has been implicated in acting upon, including lesion repair by HR (Lawrence, 2002; Lundin *et al.*, 2005).

The relatively weak MMS sensitivity phenotype of the *Tbrev3-/-* cells could be explained by the redundancy that characterizes TLS Pols. It is well known that in multicellular organisms it is common to observe the exchange of roles between TLS Pols, where the loss of one can be easily replaced by another (Waters et al. 2009). There is a possibility that this could also happen in unicellular organisms, such as *T. brucei*. PolZ is known to interact with several TLS pols in order to repair lesions: Polη, Polι and PolK. During these interactions, the polymerases are normally in charge of inserting the nucleotides prior to PolZ performing the extension process (Zhao & Washington 2017a). However, it has also been documented that in the absence of Polη, Polι or PolK, PolZ has the ability to insert the nucleotides and complete the extension process (Johnson *et al.*, 2000; Ziv *et al.*, 2009; Stone *et al.*, 2011). Thus, there is the possibility that in the absence of TbPolZ, or at least TbRev3, other polymerases can take over the role of this putative TLS Pol. Testing this is complicated by the lack of functional characterization of other TLS Pols in *T. brucei*.

An alternative explanation for the relatively mild MMS sensitivity phenotype of TbRev3 null mutants is that the putative TLS Pol plays a more pronounced role in tackling other forms of genome damage. Considering that *T. brucei* is a unicellular organism, the collapse of the replication fork may be lethal for the cell, which gives the possibility that in the absence of the protein, there is the action of an alternative repair pathway that is not mediated by TbPolZ. In this regard, if there had been time it would have been valuable to assess growth of the mutants in the presence of, for example, UV or hydrogen peroxide.

4.5.3 **Attempting to elucidate the role of PolZ in *T. brucei***

The immunoprecipitation of TbRev3-12myc was performed with the aim of beginning to understand the role of TbPolZ in *T. brucei*. However, given the complexity of the peptide hits obtained from the mass spectrometry analysis, it was not possible to clearly elucidate the pathway in which this protein is involved in in the parasite. Nonetheless, the recovery of several possible interaction partners suggests potential routes for future investigation.

The strongest potential interactor recovered was a putative subunit of *T. brucei* Polδ, though it should be noted that functional or biochemical characterization of this replicative Pol has not been reported. As mentioned above, *S. cerevisiae* Polδ is composed of three subunits, the catalytic subunit (Pl3) and two accessories subunits (Pol31 and Pol32) (Johansson, Majka and Burgers, 2001). The C-terminal domain of the catalytic subunit is connected to the rest of the structure by a linker, providing the ability to dissociate from Pol31 and Pol32 and allowing the recruitment of Rev3 and Rev7, activating the TLS pathway (Baranovskiy *et al.*, 2012). Thus the TbRev3-12myc IP suggests that TbPolZ might also be under the regulation of TbPolδ. However, at the moment this putative interaction needs to be confirmed, in particular as we did not recover proteins corresponding to Pol32 and Rev7 counterparts in TbPolZ, and no homologues were found with the Blastp analysis. Further studies are needed to understand the structure of TbPolZ.

HSP40 was another protein that was recovered specifically in the TbRev3-12myc IP and belongs to the heat shock protein family, which is activated during

cellular stress and localises both in the nucleus and in the mitochondrion (Deka *et al.*, 2016). Studies have demonstrated that another member of the HSP family is involved in the regulation of TLS Pols: HSP90 regulates the activation of Polη and Rev1 by inhibiting the binding of the polymerases to PCNA (Yamashita, Oda and Sekimoto, 2012). It is, therefore, a possibility that HSP40 plays a similar role in the parasite, but further studies are required. As it was mentioned in section 3.5.1, TbPolZ lacks the zinc finger domain, which is associated with the interaction with the proliferating cell nuclear antigen (PCNA) and with Polδ accessory subunits. The question is how HSP40 may regulate TbPolZ activity if there is no evidence of interaction between the TLS pol and the PCNA. Despite the lack of this structure, the immunoprecipitation results suggest that there is an interaction between TbPolZ and TbPolδ accessory subunit 2. Studies in *S. cerevisiae* have shown that the PCNA binding motif (PIP box) is localised in the C-terminal domain of the Pol32 subunit (accessory subunit) (Acharya *et al.*, 2011). Even though *T. brucei* seems to lack a Polδ Pol32 homologue, there is the possibility that Polδ subunit 2 is the one interacting with the PCNA. Though the general sequence of the PIP box (Q-x-x-(L,V,I,M)-x-x(Y,F)) is missing in TbPolδ subunit 2, this could be explained by a mutation of the motif, changing the sequence of the PIP box without affecting the interaction with the PCNA. This could mean that HSP40 could be regulating the activity of TbPolZ only if the TLS pol is interacting with the accessory subunit of TbPolδ. Further studies are needed in order to confirm this hypothesis.

Given the demonstration of TbRev3-12myc localisation in the kinetoplast, it was intriguing that a number of mitochondrial proteins were recovered in the IP. Amongst these were mitochondrial carrier proteins, which have an important role in the cell due to their ability to transport molecules into this organelle. Several proteins involved in the organization, regulation and replication of the mitochondrion are synthesized in the nucleus and transported into the mitochondria using the carrier proteins (Bailey and Doherty, 2017). It may be possible that TbRev3 (and TbPolZ) interacts with these carriers to be mobilized from the nucleus to the mitochondrion. It is known that during the replication of the kinetoplast, the minicircles need to close the gaps that are left during the process (Klingbeil and Englund, 2004). The possibility that TbRev3 might have a function during this process is raised by the IP of a kinetoplast binding protein

(Tb927.8.726), which preferentially binds to the minicircles and is also involved in the compaction of the structure (Pfam domain prediction). In other kinetoplastids such as *Chrithidia fasciculata,* the kinetoplast binding protein (UMSBP) has an important role during the replication of the minicircles by recognizing and binding to the replication origins. The interaction of the kinetoplast binding protein and TbRev3, may suggest that TbRev3 repair activity may be involved during the replication process. Of course, the recovery of mitochondrial proteins after TbRev3-12myc IP may simply reflect artefactual localisation of the protein to the organelle, and therefore further tests are needed. It can be noted, however, that myc-tagging of no other *T. brucei* repair protein has so far caused artefactual kinetoplast localisation, and further TLS Pol IPs described here have not recovered mitochondrial carrier proteins (chapter 5, see section 5.7.1).

5 Understanding the function of DNA Polymerase Nu (PolN) in *T. brucei*

5.1 Introduction

The eukaryotic DNA polymerase Nu (PolN) is a member of the A family polymerases. These polymerases are known to be involved in both DNA replication and repair (Garcia-Diaz and Bebenek, 2007). They are characterized by their high fidelity, due to the presence of 3'-5'exonuclease proofreading activity (Garcia-Diaz and Bebenek, 2007). PolN, together with PolQ, are the only members of the A family of polymerases that lack such exonuclease activity (Arana *et al.*, 2007; Garcia-Diaz and Bebenek, 2007). PolN has been associated with several genome maintenance pathways such as TLS, cross-link repair and homologous recombination (HR) (Arana *et al.*, 2007; Moldovan *et al.*, 2010; Gowda, Moldovan and Spratt, 2015). Studies in human cells have suggested an important role of PolN during the repair of cross-link lesions by HR (Moldovan *et al.*, 2010). It has been proposed that Rad51 stimulates PolN in order to initiate DNA synthesis after strand invasion (Moldovan *et al.*, 2010). In *Leishmania infantum* LiPolθ (PolN) has TLS activity, permitting the bypass of oxidative lesions such as 8-oxoguanine, thymidine glycol and abasic sites (Fernández-Orgiler *et al.*, 2016). However, functional analysis of the consequences of loss of PolN has not been reported in any kinetoplastid.

Previous studies have shown high homology between PolN and the polymerase domain of PolQ (Li, Gao and Wang, 2011). PolQ is a highly conserved polymerase among multicellular eukaryotes and consists of a C-terminal polymerase domain and an N-terminal helicase domain (Bebenek and Kunkel, 2004). Although the helicase activity is still uncertain, in some organisms, such as *D. melanogaster,* the PolQ (Mus308) polymerase domain has been associated with cross-link repair (Moldovan *et al.*, 2010). Biochemical analyses have shown the ability of PolQ to add nucleotides opposite abasic sites and bypass thymidine glycol lesions (Li, Gao and Wang, 2011). PolQ has also been associated with other repair pathways such as HR, microhomology-mediated end joining (MMEJ) and base excision repair (BER) (Beagan *et al.*, 2017). Interestingly, a helicase (HelQ) has been found that shares high homology with the PolQ helicase domain. *In vitro* experiments demonstrated the ability of the protein to unwind the DNA duplex, confirming its helicase activity (Beagan and McVey, 2016). Recent studies in human cells proposed a role for HelQ in DSB repair (Wu *et al.*, 2001).

Due to the high sequence homology PolN and HelQ share with PolQ's polymerase and helicase domains, respectively, it has been suggested that there is a possible interaction between PolN and HelQ (Beagan and McVey, 2016).

In *T. brucei*, the role of PolN (TbPolN) and its possible interaction with HelQ (TbHelQ) is still uncertain. Chapter 3 revealed that RNAi of TbPolN had a transient, severe impact on growth, but similar RNAi against TbHelQ was ineffective. Unpublished data suggests that in *T. brucei* TbHelQ in procyclic form cells interacts with BRCA2, a regulator of homologous recombination (Prorocic and McCulloch, unpublished), but this has not been evaluated in bloodstream form cells, where the RNAi studies were performed (Chapter 3). Due to the lack of information about these proteins, the aim of this chapter was to make a more in-depth characterisation of the effects of TbPolN loss, in order to have a better understanding of the function that the protein plays in the parasite and, perhaps, to ask how this compares with PolN and PolQ in other eukaryotes, given that there is no evidence that *T. brucei* encodes a PolQ homologue.

5.2 Cell structural analysis after RNAi depletion of TbPolN

It was shown in Chapter 3, section 3.4.1, that RNAi depletion of TbPolN results in significant changes in cell morphology, especially at 48 hours post induction, and the accumulation of aberrant cells with abnormal nuclei and multiple kinetoplasts. In order to evaluate these observations further, two electron microscopy imaging methods were employed: transmission electron microscopy (TEM) and scanning electron microscopy (SEM). These techniques have already been used successfully in *T. brucei* and *L. mexicana*, permitting analysis of the flagellum architecture, for instance (Gluenz *et al.*, 2015).

TEM was performed in order to examine the ultrastructure of TbPolN RNAi depleted cells relative to uninduced controls, facilitating the visualization of the nucleus, kinetoplast and flagellar pocket. SEM allowed the 3D visualization of the external architecture of BSF cells, following the loss of TbPolN, to try and reveal possible changes in the body shape. The fixation and imaging of the cells is described in section 2.11. The below images were taken by L. Lemgruber-Soares after RNAi induction for 48 hours by the addition of tetracycline, since this was when the most severe defects were observed.

5.2.1 Transmission electron microscopy and scanning electron microscopy

Due to the cross-sectioning that is performed before imaging with TEM, not all structures are visible in each sample. For this reason, four images of RNAi induced cells were chosen, from a total of thirteen examined, in which it was possible to observe the main internal structures. Upon depletion of TbPolN, significant alterations were observed in the internal morphology of the cell (Figure 5-1). Unlike in uninduced cells (Figure 5-1), the kinetoplast could not clearly be detected in the images of the TbPolN RNAi depleted cells, even though DAPI staining suggested this DNA was present (chapter 3). However, there were cells with multiple flagellar pockets (Figure 5-2 B). In *T. brucei* the kinetoplast is connected to the flagellum basal body (Sunter and Gull, 2016). Due to this, the number of kinetoplasts is directly related with the number of flagellar pockets, corroborating the IFA images showing the accumulation of multiple kinetoplasts after the depletion of TbPolN (Figure 3-12). The SEM images support this observation, with the presence of cells with multiple flagella (Figure 5-3), suggesting that TbPolN may be involved in cell division. Why, given these observations, the kinetoplast DNA was undetectable in the TEM is unclear.

RNAi cells also presented an irregular nucleus (Figure 5-2 A).Though this phenotype was not detected in all cells, it is consistent with the aberrant nuclear staining after DAPI (chapter 3) and suggests problems associated with replication or division of the nucleus. In addition, swollen 'vacuole-like' structures were identified in a few of the cells (Figure 5-2 B). These structures seem to be lacking any content and how they arose is unclear. SEM analysis revealed that the aberrant cells previously visualized by light microscopy had, in addition to multiple flagella, a contorted body shape, consistent with an impediment in completing cell division (Figure 5-3).
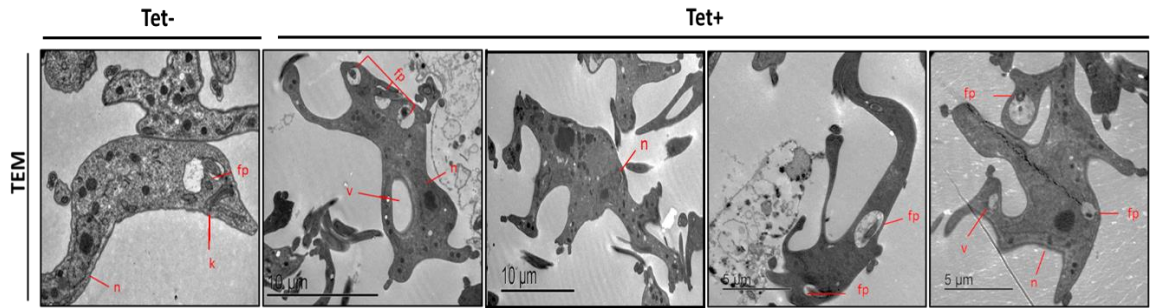
Figure 5-1. Internal cellular architecture with and without TbPolN RNAi. The first panel shows a cell with a regular architecture, before the depletion of TbPolN (Tet-). The other four panels show representative images of aberrant cells 48 h post RNAi induction (Tet+), presenting abnormal internal architecture. Important features of the cells are indicated in red (n-nucleus; fp- flagellar pocket; and v-vacuole). Images were captured on a Tecnai T20 transmission electron microscope and processed by L.Lemgruber-Soares. Scale bars 5-10 μm.
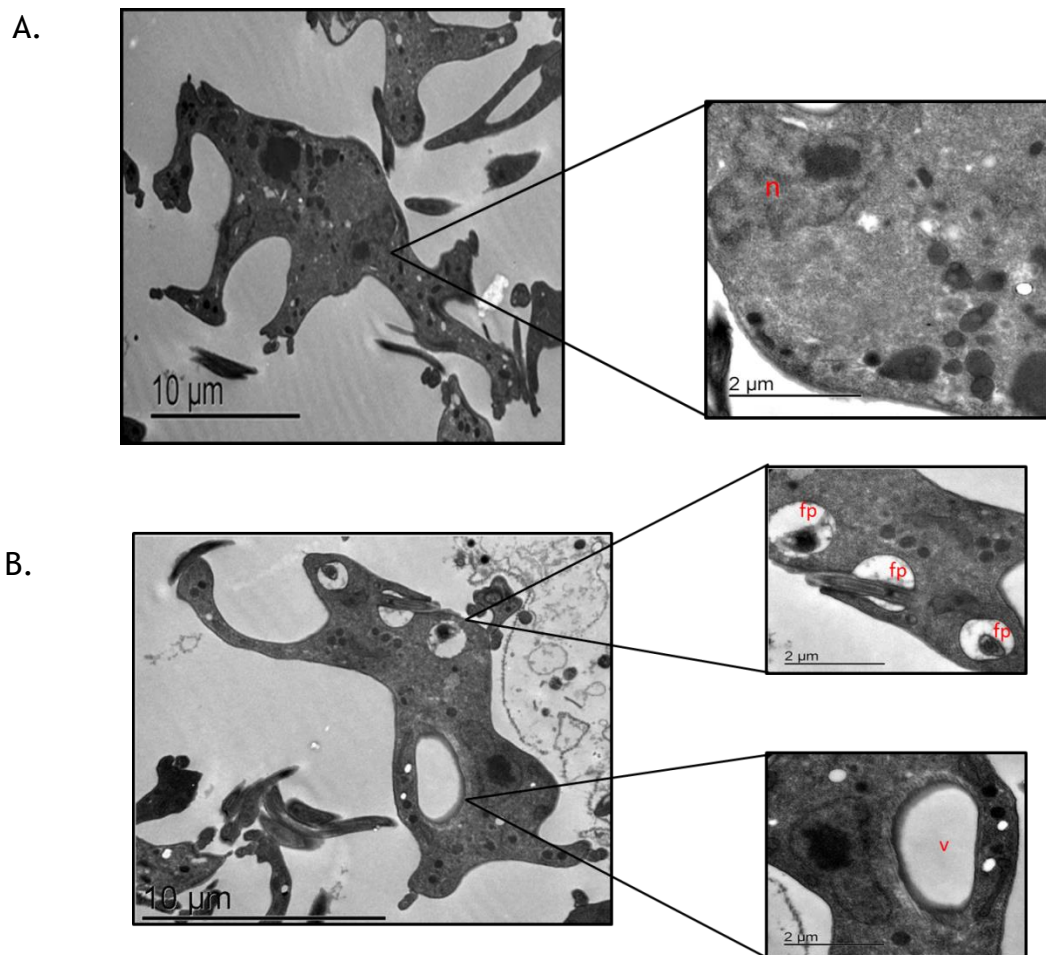
Figure 5-2. Abnormal cellular structures associated with the RNAi depletion of TbPolN. A. Cell showing irregular nucleus 48 hours after the depletion of TbPolN. **B.** Cell showing the presence of multiple flagellar pockets and an

enlarged vacuole-like structure, 48 hours post induction. Important features of the cells are indicated in red (n-nucleus; fp- flagellar pocket; and v-vacuole). Scale bars 2-10 µm.
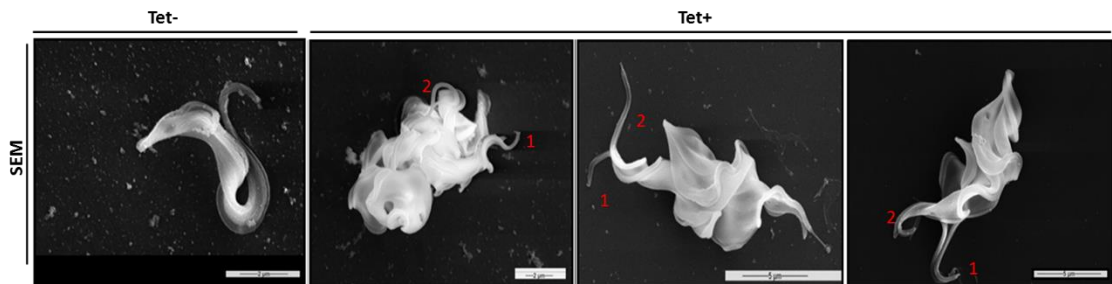
Figure 5-3. TbPolN loss is associated with aberrant cell morphology. The left panel shows a BSF *T. brucei* cell before RNAi induction (Tet-). The other three panels show representative images of aberrant cells, presenting two flagella, 48 h post RNAi induction of TbPolN (Tet+). Images were captured on a Jeol 6400 scanning electron microscope and processed by L.Lemgruber-Soares. Scale bars: 5 - 2 µm.

5.3 Intracellular localisation of Polymerase Nu in *T. brucei*

5.3.1 Verification of TbPolN endogenous epitope tagging via Western blot analysis

Previous studies in human cells have shown that GFP-tagged PolN localises to the nucleus (Marini *et al.*, 2003). To ask if this is also true in the parasite, the TbPolN gene was modified *in situ* in BSF cells in order to express the protein as a C-terminal fusion with 12 copies of the myc epitope. This manipulation was achieved using the 12Myc pNAT BSD vector (Figure 5-4) (Alsford & Horn 2008), inserting 686 bp coding for the C-terminal end of *TbPolN*, generated by PCR-amplification with the primers Fw- gcatgagctcacgagttgctcattaagcac (SacI site) and Rv-gcattctagaaggaacatcaagtttctcga (XbaI site) (Figure 5-4 A), into the construct. Plasmid and PCR fragment were digested with SacI and XbaI, followed by ligation. The cloning strategy was employed as described in section 2.3, and the construct was checked by sequencing. The construct was then linearised with PstI and transformed into wild type (WT) Lister 427 BSF cells. Transformants were selected with blasticidin (10 µg/ml).

To check if the TbPolN variant was expressed as a fusion to the 12 myc tag, a Western blot was performed using an anti-myc antibody. A band of

approximately 113 kDa (98.8kDa for TbPolN, 14.4 kDa for 12Myc), was seen in a whole cell extract of one blasticidin resistant transformant (Figure 5-4 B).
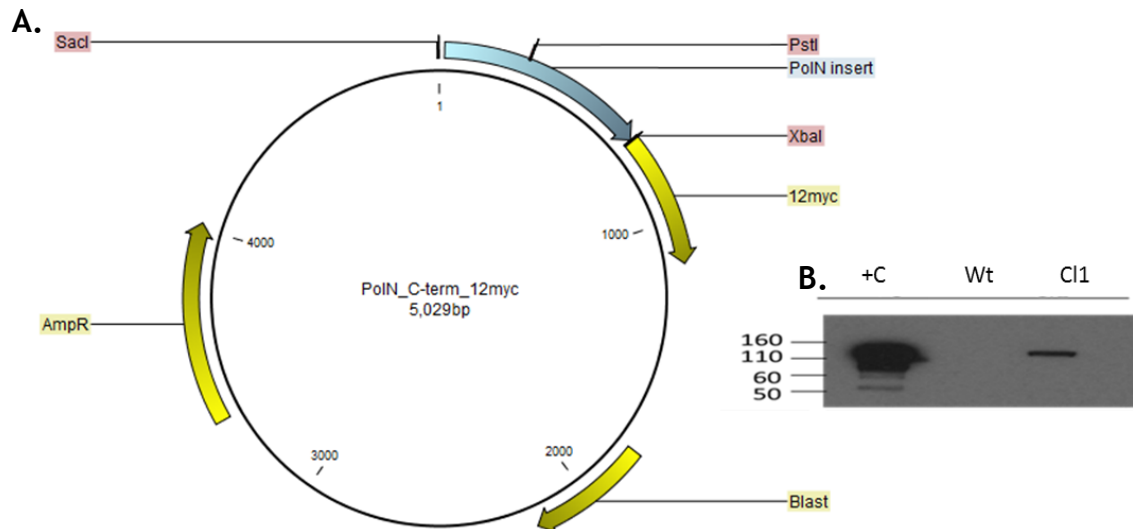
Figure 5-4. Expression of TbPolN as a 12myc C-terminal fusion variant. A. Map of the C-terminal tagging vector pNAT BSD containing a 12 Myc tag sequence (represented in yellow) and (in blue) the *TbPolN* insert, derived from the C-terminus of the complete ORF. Cloning restriction sites are labelled in pink (SacI and XbaI). **B.** Western blot of whole cell extracts from a blasticidin resistant transformant (cl1), wild type (WT, untransformed) cells and from a cell line expressing CRK11-12 myc kinase as a control (+C). The blot was probed with anti-myc antibody.

5.3.2 TbPolN localisation in the absence and presence of damage

Localisation of TbPolN-12myc was assessed with immunofluorescence of permeabilised cells, using a conjugated Alexa Fluor® 488 anti-myc antibody. The intracellular localisation of the protein was tested with and without growth of the cells in the presence of the alkylating agent MMS (0.0003%) for 18 hours. Images were captured on an Axioscope 2 (Figure 5-5).

The anti-myc signal was strongest in the nucleus in the absence of MMS, with a less intense signal in the cytoplasm, suggesting TbPolN-12myc predominantly localises to the nucleus in the absence of damage. After treatment with MMS, the nuclear signal appeared to be more intense, but retained the non-uniform distribution seen before damage (Figure 5-5). The

nuclear signal appeared to be present throughout the different cell cycle stages Figure 5-6.
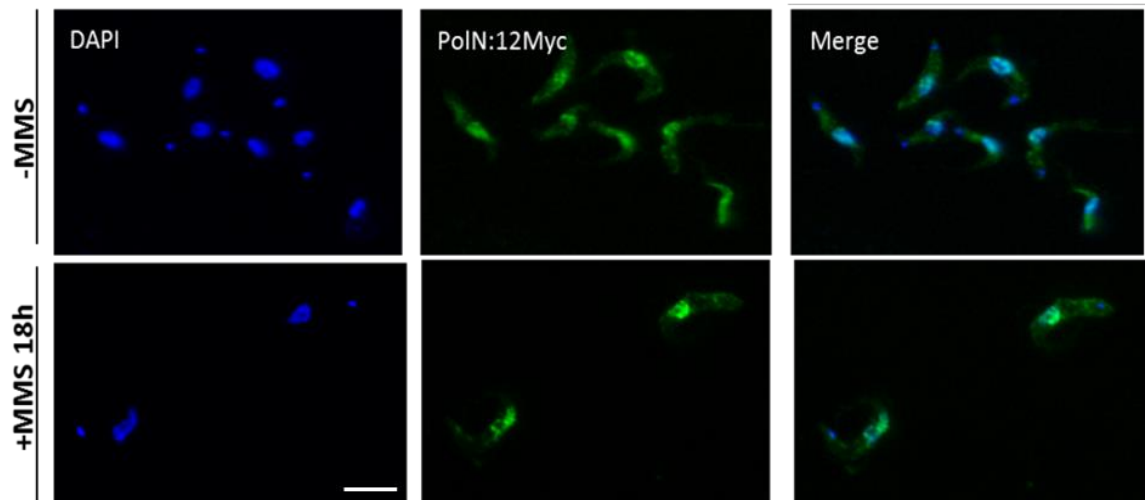
Figure 5-5.Immunolocalisation of C-terminally 12myc-tagged TbPolN in the absence and presence of MMS damage. Immunolocalisation of TbPolN-12myc in *T. brucei* BSF cells: the left panel shows DAPI staining of the nucleus and kinetoplast, the middle panel shows localisation of TbPolN-12myc using a conjugated Alexa Fluor® 488 anti-myc antibody, and the right panel is merged images of both signals. Cells are shown after culture without damage (-MMS) or after growth for 18 hrs in the presence of 0.0003% methyl methanosulphonate (+MMS 18 h). Images were captured on an Axioscope 2. Scale bar represents 5 µm.
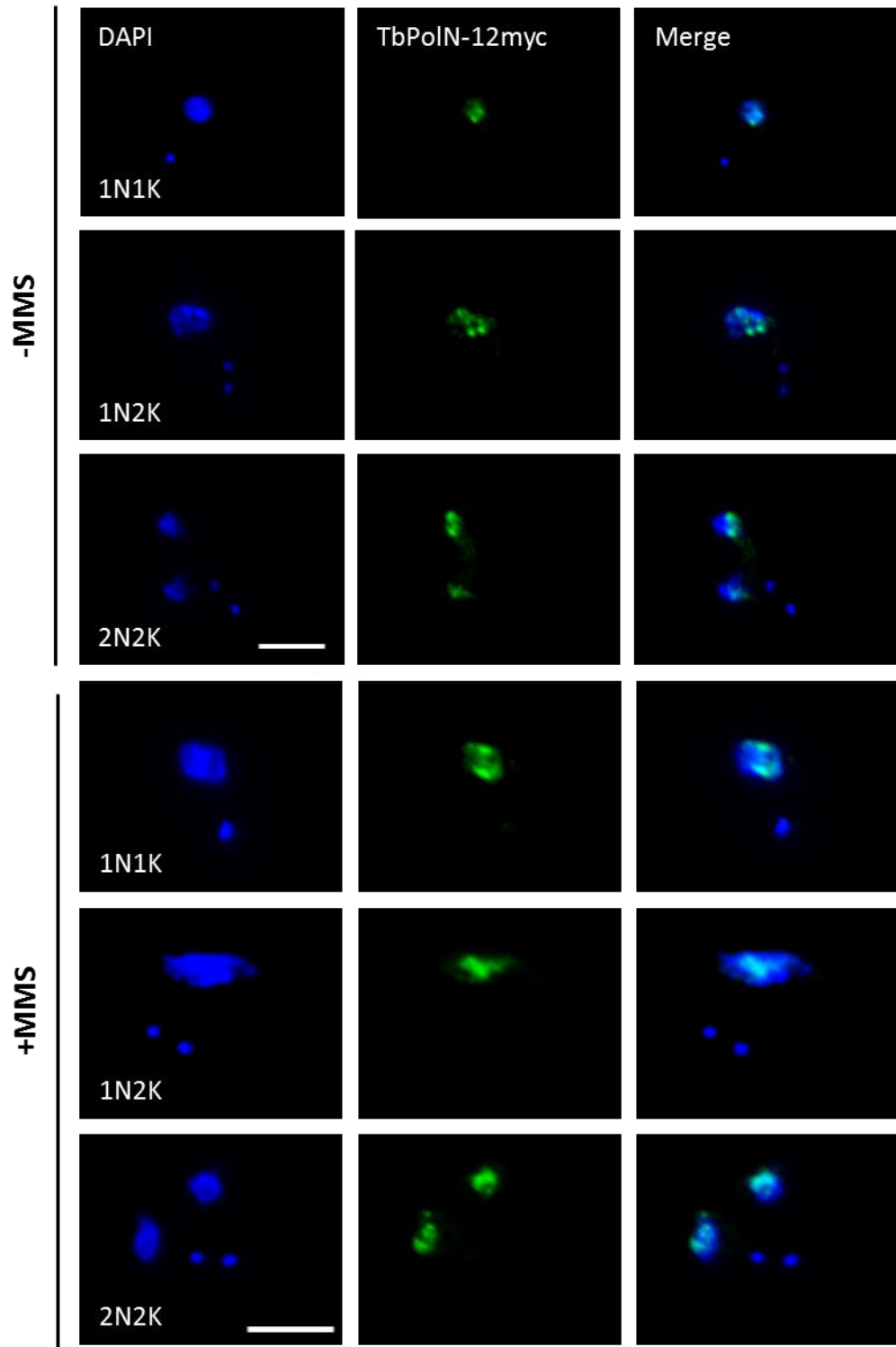
Figure 5-6. Immunolocalisation of TbPolN-12myc throughout the different cell cycle stages. The left panel shows DAPI staining of the nucleus and kinetoplast, the middle panel shows localisation of TbPolN-12myc using a conjugated Alexa Fluor® 488 anti-myc antibody, and the right panel is merged images of both signals. Cells are shown after culture without damage (-MMS) or after growth for 18 hrs in the presence of 0.0003% methyl methanosulphonate (+MMS 18 h). Images were captured on an Axioscope 2. Scale bar represents 5 µm.

Because the TbPolN-myc localisation in the nucleus seen using the Axioscope microscope appeared non-uniform, high resolution images were captured on a Delta Vision RT deconvolution microscope (Figure 5-7) and Zeiss Elyra Super Resolution Microscope (Figure 5-8). In the absence of MMS treatment, localisation of the anti-myc signal was predominantly at the nuclear periphery, and was normally composed of intense puncta (Figure 5-7 A). In the case of the Elyra images a pattern composed of two distinct puncta was observed (Figure 5-8 A). After growth in MMS, greater subnuclear signal was seen throughout the nucleoplasm (Figure 5-7 B, Figure 5-8 B), suggesting redistribution of TbPolN-myc in the presence of damage. What features of the nuclear genome are localised in the periphery of the nucleus and might coincide with TbPolN-myc localisation in undamaged cells, still unclear. On the other hand the rearrangement of the signal inside the nucleus after MMS damage may indicate that the putative TLS pol migrates from its predominant sites of action to sites of exogenously generated damage in order to repair the resulting lesions.
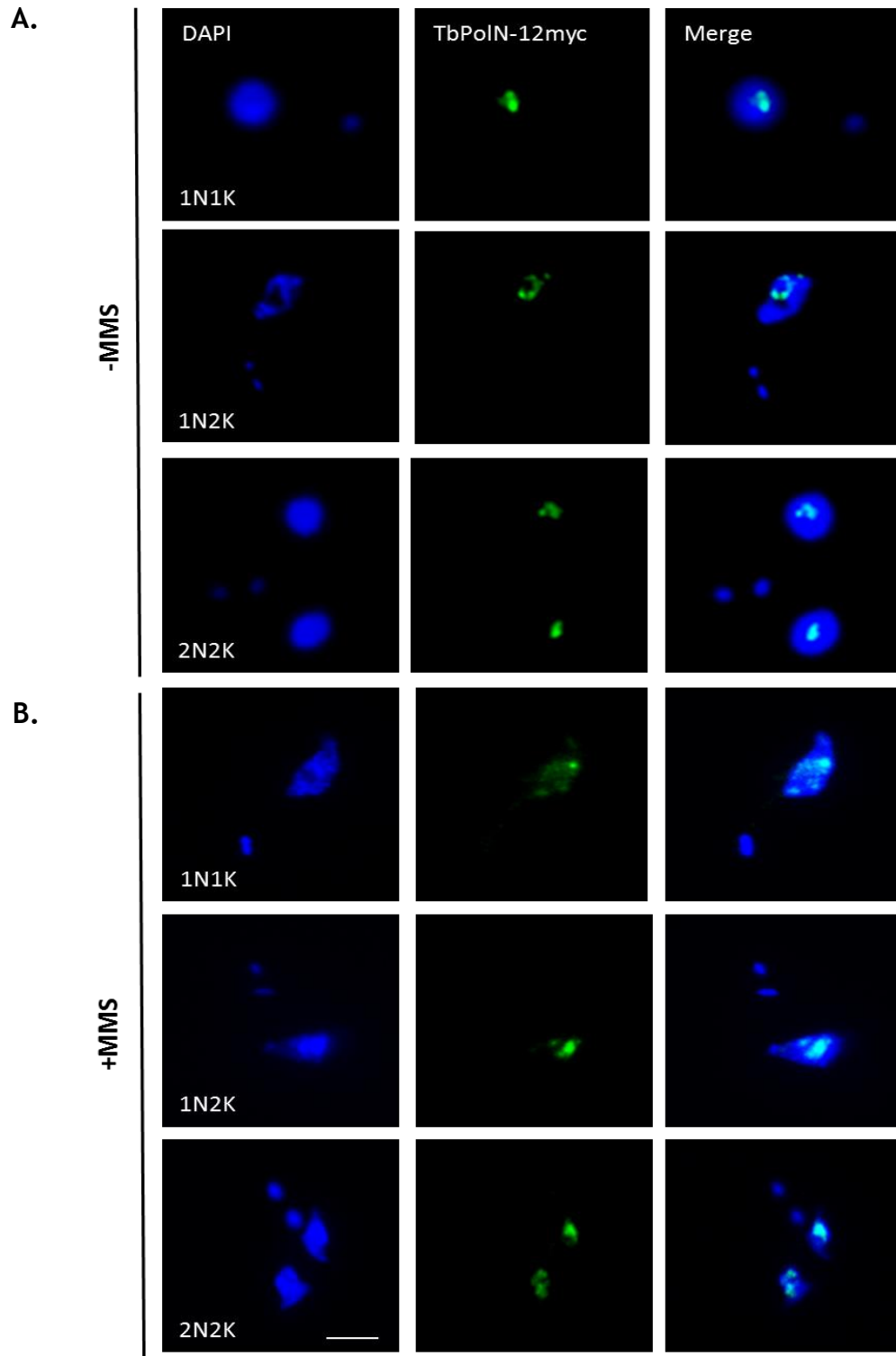
Figure 5-7. TbPolN-12myc nuclear loicalisation throughout the different cell cycle stages in the absence and presence of MMS damage. Immunolocalisation of TbPolN-12myc in *T. brucei* BSF cells: the left panel shows DAPI staining of the nucleus and kinetoplast, the middle panel shows localisation of TbPolN-12myc using a conjugated Alexa Fluor® 488 anti-myc antibody, and the right panel is merged images of both signals. **A.** Cells are shown after culture without damage (-MMS) or **B.** after growth for 18 hrs in the presence of 0.0003% methyl methanosulphonate (+MMS 18 h). Images were captured on a Delta Vision RT deconvolution microscope. Scale bar represents 2 μm.
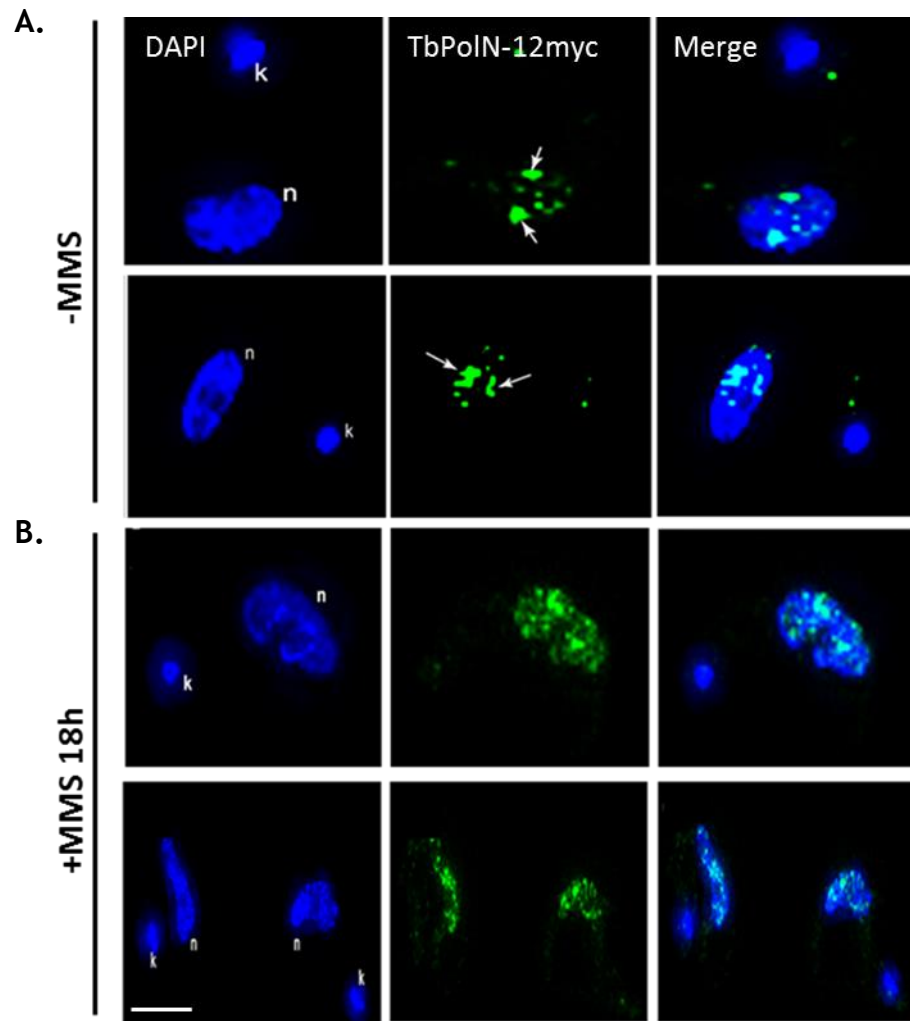
Figure 5-8. High resolution images of TbPolN-12myc localisation. Immunolocalisation of TbPolN-12myc in *T. brucei* BSF cells: left panels show DAPI staining of the nucleus and kinetoplast, the middle panels shows localisation of TbPolN-12myc using a conjugated Alexa Fluor® 488 anti-myc antibody, and the right panels are merged images of both signals. **A.** Cells are shown after culture without damage (-MMS) or **B.** after growth for 18 hrs in the presence of 0.0003% methyl methanosulphonate (+MMS 18 h). Images were captured on a Zeiss Elyra Super Resolution Microscope. Arrows show the agglomeration of TbPolN-12myc signal in the periphery of the nucleus, forming two distinct puncta. Scale bar represents 2 µm

5.4 TbPolN depletion is associated with damage accumulation and replication impairment

As described in chapter 3, the depletion of TbPolN by RNAi provokes a decrease of proliferating cells and the rise of aberrant cells. In studies in other eukaryotes, PolN has been associated with the repair of different lesions, such as DSBs and lesions caused by oxidative agents (Moldovan *et al.*, 2010; Fernández-Orgiler *et al.*, 2016). To ask if similar roles might be provided by TbPolN, expression of the DNA damage marker γH2A was determined after RNAi, asking if loss of the putative TLS resulted in nuclear DNA damage. In addition, incorporation of 5-ethynyl-2'-deoxyuridine (EdU), a thymidine analogue, was tested at the same time, asking if loss of the protein impedes genome replication.

5.4.1 Analysis of γH2A expression in TbPolN depleted cells.

The eukaryotic nucleosome consists of four core histones: H2A, H2B, H3 and H4. Histone post-translational modification is a widespread strategy to alter chromatin, in order to prepare chromatin for the repair machinery. In *T. brucei* it has been demonstrated that phosphorylation of H2A^{Thr130} occurs in the presence of diverse types of damage, suggesting this histone modification is the kinetoplastid variant of serine phosphorylation of either H2A or the H2Ax variant in other eukaryotes (Glover and Horn, 2012). Indeed, elevated levels of γH2A are seen in *T. brucei* following RNAi of a range of protein kinases, and in *Leishmania major* after mutation of components of the 9-1-1 repair complex (Damasceno *et al.*, 2016; Stortz *et al.*, 2017), indicating abundance of the modified histone is a marker of levels of nuclear damage.

Two techniques were used for the analysis of γH2A levels after TbPolN RNAi: IFA imaging and Western blot. In the case of the IFA, uninduced and RNAi induced cells were collected after 24 hours, 48 hour and 72 hours growth and the cells prepared as described in section 2.10. In the case of the Western blot, cell lysates of uninduced and RNAi induced cells were collected at 24 hours and 48 hours; detailed explanation of the lysate preparation can be found in section 2.12 . For this assay, WT cells in the absence of damage or after the addition of

phleomycin (1 µg/ml) for 24 hours were used as negative and positive controls, respectively. Phleomycin is known to cause DBS breaks, which induces the phosphorylation of γH2A making possible its detection. For both approaches anti-γH2A antibody (provided by Dr. Tiago D. Serafim), which recognised the phosphorylated γH2A, was diluted to a concentration of 1:1000 and detected with α-rabbit HRP conjugate (1:3000) for the Western blot and Alexa Fluor® 594 α- rabbit (1:1000) for the immunofluorescence.

In both the IFA and Western blot experiments, it was possible to observe an increase in the expression of γH2A after TbPolN RNAi (Figure 5-9). In the Western blot an increase of γH2A expression levels was seen at both 24 hours and 48 hours post RNAi induction relative to the uninduced cells (Figure 5-9 A). Unlike the IFA results (see below), there was not a visible difference between the γH2A levels at 24 hours and 48 hours post RNAi induction. In the case of the IFA (Figure 5-9 B), a small amount of γH2A signal was seen in most uninduced cells, and this did not alter over the time course, though was variable within individual cells in the populations. After RNAi, a modest increase in γH2A signal was seen in some cells after 24 hrs, and this signal was substantially stronger at 48 hours post RNAi induction. At 72 hour the expression levels of γH2A appeared to decrease relative to the 48 hours RNAi induced cells and appeared more comparable with the increased signal seen after 24 hrs. The fluorescence intensity was quantified by calculating the corrected total cell fluorescence (CTCF) (section 2.10.3), supporting the results obtained in the IFA. At 24 hours the γH2A intensity levels were close to zero. At 48 hours the γH2A intensity was stronger, showing a wider distribution along the Y-axis. Meanwhile, at 72h the cells show a decrease in γH2A intensity. Intriguingly, the IFA results closely mirror the cell cycle analysis in section 3.3.1, in which the strongest accumulation of aberrant cells was seen 48 hours post RNAi induction and diminished by 72 hrs. The results obtained in both assays suggest that loss of TbPolN results in an accumulation of nuclear DNA damage, suggesting the protein contributes to genome maintenance.

A.

B.

C.
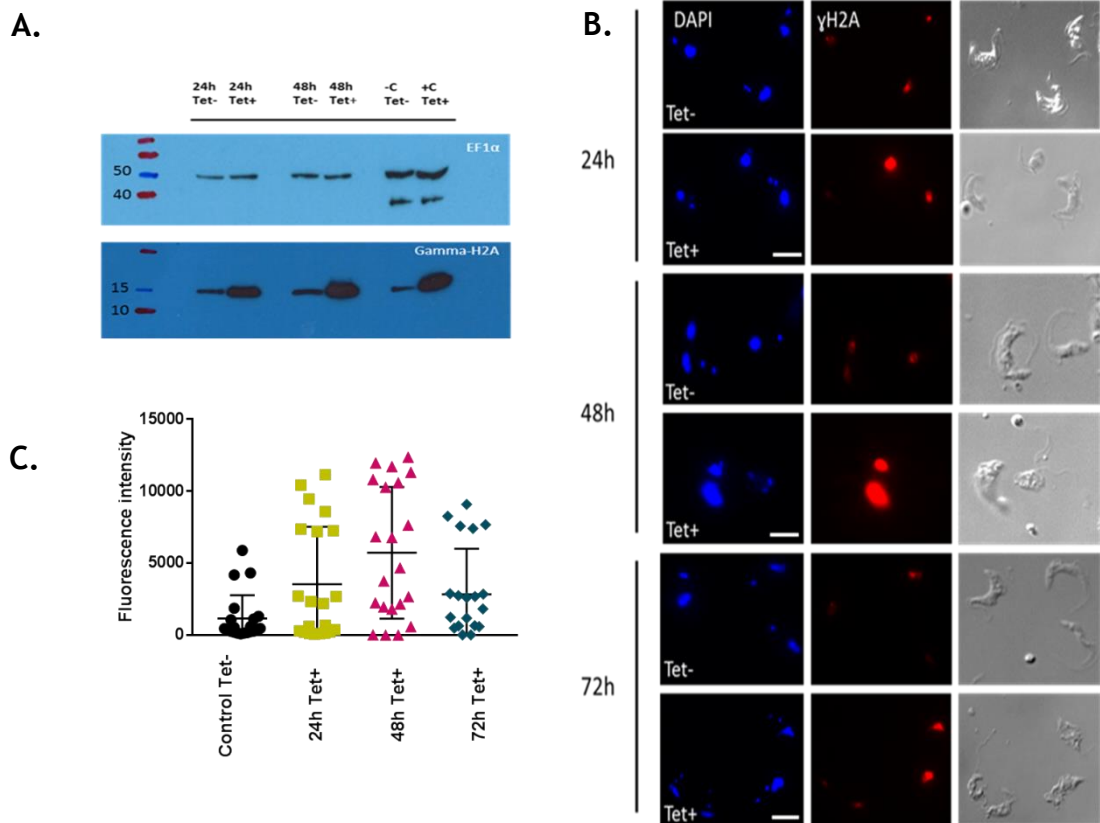
Figure 5-9. Acummulation of DNA damage after RNAi of TbPolN. A. Western blot showing γH2A expression levels after the RNAi depletion of TbPolN relative to uninduced cells. Signal is shown after 24 h and 48 h of growth and detected with anti-γH2A antiserum. WT cells in the absence and presence of phleomycin (2.5 µg/ml) were used as negative (-C) and positive (+C) control respectively. Anti-Ef1α antiserum was used as a loading control. Size markers (kDa) are shown. **B.** Immunolocalisation of *T. brucei* γH2A: left panels show DAPI staining of the nucleus and kinetoplast, the middle panel shows γH2A, detected with anti-γH2A antiserum, and the right panels are merged images of both signals. Cells are shown 24 hours, 48 hours and 72 hours with (Tet+) and without (Tet-) RNAi induction. Images were captured on an Axioscope 2. Scale bar represents 5 µm. **C.** Quantitative measurement of fluorescence intensity of γH2A after 24h, 48h and 72h RNAi induction. The fluorescence was measured by calculating the corrected total cell fluorescence (CTCF). Dots represent the signal obtained for each individual cell. A total of 20 cells were analysed for each group.

5.4.2 Possible role of TbPolN in DNA repair

Increased expression of γH2A in the cell following the depletion of TbPolN suggests an accumulation of DNA damage after the loss of the protein. To ask if TbPolN associates with DNA lesions, a double immunofluorescence assay was

performed assessing a possible co-localisation of the modified histone γH2A and TbPolN-12Myc after the generation of damage.

For the assay, the TbPolN-12 myc tagged cell line was used. Signal co-localisation was tested in the absence and presence of the alkylating agent MMS (0.0003%) for 18 hours. Permeabilised cells were incubated in a mixture of two primary antibodies, rabbit anti- γH2A (1:1,000 dilution) and mouse unconjugated anti-Myc (1:1,000). The signal was detected with Alexa Fluor® 488 α- rabbit (1:1,000) and Alexa Fluor® 594 α- mouse (1:1,000), respectively.

Some overlap of the fluorescent signals was seen after the addition of MMS. As described before, the TbPolN-myc signal after MMS treatment was spread throughout the cells, whereas the γH2A signal was seen as a discrete focus in some cells, or not at all in others. After MMS treatment, γH2A signal was much more widespread in the nucleus and the overlap of both fluorescent signals was modest (Figure 5-10). The partial co-localisation of TbPolN and γH2A suggests a putative role of TbPolN during the repair of MMS damage.
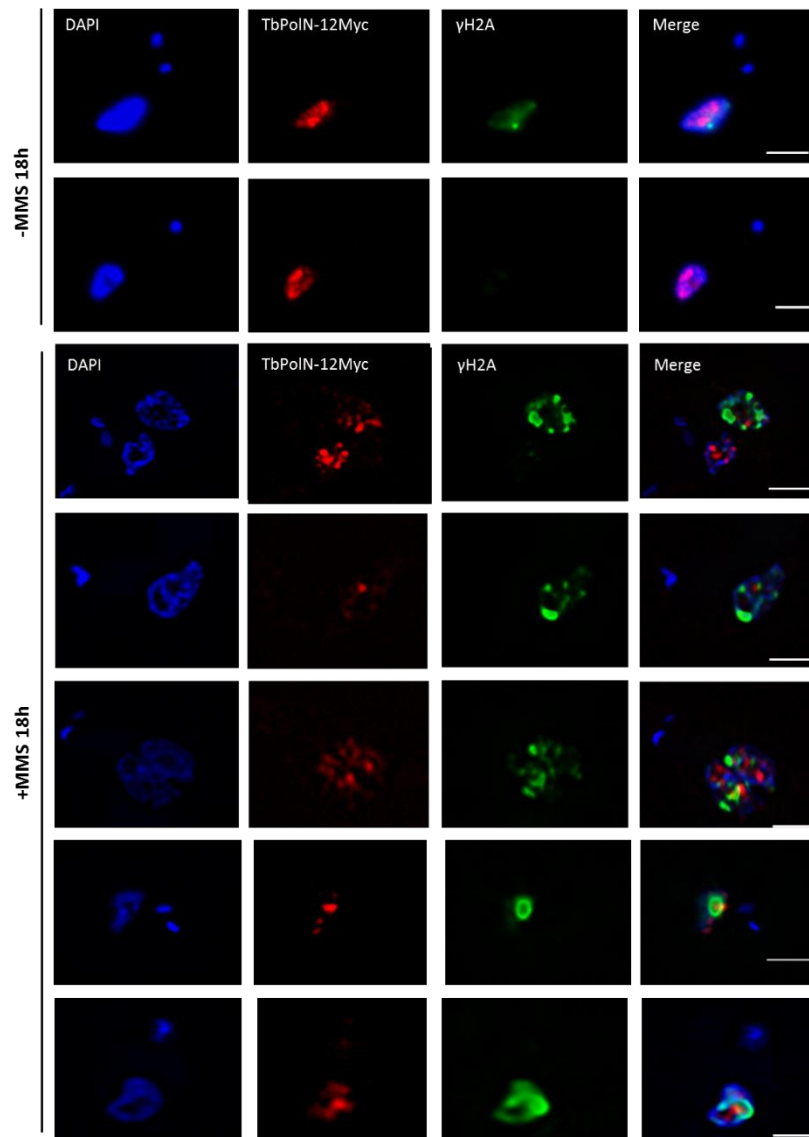
Figure 5-10. Co-localisation of TbPolN-12myc and γH2A. Immunolocalisation of *T. brucei* γH2A and TbPolN-12myc: first (left to right) panel shows DAPI staining of the nucleus and kinetoplast, the second panel shows TbPoN-12myc using a unconjugated anti-myc antibody, third panel shows γH2A signal and the fourth panel is merged images of the three signals. Cells are shown before (Tet-) and after (Tet+) RNAi induction in the presence of 0.0003% of MMS. Images were captured on a Delta Vision RT deconvolution microscope. Scale bar represents 2 μm.

5.4.3 Analysis of EdU incorporation in TbPolN depleted cells

Damage accumulation, increase of aberrant cells and decrease of cell proliferation are all the result of RNAi depletion of TbPolN. One explanation for this range of phenotypes is a role of TbPolN during nuclear genome replication, which results in genome instability when the protein is lost.

To assess a possible role of TbPolN during replication, uptake of EdU, which has the capacity to incorporate into the DNA of proliferating cells (Salic and Mitchison, 2008), was assessed. This synthetic nucleoside is characterized by the replacement of the terminal methyl group by an alkaline group. The alkaline group can form a covalent bond with a fluorescent azide using a copper Cu(I) catalyzed-[3+2] cycloaddition ('Click') reaction, facilitating the detection of EdU inside the cell (Salic and Mitchison, 2008).

In order to test if the depletion of TbPolN affects DNA replication, EdU incorporation was tested in cells after 12 hours, 24 hours, 36 hours and 48 hours growth, in the absence (Tet-) or presence (Tet+) of tetracycline RNAi induction. In procyclic forms, nuclear S phase has a duration of 1.5 hours (Woodward and Gull, 1990). Assuming that the nuclear DNA synthesis timing is similar or slightly shorter in blood stream forms, it was decided to incubate the cells with EdU for a period of four hours. The cells used in this assay were not synchronized. For this reason, the four hour incubation period was considered optimal to ensure the labeling of the majority of cells undergoing DNA synthesis. Previous work, in both procyclic from and bloodstream form *T. brucei,* has shown that RNAi depletion of components of the origin recognition complex (ORC), which initiates DNA replication, leads to loss of EdU uptake (Marques *et al.,* 2016). In all cases, the timing of EdU uptake loss preceded further growth and cell cycle impairment, suggesting ORC loss led to DNA replication reduction, which then led to growth defects (Marques *et al.*, 2016).

IFA imaging of EdU positive cells was performed for both uninduced and RNAi induced cells after 12 hours, 24 hours, 36 hours and 48 hours growth. In these conditions, the proportion of uninduced cells that displayed nuclear EdU signal was 90%. To allow comparison with EdU uptake after RNAi, the proportion of Tet- EdU positive cells at each time point were considered to be a 100% and the proportion of the Tet+ EdU positive cells were calculated relative to the Tet- value. 2T1 cells, which do not induce RNAi, were used as a control.

A small decrease in the number of EdU stained cells, 5% and 6%, was observed 12 hours and 24 hours post induction, respectively (Figure 5-11). A decrease in the number of EdU stained cells (22%) was also detected 36 hours

after RNAi induction (Figure 5-12), suggesting that replication impairment starts before the most pronounced cell cycle defects were seen at 48 hours (section 3.3.1, 3.3.2). At 48 hours post-RNAi induction, when there was a very pronounced decrease of 1N1K cells and an accumulation of aberrant cells, 45% of the population stopped incorporating EdU (Figure 5-12). Closer examination of the EdU positive and EdU negative cells 48 hours after RNAi, suggested a possible connection between a lack of EdU incorporation and aberrant cells. In the damage accumulation assay (Section 5.3.2), aberrant cells commonly presented γH2A signal. Thus, we decided to ask if the defect in replication and damage accumulation phenotypes were also connected.
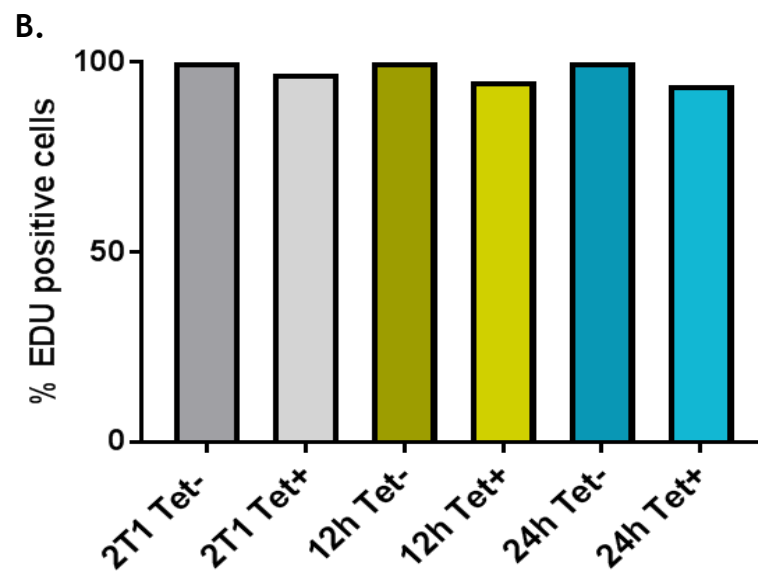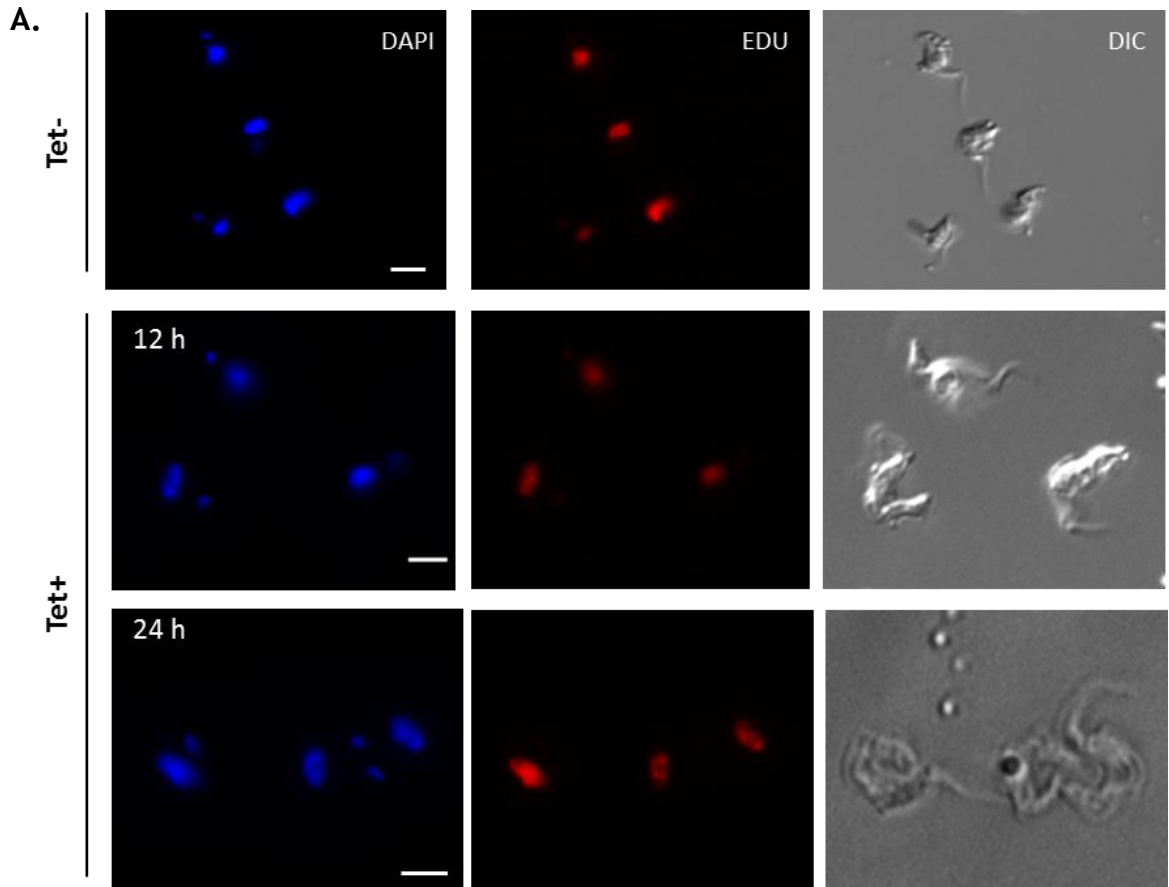
Figure 5-11. EDU labelling to determine the effect on nuclear DNA replication at 12 hours and 24 hours of TbPolN loss. A. Left panels shows DAPI staining of the nucleus and kinetoplast, middle panels show EdU signal, and right panels show the cell outline by DIC. **B.** EdU stained cells in the absence (Tet-) and presence (Tet+) of tetracycline induction at 12 hours and 24 hours are shown, with the graph depicting the percentage of the total population after induction relative to uninduced control at the same time points (set at 100%). A minimum of 100 cells were analysed per time point.
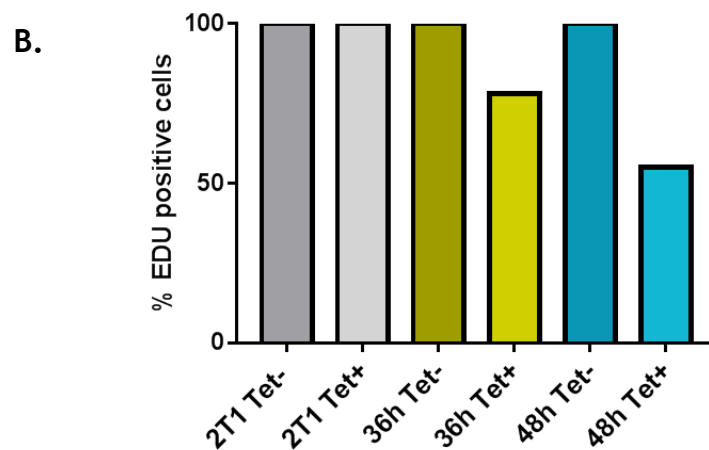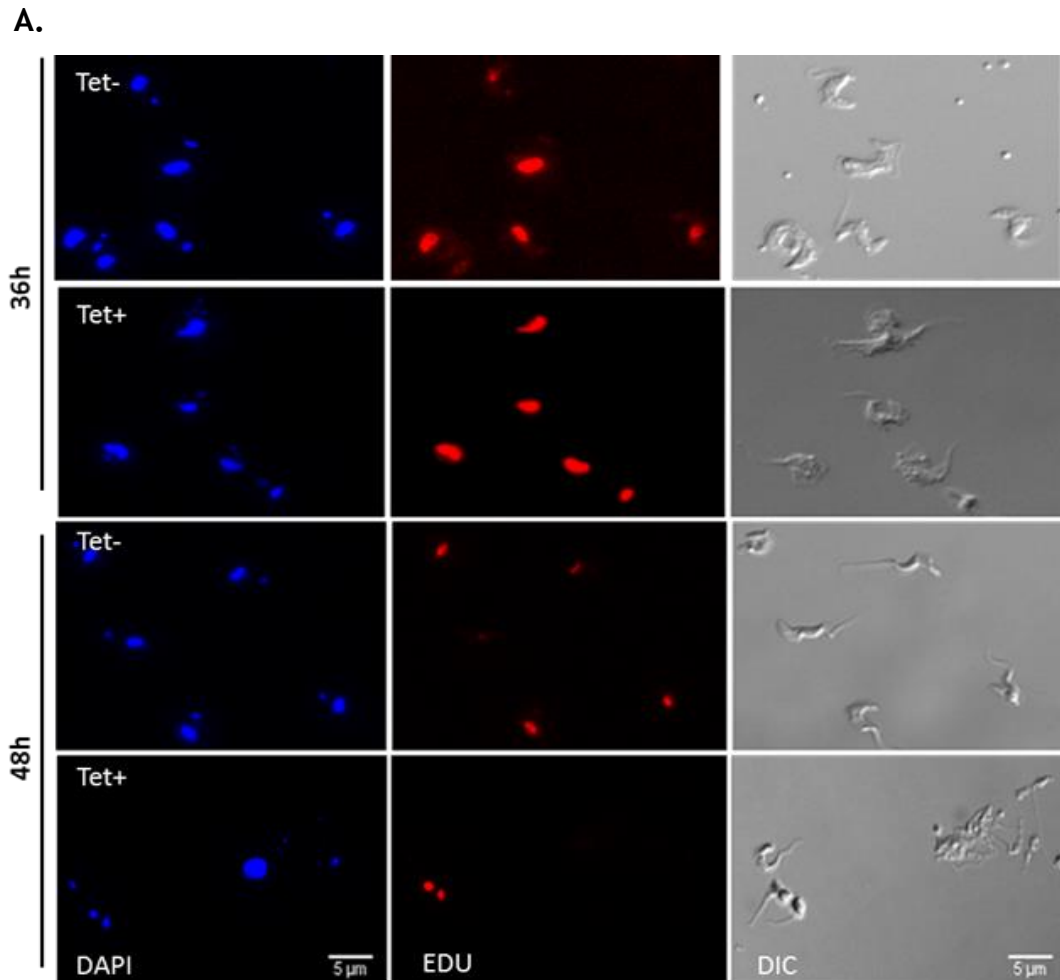
Figure 5-12. EdU labelling to determine the effect of TbPolN RNAi on nuclear DNA replication. A. Left panels shows DAPI staining of the nucleus and kinetoplast, middle panels show EdU signal, and right panels show the cell outline by DIC. **B.** EdU stained cells in the absence (Tet-) and presence (Tet+) of tetracycline induction at 36 hours and 48 hours are shown, with the graph depicting the percentage of the total population after induction relative to

uninduced control at the same time point (set at 100%). A minimum of 100 cells were analysed per time point.

In order to test for a correlation between damage accumulation and the decrease of EdU incorporation at 48 hours post induction, a double immunofluorescence was performed using permeabilised cells. The cells where first stained for EdU (section 2.8) and subsequently stained for γH2A (1:1,000).

This experiment suggests an association between damage accumulation and lack of EdU incorporation. In the uninduced population most cells that had nuclear EdU signal did not display γH2A signal (Figure 5-13 A). In contrast, many cells could be detected after RNAi against TbPolN that did not display EdU signal and had γH2A signal; indeed, this was commonly observed in aberrant cells (Figure 5-13(1)). This appears consistent with stalling of nuclear replication in the absence of TbPolN leading to damage. Cells were also detected, though less often, which were positive for EdU and γH2A, as well as healthy cells that appeared to be incorporating EdU and had no γH2A (Figure 5-13 (2-3)). These latter events suggest that not all cells lacking TbPolN suffer this fate, which may be explained by redundancy of TLS pols, with the role of TbPolN being assumed by another TLS pol. Alternatively, the levels of TbPolN loss after RNAi are variable in the cells of the population, or the features of the genome that need to be tackled by TbPolN are at variable levels in individual cells.

The results were confirmed by performing a quantitative measurement of EdU and γH2A fluorescence intensity by calculating the corrected total cell fluorescence (CTCF) with the software Fiji (ImageJ) (section 2.10.3). The CTCF was calculated separately for each fluorescent channel. The measurement of the intensity of EdU and γH2A signal, in uninduced cells, resembles the data obtained in the IFA, where the γH2A signal in the majority of the analysed cells was limited, suggesting the absence of damage accumulation in most cells. In the same cells, the EdU fluorescence intensity ranged between ~ 50 – 100 pixels, meaning that the cells were incorporating EdU, and therefore showing evidence of ongoing replication (Figure 5-13 B). On the other hand, the 48 hours induced cells show EdU intensity levels closer to zero, suggesting replication stalling. At the same time, a much larger proportion of the RNAi induced cells displayed γH2A signal (which was more distributed along the Y-axis), suggesting

accumulation of damage after the depletion of the protein. It was also possible to observe an overlap of both signals, which support the data obtained in the IFA, where few cells accumulate damage and incorporate EdU (Figure 5-13).
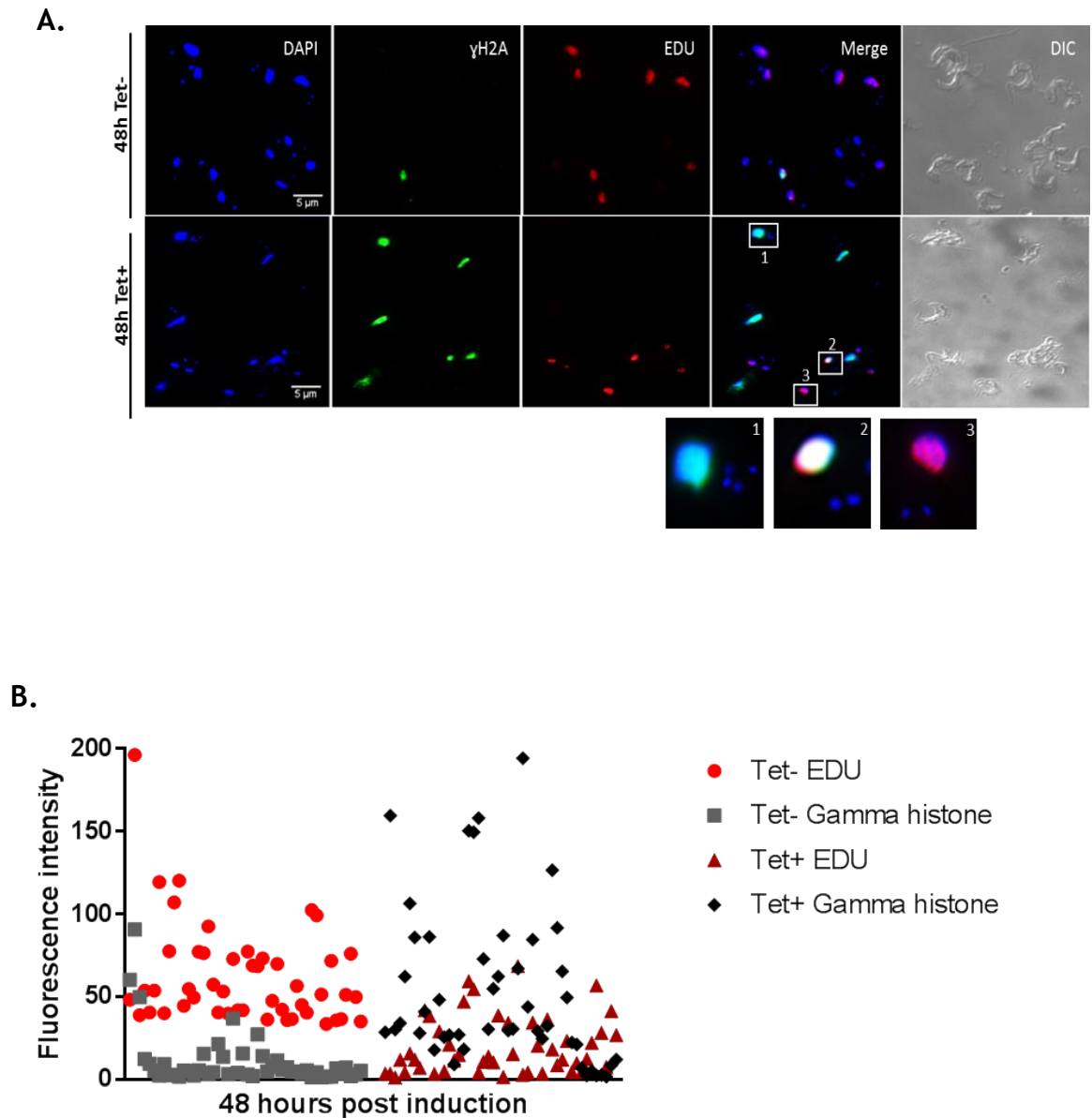
Figure 5-13. Double staining immunofluorescence of γH2A and EdU before and after TbPolN RNAi. Cells are shown after 48 h growth in the absence (Tet-) or presence (Tet+) of tetracycline. **A.** The first panels (left to right) show DAPI staining of the nucleus and kinetoplast, second panels show γH2A signal detected with anti- γH2A antiserum, third panels show EdU signal, the fourth panels show a merge of the γH2A and EdU signals, and the fifth panels show the cell outline by DIC. Larger images of boxes show three different scenarios: (1) cells lacking EdU signal but showing accumulation of damage; (2) cells presenting γH2A and EdU signal; and (3) cells incorporating EdU and not showing

γH2A signal. Scale bar 5 μm. **B.** Quantitative measurement of fluorescence intensity of EdU and γH2A by calculating the corrected total cell fluorescence (CTCF). The CTCF was calculated separately for each fluorescent channel (ROI - 21x21 pixels). Dots represent the signal obtained for each individual cell. A total of 50 cells were analysed for each group

5.4.4 Association of TbPolN with chromosome integrity

Although PolN has not been associated with chromosomal rearrangements in other organisms, the severe phenotype shown after the depletion of the protein suggested this was a possibility in *T. brucei* after RNAi. Previous studies have demonstrated a link between polymerases and chromosomal segregation; for instance, *S. cerevisiae* trf4/polymerase σ, a member of X family of polymerases, is associated with the sister chromatid cohesion complex, and loss of the protein affects the assembly of the complex and the subsequent transition from metaphase to anaphase (Wang *et al.*, 2002; Haracska *et al.*, 2005).

In order to test for a role for TbPolN and the maintenance of chromosome integrity in BSF parasites, a telomere-fluorescence *in situ* hybridisation (Telo-Fish) assay was performed using a telomeric probe recognizing the TTAGGG repeats in *T. brucei*. The assay was performed with the TbPolN RNAi cell line in the presence and absence of tetracycline at 24 hours and 48 hours. $2x10^6$ cells were collected and fixed (section 2.9); subsequently the probe was applied to the cells and incubated for 16 hours. Several washes were performed in order to remove unhybridized probes (section 2.9). Images were taken using the Delta Vision RT Epifluorescence Imaging System. Because mini-chromosomes are more abundant than megabase-chromosomes, it is likely that most Telo-FISH signal corresponds to the former. As seen in previous work (DuBois *et al.*, 2012), in uninduced RNAi cells, telomeres are localised diffusely around the nucleus during interphase, with a stronger signal towards the nuclear envelope (Ogbadoyi *et al.*, 2000) (Figure 5-14). During metaphase the telomeres were detected in the centre of the nucleus and later in mitosis (anaphase) the telomeres were localised towards the nucleus poles (Figure 5-14)(Ogbadoyi *et al.*, 2000; DuBois *et al.*, 2012). It appears that the telomere distribution 24 hours post RNAi induction was mainly not affected (Figure 5-15), resembling the telomere segregation of the uninduced cells.
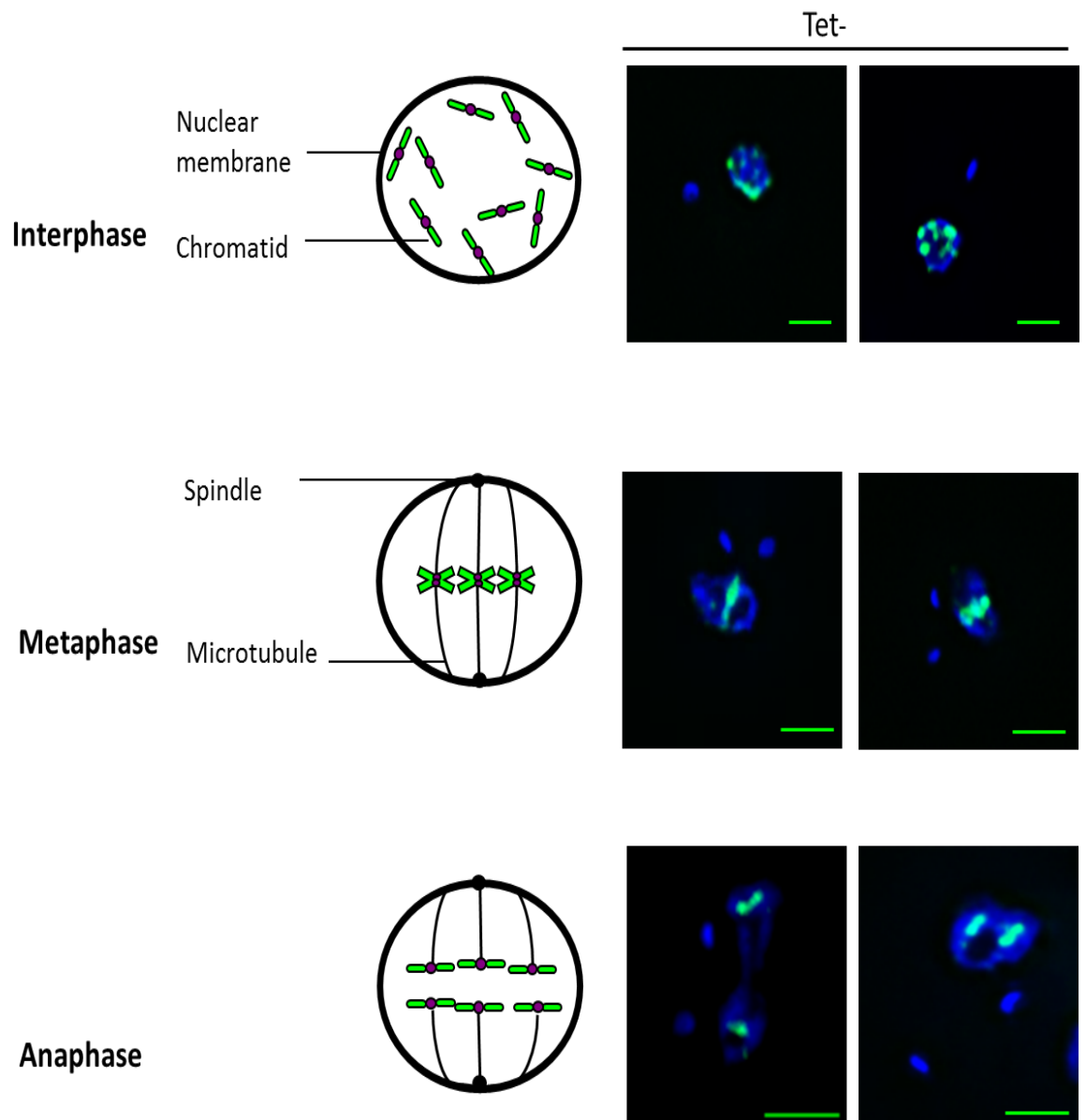
Figure 5-14. Fluorescence *in situ* hybridisation analysis of the distribution of telomeres during the cell cycle in *T. brucei*. Schematic representation of chromosome distribution. Chromatids are represented in green, kinetochores in purple and nuclear membrane, spindle and microtubules in black. Representative images of uninduced cells (Tet-), which were captured on a Delta Vision RT. DNA (blue) is stained with DAPI and telomere signal is in green. Scale, 2 μm.

Interphase

Metaphase

Anaphase
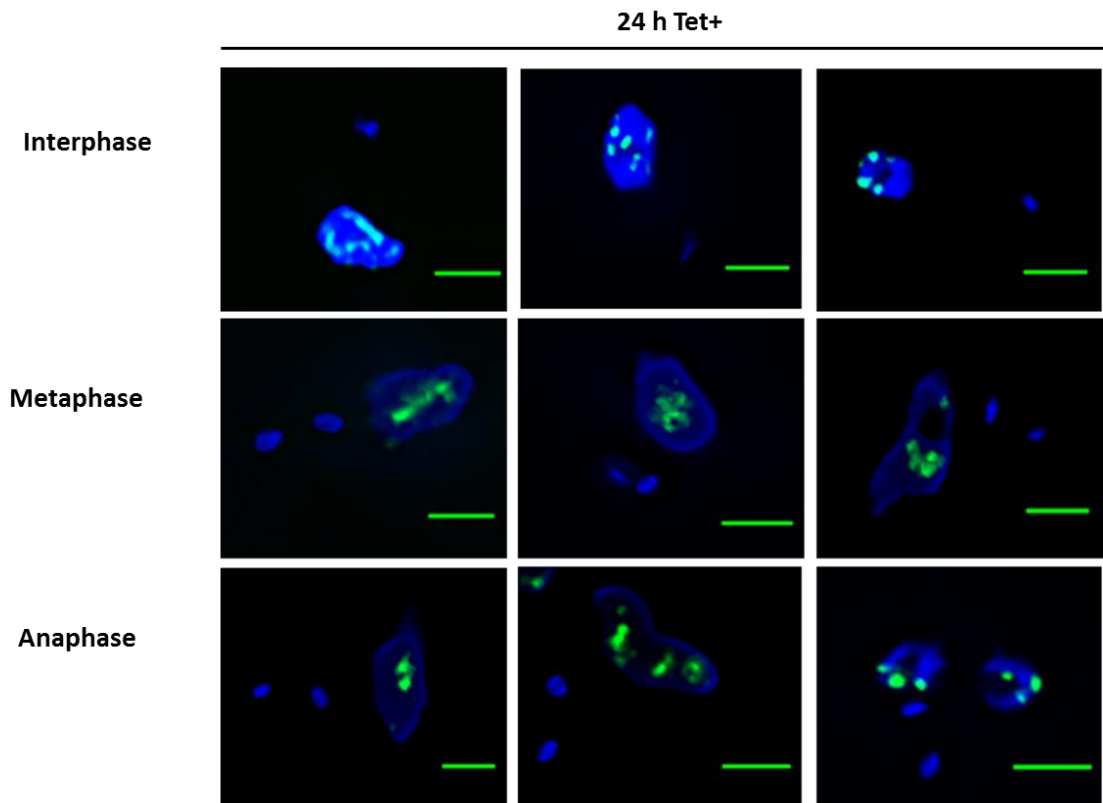
Figure 5-15.Fluorescence *in situ* **hybridisation analysis of telomere distribution 24 hours post RNAi induction against TbPolN.** Fluorescence in situ hybridization using telomeres as a probe (green), in the presence (Tet+) of tetracycline for 24 hours. Top three panels show telomere distribution during interphase, middle panels show telomere localisation during metaphase and bottom panels show telomere distribution during anaphase. Images captured on a Delta Vision RT. Scale bar 2 μm.

On the other hand, after 48 hours of TbPolN RNAi it was possible to observe potentially aberrant chromosome segregation. In cells that appeared to be going through mitosis, the typical telomere distribution during metaphase could be lost, with cells presenting an abnormal alignment at the equator of the nucleus. During anaphase the ordered segregation of the telomeres into each of the two progeny cells could be seen to be compromised, with unequal distribution in the nuclei (Figure 5-16 A). In interphase cells the telomere signal resembles the localisation of uninduced cells, with a large part of the signal localised to the nuclear periphery (Figure 5-16 A)(Ogbadoyi *et al.*, 2000). Finally, defective telomere distribution was also observed in aberrant cells, which could be the result of anomalous nucleus architecture or of previous inaccurate chromosome segregation events during mitosis (Figure 5-16 B).
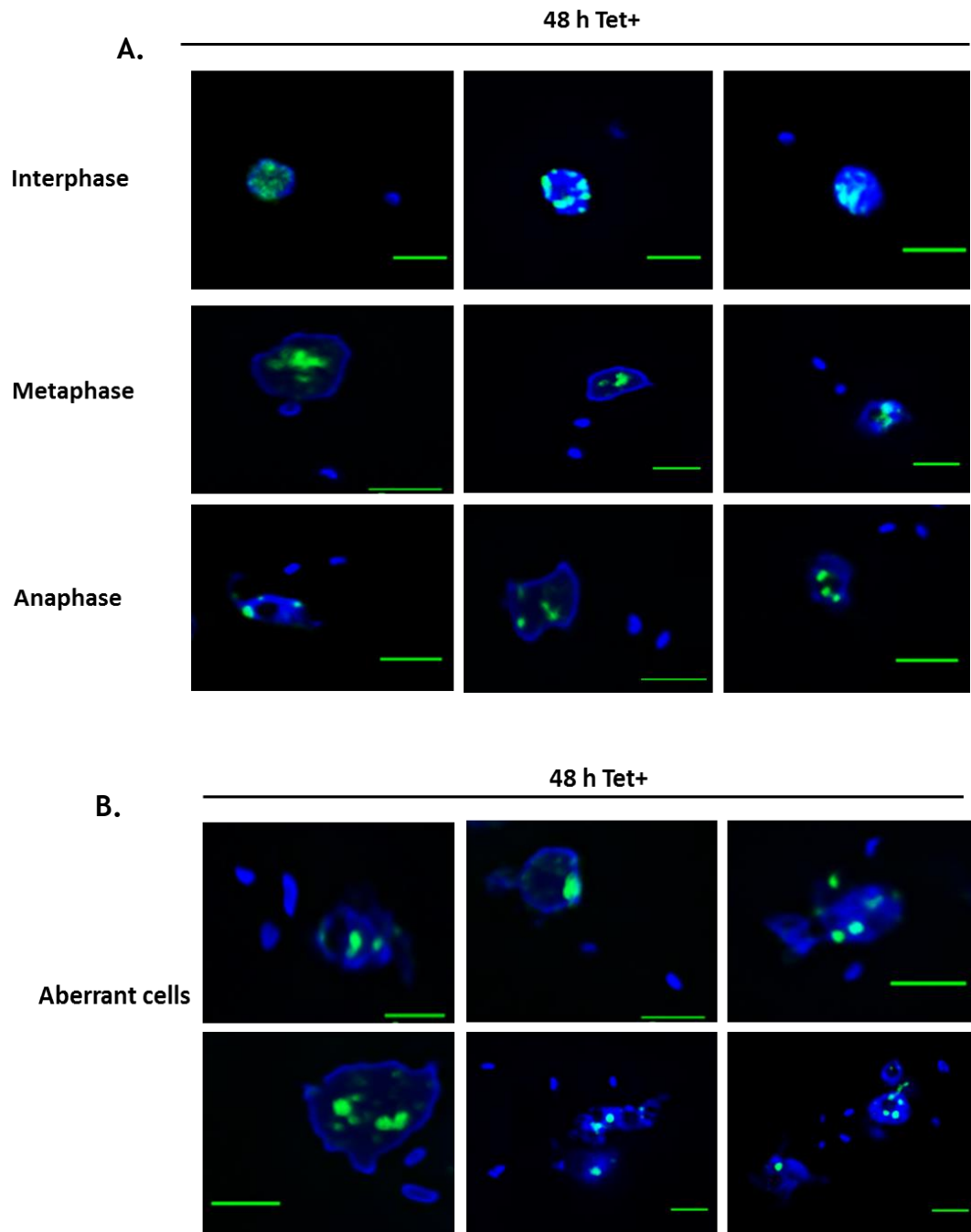
Figure 5-16. Fluorescence in situ hybridization of telomeres after the depletion of TbPolN. Fluorescence in situ hybridization using telomeres as a probe (green), in the absence (Tet-) and presence (Tet+) of tetracycline for 48h. **A.** Top panels show telomere distribution during interphase, middle panels show telomere distribution during metaphase and bottom panels show telomere localisation during anaphase. **B.** Aberrant cells, such as with abnormal nuclei or increased kinetoplast numbers, showing examples of telomere distribution. Images captured on Delta Vision RT. Scale bar 2 µm.

5.5 Depletion of TbPolN is associated with deregulation of silent VSG expression sites

It was shown above that TbPolN may be associated with chromosome stability, with depletion of the protein resulting in alteration of chromosome segregation during metaphase and anaphase. As in other eukaryotes, *T. brucei* regulates the transition from metaphase to anaphase through the cohesin complex (Gluenz *et al.*, 2008). Earlier studies in *T. brucei* suggest that alterations in the cohesin complex result in activation of silent VSG expression sites (ESs) (Landeira and Navarro, 2007). Thus, it was considered a possibility that loss of TbPolN might also result in an alteration in VSG expression controls.

Previous studies have identified the presence of 15 unique bloodstream ESs (BESs) in Lister 427 (Figure 5-17) (Hertz-Fowler *et al.*, 2008; Landeira *et al.*, 2009). The cell lines used for this assay predominantly express VSG221, which is localised in BES1 (the 'active' expression site). In order to investigate whether the loss of TbPolN resulted in the increase in transcription of silent VSGs RT-qPCR was performed; 48 hours post induction of TbPolN RNAi, to assess levels of RNA for four silent ES genes (VSG13, VSG800, VSG224 and VSGVO2). The RNA extraction and its conversion to cDNA, prior to the RT-qPCR analysis, was performed as per section 2.3.4. The primers used for the assay are described in Table 2-2.

An increase in VSG transcript levels from the silent ESs could be detected 48 hours after TbPolN RNAi relative to the uninduced cells. In the case of VSG13, VSGVO2 and VSG224 an increase, ranging from ~2-3 fold was seen (Figure 5-18), with a smaller increase for VSG800. Although the changes are modest, the data suggest that the depletion of TbPolN results in activation of silenced VSG ESs. Similar results were obtained after the depletion of the cohesin complex subunit, TbSCC1 (Landeira *et al.*, 2009). However, a small increase in VSG221 RNA, to a similar extent to that of VSG800, was also seen. This observation may suggest subtly different effects to that of TbSCC1 RNAi, but may also suggest that these preliminary observations need to be validated by further experimental repeats.

Figure 5-17. Schematic representation of bloodstream VSG expression sites in *T. brucei* Lister 427. The diagram shows the bloodstream expression sites (BESs) annotated in the *T. brucei* Lister 427 genome following TAR (transformation-associated recombination) cloning. ESAGs (expression site associated genes), VSGs (variant surface glycoprotein), pseudogenes and other ES features are represented above. Figure reproduced in full from (Hertz-Fowler et al. 2008) (all rights reserved).

Figure 5-18. Loss of TbPolN is associated with the increase in transcription of silent ES VSGs. Levels of RNA were assessed by RT-qPCR of TbPolN RNAi cell line after growth for 48 hour in the presence or absence of tetracycline induction. The CT values for each sample were calculated by averaging the CT values across the triplicate technical repeats. The relative fold change for each gene examined was determined by calculating the ΔΔCT value (equation shown in section **RT-qPCR**) for each gene normalised to an endogenous control (actin). The levels of RNA for the uninduced samples were set to 1 (represented by the black line), and the levels in the RNAi induced expressed relative that control. The following VSGs were examined: VSG221, VSG13, VSGVO2, VSG224 and VSG800 (named as detailed in Hertz-Fowler et al. 2008).

5.6 Generation of TbPolN knockout cell lines

As discussed previously (section 3.3.1), depletion of TbPolN by RNAi results in a decrease in cell proliferation. Interestingly, however, the defects observed during reduced growth represent transient phenotypes, with less aberrant cells and less nuclear damage beyond 48 hour post induction.

For these reasons, a full knockout of Tb*PolN* was attempted in order to ask if TbPolN is truly essential. In order to accomplish this, a disruption of the *TbPolN* gene was attempted by two sequential rounds of transformation into wild type (WT) BSF cells (*T. brucei* Lister 427) using two constructs: one containing a blasticidin resistance cassette (*ΔPolN::BSD*) and the other a G418 resistance cassette (*ΔPolN:: NEO*) (Figure 5-19).

A region of approximately 500 bp was amplified, which includes a part of the UTR and ORF of the Tb*PolN* gene, from both the 5'and 3' regions. The forward and reverse primers used for the amplification were designed to include a specific restriction site. For the 5' region, the forward primer contains HindIII and NotI sites (gcataagcttgcggccgcaaacatgcttatgtttttgt) and the reverse primer contains an XbaI restriction (gcattctagattcccttcagtggttgtgta). The 3' region forward primer contains a SacI restriction site (gcatgagctcttcacgaaaggcgtcacgac), and ClaI and NotI were included in the reverse primer (gcatatcgatgcggccgcccccacaacaataacaacaa).
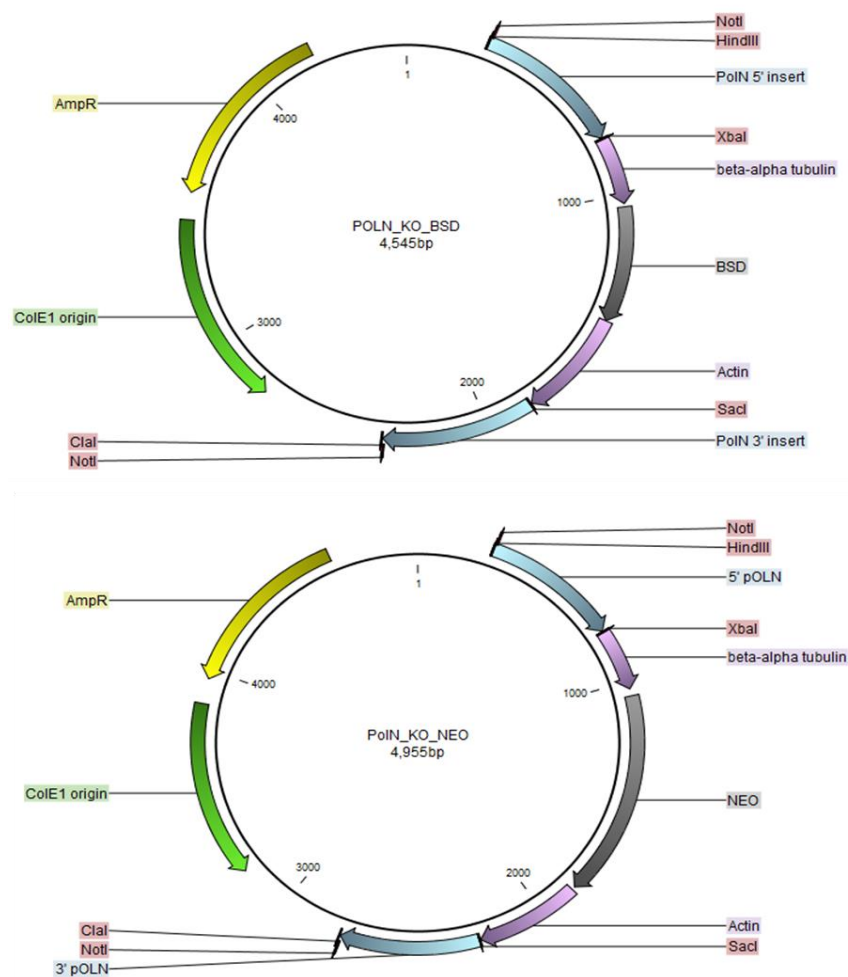
Figure 5-19. Plasmid maps of the constructs used for the deletion of TbPolN. In grey are the *BSD* and *NEO* cassettes, encoding the drug resistance markers used for the selection of transformant clones. Β-α tubulin and actin represented in purple, flanking the drug cassette.In blue are represented sequences of approximately 200 bp that have homology with the 5' and 3' regions surrounding the *TbPolN* ORF, respectively, which provide homology for recombination and integration of the cassettes after transformation.

The PCR products and the *ΔPolN::BSD* and *ΔPolN::NEO* plasmid were digested (HindIII+XbaI and SacI+ClaI) and ligated as described in section 2.3.8. The resulting knockout constructs were checked by sequencing prior to transfection, after the DNA fragment was liberated from the plasmid with NotI. If successful, two rounds of transformation in WT cells should replace both alleles of the gene with the antibiotic resistance cassettes (Chapter 4, Section 4.3).

ΔPolN:: NEO was first transformed into WT cells, generating putative heterozygous mutants (*TbPolN-/+*). As mentioned in section 4.3, the addition of the antibiotic G418 caused slowed growth of the transformant cells in comparison to WT (data not shown). As in the case of *TbRev3 -/+* transformants, the drug was removed after clonal selection, permitting optimal outgrowth of the cells for transformation of the putative *TbPolN-/+* cells with the *ΔPolN:: BSD* construct.

The first transformation with the *ΔPolN::NEO* construct was successful, recovering two G418 resistant transformant clones. For the verification of the heterozygous cell line, two PCRs were performed: the first PCR targeting the drug resistance cassette, and the second PCR targeting a region of the *TbPolN* ORF (Figure 5-20). For both clones, the PCRs confirmed the presence of integrated NEO and retention of the ORF, as expected for a heterozygous cell line (-/+)(Figure 5-20).

Having generated *TbPolN-/+* cells, a second transformation with the ΔPolN::BSD construct was attempted, but no blasticidin resistant transformants were recovered. Further attempts were performed to obtain null mutants, reducing the drug concentration from 10 µg/ml to 7 µg/ml and 5 µg/ml. Before changing the drug concentration a titration was performed to ensure the drug concentration was still optimal for the selection of positive clones (data not shown). The retrieval of null mutants was not successful, suggesting that TbPolN protein may have an essential role in survival of the parasite.
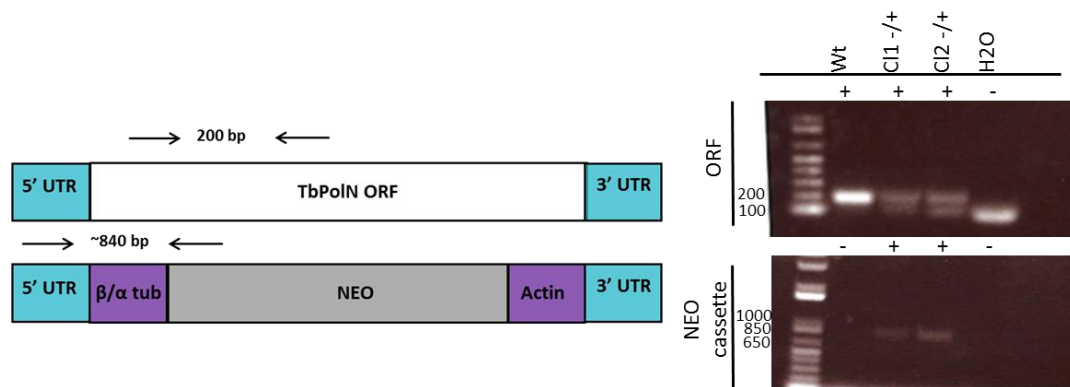
Figure 5-20. Confirmatory PCR of *TbPolN* heterozygote mutants.Schematic representation of expected fragment sizes amplified by PCR (bp), including diagnostic primers used (black arrows) and their position in the genome or construct (not to scale). Primer sequences are available in Chapter2, Table 2-1. Agarose gels of diagnostic PCRs, testing the presence of *TbPolN* ORF and integration of the *NEO* cassette. WT cells and ddH$_2$O were used as negative controls. All PCRs were performed on the same gDNA samples. Size markers (bp) are shown.

5.7 Identifying TbPolN potential interaction partners

To attempt to further understand the functions of TbPolN, it was decided to search for possible interaction partners. To do this, immunoprecipitation (IP) of TbPolN-myc was performed with anti-myc antiserum. For this purpose, the *TbPolN-/+* cell line was transformed with C-terminal myc-tag construct as described in section 5.3.1. The expression of TbPolN-myc was verified by Western blot of cell extracts with anti-myc antiserum (Figure 5-21 A).

5.7.1 Immunoprecipitation

In order to perform the IP, extracts from WT (1x10^8) and *TbPolN-/+::12myc* cells (1x10^8) were incubated with Dynabeads® (Invitrogen) coated with anti-myc antibody. After five washes with washing buffer (50 mM Hepes pH 7.55, 100 mM NaCl, 1 mM EDTA pH 8.0, 1 mM EGTA pH 8.0, 10 % glycerol, 0.1 % Triton X-100, and 2x complete protease and phosphatase inhibitor cocktail; Roche), the eluate was collected and re-suspended in 15 µl of 1X NuPAGE® LDS Sample Buffer (described in chapter 2, section 2.12.2). For both WT and *TbPolN-/+::12myc* duplicate IPs were performed. One of the eluates from each of the WT and TbPolN-/+::12myc cells was separated on a 10% Bis-Tris SDS-PAGE gel and stained with SYPRO® Ruby. It was not possible to differentiate specific bands when comparing the WT control and *TbPolN-/+::12myc* IPs (Figure 5-21 B).

However, using the second eluate, specific IP of TbPolN-myc was confirmed by Western blot (1µl of eluate, 9µl of protein loading buffer), where the presence of tagged protein was exclusively detected in the *TbPolN-/+::12myc* IP eluate and not WT (Figure 5-21 C). Thus, the remaining eluate of both the WT and TbPolN-/+::12Myc IPs were analysed by mass spectrometry (Glasgow Polyomics Facility).
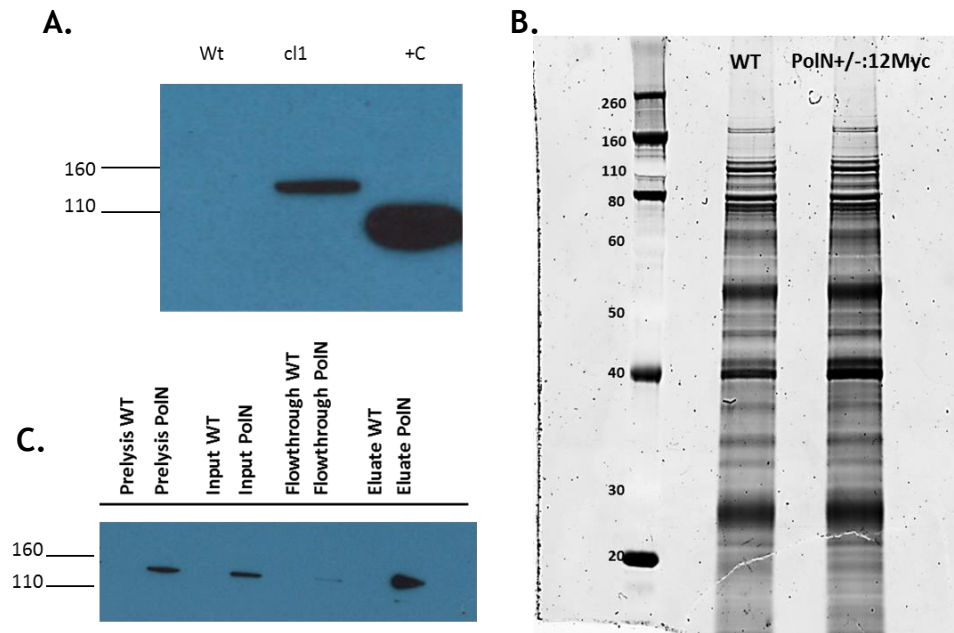
Figure 5-21. Immunoprecipitation of TbPolN-12Myc. A. Western blot of whole cell extracts from WT, a blasticidin resistant transformants and from a cell line expressing CRK11-12 myc as a control (+C), detected using anti-myc antibody. **B.** Sypro ruby stained gel of anti-myc immunoprecipitated proteins from WT427 (un-tagged cell line) and TbPolN+/-12myc lysates. **C.** Western blot on all fractions of the IP from TbPolN-12myc and WT. Fractions from left to right: prelysis, input, flow-through and eluate from TbPolN-12myc and WT, showing the absence of bands in the untagged cell line.

The mass spectrometry data revealed the IP of several possible TbPolN-myc interacting partners. In order to evaluate the data, *TbPolN -/+::12Myc* IP 'hits' were compared against WT 'hits', excluding common proteins. From a total of 59 proteins identified by MS in the *TbPolN -/+::12Myc* IP, four proteins were shared with the WT control IP (which identified 36 proteins), leaving 55 proteins specific to the former (Table 5-1). These 55 proteins were assessed for possible contaminants (e.g. VSGs, ESAGs and ribosomal proteins), which were

excluded, leaving 34 proteins. All of these hits were analysed by BLASTp, in an attempt to derive potential functional information beyond the existing TriTrypDB annotations. For many proteins no further information could be discerned beyond that provided by existing annotations, and for others, annotated as 'hypothetical', the Blast and conserved domain predictions gave only very weak homologies. However, four potential proteins were revealed as potentially of interest (Table 5-2). Three of the four possible interaction partners are annotated in TriTrypDB as hypothetical proteins (Tb927.5.3280, Tb927.2.3990 and Tb11.01.3060), but BLASTp revealed each to have putative domains conserved with structural maintenance of chromosome (SMC) proteins, perhaps suggesting roles in chromosomal condensation or cohesion (Harvey, Krien and O'Connell, 2002). The other 'hit' was a putative Poly(A) polymerase (putative Polσ), which has been suggested to have a role in DNA repair (Garcia-Diaz and Bebenek, 2007) in other eukaryotes. It has also been associated with chromosome cohesion in yeast (Edwards *et al.*, 2003b). Thus, though the IP is highly unspecific, a cohort of proteins potentially associated with genome transmission were specifically recovered in the TbPolN-12myc IP, perhaps consistent with the impaired genome maintenance functions seen after TbPolN RNAi.

Gene ID	Annotation	Score
Tb927.8.7590	receptor-type adenylate cyclase GRESAG 4, putative	33
Tb927.6.1130	hypothetical protein, conserved	33
Tb927.1.2330	beta tubulin 570482:571810 forward	33
Tb927.5.3280	hypothetical protein, conserved	31
Tb11.01.3980	hypothetical protein, conserved	30
Tb927.4.5610	variant surface glycoprotein (VSG, pseudogene),	29
Tb927.7.1140	GPX3 trypanothione/tryparedoxin dependent peroxidase	29
Tb11.30.0013	variant surface glycoprotein (VSG, pseudogene)	29
Tb927.2.2340	hypothetical protein, conserved	26
Tb11.01.4960	Tb11.01.4960 regulator of nonsense transcripts 1, putative (pseudogene)	25
Tb927.8.5200	hypothetical protein, conserved	25
Tb927.8.7260	kinetoplast-associated protein, putative	25
Tb927.5.3250	hypothetical protein, conserved	25
Tb927.8.5700	hypothetical protein, conserved	25
Tb927.5.2800	hypothetical protein, conserved	25
Tb927.4.5650	variant surface glycoprotein (VSG, pseudogene)	24
Tb927.2.6050	beta prime COP protein	24
Tb10.70.0070	tyrosine specific protein phosphatase, putative	22
Tb927.8.4230	hypothetical protein, conserved	22
Tb11.01.2440	glycosyl hydrolase, putative	22
Tb927.8.7800	hypothetical protein, conserved	20
Tb11.03.0970	receptor-type adenylate cyclase GRESAG 4, putative	20
Tb927.8.3830	ATP-dependent DEAD/H RNA helicase, putative	19
Tb927.8.600	hypothetical protein, conserved	19
Tb05.5K5.310	expression site-associated gene (ESAG) protein, putative	19
Tb927.5.4660	expression site-associated gene (ESAG, pseudogene), putative	19
Tb11.03.0670	transcription factor, putative; transcription factor IIIb, putative	18
Tb927.2.3990	hypothetical protein, conserved	18
Tb10.6k15.1200	hypothetical protein, conserved	18
Tb927.4.1700	protein kinase, putative	17
Tb11.01.0300	hypothetical protein, conserved	17
Tb927.1.2670	axoneme central apparatus protein, putative	16
Tb09.211.2310	Bem46-like serine peptidase	16
Tb05.5K5.540	variant surface glycoprotein (VSG, pseudogene), putative	16
Tb927.3.5850	variant surface glycoprotein (VSG, pseudogene), putative	15
Tb09.160.1290	hypothetical protein, conserved	15
Tb11.01.3730	hypothetical protein, conserved	15
Tb927.6.5830	variant surface glycoprotein (VSG, pseudogene), putative	15
Tb09.211.4580	hypothetical protein, conserved	14
Tb11.01.2490	hypothetical protein, conserved	14
Tb09.244.0750	variant surface glycoprotein (VSG, pseudogene), putative	14
Tb09.160.3240	hypothetical protein, conserved	14
Tb10.v4.0092	variant surface glycoprotein (VSG, pseudogene), putative	13
Tb11.02.1370	katanin, putative;	13
Tb927.8.7310	hypothetical protein	13
Tb10.70.7360	hypothetical protein, conserved	13
Tb09.244.0190	hypothetical protein, unlikely	13
Tb927.6.1220	hypothetical protein, conserved	13
Tb927.8.1090	DNA polymerase sigma, putative	13
Tb09.244.1250	variant surface glycoprotein (VSG, pseudogene), putative	13
Tb927.4.1090	endosomal integral membrane protein, putative	13
Tb11.01.3060	hypothetical protein, conserved	13
Tb11.01.0200	katanin, putative	13
Tb927.8.6120	hypothetical protein, conserved	13
Tb10.61.3120	hypothetical protein, conserved	13
Tb927.7.2160	hypothetical protein, conserved	13

Table 5-1. Recovered proteins from TbPolN-12myc IP after mass spectrometry analysis. Proteins shown were only present in TbPolN anti-myc IP; hits also identified in IP from WT cells were excluded. Interesting 'hits' are labelled in red. Samples were analysed using MASCOT software.

Gene ID	Annotation	Predicted domains	Potential Function	Protein Score
Tb927.5.3280	hypothetical protein	Structural maintenance of chromosomes (SMC) domain	chromosome segregation	31
Tb927.2.3990	hypothetical protein	SMC domain	chromosome segregation	18
Tb927.8.1090	DNA polymerase sigma putative	Poly A polymerase domain	repair, sister chromatin cohesion	13
Tb11.01.3060	hypothetical protein	SMC domain	chromosome partition	13

Table 5-2. Potential TbPolN interaction partners identified by Mass Spectrometry and homology analyses. Proteins shown were only present in IP from TbPolN-12Myc. Proteins were analysed using MASCOT. Proteins sequence for each 'hit' was examined by BLASTp.

5.7.2 Co-Immunoprecipitation and Co-localisation of TbPolN and putative Poly(A) polymerase (putative Polσ)

To evaluate the possible TbPolN interaction partners further, one of the candidates, a putative Pol σ homologue, was chosen for further study as it has been characterised to some extent in *T. brucei* (Cristodero and Clayton, 2007). The potential role of Polσ in RNA degradation was tested, showing no clear interaction with MTr4. In *S. cerevisiae,* Mtr4 forms part of the TRAMP complex together with a Poly-A polymerase (Cristodero and Clayton, 2007; Callahan and Butler, 2010). This complex is known to be involved in the degradation of RNA in the nucleus (Callahan and Butler, 2010). Interestingly it was possible to detect a growth effect after the depletion of Pol σ by RNAi (Cristodero and Clayton, 2007).

In order to test the predicted interaction, a double-tagged cell line was generated, in which TbPolN was tagged with a myc epitope and TbPolσ with six copies of the HA tag. In order to create the double-labelled cell line, the *TbPolN-/+::12 Myc* cell line was used as the parental line (section 5.7.1). To tag TbPolσ a 620 bp DNA fragment of the C-terminal end of the putative Polσ ORF was inserted into the 6 HA pNAT Phl vector (Alsford and Horn, 2008)(Figure 5-22 A). The fragment was amplified using the following primers: Fw-gcatgagctcagatgctttaaacgtacgga (SacI site) and Rv-gcattctagaacgtcgggtcaatgaccgag (XbaI site). The construct was digested with HpaI and transformed into *TbPolN-/+::12 Myc* cells and transformants selected with phleomycin (2.5 µg/ml). The cloning strategy is described in section 2.5.1.

To check if TbPolN and TbPolσ were expressed as fusions with 12 Myc and 6 HA tags, respectively, a Western blot was performed. A band of approximately

113 kDa (98.8kDa for TbPolN, 14.4 kDa for 12Myc) for TbPolN-myc and a band of approximately 88 kDa for putative Polσ-HA (81.6 kDa for Polσ, 6.6 kDa 6HA) were expected. Two bands of the expected size were seen in a cell extract of one transformant, confirming a successful double tagged cell line (Figure 5-22 B).
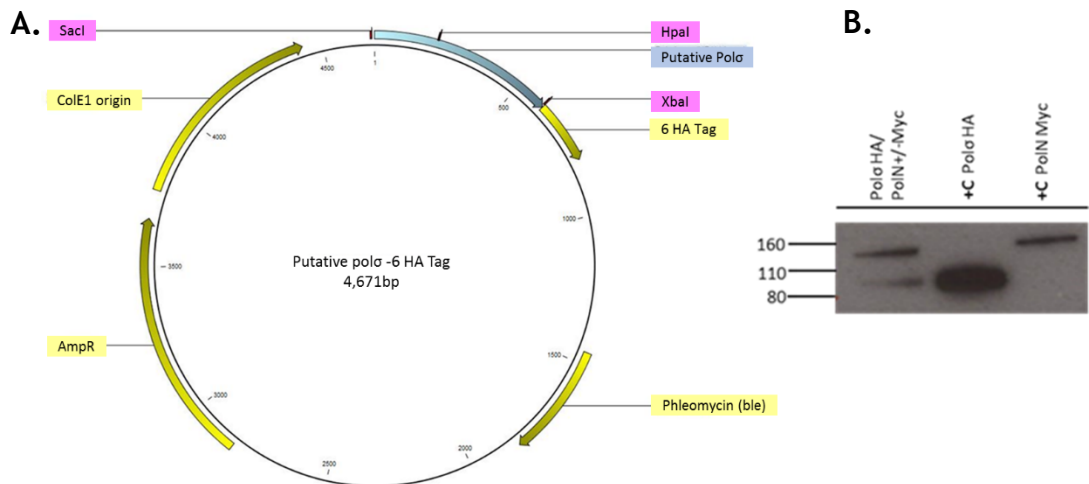
Figure 5-22. Expression of TbPolσ as a 6HA C-terminal fusion variant A. Map of the C-terminal tagging vector containing a 12 Myc tag sequence (represented in yellow) and (in blue) the TbPolσ insert, derived from the C-terminus of the complete ORF. **B.** Western blot of whole cell extracts from a blasticidin and phleomycin resistant individual transformant, Polσ-6HA and PolN-12myc transformants as controls (+C), detected using anti-myc and anti HA antibody. WT, untagged cell line is not present in the gel.

To test interaction between TbPolN and TbPolσ, co-localisation of TbPolN-myc and TbPolσ-HA was first assessed by a double immunofluorescence assay. For this approach, permeabilised cells were incubated in a mixture of two primary antibodies: conjugated Alexa Fluor® 488 mouse anti-myc (1:500 dilution) and mouse anti- HA (1:1,000), detected with Alexa Fluor® 594 α- mouse (1:1,000). Images were captured on a Delta Vision RT deconvolution microscope (Figure 5-23 A) and on a super-resolution Elyra microscope (Figure 5-23B).

Both sets of images suggest some co-localisation of the proteins, presenting as an overlap of staining inside the nucleus (Figure 5-23 A-B). Though

the anti-HA signal for TbPolσ-HA was more widespread in the nucleoplasm, loci of discrete overlap with TbPolN-myc were apparent, and overlay of the signals (Myc and HA) could be seen by the generation of a fluorescence intensity graph, using the super-resolution images (Figure 5-23 B). However, in spite of the overlap, the interaction still needed to be confirmed as the broad distribution of TbPolσ-HA across the nucleus may result in false-positive co-localisatio.
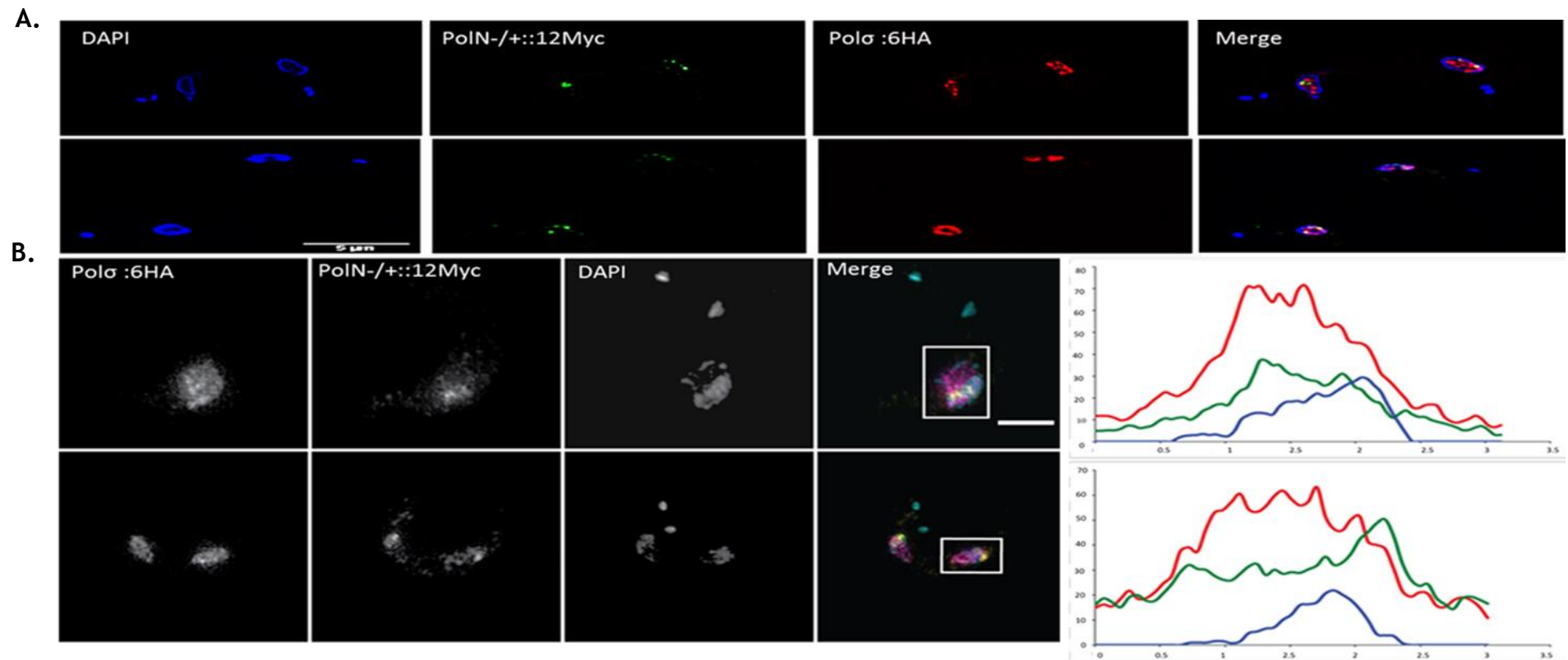
Figure 5-23. Co-localisation of TbPolN and TbPolσ. A. First panels (left to right) shows DAPI staining of the nucleus and kinetoplast, second panels show anti-myc signal, third panels show anti-HA signal, and fourth panels are a merge of the three signals. **B.** First panels show putative Pol σ signal, second panels show PolN-/+::12myc signal, third panels show DAPI staining of the nucleus and kinetoplast and fourth panels are a merge of the three signals. Diagrams show fluorescence intensity for the DAPI (red), anti-HA (green) and anti-myc (blue) signals. The white box represents the area from which the fluorescence intensity was measured in order to elaborate the graph (using image J). Fluorescence intensity is plotted (X-axis) over distance (µm; Y-axis). Scale bar = 5 µm

To more directly test for interaction of TbPolN and TbPolσ, a co-immunoprecipitation (co-IP) was performed. The co-IP methodology is an extension of the IP method, the conditions used for this assay are those described for the IP in section 5.7.1.

The co-immunoprecipitation was assessed by Western blot, using anti-myc and anti-HA to IP proteins from the TbPolN-myc and TbPolσ-HA double tagged cells, as well as from cells expressing only TbPolN-myc or TbPolσ-HA. In the eluate of the double tagged cell line, anti-myc IP revealed a band of ~88kDa recognized by the anti-HA antibody, confirming recovery of Polσ-HA (Figure 5-24 A) . In addition, in the eluate of the double tag cell line after anti-HA IP, a band of ~113 kDa was recognized by the anti-myc antibody, confirming the presence of TbPolN-myc (Figure 5-24 B). To check that the co-IPs were not false positives, controls were performed to test the specificity of the antibodies. While both TbPolN12-myc and TbPolσ-6 HA are successfully detected by anti-myc and anti-HA antibodies after anti-myc and anti-HA IPs, respectively, from cells expressing only TbPolN12-myc or TbPolσ-6 HA, IPs of the same cells with anti-HA or anti-myc, respectively, did not recover the same proteins (Figure 5-24 C,D). Thus, the antibodies uniquely bind to the target epitopes and the coIP in the double tagged cells is because of TbPolN12-myc and TbPolσ-6 HA interaction.
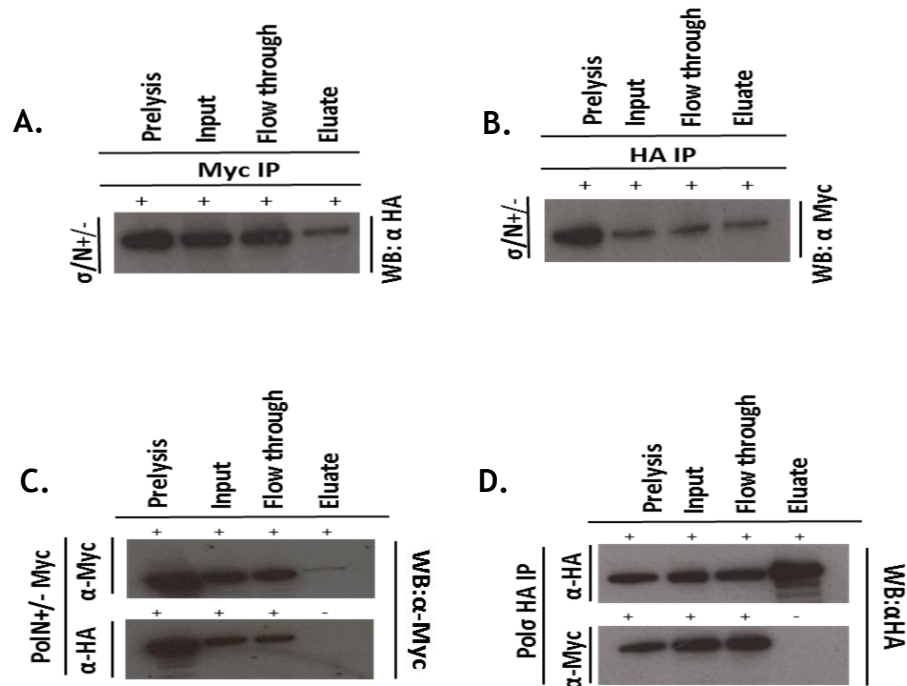
Figure 5-24. TbPolN and TbPolσ co-immunoprecipitation. A. Western blot showing anti-myc IP from cell line expressing TbPolN12-myc and TbPolσ-6 HA , detected using anti-HA antibody. **B.** Western blot showing anti-HA IP from the same double tagged cells, detected using anti-Myc antibody. **C.** Western blot of anti-Myc and anti-HA IPs from a PolN+/-12Myc lysate, detected using anti-Myc antibody. **D.** Western blot of anti-Myc and anti-HA IPs from a TbPolσ-6HA lysate, detected using anti-HA antibody. In each blot the prelysis, input, flow through and eluate samples are shown.

5.7.3 Possible interaction partners of Polymerase theta (helicase domain)

In higher eukaryotes a possible interaction between the helicase domain-containing protein HelQ and the polymerase domain protein PolN has been suggested (Bebenek and Kunkel, 2004). For this reason, it was decided to ask if the two putative *T. brucei* homologues interact, in particular because RNAi against TbHelQ was ineffective. Though the results obtained from the TbPolN-myc IP and MS analysis did not reveal TbHelQ as a possible interaction partner, it is possible it was not efficiently recovered. Therefore, a reverse IP was performed, this time using TbHelQ-HA as the target protein.

For the analysis, TbHelQ was tagged using the 6 HA pNAT vector (Alsford and Horn, 2008) containing 1160 bp of the C-terminal end of the TbHelQ ORF

(Figure 5-25 A). The insert was amplified using the following primers: Fw-gcatgagctcctggagtttgtcgcgattgg (SacI site) and Rv-gcattctagagtaggttgaagattggaggg (XbaI site). Plasmid and fragment were digested with SacI and XbaI, followed by a ligation process. The vector was linearised with XhoI and transformed into WT Lister 427 BSF (section 2.3.7, 2.3.8). The cloning strategy is described in detail in section 2.5.1. To verify if TbHelQ was expressed as a fusion with the 6 HA tag, a Western blot was performed, where a band of approximately 121.6 kDa (115 kDa TbHelQ, 6.6 kDa HA tag) was observed (Figure 5-25 B).
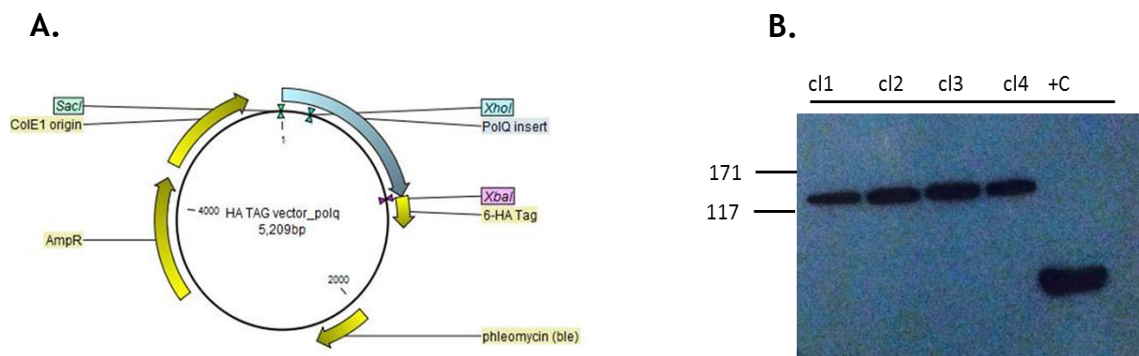
Figure 5-25. Expression of TbPolQ as a 6HA C-terminal fusion variant. A. Map of the C-terminal tagging vector containing a 6 HA tag sequence (represented in yellow) and (in blue) the TbHelQ insert, derived from the C-terminus of the complete ORF. **B.** Western blot of whole cell extracts from four phleomycin resistant transformants (cl1-4) and from a cell line expressing Polσ-6HA as a control (+C). The blot was probed with anti-HA antibody. WT untagged cell line was not loaded in the gel.

The IP conditions used for this assay are the same as those described for the TbPolN-myc IP in section 5.7.1, but using anti-HA antiserum. The SYPRO®Ruby gel did not show any specific bands in TbHelQ-HA IP in relation to the control WT IP (Figure 5-26 A). However, IP of the HA-tagged protein was confirmed by Western blot, detecting the presence of TbHelQ-HA uniquely in the TbHelQ-HA IP (Figure 5-26 B). The eluates from both the WT and TbHelQ IPs were analysed by mass spectrometry (Glasgow Polyomics Facility).
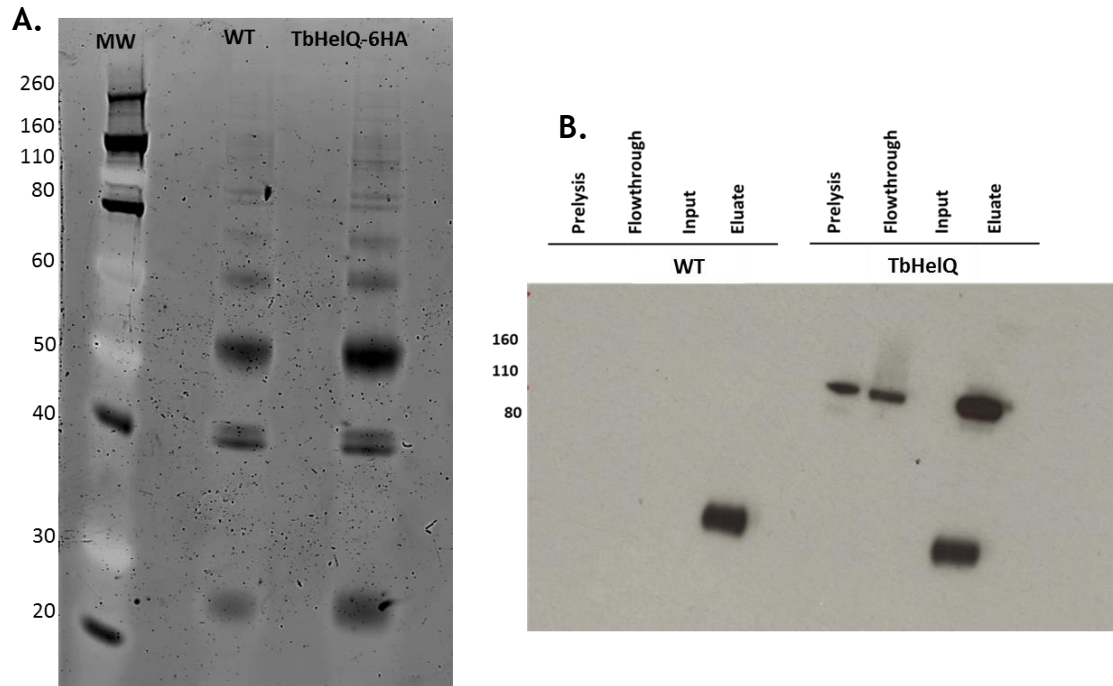
Figure 5-26. Validation of TbHelQ immunoprecipitation.A. Sypro ruby stained gel of anti-myc immunoprecipitated proteins from WT427 (un-tagged cell line) and TbHelQ-6HA lysates. **B.** Western blot on all fractions of the IP from TbHelQ-HA and WT. Fractions from left to right: prelysis, flow-through, input and eluate from WT and TbHelQ, showing the absence of bands in the untagged cell line. The extra bands represent the heavy chain of the antibody.

As for TbPolN-myc IP, the TbHelQ-HA IP mass spectrometry results were analysed against WT (which identified 143 proteins), excluding common proteins, leaving a total of 49 possible interaction partners (Table 5-3). None of these proteins corresponded to TbPolN. After the elimination of possible contaminants and proteins with insufficient information, 4 possible TbHelQ interactors were highlighted as potentially worthy of further analysis (Table 5-4). Three of these proteins, Rad50 (Tb11.01.0340), Rad51 (Tb09.211.1210), and BRCA2 (Tb927.1.640), are known to play an important role during HR in the parasite. BRCA2 is of particular interest, because it is known to be essential for the regulation of Rad51 in *T. brucei* (Trenaman *et al.*, 2013) and previous work in which IP was used against procyclic form *T. brucei* cells expressing BRCA2-myc recovered TbHelQ (Prorocic and McCulloch, unpublished). Though Rad50 and Rad51, which also act during the repair of DSBs (Passos-Silva *et al.*, 2010), were not recovered in the BRCA2-myc IP, selected bands, rather than a whole eluate, were analyzed by MS in that approach. One further repair protein, *T. brucei*

PMS1 (Tb09.211.4840), was also recovered by TbHelQ-HA IP and is known to have an important role in mismatch repair (Passos-Silva *et al.*, 2010).

Gene ID	Protein	Score
Tb927.1.710	PGKB phosphoglycerate kinase	356
Tb09.160.2550	ribosomal protein S7, putative	322
Tb09.160.0700	60S ribosomal protein L35, putative	181
Tb927.4.1860	ribosomal protein S19, putative	83
Tb10.70.4800	ribosomal protein S25, putative	83
Tb10.61.2090	60S ribosomal protein L17, putative	80
Tb927.7.2820	histone H2A, putative	79
Tb09.211.3270	60S ribosomal subunit protein L31, putative	78
Tb11.01.7535	60S ribosomal protein L27, putative	77
Tb11.02.0740	60S ribosomal protein	75
Tb11.01.0355	ribosomal protein S26, putative	73
Tb09.211.0865	60S ribosomal protein L37, putative	65
Tb927.8.1330	60S ribosomal protein L7a, putative	56
Tb09.v4.0067	retrotransposon hot spot protein, pseudogene	34
Tb927.4.2180	60S ribosomal protein L35A, putative	33
Tb10.70.4700	TSR1IP splicing factor PTSR1 interacting protein	41
Tb927.5.940	NADH-dependent fumarate reductase	31
Tb11.02.1630	hypothetical protein	31
Tb10.70.4680	hypothetical protein, conserved	30
Tb927.6.150	retrotransposon hot spot protein (RHS, pseudogene), putative	30
Tb927.7.3050	hypothetical protein, conserved	29
Tb09.244.2760	cytosolic coat protein, putative	28
Tb11.13.0006	variant surface glycoprotein (VSG, pseudogene), putative	27
Tb927.4.3160	dihydroxyacetone phosphate acyltransferase, putative	26
Tb11.14.0008	variant surface glycoprotein (VSG, atypical), putative	25
Tb09.160.5400	expression site-associated gene 9 (ESAG9) protein, putative	25
Tb09.160.0010	variant surface glycoprotein (VSG, pseudogene), putative	24
Tb927.3.3620	hypothetical protein, conserved	24
Tb10.v4.0231	variant surface glycoprotein (VSG, pseudogene), putative	23
Tb09.v4.0057	variant surface glycoprotein (VSG, pseudogene), putative	23
Tb10.v4.0004	variant surface glycoprotein (VSG, pseudogene), putative	23
Tb09.160.1290	hypothetical protein, conserved	23
Tb927.5.2140	regulator of nonsense transcripts 1, putative	22
Tb927.4.1730	hypothetical protein, conserved	21
Tb05.5K5.530	variant surface glycoprotein (VSG), putative	19
Tb09.v4.0114	variant surface glycoprotein (VSG, atypical), putative	18
Tb11.52.0008	hypothetical protein, conserved	33
Tb927.3.1850	hypothetical protein, conserved	33
Tb927.8.1840	hypothetical protein, conserved	29
Tb927.7.3160	dynein heavy chain, cytosolic, putative	28
Tb11.01.4210	hypothetical protein, conserved	18
Tb927.6.4070	hypothetical protein, conserved	18
Tb927.7.1200	hypothetical protein, conserved	18
Tb11.02.1340	AMP deaminase, putative	18
Tb11.01.2310	hypothetical protein, conserved	17
Tb09.211.1210	RAD51/dmc1 protein, putative	48
Tb11.01.0340	RAD50 DNA repair-like protein	16
Tb09.211.4840	mismatch repair protein PMS1, putative	15
Tb927.1.640	hypothetical protein, conserved (BRCA2)	13

Table 5-3.Recovered proteins from the TbHelQ-6HA IP after mass spectrometry analysis. Proteins shown were only present in TbHelQ anti-HA IP; hits also identified in IP from WT cells were excluded. Interesting 'hits' are labelled in red. Samples were analysed using MASCOT software.

Gene ID	Annotation	Predicted domain	Score
Tb09.211.1210	RAD51/dmc1 protein, putative	NTP binding domain, Rad51	48
Tb11.01.0340	RAD50 DNA repair-like protein	ATP-binding domain, exonuclease domain, AAA domain	16
Tb09.211.4840	mismatch repair protein PMS1, putative	MutL dimerisation domain	15
Tb927.1.640	hypothetical protein, conserved (BRCA2)	BRCA2, oligonucleotide/oligosaccharide-binding, domain 1	13

Table 5-4.Potential TbHelQ interaction partners identified by Mass Spectroscopy and homology analyses. Proteins shown were only present in IP from TbPHelQ-HA. Proteins were analysed using MASCOT. Proteins sequence for each 'hit' was examined by BLASTp for predicted domains.

5.7.4 A possible role for HelQ during Homologous Recombination

BRCA2 was chosen for further analysis to try and elucidate a possible role for TbHelQ. In order to assess a possible interaction, a double tagged BSF cell line expressing TbHelQ-HA and BRCA2-Myc was generated. The generation of the double tagged cell line was performed by using a BRAC2-12 Myc cell line (kindly provided by A. Trenaman) as the parental cell line, into which the TbHelQ-6HA pNAT Phl vector was transformed (section 2.3.9). To verify if both tagged proteins were expressed, a Western blot was performed and probed with anti-myc and anti-HA antisera, revealing bands of ~120 kDa (115 kDa TbHelQ, 6.6 kDa HA tag) and ~200 kDa (181.28 kDa BRCA2, 14.4 kDa Myc) (Figure 5-27).

For immunofluorescence, permeabilised cells were incubated in a mixture of two primary antibodies, conjugated Alexa Fluor® 488 mouse anti-Myc (1:500 dilution) and mouse anti- HA (1:1000), which was detected with Alexa Fluor® 594 α- mouse (1:1000). The images were captured on a Delta Vision RT deconvolution microscope. It was possible to observe a very substantial overlap of the anti-HA and anti-myc signals, suggesting TbHelQ-HA and BRCA2-myc co-localise in the same regions of the nucleus (Figure 5-27). Indeed, the pattern of BRCA2-myc localisation is highly similar to previous studies, with the protein present in multiple puncta across the nucleus in the absence of damage (Trenaman *et al.*, 2013).
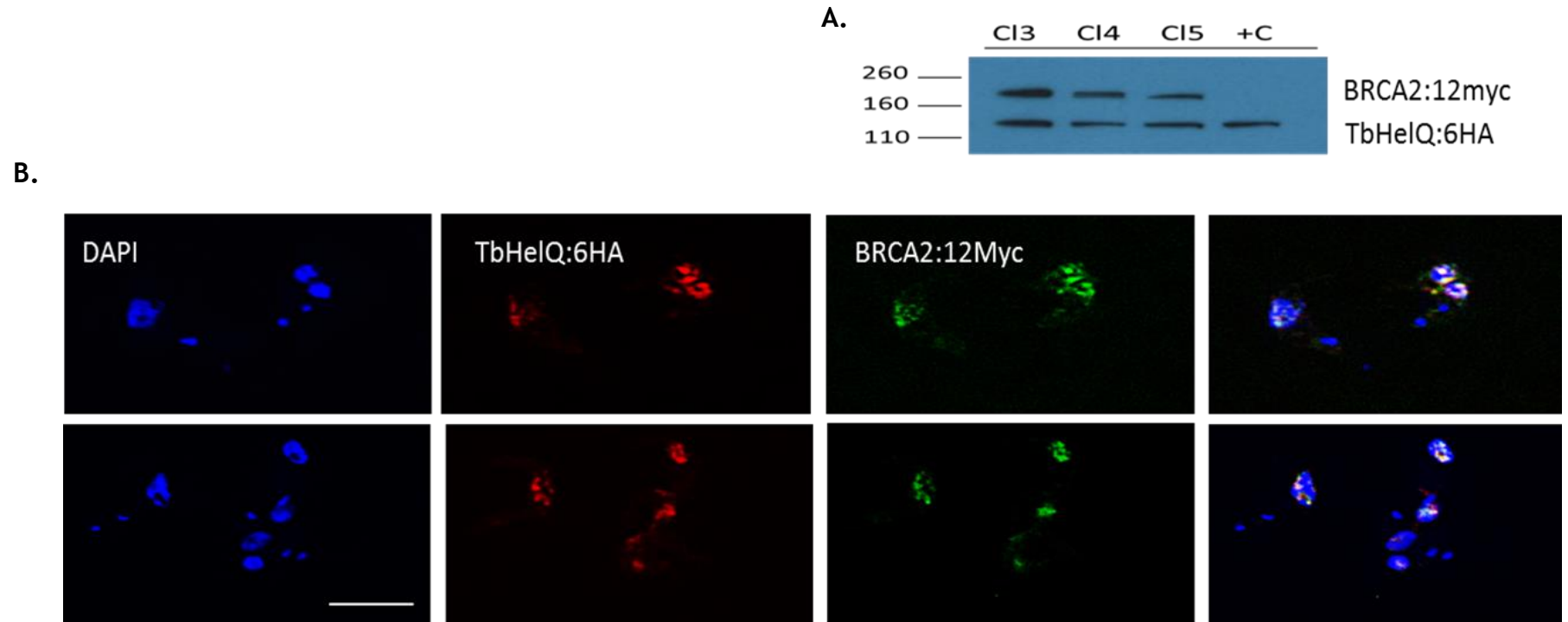
Figure 5-27. TbHelQ and BRCA2 nuclear co-localisation. A. Western blot of whole cell extracts from 3 blasticidin and phleomycin resistant transformants (cl3, 4, 5), and from a cell line expressing only TbHelQ-6HA as a control (+C), detected using anti-myc and anti-HA antibody. **B.** First panel show DAPI staining of the nucleus and kinetoplast, second panel show anti -HA signal, third panel show anti-myc signal, and fourth panel is a merge of the three signals. Images captured on a Delta Vision RT deconvolution microscope. Scale bar 5μm.

In order to ensure the putative co-localisation of TbHelQ and BRCA2 did not result from antibody cross-reaction in the IFA, the TbHelQ 6HA pNAT Phl vector was transformed into a WT Lister 427 cell line (Section 5.7.3). For the immunofluorescence assay, permeabilised cells were incubated in a conjugated mouse anti-HA (1:500 dilution) antibody and images were taken on a Delta Vision RT deconvolution microscope. The anti-HA signal was detected along the nucleus (Figure 5-28), resembling the localisation observed in the co-localisation assay (Figure 5-27).
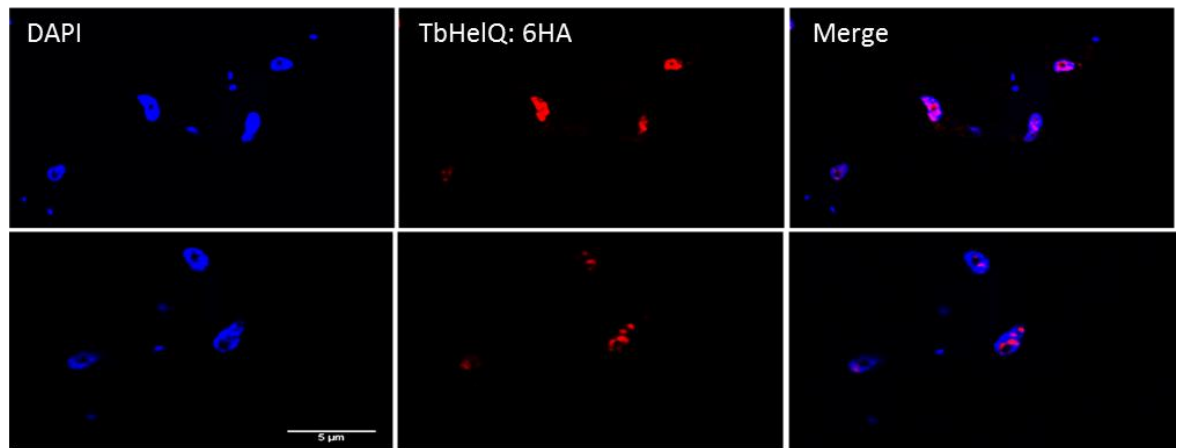
Figure 5-28. TbHelQ nuclear localisation. First panel shows DAPI staining of the nucleus and kinetoplast, second panel shows TbHelQ-6HA signal and third panel is a merge of the two signals. Images captured on a Delta Vision RT deconvolution microscope. Scale bar 5µm.

5.8 Discussion

This section describes the activity of the putative TLS Pol, Tb Pol Nu (PolN) in bloodstream form *T. brucei* cells. Epitope tagging demonstrates that TbPolN localises in discrete sites at the periphery of the nucleus in the absence of DNA damage, with a more widespread, but non-uniform localisation after MMS damage. Morphological defects arise ~48 hours post RNAi induction, with the appearance of multiple flagellar pockets and aberrant nuclei. EdU labelling and γH2A analysis after TbPolN knockdown reveal a decrease in proliferating cells, which accumulate nuclear DNA damage. The depletion of TbPolN is also associated with aberrant chromosome segregation. Finally, we show that TbPolN interacts with a nuclear putative non-canonical PolyA polymerase (putative Polσ).

In addition to the above data on TbPolN, IP and colocalisation analysis indicate that TbHelQ provides a quite distinct function in *T. brucei* to TbPolN. TbHelQ appears not to interact with TbPolN, but to interact with TbBRCA2, and perhaps further repair factors, suggesting a role in HR.

5.8.1 Possible roles of Polymerase theta (helicase domain) in *T. brucei*

Helicases are known for their ability to catalyse the separation of double-stranded nucleic acids in an ATP dependent manner (Byrd and Raney, 2012). The resulting substrate - single-stranded nucleic acids - play important roles during cellular reactions (Byrd and Raney, 2012). The helicase members of the Sf1 and Sf2 superfamilies are known to have important roles in DNA and RNA metabolism (Fairman-Williams, Guenther and Jankowsky, 2010; Byrd and Raney, 2012). The members of the SF2 superfamily (RecQ-like, RecG-like, DEAH/RHA box and DEAD-box) are active during replication, transcription, DNA repair and chromatin rearrangement (Byrd and Raney, 2012). Alterations of the SF2 helicases are associated with mental retardation, immunodeficiency, premature aging and predisposition to cancer in humans (Byrd and Raney, 2012).

As it was shown in chapter 3, TbHelQ belongs to the SF2 superfamily, suggesting a role in DNA metabolism, with the possibility of being involved in

DNA repair. TbHelQ-HA immunoprecipitation revealed that BRCA2, and perhaps RAD51, are interaction partners of TbHelQ (section 5.7.3). These two molecules are known to be involved in repair of double strand breaks (DSB) in eukaryotes (Jasin and Rothstein, 2013). An important question, therefore, is if and how this helicase might act in HR.

Several members of the SF2 superfamily have been linked with the repair of DSBs. For instance, mutation in the BLM helicase, a member of the RecQ family, has been associated with Bloom's disorder. This disorder is responsible for growth delay, facial sun sensitivity, immunodeficiency, fertility problems and cancer (Wu *et al.*, 2001). It is suggested that this is provoked by an inefficient HR pathway (Wu *et al.*, 2001). The interaction was tested by immunofluorescence, which confirmed co-localisation of BLM and Rad51 in response to ionizing radiation (resulting in interstrand cross-links (ICL)) (Wu *et al.*, 2001). It has been proposed that BLM activity is important for impeding the crossover of the DNA strands, facilitating the recruitment of Rad51 (Wu *et al.*, 2001). *T. brucei* RecQ2, a putative BLM homologue, shows a role during DNA repair and VSG switching. The loss of TbRecQ2 in the parasite impairs the survival of the cells in the presence of DSB (Devlin *et al.*, 2016). In addition, Co-localisation of TbRecQ and TbRad51 was detected after inducing damage with phleomycin (generates DSBs) and loss of TbRecQ results in an increase in VSG switching, which is a consequence of altered recombination pathways (Devlin *et al.*, 2016).

In contrast to a clear role for RecQ helicases in Rad51-mediated HR, the human HelQ helicase has only so far been related to ICL repair in cancer, since HelQ heterozygous cells show increased sensitivity to ICL inducing agents (Takata *et al.*, 2013). In addition, immunoprecipitation of HelQ revealed interaction with ATR and Rad51 paralogs (Rad51B, Rad51C and Rad51D), not Rad51 or BRCA2 (Takata *et al.*, 2013). CL lesions are highly lethal for the cell, impeding the pass of the replication and transcription machinery by blocking DNA strand separation (Takata *et al.*, 2013). Tackling these lesions involves different pathways such as NER, TLS and HR. These pathways work together in order to excise, bypass and homologously pair the resulting strand (Zhang *et al.*, 2009; Moldovan *et al.*, 2010). Interestingly, several genes that are known to be

involved in CL repair by HR are present in the Fanconi anemia (FA) pathway (Moldovan and D'Andrea, 2009; Moldovan *et al.*, 2010; Michl, Zimmer and Tarsounas, 2016). FA is a recessive disorder, which is characterized by the inability to repair CL lesions, provoking bone marrow failure, genomic instability and predisposition to cancer (Moldovan and D'Andrea, 2009). In humans, 13 genes have been shown to be involved in this pathway, and are conserved among vertebrates (Zhang *et al.*, 2009). In contrast to humans, trypanosomes have only been described as having one FA gene conserved; this is FANCDI, also known as BRCA2 (Zhang *et al.*, 2009). In the parasite, BRCA2 is involved in HR, which is critical for the repair of DSBs (Hartley and McCulloch, 2008; Trenaman *et al.*, 2013). BRCA2 interacts with Rad51 through the BRC repeats, and an expanded number of BRC repeats in TbBRCA2 appears to regulate RAD51 nuclear redistribution after damage (Trenaman *et al.*, 2013).

Studies have suggested that the signaling of the stress checkpoint, involving ATR, is necessary for the activation of the FA pathway (Collis *et al.*, 2008; Takata *et al.*, 2013). The ATR kinase responds to a variety of lesions, including DSBs and SSBs (Maréchal and Zou, 2013; Takata *et al.*, 2013). In *C. elegans* Hel-308, the likely homologue of HelQ, has recently been suggested to be involved in the FA pathway. Analysis has shown that the deletion of Hel-308 followed by the mutation of Brc-1 (BRCA-1 homologue) is lethal for the worm after crosslinking treatment (Muzzini *et al.*, 2008). Nontheless, a specific role of the helicase during the FA pathway is still uncertain (Muzzini *et al.*, 2008). Together, these data suggest a possible interaction between HelQ and the checkpoint machinery, but to date a direct link with Rad51 and BRCA2 during HR, as potentially observed in *T. brucei,* has not been seen. Whether TbHelQ works with TbATR to activate checkpoint signaling and recruitment of the repair machinery is also unknown.

Taken together, the available data from other eukaryotes suggest TbHelQ interaction and co-localisation with BRCA2 is either novel, or so far undetected. The pronounced overlap of signals for the two proteins was of particular interest, suggesting almost exactly matching distributions of the proteins across the nucleus (Section 5.7.4). Though BRCA2 is known to interact with Rad51, a key molecule in the HR pathway in the parasite, the co-localisation of RAD51 and

BRCA2 is not nearly as extensive (Trenaman *et al.*, 2013). Thus, though the potential interaction of TbHelQ and TbRad51 revealed by IP is of interest, it will be necessary to test this further, since the data to date suggest a more pronounced co-ordination with BRCA2, for reasons that are unclear. Whether this relates to possible interaction with Rad50 is also unclear. In eukaryotes, Rad50 is part of the MRN complex (Mre11/Rad50/Nbs1), which is essential for the initial recognition of a DSB (Lamarche, Orazio and Weitzman, 2010), subsequently activating the HR repair pathway, including Rad51. In *T. brucei*, all MRN homologous proteins have been found (Passos-Silva *et al.*, 2010), but to date only MRE11 has been analysed (Robinson *et al.*, 2002; Tan, Leal and Cross, 2002). Intriguingly, loss of MRE11, like loss of BRCA2, leads to attrition of the VSG archive (Robinson *et al.*, 2002; Hartley and McCulloch, 2008; Trenaman *et al.*, 2013); it would be valuable to test if TbHelQ acted in the same way.

5.8.2 Possible role of *T. brucei* Polymerase Nu

Despite work in other eukaryotes suggesting a role for PolN in HR, unlike TbHelQ (Moldovan *et al.*, 2010; Gowda, Moldovan and Spratt, 2015), immunoprecipitation of TbPolN-12myc did not reveal proteins involved in the HR pathway. Instead, four proteins associated with chromosome integrity, including three hypothetical proteins (Tb927.5.3280, Tb927.2.3990, Tb11.01.3060) that contain putative conserved domains belonging to structural maintenance of chromosomes proteins (SMC) (Harvey, Krien and O'Connell, 2002), were highlighted. Interaction with a fourth protein that provides similar roles was validated by targeted coIP. The fourth potential interaction partner is a putative homologue of Pol σ. In yeast Trf4/Trf5, also known as Pol σ, is encoded by two redundant genes (Trf4 or Trf5), and is known to have Poly(A) activity (Edwards *et al.*, 2003b; Haracska *et al.*, 2005). In this organism, Polσ is involved in chromosome condensation and sister chromatid cohesion (Haracska *et al.*, 2005), activities similar to SMC proteins (Harvey, Krien and O'Connell, 2002). Indeed, studies have suggested that Pol σ directly interacts with SMC1 and SMC2 in order to accomplish the cohesion of sister chromatids (Haracska *et al.*, 2005).

Recent studies in *S. cerevisiae* have also shown a possible interaction of Pol σ and Polε. Polε is a high fidelity polymerase, involved in replicative strand

synthesis. However, it has been suggested that this polymerase may also have an alternative role, apart from the polymerase activity (Edwards *et al.*, 2003b). A co-immunoprecipitation of Trf4-6His and Pol2 (catalytic subunit of Polε)-Flag cells was performed, confirming the interaction between these two polymerases (Edwards *et al.*, 2003b). This was further studied by mutating the Polε binding domain of Polσ (trf4), showing deficient sister chromatid cohesion in the absences of the Polσ-Pol2 interaction. Hence, Polε may also have a role in chromatid cohesion (Edwards *et al.*, 2003b). Although TbPolσ has not been implicated in such a role, and neither has PolN in any eukaryote, their co-immunoprecipitation may reveal a role for both in similar strategies of chromosome cohesion.

In yeast and metazoans, SSC1 is associated with SMC1 and SMC3, forming the chromosome cohesin complex, whose role is to maintain the chromosomes together through S phase until anaphase (Gluenz *et al.*, 2008). The cleavage of SSC1 allows the separation of sister chromatids during anaphase, preparing the cell for division (Gluenz *et al.*, 2008).

SSC1 (Tb927.7.6900) has been studied in *T. brucei* in order to understand the cohesion mechanism in the parasite. Mutants were generated by depleting SSC1 by RNAi. The depletion of the protein in BSF cells lead to a decrease of proliferating cells, a decrease of 1N1K cells and an increase of 1N2K, 24 hours post induction (Gluenz *et al.*, 2008). Intriguingly, a similar effect was observed after TbPolN depletion. Moreover, depletion of SSC1 also results in accumulation of aberrant cells, which consist of an irregular nucleus, multiple kinetoplasts and multiple flagella, a phenotype more obvious 48 hours post induction (Gluenz *et al.*, 2008). Interestingly, the cells appear to recover from the phenotype after three days, though through reappearance of the protein (Gluenz *et al.*, 2008). In the case of TbPolN, depletion of the protein also resulted in an accumulation of aberrant cells, which was also a transient phenotype. Unlike SSC1, however, the TbPolN depletion was maintained through the 72 hours after RNAi activation. This either suggests that the parasites have the ability to compensate the loss of TbPolN or part of the population escapes the RNAi mechanism, since we have not yet detected re-expression of the putative TLS pol.

Loss of SSC1 is responsible for aberrant chromosome distribution, impeding the separation of the sister chromatids and generating an arrest in anaphase (Gluenz *et al.*, 2008). Depletion of TbPolN also results in an irregular chromosome distribution, as suggested by telo-FISH, which indicated an abnormal distribution of DNA in cells going through metaphase and anaphase. It would be valuable to investigate if the correct separation of sister chromatids is impaired after TbPolN loss, as this would more closely link the two sets of data.

Studies in yeast have linked SSC1 with the release of CDC14 phosphatase from the nucleus, a protein necessary for mitotic exit. For this reason, absence of SSC1 affects the culmination of mitosis, impeding cell division (Gluenz *et al.*, 2008). This may explain the presence of an enlarged aberrant nucleus after the depletion of TbPolN. All these data raise the possibility that TbPolN is part of the cohesin complex, and its absence in this context would explain the effect of TbPolN loss on mitosis in *T. brucei*, resulting in the inability of the parasite to correctly conclude cytokinesis (Hammarton *et al.*, 2003).

Interestingly, studies in yeast have shown that the cohesin complex is not only involved in sister chromatid cohesion, but may also affect the repair of DSB during S phase (Sjogren and Nasmyth, 2001). It has been proposed that this complex is essential during post-replication repair by maintaining chromatids close together. In this way, the complex facilitates homologous pairing and preventing chromosome fragmentation (Sjogren & Nasmyth 2001). This hypothesis was tested with SSC1 deficient mutants, where the loss of the protein results in mutants incapable of repairing γ irradiation damage (Sjogren and Nasmyth, 2001). This may explain the data obtained after the depletion of TbPolN, where the cells show sensitivity to UV and MMS exposure, accumulation of damage, decrease of EdU incorporation and redistribution of the protein in the presence of damage. This suggests that in the presence of DNA damage, TbPolN is redistributed in order to facilitate damage repair by maintaining chromosome integrity. The cohesion complex has also been associated with VSG switching in *T. brucei*. The depletion of SSC1 by RNAi was shown to lead to an increase in the expression levels of inactive VSG genes, which was also observed after the depletion of TbPolN. It was suggested that alteration of the cohesin

complex may alter the monoallelic VSG expression mechanism (Landeira and Navarro, 2007).

These data propose a new role for TbPolN in the maintenance of chromosome integrity and DNA repair, where TbPolN interacts with SMC-related proteins and a putative Polσ. As it was shown in yeast, the complex may be involved in the repair of DSB and maintenance of chromosomal integrity by promoting sister chromatid cohesion. How exactly the coordination of such interactions compares between *T. brucei* and yeast is, however, currently unknown.

6 Conclusion

Cells are constantly exposed to DNA damage, which can arise from sources such as UV light, genotoxic agents and reactive oxygen species (ROS), to name just a few (Giglia-Mari, Zotter and Vermeulen, 2011). In order to maintain genome integrity, cells have developed diverse repair mechanisms that are capable of tackling the resulting lesions (Iyama and Wilson, 2013; Gao *et al.*, 2017). Although these mechanisms are highly efficient, they are not always able to completely resolve the damage. In order to avoid collapse of the DNA replication fork when a DNA lesion is encountered, the translesion synthesis pathway (TLS) has the ability to bypass through damage, ensuring complete replication and the survival of the cell (Goodman and Woodgate, 2013). Translesion polymerases play an important role in this error tolerance mechanism and so eukaryotes possess several TLS polymerases (pols), such as PolZ, PolN, PolQ, Polι, Polη, PolK and Rev1 (Goodman, 2002).

TLS is known as a low fidelity pathway due to the absence of proofreading activity by the TLS pols involved in this process, increasing the probability of the insertion of mutations (Sale, 2013). Despite the fact that TLS is prone to insertion of mutations, it has been conserved throughout evolution, suggesting a critical role for the process in the maintenance of eukaryotic genome integrity (Rosenberg, 2001; Friedberg, Wagner and Radman, 2002). For example, the loss of PolZ results in embryonic lethality in mice, suggesting that PolZ cannot be replaced by any other polymerase during early development (Esposito *et al.*, 2000). TLS pols are not only involved in the error tolerance repair pathway. It has also been demonstrated that they have an active role in diverse repair mechanisms such as homologous (HR) recombination, base excision repair (BER), nucleotide excision repair (NER) and mismatch repair (MMR) (Goodman, 2002; Lange, Takata and Wood, 2011). For instance, in humans, PolN has been associated with crosslink repair by HR (Moldovan *et al.*, 2010). Meanwhile, PolZ has been linked with TLS in *S. cerevisiae* and in HR in human cells (Gibbs *et al.*, 2005; Lange, Wittschieben and Wood, 2012; Sharma, Helchowski and Canman, 2013a).

T. brucei encodes ~15 TLS pols, only two of which have been analysed at all. A single recent study demonstrated that two related proteins, termed PPL1 and PPL2, have TLS activity and that PPL2 is essential for the survival of the cell. PPL2 has a critical role in cell cycle progression, where the protein is involved in the transition from late S-phase into mitosis, since depletion of the protein was found to result in arrest in the G2 phase of the cell cycle (Rudd *et al.*, 2013). The unconventional structure of PPL1 and PPL2 has meant that they are frequently overlooked as TLS pols, and instead are classified as members of the archaeo-eukaryotic primase superfamily, though in common with other factors in this class they can synthesise DNA (Iyer *et al.*, 2005).

At the start of this work, no other functional data was available for TLS pols in *T. brucei*. In order to have a better understanding of the function of TLS pols in *T. brucei*, TbPolN, TbPolZ's catalytic subunit (TbRev3) and a putative TbPolQ helicase domain protein (TbHelQ) were studied. The first step was the analysis of the protein sequences, showing that TbRev3 and TbPolN are highly conserved when compared to human and *A. thaliana* homologues. Each harbours motifs which characterise them as members of the B and A family of polymerases, respectively. On the other hand, TbPolQ (HelQ) resembles the structure of helicase HelQ, rather than the translesion polymerase PolQ: rather than encoding both a polymerase and helicase domain, the *T. brucei* protein only harbours a helicase domain. Thus, the protein is unlikely to be a TLS pol. Despite this, TbHelQ maintains the conserved motifs corresponding to the SF2 helicase superfamily, which are also found in the helicase domain of PolQ in other eukaryotes (Fairman-Williams, Guenther and Jankowsky, 2010). These sequence comparisons indicate a separation of activities found in PolQ into two proteins in *T. brucei*, which led to the question of whether the function of *T. brucei* TLS pols is conserved.

In order to answer the above question, RNAi analysis was performed for each gene. The loss of TbPolN appeared to slow growth after ~24 hours, which was associated with observable phenotypic changes in which the cells lose their regular structure and accumulate aberrant DNA content, with these phenotypic effects being most pronounced at 48 hours post RNAi induction. The timing of the growth effect seen after TbPolN RNAi also coincided with increased

sensitivity of the cells after exposure to MMS and UV light. EdU labelling and γH2A analysis after TbPolN knockdown revealed a decrease in proliferating cells, which accumulate nuclear DNA damage. In addition, irregular chromosome segregation was detected after the loss of the protein. Localisation of TbPolN-myc revealed a pronounced and localised signal in the nucleus periphery, with some redistribution after the generation of damage. To understand these observations further an immunoprecipitation (IP) assay was performed, which revealed putative interaction with a putative Polσ and several further hypothetical proteins that harbour structural maintenance of chromosome (SMC) domain homology. SMC proteins are involved in chromosome segregation, forming part of the cohesin complex which holds sister chromatids together until the cell cycle transitions to anaphase (Harvey, Krien and O'Connell, 2002; Haracska *et al.*, 2005). Interestingly, the TbPolN cell cycle phenotype after RNAi resembles the phenotypes obtained after the depletion of SCC1 by RNAi, a molecule that forms part of the cohesin complex (Gluenz *et al.*, 2008). However, this is not the only role which has been conferred to the cohesion complex, as it has also been suggested that the complex is involved in the repair of DSBs, also by maintaining the sister chromatids close together, permitting homologous pairing (Sjogren and Nasmyth, 2001). All the data together may suggest that TbPolN interacts with the cohesin-like complex and be involved in chromosome segregation and promoting HR. However, only interaction with Polσ was confirmed, and the remaining factors are not canonical cohesin factors, meaning further work is needed to explore this hypothesis and to understand the roles played by each factor. In addition, what feature of the nucleus or genome is bound by TbPolN in undamaged cells remains unclear, though this may provide important insight. Finally, at this time it remains somewhat speculative that TbPolN is a TLS Pol, since no enzymatic activity of the protein was tested, though the syntenic gene in *L. infantum* encodes a protein that does display TLS Pol activity (Fernández-Orgiler *et al.*, 2016).

In higher eukaryotes an interaction between PolN and HelQ has been proposed (Bebenek and Kunkel, 2004). The results obtained from the IPs of TbPolN and TbHelQ, suggest that there is no such interaction between these proteins in the parasite. Instead, TbHelQ was confirmed to interact and colocalise with BRCA2, which is involved in HR. Further, as yet unconfirmed,

proteins were recovered from the TbHelQ IP that are also involved in HR, including Rad51 and Rad50. These data suggest a role for TbHelQ in the HR pathway, but this is complicated by the differing subnuclear localisations of TbBRCA2 and TbRAD51 (Trenaman *et al.*, 2013), with TbHelQ more closely resembling the former. Thus, it will be important to evaluate further if TbHelQ acts in HR, and wider roles in the DNA damage response might be considered. In humans HelQ appears to activate the checkpoint via ATR, allowing recruitment of the repair machinery (Takata *et al.*, 2013). Further studies to test for an interaction between TbHelQ and TbATR in *T. brucei* may therefore be valuable.

A damage sensitivity effect was observed after the growth of TbRev3 RNAi and TbRev3 KO cells in the presence of MMS and UV radiation, suggesting a role of the protein in DNA damage repair. Interestingly, the growth effect after UV exposure was not as severe as expected, considering PolZ has been characterised by its ability to repair UV damage (Zhao & Washington 2017b; Gueranger et al. 2008). The data might therefore suggest that UV damage is tackled by another repair mechanism that does not involve TbRev3, and that TbRev3 may mainly act in another pathway. TbRev3-12myc immunolocalisation reveals both nuclear and mitochondrial signals, which became stronger after the generation of damage. In mammals and yeast, the PolZ catalytic subunit has also been detected in the mitochondrion, suggesting a role in the maintenance of this organelle (Kaniak-Golik and Skoneczna, 2015; Singh *et al.*, 2015). TbRev3 mitochondrial localisation was supported by IP, where mitochondrial proteins were recovered as potential interaction partners. All these findings, taken together, suggest a possible role for TbPolZ in the maintenance of both the mitochondrion and nucleus in *T. brucei*. In both cases, however, the precise roles played by the factor need to be further evaluated.

Taken as a whole, the work in this thesis reveals widespread and variant functions for TbPolN, TbRev3 and TbHelQ in *T. brucei* genome biology. It might be anticipated that the functions provided by the other putative *T. brucei* TLS pols, TbPolK and TbPolH, which were not examined here, will reveal yet further activities.

7 Reference

Acharya, N., Klassen, R., Johnson, R. E., Prakash, L. and Prakash, S. (2011) 'PCNA binding domains in all three subunits of yeast DNA polymerase modulate its function in DNA replication', *Proceedings of the National Academy of Sciences*, 108(44), pp. 17927–17932.

Acosta-Serrano, A., Vassella, E., Liniger, M., Kunz Renggli, C., Brun, R., Roditi, I. and Englund, P. T. (2001) 'The surface coat of procyclic Trypanosoma brucei: Programmed expression and proteolytic cleavage of procyclin in the tsetse fly', *Proceedings of the National Academy of Sciences*, 98(4), pp.1513-1518.

Adelman, C. A., Lolo, R. L., Birkbak, N. J., Murina, O., Matsuzaki, K., Horejsi, Z., Parmar, K., Borel, V., Skehel, J. M., Stamp, G., D 'andrea, A., Sartori, A. A., Swanton, C. and Boulton, S. J. (2013) 'HELQ promotes RAD51 paralogue-dependent repair to avert germcell loss and tumorigenesis', *Nature*, 502, pp. 381–384.

Akhmedov, A. T. and Marin-Garcia, J. (2015) 'Mitochondrial DNA maintenance: an appraisal', *Molecular and Cellular Biochemistry*, 409, pp. 283–305.

Akiyoshi, B. and Gull, K. (2014) 'Discovery of Unconventional Kinetochores in Kinetoplastids', *Cell*, 156(6), pp. 1247–1258.

Alonso, A., Terrados, G., Picher, A. J., Giraldo, R., Blanco, L. and Larraga, V. (2006) 'An intrinsic 5'-deoxyribose-5-phosphate lyase activity in DNA polymerase beta from Leishmania infantum supports a role in DNA repair.', *DNA repair*, 5(1), pp. 89-101.

Alsford, S. and Horn, D. (2008) 'Single-locus targeting constructs for reliable regulated RNAi and transgene expression in Trypanosoma brucei', *Molecular and Biochemical Parasitology*, 161(1), pp. 76–79.

Alsford, S. and Horn, D. (2012) 'Cell-cycle-regulated control of VSG expression site silencing by histones and histone chaperones ASF1A and CAF-1b in Trypanosoma brucei', *Nucleic Acids Research*, 40(20), pp. 10150–10160.

Altschul, S. F., Gish, W., Miller, W., Myers, E. W. and Lipman, D. J. (1990) 'Basic local alignment search tool', *Journal of molecular biology*, 215(3), pp. 403–10.

Andersen, P. L., Xu, F. and Xiao, W. (2008) 'Eukaryotic DNA damage tolerance and

translesion synthesis through covalent modifications of PCNA', *Cell Research*, 18(1), pp. 162–173.

Antonin, W. and Neumann, H. (2016) 'Chromosome condensation and decondensation during mitosis', *Current Opinion in Cell Biology*, 40, pp. 15–22.

Arana, M. E., Takata, K. ichi, Garcia-Diaz, M., Wood, R. D. and Kunkel, T. A. (2007) 'A unique error signature for human DNA polymerase nu', *DNA Repair*, 6(2), pp. 213–223.

Aslett, M., Aurrecoechea, C., Berriman, M., Brestelli, J., Brunk, B. P., Carrington, M., Depledge, D. P., Fischer, S., Gajria, B., Gao, X., Gardner, M. J., Gingle, A., Grant, G., Harb, O. S., Heiges, M., Hertz-Fowler, C., Houston, R., Innamorato, F., Iodice, J., Kissinger, J. C., Kraemer, E., Li, W., Logan, F. J., Miller, J. A., Mitra, S., Myler, P. J., Nayak, V., Pennington, C., Phan, I., Pinney, D. F., Ramasamy, G., Rogers, M. B., Roos, D. S., Ross, C., Sivam, D., Smith, D. F., Srinivasamoorthy, G., Stoeckert, C. J., Subramanian, S., Thibodeau, R., Tivey, A., Treatman, C., Velarde, G. and Wang, H. (2009) 'TriTrypDB: A functional genomic resource for the Trypanosomatidae', *Nucleic Acids Research*, 38, pp.457-462.

Augusto-Pinto, L. and Bartholomeu, D. (2001) 'Molecular cloning and characterization of the DNA mismatch repair gene class 2 from the Trypanosoma cruzi', *Gene*, 272(1–2), pp. 323–33.

Badie, S., Liao, C., Thanasoula, M., Barber, P., Hill, M. A. and Tarsounas, M. (2009) 'RAD51C facilitates checkpoint signaling by promoting CHK2 phosphorylation', *Journal of Cell Biology*, 185(4), pp. 587–600.

Badjatia, N., Nguyen, T. N., Lee, J. H. and Günzl, A. (2013) 'Trypanosoma brucei harbours a divergent XPB helicase paralogue that is specialized in nucleotide excision repair and conserved among kinetoplastid organisms', *Molecular Microbiology*, 90(6), pp. 1293–1308.

Bailey, L. J. and Doherty, A. J. (2017) 'Mitochondrial DNA replication: a PrimPol perspective', *Biochemical Society Transactions*, 45(2), pp. 513–529. .

Baranovskiy, A. G., Lada, A. G., Siebler, H. M., Zhang, Y., Pavlov, Y. I. and Tahirov, T. H. (2012) 'DNA polymerase δ and ζ switch by sharing accessory subunits of DNA polymerase δ.', *The Journal of biological chemistry*, 287(21), pp. 17281–7.

Barnum, K. J. and O'Connell, M. J. (2014) 'Cell cycle regulation by checkpoints', *Methods in Molecular Biology*, 1170, pp. 29–40.

Barry, J. D., Ginger, M. L., Burton, P. and McCulloch, R. (2003) 'Why are parasite contingency genes often associated with telomeres?', *International Journal for Parasitology*, pp. 29–45.

Barry, J. D., Hall, J. P. J. and Plenderleith, L. (2012) 'Genome hyperevolution and the success of a parasite.', *Annals of the New York Academy of Sciences*, 1267, pp. 11–7.

Bartossek, T., Jones, N. G., Schäfer, C., Cvitković, M., Glogger, M., Mott, H. R., Kuper, J., Brennich, M., Carrington, M., Smith, A.-S., Fenz, S., Kisker, C. and Engstler, M. (2017) 'Structural basis for the shielding function of the dynamic trypanosome variant surface glycoprotein coat', *Nature Microbiology*, 2, pp. 1523–1532.

Batram, C., Jones, N. G., Janzen, C. J., Markert, S. M. and Engstler, M. (2014) 'Expression site attenuation mechanistically links antigenic variation and development in Trypanosoma brucei', 3(2324),pp. 1–18.

Beagan, K., Armstrong, R. L., Witsell, A., Roy, U., Renedo, N., Baker, A. E., Schärer, O. D. and McVey, M. (2017) 'Drosophila DNA polymerase theta utilizes both helicase-like and polymerase domains during microhomology-mediated end joining and interstrand crosslink repair', *PLOS Genetics*. Edited by L. S. Symington. Public Library of Science, 13(5), pp.1-19.

Beagan, K. and McVey, M. (2016) 'Linking DNA polymerase theta structure and function in health and Disease', *Cell Molecular Life Science*, 73(3), pp. 603–615.

Bebenek, K. and Kunkel, T. A. (2004) 'Functions of DNA polymerases', *Advances in Protein Chemistry*, 69, pp. 137–165.

Bell, J. S., Harvey, T. I., Sims, A. M. and McCulloch, R. (2004) 'Characterization of components of the mismatch repair machinery in Trypanosoma brucei', *Molecular Microbiology*, 51(1),pp. 159–173.

Belli, S. I. (2000) 'Chromatin remodelling during the life cycle of trypanosomatids', *International Journal for Parasitology*, 30, pp. 679–687.

Benmerzouga, I., Concepción-Acevedo, J., Kim, H. S., Vandoros, A. V, Cross, G. A. M.,

Klingbeil, M. M. and Li, B. (2013) 'Trypanosoma brucei Orc1 is essential for nuclear DNA replication and affects both VSG silencing and VSG switching', *Molecular Microbiology*. NIH Public Access, 87(1), pp. 196–210.

Berriman, M., Ghedin, E., Hertz-Fowler, C., Blandin, G., Renauld, H., Bartholomeu, D. C., Lennard, N. J., Caler, E., Hamlin, N. E., Haas, B., Böhme, U., Hannick, L., Aslett, M. a, Shallom, J., Marcello, L., Hou, L., Wickstead, B., Alsmark, U. C. M., Arrowsmith, C., Atkin, R. J., Barron, A. J., Bringaud, F., Brooks, K., Carrington, M., Cherevach, I., Chillingworth, T.-J., Churcher, C., Clark, L. N., Corton, C. H., Cronin, A., Davies, R. M., Doggett, J., Djikeng, A., Feldblyum, T., Field, M. C., Fraser, A., Goodhead, I., Hance, Z., Harper, D., Harris, B. R., Hauser, H., Hostetler, J., Ivens, A., Jagels, K., Johnson, D., Johnson, J., Jones, K., Kerhornou, A. X., Koo, H., Larke, N., Landfear, S., Larkin, C., Leech, V., Line, A., Lord, A., Macleod, A., Mooney, P. J., Moule, S., Martin, D. M. a, Morgan, G. W., Mungall, K., Norbertczak, H., Ormond, D., Pai, G., Peacock, C. S., Peterson, J., Quail, M. a, Rabbinowitsch, E., Rajandream, M.-A., Reitter, C., Salzberg, S. L., Sanders, M., Schobel, S., Sharp, S., Simmonds, M., Simpson, A. J., Tallon, L., Turner, C. M. R., Tait, A., Tivey, A. R., Van Aken, S., Walker, D., Wanless, D., Wang, S., White, B., White, O., Whitehead, S., Woodward, J., Wortman, J., Adams, M. D., Embley, T. M., Gull, K., Ullu, E., Barry, J. D., Fairlamb, A. H., Opperdoes, F., Barrell, B. G., Donelson, J. E., Hall, N., Fraser, C. M., Melville, S. E. and El-Sayed, N. M. (2005) 'The genome of the African trypanosome Trypanosoma brucei.', *Science*, 309(5733), pp. 416–22.

Bessat, M., Knudsen, G., Burlingame, A. L. and Wang, C. C. (2013) 'A Minimal Anaphase Promoting Complex/Cyclosome (APC/C) in Trypanosoma brucei', *PLoS ONE*, 8(3), pp.1-14.

Boehm, E. M., Spies, M. and Washington, M. T. (2016) 'PCNA tool belts and polymerase bridges form during translesion synthesis', *Nucleic Acids Research*, 44(17), pp. 8250–8260.

Boettcher, B. and Barral, Y. (2012) 'The cell biology of open and closed mitosis.', *Nucleus (Austin, Tex.)*. Taylor & Francis, 4(3), pp. 160–165.

Boothroyd, C. E., Dreesen, O., Leonova, T., Ly, K. I., Figueiredo, L. M., Cross, G. a M. and Papavasiliou, F. N. (2009) 'A yeast-endonuclease-generated DNA break induces antigenic switching in Trypanosoma brucei.', *Nature*. Nature Publishing Group, 459(7244), pp. 278–81.

Borst, P. and Ulbert, S. (2001) 'Control of VSG gene expression sites', *Molecular and Biochemical Parasitology*,114, pp. 17–27.

Bruhn, D. F., Mozeleski, B., Falkin, L. and Klingbeil, M. M. (2010) 'Mitochondrial DNA polymerase POLIB is essential for minicircle DNA replication in African trypanosomes', *Molecular Microbiology*, 75(6), pp. 1414–1425.

Bruhn, D. F., Sammartino, M. P. and Klingbeil, M. M. (2011) 'Three mitochondrial DNA polymerases are essential for kinetoplast DNA replication and survival of bloodstream form Trypanosoma brucei', *Eukaryotic Cell*, 10(6), pp. 734–743.

Bruhn, D. F., Sammartino, M. P. and Klingbeil, M. M. (2011) 'Three mitochondrial DNA polymerases are essential for kinetoplast DNA replication and survival of bloodstream form Trypanosoma brucei.', *Eukaryotic cell*, 10(6), pp. 734–43.

Burton, P., McBride, D. J., Wilkes, J. M., Barry, J. D. and McCulloch, R. (2007) 'Ku heterodimer-independent end joining in Trypanosoma brucei cell extracts relies upon sequence microhomology', *Eukaryotic Cell*, 6(10), pp. 1773–1781.

Byrd, A. K. and Raney, K. D. (2012) 'Superfamily 2 helicases.', *Frontiers in bioscience*, 17, pp. 2070–88.

Callahan, K. P. and Butler, J. S. (2010) 'TRAMP Complex Enhances RNA Degradation by the Nuclear Exosome Component Rrp6, *The Journal of biological chemistry*, 285(6), pp. 3540–3547.

Callejas, S., Leech, V., Reitter, C. and Melville, S. (2006) 'Hemizygous subtelomeres of an African trypanosome chromosome may account for over 75% of chromosome length.', *Genome research*, 16(9), pp. 1109–18.

Capewell, P., Cren-Travaille, C., Marchesi, F., Johnston, P., Clucas, C., Benson, R. A., Gorman, T.-A., Calvo-Alvarez, E., Crouzols, A., Jouvion, G., Jammoneau, V., Weir, W., Stevenson, M. L., O'Neill, K., Cooper, A., Swar, N.-R. K., Bucheton, B., Ngoyi, D. M., Garside, P., Rotureau, B. and MacLeod, A. (2016) 'The skin is a significant but overlooked anatomical reservoir for vector-borne African trypanosomes.', *eLife*, 5, pp. 157–167.

Carreira, A. and Kowalczykowski, S. C. (2011) 'Two classes of BRC repeats in BRCA2 promote RAD51 nucleoprotein filament function by distinct mechanisms', *Proceedings of*

the National Academy of Sciences, 108(26), pp. 10448–10453.

Chandler, J., Vandoros, A. V, Mozeleski, B. and Klingbeil, M. M. (2008) 'Stem-loop silencing reveals that a third mitochondrial DNA polymerase, POLID, is required for kinetoplast DNA replication in trypanosomes', *Eukaryotic Cell*, 7(12), pp. 2141–2146.

Chun, A. C. S. and Jin, D.-Y. (2010) 'Ubiquitin-dependent regulation of translesion polymerases.', *Biochemical Society transactions*, 38, pp. 110–5.

Cline, S. D. (2012) 'Mitochondrial DNA damage and its consequences for mitochondrial gene expression.', *Biochimica et biophysica acta*, 1819(9–10), pp. 979–91.

Colasante, C., Peña Diaz, P., Clayton, C. and Voncken, F. (2009) 'Mitochondrial carrier family inventory of Trypanosoma brucei brucei: Identification, expression and subcellular localisation', *Molecular and Biochemical Parasitology*, 167(2), pp. 104–117.

Collis, S. J., Ciccia, A., Deans, A. J., Hořejší, Z., Martin, J. S., Maslen, S. L., Skehel, J. M., Elledge, S. J., West, S. C. and Boulton, S. J. (2008) 'FANCM and FAAP24 Function in ATR-Mediated Checkpoint Signaling Independently of the Fanconi Anemia Core Complex', *Molecular Cell*, 32(3), pp. 313–324.

Compe, E. and Egly, J.-M. (2012) 'TFIIH: when transcription met DNA repair', *Nature Reviews Molecular Cell Biology*, 13(6), pp. 343–354.

Costes, A. and Lambert, S. A. E. (2013) 'Homologous recombination as a replication fork escort: Fork-protection and recovery', *Biomolecules*,3, pp. 39–71.

Cotterill, S. and Kearsey, S. (2002) 'Eukaryotic DNA Polymerases', *Encyclopedia of Life Sciences*, pp. 1–6.

Cristodero, M. and Clayton, C. E. (2007) 'Trypanosome MTR4 is involved in rRNA processing', *Nucleic Acids Research*, 35(20), pp. 7023–7030.

Cristodero, M., Seebeck, T. and Schneider, A. (2010) 'Mitochondrial translation is essential in bloodstream forms of Trypanosoma brucei', *Molecular Microbiology*, 78(3), pp. 757–769.

D'Archivio, S. and Wickstead, B. (2017) 'Trypanosome outer kinetochore proteins suggest conservation of chromosome segregation machinery across eukaryotes', *Journal*

of Cell Biology, 216(2), pp. 379–391.

Damasceno, J. D., Obonaga, R., Santos, E. V., Scott, A., McCulloch, R. and Tosi, L. R. O. (2016) 'Functional compartmentalization of Rad9 and Hus1 reveals diverse assembly of the 9-1-1 complex components during the DNA damage response in Leishmania', *Molecular Microbiology*, 101(6), pp. 1054–1068.

Dang, H. Q. and Li, Z. (2011) 'The Cdc45-Mcm2-7-GINS protein complex in trypanosomes regulates DNA replication and interacts with two Orc1-like proteins in the origin recognition complex', *Journal of Biological Chemistry*. American Society for Biochemistry and Molecular Biology, 286(37), pp. 32424–32435.

Deitsch, K. W., Lukehart, S. a and Stringer, J. R. (2009) 'Common strategies for antigenic variation by bacterial, fungal and protozoan pathogens.', *Nature reviews. Microbiology*, 7(7), pp. 493–503.

Deka, K., Singh, A., Chakraborty, S., Mukhopadhyay, R. and Saha, S. (2016) 'Protein arginylation regulates cellular stress response by stabilizing HSP70 and HSP40 transcripts.', *Cell death discovery*,2, pp. 1-8.

Delarue, M., Poch, O., Noel, T., Moras, D. and Argos, P. (1990) 'An attempt to unify the structure of polymerases', *Protein Engineering, Design and Selection*, 3(6), pp. 461–467.

Della, M., Palmbos, P. L., Tseng, H.-M., Tonkin, L. M., Daley, J. M., Topper, L. M., Pitcher, R. S., Tomkinson, A. E., Wilson, T. E. and Doherty, A. J. (2004) 'Mycobacterial Ku and ligase proteins constitute a two-component NHEJ repair machine.', *Science (New York, N.Y.)*. American Association for the Advancement of Science, 306(5696), pp. 683–685.

Devlin, R., Marques, C. A., Paape, D., Prorocic, M., Zurita-Leal, A. C., Campbell, S. J., Lapsley, C., Dickens, N. and McCulloch, R. (2016) 'Mapping replication dynamics in Trypanosoma brucei reveals a link with telomere transcription and antigenic variation', *eLife*,5, pp. 1-30.

Ding, H., Guo, M., Vidhyasagar, V., Talwar, T. and Wu, Y. (2015) 'The Q motif is involved in DNA binding but not ATP binding in ChlR1 helicase', *PLoS ONE*, 10(10).pp.1-22.

Dobson, R., Stockdale, C., Lapsley, C., Wilkes, J. and McCulloch, R. (2011) 'Interactions

among Trypanosoma brucei RAD51 paralogues in DNA repair and antigenic variation.', *Molecular microbiology*, 81(2), pp. 434–56..

Downey, N., Hines, J. C., Sinha, K. M. and Ray, D. S. (2005) 'Mitochondrial DNA ligases of Trypanosoma brucei.', *Eukaryotic cell*. American Society for Microbiology (ASM), 4(4), pp. 765–74.

DuBois, K. N., Alsford, S., Holden, J. M., Buisson, J., Swiderski, M., Bart, J. M., Ratushny, A. V, Wan, Y., Bastin, P., Barry, J. D., Navarro, M., Horn, D., Aitchison, J. D., Rout, M. P. and Field, M. C. (2012) 'NUP-1 is a large coiled-coil nucleoskeletal protein in trypanosomes with lamin-like functions', *PLoS Biology*, 10(3), pp. 1-20.

Duraisingh, M. T. and Horn, D. (2016) 'Epigenetic Regulation of Virulence Gene Expression in Parasitic Protozoa', *Cell Host and Microbe*, 19 (5),pp. 629–640.

Ebrahimi, H. and Cooper, J. P. (2012) 'Closed mitosis: A timely move before separation', *Current Biology*, 22(20), pp. R880–R882.

Echeverry, M. C., Bot, C., Obado, S. O., Taylor, M. C. and Kelly, J. M. (2012) 'Centromere-associated repeat arrays on Trypanosoma brucei chromosomes are much more extensive than predicted', *BMC Genomics*. BioMed Central, 13(29), p. 1-8.

Edwards, S., Li, C. M., Levy, D. L., Brown, J., Snow, P. M. and Campbell, J. L. (2003a) 'Saccharomyces cerevisiae DNA polymerase epsilon and polymerase sigma interact physically and functionally, suggesting a role for polymerase epsilon in sister chromatid cohesion.', *Molecular and cellular biology*, 23(8), pp. 2733–2748.

Edwards, S., Li, C. M., Levy, D. L., Brown, J., Snow, P. M. and Campbell, J. L. (2003b) 'Saccharomyces cerevisiae DNA polymerase epsilon and polymerase sigma interact physically and functionally, suggesting a role for polymerase epsilon in sister chromatid cohesion.', *Molecular and cellular biology*, 23(8), pp. 2733–2748.

Eeken, J. C. J., Romeijna, R. J., De Jong, A. W. M., Pastink, A. and Lohman, P. H. M. (2001) 'Isolation and genetic characterisation of the Drosophila homologue of (SCE)REV3, encoding the catalytic subunit of DNA polymerase ζ', *Mutation Research - DNA Repair*, 485(3), pp. 237–253.

Engel, M. L. and Ray, D. S. (1999) 'The kinetoplast structure-specific endonuclease I is related to the 5' exo/endonuclease domain of bacterial DNA polymerase I and

colocalizes with the kinetoplast topoisomerase II and DNA polymerase beta during replication.', *Proceedings of the National Academy of Sciences of the United States of America*. National Academy of Sciences, 96(15), pp. 8455–60.

Esposito, G., Godindagger, I., Klein, U., Yaspo, M. L., Cumano, A. and Rajewsky, K. (2000) 'Disruption of the Rev3l-encoded catalytic subunit of polymerase zeta in mice results in early embryonic lethality.', *Current biology : CB*. Cell Press, 10(19), pp. 1221–1224.

Fairman-Williams, M. E., Guenther, U. P. and Jankowsky, E. (2010) 'SF1 and SF2 helicases: Family matters', *Current Opinion in Structural Biology*, 20(3), pp. 313–324.

Fenn, K. and Matthews, K. R. (2007) 'The cell biology of Trypanosoma brucei differentiation', *Current Opinion in Microbiology*,10, pp. 539–546.

Fernández-Orgiler, A., Martínez-JimCrossed, M. I., Alonso, A., Alcolea, P. J., Requena, J. M., Thomas, M. C., Blanco, L. and Larraga, V. (2016) 'A putative Leishmania DNA polymerase theta protects the parasite against oxidative damage', *Nucleic Acids Research*, 44(10), pp. 4855–4870.

Field, M. C. and Carrington, M. (2009) 'The trypanosome flagellar pocket', *Nature Reviews Microbiology*, 7(11), pp. 775–786.

Figueiredo, L. M. and Cross, G. A. M. (2010) 'Nucleosomes are depleted at the VSG expression site transcribed by RNA polymerase I in African trypanosomes', *Eukaryotic Cell*. American Society for Microbiology (ASM), 9(1), pp. 148–154.

Figueiredo, L. M., Janzen, C. J. and Cross, G. A. M. (2008) 'A histone methyltransferase modulates antigenic variation in African trypanosomes', *PLoS Biology*, 6(7), pp. 1539–1548.

Finn, R. D., Attwood, T. K., Babbitt, P. C., Bateman, A., Bork, P., Bridge, A. J., Chang, H.-Y., Dosz Anyi, Z., El-Gebali, S., Fraser, M., Gough, J., Haft, D., Holliday, G. L., Huang, H., Huang, X., Letunic, I., Lopez, R., Lu, S., Marchler-Bauer, A., Mi, H., Mistry, J., Natale, D. A., Necci, M., Nuka, G., Orengo, C. A., Park, Y., Pesseat, S., Piovesan, D., Potter, S. C., Rawlings, N. D., Redaschi, N., Richardson, L., Rivoire, C., Sangrador-Vegas, A., Sigrist, C., Sillitoe, I., Smithers, B., Squizzato, S., Sutton, G., Thanki, N., Thomas, P. D., Tosatto, S. C. E., Wu, C. H., Xenarios, I., Yeh, L.-S., Young, S.-Y. and Mitchell, A. L. (2017) 'InterPro in 2017––beyond protein family and domain annotations',

Nucleic Acids Research, 45, pp. 190-199.

Franco, J. R., Simarro, P. P., Diarra, A., Ruiz-Postigo, J. A. and Jannin, J. G. (2014) 'The journey towards elimination of gambiense human African trypanosomiasis: not far, nor easy.', *Parasitology*, 141, pp. 748–60.

Friedberg, E. C., Lehmann, A. R. and Fuchs, R. P. P. (2005) 'Trading places: how do DNA polymerases switch during translesion DNA synthesis?', *Molecular cell*, 18(5), pp. 499–505.

Friedberg, E. C., Wagner, R. and Radman, M. (2002) 'Specialized DNA polymerases, cellular survival, and the genesis of mutations.', *Science (New York, N.Y.)*, 296(5573), pp. 1627–30.

Gan, G. N., Wittschieben, J. P., Wittschieben, B. Ø. and Wood, R. D. (2008) 'DNA polymerase zeta (pol zeta) in higher eukaryotes.', *Cell research*, 18(1), pp. 174-83.

Gao, Y., Mutter-Rottmayer, E., Zlatanou, A., Vaziri, C. and Yang, Y. (2017) 'Mechanisms of post-replication DNA repair', *Genes*, 8(2)pp. 1-16.

Garcia-Diaz, M. and Bebenek, K. (2007) 'Multiple Functions of DNA Polymerases', *CRC Crit Rev Plant Sci*, 26(2), pp. 105–122.

Genois, M.-M., Paquet, E. R., Laffitte, M.-C. N., Maity, R., Rodrigue, A., Ouellette, M. and Masson, J.-Y. (2014) 'DNA Repair Pathways in Trypanosomatids: from DNA Repair to Drug Resistance', *Microbiology and Molecular Biology Reviews*, 78(1), pp. 40–73.

Genois, M. M., Mukherjee, A., Ubeda, J. M., Buisson, R., Paquet, E., Roy, G., Plourde, M., Coulombe, Y., Ouellette, M. and Masson, J. Y. (2012) 'Interactions between BRCA2 and RAD51 for promoting homologous recombination in Leishmania infantum', *Nucleic Acids Research*, 40(14), pp. 6570–6584.

Gibbs, P. E. M., McDonald, J., Woodgate, R. and Lawrence, C. W. (2005) 'The relative roles in vivo of Saccharomyces cerevisiae Pol eta, Pol zeta, Rev1 protein and Pol32 in the bypass and mutation induction of an abasic site, T-T (6-4) photoadduct and T-T cis-syn cyclobutane dimer', *Genetics*. Genetics, 169(2), pp. 575–82.

Giglia-Mari, G., Zotter, A. and Vermeulen, W. (2011) 'DNA damage response', *Cold Spring Harbor Perspectives in Biology*, 3(1), pp. 1–19.

Ginger, M. L., Blundell, P. A., Lewis, A. M., Browitt, A., Günzl, A. and Barry, J. D. (2002) 'Ex vivo and in vitro identification of a consensus promoter for VSG genes expressed by metacyclic-stage trypanosomes in the tsetse fly', *Eukaryotic Cell*. American Society for Microbiology, 1(6), pp. 1000–1009.

Glover, L. and Horn, D. (2012) 'Trypanosomal histone γh2A and the DNA damage response', *Molecular and Biochemical Parasitology*, 183(1), pp. 78–83.

Glover, L., Hutchinson, S., Alsford, S. and Horn, D. (2016) 'VEX1 controls the allelic exclusion required for antigenic variation in trypanosomes', *Proceedings of the National Academy of Sciences*. National Academy of Sciences, 113(26), pp. 7225–7230.

Glover, L., Hutchinson, S., Alsford, S., McCulloch, R., Field, M. C. and Horn, D. (2013) 'Antigenic variation in African trypanosomes: the importance of chromosomal and nuclear context in VSG expression control', *Cellular microbiology*, 15(12), pp. 1984–93.

Glover, L., Jun, J. and Horn, D. (2011) 'Microhomology-mediated deletion and gene conversion in African trypanosomes', *Nucleic Acids Research*, 39(4), pp. 1372–1380.

Gluenz, E., Sharma, R., Carrington, M. and Gull, K. (2008) 'Functional characterization of cohesin subunit SCC1 in Trypanosoma brucei and dissection of mutant phenotypes in two life cycle stages', *Molecular Microbiology*, 69(3), pp. 666–680.

Gluenz, E., Wheeler, R. J., Hughes, L. and Vaughan, S. (2015) 'Scanning and three-dimensional electron microscopy methods for the study of Trypanosoma brucei and Leishmania mexicana flagella', *Methods in Cell Biology*, 127, pp. 509–542.

Gómez-Llorente, Y., Malik, R., Jain, R., Choudhury, J. R., Johnson, R. E., Prakash, L., Prakash, S., Ubarretxena-Belandia, I. and Aggarwal, A. K. (2013) 'The architecture of yeast DNA polymerase ζ.', *Cell reports*, 5(1), pp. 79–86.

Goodman, M. F. (2002) 'Error-prone repair DNA polymerases in prokaryotes and eukaryotes.', *Annual review of biochemistry*, 71, pp. 17–50.

Goodman, M. F. and Woodgate, R. (2013) 'Translesion DNA polymerases', *Cold Spring Harbor Perspectives in Biology*. Cold Spring Harbor Laboratory Press, 5(10), p. a010363.

Gowda, a. S. P., Moldovan, G.-L. and Spratt, T. E. (2015) 'Human DNA Polymerase v Catalyzes Correct and Incorrect DNA Synthesis with High Catalytic Efficiency', *Journal*

of Biological Chemistry, 290(26), pp. 16292–16303.

Grams, J., Morris, J. C., Drew, M. E., Wang, Z., Englund, P. T. and Hajduk, S. L. (2002) 'A trypanosome mitochondrial RNA polymerase is required for transcription and replication', *Journal of Biological Chemistry*, 277(19), pp. 16952–16959.

Griffin, C. S., Simpson, P. J., Wilson, C. R. and Thacker, J. (2000) 'Mammalian recombination-repair genes XRCC2 and XRCC3 promote correct chromosome segregation.', *Nature cell biology*, 2(10), pp. 757–761.

Gueranger, Q., Stary, A., Aoufouchi, S., Faili, A., Sarasin, A., Reynaud, C.-A. and Weill, J.-C. (2008) 'Role of DNA polymerases eta, iota and zeta in UV resistance and UV-induced mutagenesis in a human cell line.', *DNA repair*, 7(9), pp. 1551–62.

Guirouilh-Barbat, J., Lambert, S., Bertrand, P. and Lopez, B. S. (2014) 'Is homologous recombination really an error-free process?', *Frontiers in Genetics, 5(175),pp.*1-24.

Gull, K., Alsford, S. and Ersfeld, K. (1998) 'Segregation of minichromosomes in trypanosomes: Implications for mitotic mechanisms', *Trends in Microbiology*, 6(8), pp. 319–323.

Günzl, A., Kirkham, J. K., Nguyen, T. N., Badjatia, N. and Park, S. H. (2015) 'Mono-allelic VSG expression by RNA polymerase I in Trypanosoma brucei: Expression site control from both ends?', *Gene*. NIH Public Access, 556(1), pp. 68–73.

Hall, B. S., Gabernet-Castello, C., Voak, A., Goulding, D., Natesan, S. K. and Field, M. C. (2006) 'TbVps34, the trypanosome orthologue of Vps34, is required for Golgi complex segregation', *Journal of Biological Chemistry*. American Society for Biochemistry and Molecular Biology, 281(37), pp. 27600–27612.

Hall, J. P. J., Wang, H. and Barry, J. D. (2013) 'Mosaic VSGs and the scale of Trypanosoma brucei antigenic variation.', *PLoS pathogens*, 9(7), pp.1-13.

Hall, M. C. and Matson, S. W. (1999) 'Helicase motifs: the engine that powers DNA unwinding.', *Molecular microbiology*, 34(5), pp. 867–877.

Hammarton, T. C. (2007) 'Cell cycle regulation in Trypanosoma brucei', *Molecular and Biochemical Parasitology*. Elsevier, pp. 1–8.

Hammarton, T. C., Clark, J., Douglas, F., Boshart, M. and Mottram, J. C. (2003) 'Stage-specific differences in cell cycle control in Trypanosoma brucei revealed by RNA interference of a mitotic cyclin', *Journal of Biological Chemistry*, 278(25), pp. 22877–22886.

Hammarton, T. C., Engstler, M. and Mottram, J. C. (2004) 'The Trypanosoma brucei cyclin, CYC2, is required for cell cycle progression through G1 phase and for maintenance of procyclic form cell morphology', *Journal of Biological Chemistry*. American Society for Biochemistry and Molecular Biology, 279(23), pp. 24757–24764.

Haracska, L., Johnson, R. E., Prakash, L. and Prakash, S. (2005) 'Trf4 and Trf5 Proteins of Saccharomyces cerevisiae Exhibit Poly (A) RNA Polymerase Activity but No DNA Polymerase Activity', 25(22), pp. 10183–10189.

Harashima, H., Dissmeyer, N. and Schnittger, A. (2013) 'Cell cycle control across the eukaryotic kingdom', *Trends in Cell Biology*, 23(7), pp. 345–356.

Hartley, C. L. and McCulloch, R. (2008) 'Trypanosoma brucei BRCA2 acts in antigenic variation and has undergone a recent expansion in BRC repeat number that is important during homologous recombination.', *Molecular microbiology*, 68(5), pp. 1237–51.

Harvey, S. H., Krien, M. J. and O'Connell, M. J. (2002) 'Structural maintenance of chromosomes (SMC) proteins, a family of conserved ATPases', *Genome Biol*, 3(2),pp.1-5.

Hays, J. B. (2002) 'Arabidopsis thaliana, a versatile model system for study of eukaryotic genome-maintenance functions', *DNA Repair*,1, pp. 579–600.

Van Hellemond, J. J., Neuville, P., Schwarz, R. T., Matthews, K. R., Mottram, J. C., Characterization, F., Cyc, O. F. and Hellemond, J. J. Van (2000) 'Isolation of Trypanosoma brucei CYC2 andCYC3 Cyclin Genes by Rescue of a Yeast G1Cyclin Mutant', *Journal of Biological Chemistry*, 275(12), pp. 8315–8323.

Hertz-Fowler, C., Figueiredo, L. M., Quail, M. a, Becker, M., Jackson, A., Bason, N., Brooks, K., Churcher, C., Fahkro, S., Goodhead, I., Heath, P., Kartvelishvili, M., Mungall, K., Harris, D., Hauser, H., Sanders, M., Saunders, D., Seeger, K., Sharp, S., Taylor, J. E., Walker, D., White, B., Young, R., Cross, G. a M., Rudenko, G., Barry, J. D., Louis, E. J. and Berriman, M. (2008) 'Telomeric expression sites are highly conserved in Trypanosoma brucei.', *PloS one*, 3(10), pp. 1-12.

Hirumi, H. and Hirumi, K. (1989) 'Continuous cultivation of Trypanosoma brucei blood stream forms in a medium containing a low concentration of serum protein without feeder cell layers.', *The Journal of parasitology*, 75(6), pp. 985–989.

Hisanaga, S. and Endo, R. (2010) 'Regulation and role of cyclin-dependent kinase activity in neuronal survival and death.', *Journal of neurochemistry*, 115(6), pp. 1309–21.

Ho, T. V. and Schärer, O. D. (2010) 'TranslesionDNA Synthesis Polymerases inDNA Interstrand Crosslink Repair', *Environmental and molecular mutagenesis*, 51(3), pp. 229–235.

Hogg, M., Seki, M., Wood, R. D., Doublié, S. and Wallace, S. S. (2011) 'Lesion bypass activity of DNA polymerase θ (POLQ) is an intrinsic property of the pol domain and depends on unique sequence inserts', *Journal of Molecular Biology*, 405(3), pp. 642–652.

Horn, D. (2014) 'Antigenic variation in African trypanosomes', *Molecular and Biochemical Parasitology*, 195, pp. 123-129.

Hovel-Miner, G., Mugnier, M., Papavasiliou, F. N., Pinger, J. and Schulz, D. (2015) 'A host–pathogen interaction reduced to first principles: Antigenic variation in T. Brucei', in *Results and Problems in Cell Differentiation*, pp. 23–46.

Iyama, T. and Wilson, D. M. (2013) 'DNA repair mechanisms in dividing and non-dividing cells.', *DNA repair*. Elsevier B.V., 12(8), pp. 620–36.

Iyer, L. M., Koonin, E. V, Leipe, D. D. and Aravind, L. (2005) 'Origin and evolution of the archaeo-eukaryotic primase superfamily and related palm-domain proteins: Structural insights and new members', *Nucleic Acids Research*, pp. 3875–3896.

Jackson, A. P., Berry, A., Aslett, M., Allinson, H. C., Burton, P., Vavrova-Anderson, J., Brown, R., Browne, H., Corton, N., Hauser, H., Gamble, J., Gilderthorp, R., Marcello, L., McQuillan, J., Otto, T. D., Quail, M. a., Sanders, M. J., van Tonder, A., Ginger, M., Field, M. C., Barry, J. D., Hertz-Fowler, C. and Berriman, M. (2012) 'Antigenic diversity is generated by distinct evolutionary mechanisms in African trypanosome species', *Pnas*, 109(9), pp. 3416-3421.

Jansen, J. G., Temviriyanukul, P., Wit, N., Delbos, F., Reynaud, C. A., Jacobs, H. and

Wind, N. D. (2014) 'Redundancy of mammalian Y family DNA polymerases in cellular responses to genomic DNA lesions induced by ultraviolet light', *Nucleic Acids Research*, 42(17), pp. 11071–11082.

Jasin, M. and Rothstein, R. (2013) 'Repair of strand breaks by homologous recombination.', *Cold Spring Harbor perspectives in biology*.

Jensen, B. C., Sivam, D., Kifer, C. T., Myler, P. J. and Parsons, M. (2009) 'Widespread variation in transcript abundance within and across developmental stages of Trypanosoma brucei', *BMC Genomics* l, 10(1), p. 482.

Johansson, E. and Dixon, N. (2013) 'Replicative DNA polymerases', *Cold Spring Harbor Perspectives in Biology*, 5(6), pp.1-14.

Johansson, E., Majka, J. and Burgers, P. M. J. (2001) 'Structure of DNA Polymerase δ from Saccharomyces cerevisiae*', *Published JBC Papers in Press*.276(47),pp. 43824-43828.

Johnson, R. E., Washington, M. T., Haracska, L., Prakash, S. and Prakash, L. (2000) 'Eukaryotic polymerases iota and zeta act sequentially to bypass DNA lesions.', *Nature*, 406(6799), pp. 1015–1019.

Jones, N. G., Thomas, E. B., Brown, E., Dickens, N. J., Hammarton, T. C. and Mottram, J. C. (2014) 'Regulators of Trypanosoma brucei cell cycle progression and differentiation identified using a kinome-wide RNAi screen.', *PLoS pathogens*, 10(1), pp.1-16.

Kabani, S., Fenn, K., Ross, A., Ivens, A., Smith, T. K., Ghazal, P. and Matthews, K. (2009) 'Genome-wide expression profiling of in vivo-derived bloodstream parasite stages and dynamic analysis of mRNA alterations during synchronous differentiation in Trypanosoma brucei', *BMC Genomics*, 10(1), p. 427.

Kaniak-Golik, A. and Skoneczna, A. (2015) 'Mitochondria-nucleus network for genome stability', *Free Radical Biology and Medicine*, 82, pp. 73–104.

Kannouche, P. L., Wing, J. and Lehmann, A. R. (2004) 'Interaction of human DNA polymerase eta with monoubiquitinated PCNA: A possible mechanism for the polymerase switch in response to DNA damage', *Molecular Cell*, 14(4), pp. 491–500.

Kannouche, P. and Stary, A. (2003) 'Xeroderma pigmentosum variant and error-prone DNA polymerases', *Biochimie*, pp. 1123-1132.

Karanam, K., Kafri, R., Loewer, A. and Lahav, G. (2012) 'Quantitative Live Cell Imaging Reveals a Gradual Shift between DNA Repair Mechanisms and a Maximal Use of HR in Mid S Phase', *Molecular Cell*, 47(2), pp. 320–329.

Karplus, M. and Kuriyan, J. (2005) 'Molecular dynamics and protein function.', *Proceedings of the National Academy of Sciences of the United States of America*, 102(19), pp. 6679–85.

Katzen, F. (2007) 'Gateway(®) recombinational cloning: a biological operating system.', *Expert Opinion Drug Discovery*, 2(4), pp. 571–89.

Kaufer, A., Ellis, J., Stark, D. and Barratt, J. (2017) 'The evolution of trypanosomatid taxonomy', *Parasites & Vectors*, 10(1), p. 287.

Kennedy, P. G. (2013) 'Clinical features, diagnosis, and treatment of human African trypanosomiasis (sleeping sickness).', *Lancet neurology*, 12(2), pp. 186–94.

Klingbeil, M. M. and Englund, P. T. (2004) 'Closing the gaps in kinetoplast DNA network replication', *Proc Natl Acad Sci U S A*, 101(13), pp. 4333-4334.

Klingbeil, M. M., Motyka, S. A. and Englund, P. T. (2002) 'Multiple Mitochondrial DNA Polymerases in Trypanosoma brucei', *Molecular Cell*, 10, pp. 175–186.

Krokan, H. E. and Bjørås, M. (2013) 'Base excision repair', *Cold Spring Harbor Perspectives in Biology*, 5(4), pp. 1–22.

Kumar, P. and Wang, C. C. (2005) 'Depletion of anaphase-promoting complex or cyclosome (APC/C) subunit homolog APC1 or CDC27 of Trypanosoma brucei arrests the procyclic form in metaphase but the bloodstream form in anaphase', *Journal of Biological Chemistry*. American Society for Biochemistry and Molecular Biology, 280(36), pp. 31783-31791.

Kunkel, T. A. (2004) 'DNA Replication Fidelity', *Journal of Biological Chemistry*, 279(17),pp. 16895–16898.

Lamarche, B. J., Orazio, N. I. and Weitzman, M. D. (2010) 'The MRN complex in double-

strand break repair and telomere maintenance', *FEBS Letters*, 584(17), pp. 3682–3695.

Landeira, D., Bart, J.-M., Van Tyne, D. and Navarro, M. (2009) 'Cohesin regulates VSG monoallelic expression in trypanosomes.', *The Journal of cell biology*, 186(2), pp. 243–54.

Landeira, D. and Navarro, M. (2007) 'Nuclear repositioning of the VSG promoter during developmental silencing in Trypanosoma brucei.', *The Journal of cell biology*, 176(2), pp. 133-9.

Lange, S. S., Takata, K. and Wood, R. D. (2011) 'DNA polymerases and cancer', *Nature Reviews Cancer*, 11(2), pp. 96–110.

Lange, S. S., Wittschieben, J. P. and Wood, R. D. (2012) 'DNA polymerase zeta is required for proliferation of normal mammalian cells', *Nucleic Acids Research*. Oxford University Press, 40(10), pp. 4473–4482.

Langousis, G. and Hill, K. L. (2014) 'Motility and more: the flagellum of Trypanosoma brucei', *Nature Reviews Microbiology*, 12(7), pp. 505-518.

Lawrence, C. W. (2002) 'Cellular roles of DNA polymerase zeta and Rev1 protein.', *DNA repair*, 1(6), pp. 425-35.

Lee, Y.-S., Gregory, M. T. and Yang, W. (2014) 'Human Pol ζ purified with accessory subunits is active in translesion DNA synthesis and complements Pol η in cisplatin bypass.', *Proceedings of the National Academy of Sciences of the United States of America*, 111(8), pp. 2954-9.

Lehmann, A. R., Niimi, A., Ogi, T., Brown, S., Sabbioneda, S., Wing, J. F., Kannouche, P. L. and Green, C. M. (2007) 'Translesion synthesis: Y-family polymerases and the polymerase switch.', *DNA repair*, 6(7), pp. 891–9. doi:

Li, W., Kondratowicz, B., McWilliam, H., Nauche, S. and Lopez, R. (2013) 'The annotation-enriched non-redundant patent sequence databases', *Database*, 2013(10), pp. 5-5.

Li, Y., Gao, X. and Wang, J.-Y. (2011) 'Comparison of two POLQ mutants reveals that a polymerase-inactive POLQ retains significant function in tolerance to etoposide and γ-irradiation in mouse B cells.', *Genes to cells : devoted to molecular & cellular*

mechanisms, 16(9), pp. 973–83.

Li, Z. (2012) 'Regulation of the cell division cycle in Trypanosoma brucei', *Eukaryotic Cell*, 11(10), pp. 1180–1190.

Li, Z., Umeyama, T., Li, Z. and Wang, C. C. (2010) 'Polo-like kinase guides cytokinesis in Trypanosoma brucei through an indirect means', *Eukaryotic Cell*, 9(5), pp. 705–716.

Li, Z., Umeyama, T. and Wang, C. C. (2009) 'The Aurora kinase in Trypanosoma brucei plays distinctive roles in metaphase-anaphase transition and cytokinetic initiation', *PLoS Pathogens*, 5(9), pp. 1-11.

Li, Z. and Wang, C. C. (2003) 'A PHO80-like cyclin and a B-type cyclin control the cell cycle of the procyclic form of Trypanosoma brucei', *Journal of Biological Chemistry*, 278(23), pp. 20652–20658.

Lin, W., Wu, X. and Wang, Z. (1999) 'A full-length cDNA of hREV3 is predicted to encode DNA polymerase ζ for damage-induced mutagenesis in humans', *Mutation Research - DNA Repair*, 433(2), pp. 89–98.

Livak, K. J. and Schmittgen, T. D. (2001) 'Analysis of Relative Gene Expression Data Using Real-Time Quantitative PCR and the 2−ΔΔCT Method', *Methods*. Academic Press, 25(4), pp. 402–408.

Lopes, D. de O., Schamber-Reis, B. L. F., Regis-da-Silva, C. G., Rajão, M. A., DaRocha, W. D., Macedo, A. M., Franco, G. R., Nardelli, S. C., Schenkman, S., Hoffmann, J. S., Cazaux, C., Pena, S. D. J., Teixeira, S. M. R. and Machado, C. R. (2008) 'Biochemical studies with DNA polymerase β and DNA polymerase β-PAK of Trypanosoma cruzi suggest the involvement of these proteins in mitochondrial DNA maintenance', *DNA Repair*, 7(11), pp. 1882–1892.

López-Farfán, D., Bart, J. M., Rojas-Barros, D. I. and Navarro, M. (2014) 'SUMOylation by the E3 Ligase TbSIZ1/PIAS1 Positively Regulates VSG Expression in Trypanosoma brucei', *PLoS Pathogens*. Public Library of Science, 10(12), pp.1-18.

Lord, C. J. and Ashworth, A. (2007) 'RAD51, BRCA2 and DNA repair: a partial resolution.', *Nature structural & molecular biology*, 14(6), pp. 461–462.

Lord, C. J. and Ashworth, A. (2016) 'BRCAness revisited', *Nature Reviews Cancer*, 16(2),

pp. 110–120.

Lukes, J., Guilbride, D. L., Votýpka, J., Zíková, A., Benne, R., Englund, P. T., Voty, J. and Zíkova, A. (2002) 'Kinetoplast DNA Network : Evolution of an Improbable Structure', *EUKARYOTIC CELL*, 1(4), pp. 495–502.

Lukeš, J., Skalický, T., Týč, J., Votýpka, J. and Yurchenko, V. (2014) 'Evolution of parasitism in kinetoplastid flagellates', *Molecular and Biochemical Parasitology*,195, pp. 115–122.

Lundin, C., North, M., Erixon, K., Walters, K., Jenssen, D., Goldman, A. S. H. and Helleday, T. (2005) 'Methyl methanesulfonate (MMS) produces heat-labile DNA damage but no detectable in vivo DNA double-strand breaks.', *Nucleic acids research*, 33(12), pp. 3799–811..

Machado, C. R., Vieira-da-Rocha, J. P., Mendes, I. C., Rajão, M. A., Marcello, L., Bitar, M., Drummond, M. G., Grynberg, P., Oliveira, D. A. A., Marques, C., Van Houten, B. and Mcculloch, R. (2014) 'Nucleotide excision repair in Trypanosoma brucei: Specialization of transcription-coupled repair due to multigenic transcription', *Molecular Microbiology*, 92(4), pp. 756–776.

Mailand, N., Gibbs-Seymour, I. and Bekker-Jensen, S. (2013) 'Regulation of PCNA–protein interactions for genome stability', *Nature Reviews Molecular Cell Biology*, 14(5), pp. 269–282.

Makarova, A. V and Burgers, P. M. (2015) 'Eukaryotic DNA polymerase ζ', *DNA Repair.*, 29, pp. 47–55.

Malumbres, M. (2014) 'Cyclin-dependent kinases', *Genome Biology*, 15(6), p. 122.

Malvy, D. and Chappuis, F. (2011) 'Sleeping sickness.', *Clinical microbiology and infection : the official publication of the European Society of Clinical Microbiology and Infectious Diseases*, 17(7), pp. 986–95.

Manchado, E., Eguren, M. and Malumbres, M. (2010) 'The anaphase-promoting complex/cyclosome (APC/C): cell-cycle-dependent and -independent functions', *Biochemical Society Transactions*, 38(1), pp. 65–71.

Marcello, L. and Barry, J. D. (2007) 'Analysis of the VSG gene silent archive in

Trypanosoma brucei reveals that mosaic gene expression is prominent in antigenic variation and is favored by archive substructure.', *Genome research*, 17(9), pp. 1344–52.

Maréchal, A. and Zou, L. (2013) 'DNA damage sensing by the ATM and ATR kinases', *Cold Spring Harbor Perspectives in Biology*, 5(9), pp.1-17.

Marini, F., Kim, N., Schuffert, A. and Wood, R. D. (2003) 'POLN, a nuclear PolA family DNA polymerase homologous to the DNA cross-link sensitivity protein Mus308.', *The Journal of biological chemistry*, 278(34), pp. 32014–9.

Marinus, M. G. (2012) 'DNA Mismatch Repair', *EcoSal Plus*. NIH Public Access, 5(1), pp. 997–1003.

Marques, C. A., Tiengwe, C., Lemgruber, L., Damasceno, J. D., Scott, A., Paape, D., Marcello, L. and McCulloch, R. (2016) 'Diverged composition and regulation of the Trypanosoma brucei origin recognition complex that mediates DNA replication initiation.', *Nucleic acids research*, 44(10), pp. 4763–84.

Matthews, K. R. (2005) 'The developmental cell biology of Trypanosoma brucei.', *Journal of cell science*, 118(Pt 2), pp. 283–90. doi: 10.1242/jcs.01649.

Matthews, K. R. and Gull, K. (1994) 'Evidence for an interplay between cell cycle progression and the initiation of differentiation between life cycle forms of African trypanosomes', *Journal of Cell Biology*. Rockefeller University Press, 125(5), pp. 1147–1156.

McCulloch, R. (2004) 'Antigenic variation in African trypanosomes: monitoring progress.', *Trends in parasitology*, 20(3), pp. 117–21.

McCulloch, R. and Barry, J. D. (1999) 'A role for RAD51 and homologous recombination in Trypanosoma brucei antigenic variation.', *Genes & development*, 13(21), pp. 2875–88.

McCulloch, R., Vassella, E., Burton, P., Boshart, M. and Barry, J. D. (2004) 'Transformation of monomorphic and pleomorphic Trypanosoma brucei.', *Methods in molecular biology*, 262(3), pp. 53–86.

McVey, M., Khodaverdian, V. Y., Meyer, D., Cerqueira, P. G. and Heyer, W.-D. (2016)

'Eukaryotic DNA Polymerases in Homologous Recombination', *Annual Review of Genetics*, 50(1), pp. 393–421.

Mejia, E., Burak, M., Alonso, A., Larraga, V., Kunkel, T. A., Bebenek, K. and Garcia-Diaz, M. (2014) 'Structures of the Leishmania infantum polymerase beta', *DNA Repair*, 18(1), pp. 1–9.

De Melo Godoy, P. D., Nogueira-Junior, L. A., Paes, L. S., Cornejo, A., Martins, R. M., Silber, A. M., Schenkman, S. and Elias, M. C. (2009) 'Trypanosome prereplication machinery contains a single functional Orc1/Cdc6 protein, which is typical of archaea', *Eukaryotic Cell.*, 8(10), pp. 1592–1603.

Michl, J., Zimmer, J. and Tarsounas, M. (2016) 'Interplay between Fanconi anemia and homologous recombination pathways in genome integrity', *The EMBO Journal*, 35(9), pp. 909–923.

Minoshima, Y., Kawashima, T., Hirose, K., Tonozuka, Y., Kawajiri, A., Bao, Y. C., Deng, X., Tatsuka, M., Narumiya, S., May, W. S., Nosaka, T., Semba, K., Inoue, T., Satoh, T., Inagaki, M. and Kitamura, T. (2003) 'Phosphorylation by Aurora B converts MgcRacGAP to a RhoGAP during cytokinesis', *Developmental Cell*, pp. 549–560.

Mitchison, T. J. and Salmon, E. D. (2001) 'Mitosis: a history of division.', *Nature cell biology*, 3(1), pp. E17-21.

Moldovan, G.-L. and D'Andrea, A. D. (2009) 'How the Fanconi Anemia Pathway Guards the Genome', *Annual Review of Genetics*, 43(1), pp. 223–249.

Moldovan, G.-L., Madhavan, M. V, Mirchandani, K. D., McCaffrey, R. M., Vinciguerra, P. and D'Andrea, A. D. (2010) 'DNA polymerase POLN participates in cross-link repair and homologous recombination.', *Molecular and cellular biology*, 30(4), pp. 1088–1096.

Monnerat, S., Almeida Costa, C. I., Forkert, A. C., Benz, C., Hamilton, A., Tetley, L., Burchmore, R., Novo, C., Mottram, J. C. and Hammarton, T. C. (2013) 'Identification and Functional Characterisation of CRK12:CYC9, a Novel Cyclin-Dependent Kinase (CDK)-Cyclin Complex in Trypanosoma brucei', *PLoS ONE*, 8(6), p. e67327.

Monnerat, S., Clucas, C., Brown, E., Mottram, J. C. and Hammarton, T. C. (2009) 'Searching for novel cell cycle regulators in Trypanosoma brucei with an RNA interference screen', *BMC Research Notes*, 2(1), p. 46.

Moreira, D., López-García, P. and Vickerman, K. (2004) 'An updated view of kinetoplastid phylogeny using environmental sequences and a closer outgroup: Proposal for a new classification of the class Kinetoplastea', *International Journal of Systematic and Evolutionary Microbiology*, 54(5), pp. 1861–1875.

Morrison, L. J., Majiwa, P., Read, A. F. and Barry, J. D. (2005) 'Probabilistic order in antigenic variation of Trypanosoma brucei.', *International journal for parasitology*, 35(9), pp. 961–72.

Morrison, L. J., Marcello, L. and McCulloch, R. (2009) 'Antigenic variation in the African trypanosome: molecular mechanisms and phenotypic complexity.', *Cellular microbiology*, 11(12), pp. 1724–34.

De Moura, M. B., Schamber-Reis, B. L. F., Silva, D. G. P., Rajão, M. A., Macedo, A. M., Franco, G. R., Pena, S. D. J., Teixeira, S. M. R. and Machado, C. R. (2009) 'Cloning and characterization of DNA polymerase η from Trypanosoma cruzi: Roles for translesion bypass of oxidative damage', *Environmental and Molecular Mutagenesis*, 50(5), pp. 375–386.

Murray, H. W., Berman, J. D., Davies, C. R. and Saravia, N. G. (2005) 'Advances in leishmaniasis', *The Lancet*, 366, pp. 1561–1577.

Muzzini, D. M., Plevani, P., Boulton, S. J., Cassata, G. and Marini, F. (2008) 'Caenorhabditis elegans POLQ-1 and HEL-308 function in two distinct DNA interstrand cross-link repair pathways', *DNA Repair*, 7(6), pp. 941–950.

Narayanan, M. S., Kushwaha, M., Ersfeld, K., Fullbrook, A., Stanne, T. M. and Rudenko, G. (2011) 'NLP is a novel transcription regulator involved in VSG expression site control in Trypanosoma brucei', *Nucleic Acids Research*, 39(6), pp. 2018–2031.

Nguyen, T. N., Müller, L. S. M., Park, S. H., Siegel, T. N. and Günzl, A. (2014) 'Promoter occupancy of the basal class I transcription factor A differs strongly between active and silent VSG expression sites in Trypanosoma brucei.', *Nucleic acids research*, 42(5), pp. 3164–76.

Nilsson, D., Gunasekera, K., Mani, J., Osteras, M., Farinelli, L., Baerlocher, L., Roditi, I. and Ochsenreiter, T. (2010) 'Spliced leader trapping reveals widespread alternative splicing patterns in the highly dynamic transcriptome of Trypanosoma brucei', *PLoS Pathogens*, 6(8), pp. 21–22.

Northall, S. J., Buckley, R., Jones, N., Penedo, J. C., Soultanas, P. and Bolt, E. L. (2017) 'DNA binding and unwinding by Hel308 helicase requires dual functions of a winged helix domain', *DNA Repair*, 57, pp. 125–132.

Ogbadoyi, E., Ersfeld, K., Robinson, D., Sherwin, T. and Gull, K. (2000) 'Architecture of the Trypanosoma brucei nucleus during interphase and', *Chromosoma*, 108, pp. 501–513.

Okada, T., Sonoda, E., Yoshimura, M., Kawano, Y., Saya, H., Kohzaki, M. and Takeda, S. (2005) 'Multiple roles of vertebrate REV genes in DNA repair and recombination.', *Molecular and cellular biology*, 25(14), pp. 6103–11.

Onn, I., Kapeller, I., Abu-Elneel, K. and Shlomai, J. (2006) 'Binding of the universal minicircle sequence binding protein at the kinetoplast DNA replication origin', *Journal of Biological Chemistry*. American Society for Biochemistry and Molecular Biology, 281(49), pp. 37468–37476.

Ooi, C.-P. and Bastin, P. (2013) 'More than meets the eye: understanding Trypanosoma brucei morphology in the tsetse.', *Frontiers in cellular and infection microbiology*, 3(71), pp. 1-12.

Oryan, A. and Akbari, M. (2016) 'Worldwide risk factors in leishmaniasis', *Asian Pacific Journal of Tropical Medicine*,9(10), pp. 925-932.

Overath, P., Chaudhri, M., Steverding, D. and Ziegelbauer, K. (1994) 'Invariant surface proteins in bloodstream forms of Trypanosoma brucei', *Parasitology Today*, 10(2),pp. 53-58.

Palmer, G. H., Bankhead, T. and Seifert, H. S. (2016) 'Antigenic Variation in Bacterial Pathogens', in *Virulence Mechanisms of Bacterial Pathogens,* 5, pp. 445–480.

Passos-Silva, D. G., Rajão, M. A., Nascimento de Aguiar, P. H., Vieira-da-Rocha, J. P., Machado, C. R. and Furtado, C. (2010) 'Overview of DNA Repair in Trypanosoma cruzi, Trypanosoma brucei, and Leishmania major', *Journal of Nucleic Acids*, 2010, pp. 1–14.

Pays, E., Vanhamme, L. and Pérez-Morga, D. (2004) 'Antigenic variation in Trypanosoma brucei: facts, challenges and mysteries.', *Current opinion in microbiology,* 7(4), pp. 369-74.

Peng, D., Kurup, S. P., Yao, P. Y., Minning, T. A. and Tarleton, R. L. (2015) 'CRISPR-Cas9-mediated single-gene and gene family disruption in Trypanosoma cruzi', *mBio*. American Society for Microbiology, 6(1), pp. e02097-14.

Peters, J. M., Tedeschi, A. and Schmitz, J. (2008) 'The cohesin complex and its roles in chromosome biology', *Genes and Development*. Cold Spring Harbor Laboratory Press, pp. 3089–3114.

Proudfoot, C. and McCulloch, R. (2005) 'Distinct roles for two RAD51-related genes in Trypanosoma brucei antigenic variation', *Nucleic Acids Research*, 33(21), pp. 6906–6919.

Rajão, M. A., Passos-Silva, D. G., DaRocha, W. D., Franco, G. R., Macedo, A. M., Pena, S. D. J., Teixeira, S. M. and Machado, C. R. (2009) 'DNA polymerase kappa from Trypanosoma cruzi localizes to the mitochondria, bypasses 8-oxoguanine lesions and performs DNA synthesis in a recombination intermediate.', *Molecular microbiology*, 71(1), pp. 185–97.

Rattray, A. J. and Strathern, J. N. (2003) 'Error-prone DNA polymerases: when making a mistake is the only way to get ahead.', *Annual review of genetics*, 37, pp. 31–66.

Renglin Lindh, A., Schultz, N., Saleh-Gohari, N. and Helleday, T. (2007) 'RAD51C (RAD51L2) is involved in maintaining centrosome number in mitosis', *Cytogenetic and Genome Research*, 116(1–2), pp. 38–45.

Renkawitz, J., Lademann, C. A. and Jentsch, S. (2014) 'Mechanisms and principles of homology search during recombination', *Nature Reviews Molecular Cell Biology*, 15(6), pp. 369–383.

Rettig, J., Wang, Y., Schneider, A. and Ochsenreiter, T. (2012) 'Dual targeting of isoleucyl-tRNA synthetase in Trypanosoma brucei is mediated through alternative trans-splicing', *Nucleic Acids Research*, 40(3), pp. 1299–1306.

Rico, E., Rojas, F., Mony, B. M., Szoor, B., Macgregor, P. and Matthews, K. R. (2013) 'Bloodstream form pre-adaptation to the tsetse fly in Trypanosoma brucei.', *Frontiers in cellular and infection microbiology*, 3 (78), pp.1-15.

Robinson, N. P., McCulloch, R., Conway, C., Browitt, A. and Barry, J. D. (2002) 'Inactivation of Mre11 does not affect VSG gene duplication mediated by homologous recombination in Trypanosoma brucei.', *The Journal of biological chemistry*, 277(29),

pp. 26185–93.

Rosenberg, S. M. (2001) 'EVOLVING RESPONSIVELY: ADAPTIVE MUTATION', *Nature Reviews Genetics*, 2, pp. 504–515.

Rothwell, P. J. and Waksman, G. (2005) 'Structure and mechanism of DNA polymerases', *Advances in Protein Chemistry*, 71, pp. 401–440.

Rotureau, B. and Van Den Abbeele, J. (2013) 'Through the dark continent: African trypanosome development in the tsetse fly.', *Frontiers in cellular and infection microbiology*, 3, p. 53.

Rotureau, B., Subota, I., Buisson, J. and Bastin, P. (2012) 'A new asymmetric division contributes to the continuous production of infective trypanosomes in the tsetse fly.', *Development (Cambridge, England)*, 139(10), pp. 1842–50.

Rudd, S. G., Glover, L., Jozwiakowski, S. K., Horn, D. and Doherty, A. J. (2013) 'PPL2 translesion polymerase is essential for the completion of chromosomal DNA replication in the African trypanosome.', *Molecular cell*. Elsevier, 52(4), pp. 554–65.

Ruepp, S., Furger, A., Kurath, U., Renggli, C. K., Hemphill, A., Brun, R. and Roditi, I. (1997) 'Survival of Trypanosoma brucei in the tsetse fly is enhanced by the expression of specific forms of procyclin', *Journal of Cell Biology*, 137(6), pp. 1369–1379.

Sale, J. E. (2013) 'Translesion DNA Synthesis and Mutagenesis in Eukaryotes', *Cold Spring Harbor Perspectives in Bioogy*, 5(3), pp. 1–22.

Sale, J. E., Lehmann, A. R. and Woodgate, R. (2012) 'Y-family DNA polymerases and their role in tolerance of cellular DNA damage.', *Nature reviews. Molecular cell biology*, 13(3), pp. 141–52.

Salic, A. and Mitchison, T. J. (2008) 'A chemical method for fast and sensitive detection of DNA synthesis in vivo', *Proceedings of the National Academy of Sciences*, 105(7), pp. 2415–2420.

Saribasak, H., Maul, R. W., Cao, Z., Yang, W. W., Schenten, D., Kracker, S. and Gearhart, P. J. (2012) 'DNA polymerase ζ generates tandem mutations in immunoglobulin variable regions', *The Journal of Experimental Medicine*, 209(6), pp. 1075–1081.

Saxowsky, T. T., Choudhary, G., Klingbeil, M. M. and Englund, P. T. (2003) 'Trypanosoma brucei has two distinct mitochondrial DNA polymerase beta enzymes.', *The Journal of biological chemistry*, 278(49), pp. 49095–49101.

Schamber-Reis, B. L. F., Nardelli, S., Régis-Silva, C. G., Campos, P. C., Cerqueira, P. G., Lima, S. A., Franco, G. R., MacEdo, A. M., Pena, S. D. J., Cazaux, C., Hoffmann, J. S., Motta, M. C. M., Schenkman, S., Teixeira, S. M. R. and MacHado, C. R. (2012) 'DNA polymerase beta from Trypanosoma cruzi is involved in kinetoplast DNA replication and repair of oxidative lesions', *Molecular and Biochemical Parasitology*, 183(2), pp. 122–131.

Schärer, O. D. (2013) 'Nucleotide excision repair in Eukaryotes', *Cold Spring Harbor Perspectives in Biology*. 5(3) , pp 1-19,

Schwede, A. and Carrington, M. (2010) 'Bloodstream form trypanosome plasma membrane proteins: antigenic variation and invariant antigens', *Parasitology*, 137(14), pp. 2029-2039.

Shah, P. and He, Y. Y. (2015) 'Molecular regulation of UV-induced DNA repair', *Photochemistry and Photobiology*, 91(2),pp. 254–264.

Sharma, S., Helchowski, C. M. and Canman, C. E. (2013a) 'The roles of DNA polymerase ζ and the Y family DNA polymerases in promoting or preventing genome instability.', *Mutation research,* 743–744, pp. 97–110.

Sharma, S., Helchowski, C. M. and Canman, C. E. (2013b) 'The roles of DNA polymerase ζ and the Y family DNA polymerases in promoting or preventing genome instability.', *Mutation research*. NIH Public Access, 743–744, pp. 97–110.

Sharma, S., Hicks, J. K., Chute, C. L., Brennan, J. R., Ahn, J.-Y., Glover, T. W. and Canman, C. E. (2012) 'REV1 and polymerase ζ facilitate homologous recombination repair.', *Nucleic acids research*, 40(2), pp. 682–91.

Shcherbakova, P. V, Bebenek, K. and Kunkel, T. a (2003) 'Functions of eukaryotic DNA polymerases.', *Science of aging knowledge environment : SAGE KE*, 2003(8), pp. 2-11.

Sheader, K., Vaughan, S., Minchin, J., Hughes, K., Gull, K. and Rudenko, G. (2005) 'Variant surface glycoprotein RNA interference triggers a precytokinesis cell cycle arrest in African trypanosomes.', *Proceedings of the National Academy of Sciences of the*

United States of America, 102(24), pp. 8716–21.

Siegel, T. N., Hekstra, D. R. and Cross, G. A. M. (2008) 'Analysis of the Trypanosoma brucei cell cycle by quantitative DAPI imaging', *Molecular and Biochemical Parasitology*, 160(2), pp. 171–174.

Simarro, P. P., Cecchi, G., Paone, M., Franco, J. R., Diarra, A., Ruiz, J. a, Fèvre, E. M., Courtin, F., Mattioli, R. C. and Jannin, J. G. (2010) 'The Atlas of human African trypanosomiasis: a contribution to global mapping of neglected tropical diseases.', *International journal of health geographics*, 9(1), p. 57.

Simarro, P. P., Jannin, J. and Cattand, P. (2008) 'Eliminating human African trypanosomiasis: where do we stand and what comes next?', *PLoS medicine*, 5(2), pp. 174-180.

Simpson, A. G. B., Stevens, J. R. and Lukeš, J. (2006) 'The evolution and diversity of kinetoplastid flagellates', *Trends in Parasitology*, 22(4),pp. 168–174.

Sinclair-Davis, A. (2013) 'Functional analysis of TOEFAZ1 uncovers protein domains essential for cytokinesis in Trypanosoma brucei', *Journal of Cell Science*, 130(22),pp. 3918-3932.

Singh, B., Li, X., Owens, K. M., Vanniarajan, A., Liang, P. and Singh, K. K. (2015) 'Human REV3 DNA polymerase zeta localizes to mitochondria and protects the mitochondrial genome', *PLoS ONE*, 10(10), pp. 1-18.

Sironi, M., Cagliani, R., Forni, D. and Clerici, M. (2015) 'Evolutionary insights into host–pathogen interactions from mammalian sequence data', *Nature Reviews Genetics*, 16(4), pp. 224–236.

Sjogren, C. and Nasmyth, K. (2001) 'Sister chromatid cohesion is required for postreplicative double-strand break repair in Saccharomyces cerevisiae', *Current biology : CB*, 11, pp. 991–995.

Van Sloun, P. P. H., Varlet, I., Sonneveld, E., Boei, J. J. W. A., Romeijn, R. J., Eeken, J. C. J. and De Wind, N. (2002) 'Involvement of Mouse Rev3 in Tolerance of Endogenous and Exogenous DNA Damage', *Molecular and Cellular Biology*, 22(7), pp. 2159-2169.

Smith, T. K., Young, B. L., Denton, H., Hughes, D. L. and Wagner, G. K. (2009) 'First small molecular inhibitors of T. brucei dolicholphosphate mannose synthase (DPMS), a validated drug target in African sleeping sickness', *Bioorganic and Medicinal Chemistry Letters*, 19(6), pp. 1749–1752.

Solomon, D. A., Cardoso, M. C. and Knudsen, E. S. (2004) 'Dynamic targeting of the replication machinery to sites of DNA damage', *Journal of Cell Biology*. The Rockefeller University Press, 166(4), pp. 455–463.

Sonnhammer, E. L. L., Eddy, S. R., Birney, E., Bateman, A. and Durbin, R. (1998) 'Pfam: multiple sequence alignments and HMM-profiles of protein domains', *Nucleic Acids Research*, 26(1). pp. 320-322.

Stelter, P. and Ulrich, H. D. (2003) 'Control of spontaneous and damage-induced mutagenesis by SUMO and ubiquitin conjugation.', *Nature*, 425(6954), pp. 188–91.

Steverding, D. (2008) 'The history of African trypanosomiasis', *Parasites & Vectors*. BioMed Central, 1(3), p. 1-8.

Stijlemans, B., Caljon, G., Van Den Abbeele, J., Van Ginderachter, J. A., Magez, S. and De Trez, C. (2016) 'Immune evasion strategies of Trypanosoma brucei within the mammalian host: Progression to pathogenicity', *Frontiers in Immunology*,7, pp . 1-14

Stone, J. E., Kumar, D., Binz, S. K., Inase, A., Iwai, S., Chabes, A., Burgers, P. M. and Kunkel, T. a (2011) 'Lesion bypass by S. cerevisiae Pol ζ alone.', *DNA repair*, 10(8), pp. 826–34..

Stortz, J. A., Serafim, T. D., Alsford, S., Wilkes, J., Fernandez-Cortes, F., Hamilton, G., Briggs, E., Lemgruber, L., Horn, D., Mottram, J. C. and McCulloch, R. (2017) 'Genome-wide and protein kinase-focused RNAi screens reveal conserved and novel damage response pathways in Trypanosoma brucei', *PLoS Pathogens*, 13(7), pp. 1-36.

Sung, P. and Klein, H. (2006) 'Mechanism of homologous recombination: mediators and helicases take on regulatory functions', *Nature Reviews Molecular Cell Biology*, 7(10), pp. 739–750.

Sunter, J. D. and Gull, K. (2016) 'The Flagellum Attachment Zone: "The Cellular Ruler" of Trypanosome Morphology', *Trends in parasitology*, 32(4), pp. 309–324.

Suwaki, N., Klare, K. and Tarsounas, M. (2011) 'RAD51 paralogs: Roles in DNA damage signalling, recombinational repair and tumorigenesis', *Seminars in Cell and Developmental Biology*22 (8), pp. 898–905.

Sykora, P., Kanno, S., Akbari, M., Kulikowicz, T., Baptiste, B. A., Leandro, G. S., Lu, H., Tian, J., May, A., Becker, K. A., Croteau, D. L., Wilson, D. M., Sobol, R. W., Yasui, A. and Bohr, V. A. (2017) 'DNA polymerase beta participates in mitochondrial DNA repair.', *Molecular and cellular biology*, 37 (16), pp.1-20.

Taddei, F., Radman, M., Maynard-Smith, J., Toupance, B., Gouyon, P. H. and Godelle, B. (1997) 'Role of mutator alleles in adaptive evolution', *Nature*, 387(6634), pp. 700–702.

Takahashi, S., Sakamoto, A., Sato, S., Kato, T., Tabata, S. and Tanaka, A. (2005) 'Roles of Arabidopsis AtREV1 and AtREV7 in translesion synthesis', *Plant Physiology*, 138(2), pp. 870–881.

Takata, K.-I., Reh, S., Tomida, J., Person, M. D. and Wood, R. D. (2013) 'Human DNA helicase HELQ participates in DNA interstrand crosslink tolerance with ATR and RAD51 paralogs', *Nat Commun*, 4 (2338), pp.1-8.

Takata, K. I., Arana, M. E., Seki, M., Kunkel, T. A. and Wood, R. D. (2010) 'Evolutionary conservation of residues in vertebrate DNA polymerase N conferring low fidelity and bypass activity', *Nucleic Acids Research*s, 38(10), pp. 3233–3244.

Takata, K. I., Reh, S., Yousefzadeh, M. J., Zelazowski, M. J., Bhetawal, S., Trono, D., Lowery, M. G., Sandoval, M., Takata, Y., Lu, Y., Lin, K., Shen, J., Kusewitt, D. F., McBride, K. M., Cole, F. and Wood, R. D. (2017) 'Analysis of DNA polymerase ν function in meiotic recombination, immunoglobulin class-switching, and DNA damage tolerance', *PLoS Genetics*, 13(6), pp. 1-35.

Taladriz, S., Hanke, T., Ramiro, M. J., García-Díaz, M., García De Lacoba, M., Blanco, L. and Larraga, V. (2001) 'Nuclear DNA polymerase beta from Leishmania infantum. Cloning, molecular analysis and developmental regulation', *Nucleic Acids Research*, 29(18), pp. 3822–3834.

Tan, K. S., Leal, S. T. and Cross, G. A. (2002) 'Trypanosoma brucei MRE11 is non-essential but influences growth, homologous recombination and DNA double-strand break repair', *Mol Biochem Parasitol*, 125(1–2), pp. 11–21.

Tanner, N. K. and Linder, P. (2001) 'Review DExD/H Box RNA Helicases: From Generic Motors to Specific Dissociation Functions', *Molecular Cell*, 8, pp. 251–262.

Taylor, J. E. and Rudenko, G. (2006) 'Switching trypanosome coats: what's in the wardrobe?', *Trends in genetics : TIG*, 22(11), pp. 614–20.

Tetaud, E., Giroud, C., Prescott, A. R., Parkin, D. W., Baltz, D., Biteau, N., Baltz, T. and Fairlamb, A. H. (2001) 'Molecular characterisation of mitochondrial and cytosolic trypanothione-dependent tryparedoxin peroxidases in Trypanosoma brucei', *Molecular and Biochemical Parasitology*, 116(2), pp. 171–183.

Tian, X., Patel, K., Ridpath, J. R., Chen, Y., Zhou, Y. H., Neo, D., Clement, J., Takata, M., Takeda, S., Sale, J., Wright, F. A., Swenberg, J. A. and Nakamura, J. (2016) 'Homologous recombination and translesion DNA synthesis play critical roles on tolerating DNA damage caused by trace levels of hexavalent chromium', *PLoS ONE*, 11(12), p. 1-16..

Tiengwe, C., Marcello, L., Farr, H., Gadelha, C., Burchmore, R., Barry, J. D., Bell, S. D. and McCulloch, R. (2012) 'Identification of ORC1/CDC6-interacting factors in trypanosoma brucei reveals critical features of origin recognition complex architecture', *PLoS ONE*, 7(3), p. e32674.

Tran, H. T., Gordenin, D. A. and Resnick, M. A. (1999) 'The 3'-->5' exonucleases of DNA polymerases delta and epsilon and the 5'-->3' exonuclease Exo1 have major roles in postreplication mutation avoidance in Saccharomyces cerevisiae.', *Molecular and cellular biology*, 19(3), pp. 2000–7.

Trenaman, A., Hartley, C., Prorocic, M., Passos-Silva, D. G., van den Hoek, M., Nechyporuk-Zloy, V., Machado, C. R. and McCulloch, R. (2013) 'Trypanosoma brucei BRCA2 acts in a life cycle-specific genome stability process and dictates BRC repeat number-dependent RAD51 subnuclear dynamics.', *Nucleic acids research*, 41(2), pp. 943–60.

Trindade, S., Rijo-Ferreira, F., Carvalho, T., Pinto-Neves, D., Guegan, F., Aresta-Branco, F., Bento, F., Young, S. A., Pinto, A., Van Den Abbeele, J., Ribeiro, R. M., Dias, S., Smith, T. K. and Figueiredo, L. M. (2016) 'Trypanosoma brucei Parasites Occupy and Functionally Adapt to the Adipose Tissue in Mice', *Cell Host and Microbe*, 19(6), pp. 837–848.

Truong, L. N., Li, Y., Shi, L. Z., Hwang, P. Y.-H., He, J., Wang, H., Razavian, N., Berns, M. W. and Wu, X. (2013) 'Microhomology-mediated End Joining and Homologous Recombination share the initial end resection step to repair DNA double-strand breaks in mammalian cells', *Proceedings of the National Academy of Sciences*, 110(19), pp. 7720–7725.

Tu, X. and Wang, C. C. (2004) 'The Involvement of Two cdc2-related Kinases (CRKs) in Trypanosoma brucei Cell Cycle Regulation and the Distinctive Stage-specific Phenotypes Caused by CRK3 Depletion', *Journal of Biological Chemistry*. American Society for Biochemistry and Molecular Biology, 279(19), pp. 20519–20528.

Týč, J., Klingbeil, M. M. and Lukeš, J. (2015) 'Mitochondrial heat shock protein machinery hsp70/hsp40 is indispensable for proper mitochondrial DNA maintenance and replication.', *mBio*. American Society for Microbiology (ASM), 6(1), pp. 1-14.

Vaisman, A. and Woodgate, R. (2017) 'Translesion DNA polymerases in eukaryotes: what makes them tick?', *Critical Reviews in Biochemestry and Molecular Biology*, 10 (53), pp. 1-30.

Vanhamme, L., Pays, E., McCulloch, R. and Barry, J. D. (2001) 'An update on antigenic variation in African trypanosomes.', *Trends in parasitology*, 17(7), pp. 338–43.

Wang, Z., Castaño, I. B., Adams, C., Vu, C., Fitzhugh, D. and Christman, M. F. (2002) 'Structure/function analysis of the Saccharomyces cerevisiae Trf4/Pol sigma DNA polymerase.', *Genetics*, 160(2), pp. 381–91.

Wastling, S. L. and Welburn, S. C. (2011) 'Diagnosis of human sleeping sickness: sense and sensitivity.', *Trends in parasitology*, 27(9), pp. 394–402.

Waters, L. S., Minesinger, B. K., Wiltrout, M. E., D'Souza, S., Woodruff, R. V and Walker, G. C. (2009) 'Eukaryotic translesion polymerases and their roles and regulation in DNA damage tolerance', *Microbiology and molecular biology reviews : MMBR*, 73(1), pp. 134–154.

Waters, L. S., Minesinger, B. K., Wiltrout, M. E., D'Souza, S., Woodruff, R. V and Walker, G. C. (2009) 'Eukaryotic translesion polymerases and their roles and regulation in DNA damage tolerance.', *Microbiology and molecular biology reviews : MMBR*, 73(1), pp. 134-54.

WHO (2013) 'Control and surveillance of human African trypanosomiasis.', *World Health Organization technical report series*, (984), pp. 1–237.

Wood, R. D. and Doublié, S. (2016) 'DNA polymerase θ (POLQ), double-strand break repair, and cancer', *DNA Repair*, pp. 22–32.

Woodward, R. and Gull, K. (1990) 'Timing of nuclear and kinetoplast DNA replication and early morphological events in the cell cycle of Trypanosoma brucei.', *Journal of cell science*, 95, pp. 49–57.

Wu, L., Davies, S. L., Levitt, N. C. and Hickson, I. D. (2001) 'Potential Role for the BLM Helicase in Recombinational Repair via a Conserved Interaction with RAD51', *Journal of Biological Chemistry*, 276(22), pp. 19375–19381.

Wyatt, D. W., Feng, W., Conlin, M. P., Yousefzadeh, M. J., Roberts, S. A., Mieczkowski, P., Wood, R. D., Gupta, G. P. and Ramsden, D. A. (2016) 'Essential Roles for Polymerase θ-Mediated End Joining in the Repair of Chromosome Breaks', *Molecular Cell*, 63(4), pp. 662–673.

Wyatt, M. D. and Pittman, D. L. (2006) 'Methylating agents and DNA repair responses: Methylated bases and sources of strand breaks', *Chemical Research in Toxicology*, 19(12)pp. 1580–1594.

Yamashita, T., Oda, T. and Sekimoto, T. (2012) 'Translesion DNA Synthesis and Hsp90', *Genes and Environment*, 34(2), pp. 89–93.

Yang, Z., Geng, J., Yen, W. L., Wang, K. and Klionsky, D. J. (2010) 'Positive or Negative Roles of Different Cyclin-Dependent Kinase Pho85-Cyclin Complexes Orchestrate Induction of Autophagy in Saccharomyces cerevisiae', *Molecular Cell*, 38(2), pp. 250–264.

Yousefzadeh, M. J. and Wood, R. D. (2013) 'DNA polymerase POLQ and cellular defense against DNA damage', *DNA Repair*, 12 (1), pp. 1–9.

Zhang, H., Chatterjee, A. and Singh, K. K. (2006) 'Saccharomyces cerevisiae polymerase zeta functions in mitochondria.', *Genetics*, 172(4), pp. 2683–8.

Zhang, X. Y., Langenick, J., Traynor, D., Babu, M. M., Kay, R. R. and Patel, K. J. (2009) 'Xpf and not the Fanconi anaemia proteins or Rev3 accounts for the extreme resistance

to cisplatin in Dictyostelium discoideum', *PLoS Genetics*, 5(9), pp. 1-13.

Zhao, L. and Todd Washington, M. (2017a) 'Translesion synthesis: Insights into the selection and switching of DNA polymerases', *Genes*, 8(1), pp. 1-25.

Zhou, Q., Gu, J., Lun, Z.-R., Ayala, F. J. and Li, Z. (2016) 'Two distinct cytokinesis pathways drive trypanosome cell division initiation from opposite cell ends.', *Proceedings of the National Academy of Sciences*, 113(12), pp. 3287–92.

Zhou, Q. and Li, Z. (2016) 'A backup cytokinesis pathway in Trypanosoma brucei', *Cell Cycle*, 15(18), pp.2379-2380.

Zhu, F. and Zhang, M. (2003) 'DNA polymerase ζ: new insight into eukaryotic mutagenesis and mammalian embryonic development', *World J Gastroenterol World Journal of Gastroenterology World J Gastroenterol*, 9(96), pp. 1165–1169.

Zhuang, Z. and Ai, Y. (2010) 'Processivity factor of DNA polymerase and its expanding role in normal and translesion DNA synthesis', *Biochimica et Biophysica Acta - Proteins and Proteomics*, 1804(5), pp. 1081–1093.

Ziv, O., Geacintov, N., Nakajima, S., Yasui, A. and Livneh, Z. (2009) 'DNA polymerase zeta cooperates with polymerases kappa and iota in translesion DNA synthesis across pyrimidine photodimers in cells from XPV patients.', *Proceedings of the National Academy of Sciences*, 106(28), pp. 11552–11557.

Ziv, O., Zeisel, A., Mirlas-Neisberg, N., Swain, U., Nevo, R., Ben-Chetrit, N., Martelli, M. P., Rossi, R., Schiesser, S., Canman, C. E., Carell, T., Geacintov, N. E., Falini, B., Domany, E. and Livneh, Z. (2014) 'Identification of novel DNA-damage tolerance genes reveals regulation of translesion DNA synthesis by nucleophosmin.', *Nature communications*, 5(5437), p. 1-13.